Role of HIR2 protein and plasma membrane microdomains in the control of iron acquisition machinery in plants

Amanda Martín-Barranco

NNT : 2019SACLS131

Thèse de doctorat

Role of HIR2 protein and plasma membrane microdomains in the control of iron acquisition machinery in plants

Thèse de doctorat de l'Université Paris-Saclay
préparée à L'Université Paris-Sud

École doctorale n°**567 : sciences du végétal : du gène à l'écosystème (SDV)**

Spécialité de doctorat: Biologie

Thèse présentée et soutenue à Gif-sur Yvette, 18 Juin 2019, par

Amanda Martín-Barranco

Composition du Jury :

- M. Marc Boutry Professeur Université catholique de Louvain, Louvain-la-Neuve Belgique	Rapporteur
- M. Doan-Trung Luu Chargé de Recherche, CNRS Montpellier	Rapporteur
- Mme. Jacqui Shykoff Directrice de Recherche, Université Paris-Sud 11, Orsay	Présidente du jury
- M. Sébastien Mongrand Directeur de Recherche, CNRS Bordeaux	Examinateur
- M. Hannetz Roschzttardtz Professeur Assistant, Pontifical Catholic University of Chile, Santiago, Chili	Examinateur
- M. Enric Zelazny Chargé de Recherche, CNRS, Gif-Sur-Yvette	Directeur de thèse

Université Paris-Saclay
Espace Technologique / Immeuble Discovery
Route de l'Orme aux Merisiers RD 128 / 91190 Saint-Aubin, France

Acknowledgments

First of all, I would like to say a big thank you to Enric Zelazny, my supervisor. You gave me the opportunity to carry out my PhD, you worked side by side with me when needed and you took care that everything could be done, whatever the "change in program" we faced. Besides, I would also like to thank you for your support and patience during difficult personal moments. Without that, I would not have been able to finish, thank you. To continue, I would like to thank Grégory Vert, the team leader. He was my first link with the team, the one that helped me to join the lab and that put me in contact with my supervisor. I thank him also for the little pieces of advice during my thesis, his useful comments and for keeping in touch and caring, being far. Of course, I would like to thank Sébastien Thomine, who is also a member of my thesis committee, and all the Minions lab. Thank you for hosting us during my third year and thank you for being so very welcoming! They represent for me my "second thesis lab" and I think I am somehow lucky to have had the opportunity to be part of them for a little while. And also a thank you to the people from ImageGif. Not only for assistance (and some good laughs) but also for rearranging so that we could use some lab facilities during this last year.

I would like to thank also the other members of my thesis committee: Dr. Sébastien Mongrand and Pr. Jean Denis Faure for their interest in my project and their guidance and for the very interesting talks. Of course, also a big thank you to the Jury members, my "repporteurs" Doan Luu and Marc Boutry, as well as to my "examinateurs" Sébastien Mongrand (thank you again), Hannetz Roschzttardtz and Jacqui Shykoff. Thank you for your time invested evaluating my work, and for the effort to be present in my defense, even if coming from far, I am very thankful.

I would like to thank now to all the present and past members of my lab, without them nothing would have been the same. Thank you Sara, my very first labmate, for the good moments and the help when I just arrived to Paris and for your friendship. Thank you Alvarillo and Nat, my good friends, for the good laughs after 7 p.m, while checking the chemidoc in distress. Thank you Aloy, Alex, Guillaume and "mama" Julie for the interesting talks and the laughs (and your help, Julie, and your help!). Thank you Virgi! We had the chance to meet and share! Finally, thank you Taozhi for your humor and your smile and thank you Michal (my Czech labmate) for good moments of work and fun. Thank you all of you for your support and care in difficult

moments! The list is long, but there is a special mention to Romain Vessely, my first student, who also thought me a lot. Of course, I also have the Minion side to thank: mi Marjorita y mi Elsa. Always there, for the good and for the bad. With a Christof, always ready for a plan, and a Julie, always ready for karaoke... And the I2BC side! Laurine, Romaine, Mahnaz, Charbel... you are too many to put all the names in a paper, but I do not forget, the same as for the other Minions and the short term students!
Now it is time for the "Spanish side". I would like to thank Luis Eduardo Hernández, who followed me during my Erasmus and gave me the opportunity to start working with metals in UAM. He also introduced me to Belen Montero, my first master Jedi, who deserves a special and big thank you for being always close and helpful year after year, in all circumstances, scientific and personal. Thanks Vanesa, for your valuable support and help and the good cooking times inside and outside the lab (más madera!). And of course, a big thank you to my Spanish "lunch" team: Elena, Sol and Vicky...and Raphaele. They were more than that, so many things that better to do not try to say more, I should write another thesis about them.

I would like to thank all the people that, being far, remind close: mi Esmeralda (always there), Marta (my common sense), Cris y Miguel (mis Erasmitos), Cris y Marta (mis parisinas and a big support) and my UAM's close friends, who I never forget (Miguel, Dani, Carlos, Clara and Chidi). Writing these lines, I realize so many people are missing, especially from Montpellier and England, but you know you also account each day. Nonetheless, I have to mention my former boss from Montpellier, Patrick Doumas, always supporting through distance, humanly and scientifically, who also helped me to find my PhD project when I had to leave Montpellier.

I would like to finish thanking my family. I thank you all for your support, for coming to see me, for being there each day, despite the distance and for your love. A special thanks a los tios parisinos, Anabel and Dioni, my "second pair of parents", who are always there, and also to my grandma. But a very special thank you to my mother, my father and my brother. They went through everything so that I could be here today, specially my mum, and that is why I dedicate this thesis specially to them.

And at least but not less: a big thank you to Lilian! who kept me alive during the writing part, providing food, water, coaching and also big smiles with lots of love, whatever the season. Thanks to him, there is no one day lost and they double count.

To Susana Barranco and
Bernardino Martín,
who gave everything to support me.

Résumé

Le fer est essentiel à la croissance et au développement des plantes. Chez *Arabidopsis thaliana*, le transporteur IRT1 permet l'absorption du fer par les cellules épidermiques de la racine et est, par conséquent, un des acteurs majeurs de la nutrition en fer. IRT1 est cependant un transporteur peu spécifique qui transporte également des métaux non ferreux, essentiels pour la plante mais toxiques dans le cas où ils sont absorbés en grandes quantités. Ainsi IRT1 est capable de transporter du zinc (Zn), du manganèse (Mn) et du cobalt, métaux qui constituent les substrats secondaires de ce dernier. Récemment, il a été démontré dans notre laboratoire que ces métaux non ferreux sont des régulateurs de l'endocytose d'IRT1, un mécanisme qui vise à éviter la toxicité de ces métaux qui pourrait survenir lors de la carence en fer. Afin d'identifier des protéines potentiellement impliquées dans le trafic ou dans la régulation de l'activité d'IRT1, nous avons isolé des interacteurs de ce transporteur via des immunopurifications d'IRT1 combinées à des analyses de spectrométrie de masse. Cette approche nous a permis d'établir le premier intéractome d'IRT1. Parmi les protéines potentiellement interagissant avec IRT1, nous avons isolé quelques-unes impliquées dans l'endocytose de ce dernier, comme la clathrine (antérieurement proposé par notre laboratoire comme médiatrice de l'internalisation d'IRT1), la tubuline et l'actine mais aussi les protéines AHA2, FRO2 et HIR2, qui pourraient avoir un rôle direct dans le processus d'acquisition du fer *per se*. AHA2 et FRO2 sont en effet bien connues comme étant des acteurs majeurs de l'acquisition du fer chez *Arabidopsis* : AHA2 contribue à la solubilisation du fer pendant que FRO2 permet la réduction du fer avant son internalisation via IRT1. En revanche, le rôle de la protéine HIR2 reste jusqu'à présent assez méconnu. Une particularité intéressante de cette dernière est le fait qu'elle contienne un domaine appelé SPFH, typique des protéines localisées dans des microdomaines membranaires chez *Arabidopsis*. Chez les animaux, les protéines à domaine SPFH ont été proposées comme étant impliquées dans la formation des microdomaines membranaires ; de plus certaines protéines à domaines SPFH appelées Flotillines interviennent dans des mécanismes d'endocytose chez les animaux et les plantes.

Ceci suggère qu'HIR2 pourrait avoir des rôles précis dans le contrôle de la dynamique intracellulaire d'IRT1. Après avoir validé les interactions entre les protéines IRT1 et FRO2/AHA2/HIR2 par des approches complémentaires, nous avons analysé la dynamique intracellulaire de ces protéines par microscopie. Nos résultats suggèrent l'existence d'un complexe protéique regroupant les trois acteurs majeurs de l'homéostasie du fer chez *Arabidopsis* : IRT1, FRO2 et AHA2, dont leur trafique dans la cellule serait partiellement corégulé, probablement afin d'optimiser l'absorption du fer dans la racine. Contrairement à ce qui est observé pour IRT1, les protéines FRO2 et AHA2 ne sont pas massivement endocytées en réponse à un excès de métaux (Zn, Mn, Co) et ceci bien qu'elles puissent être présentes au sein d'un complexe contenant IRT1. Nous avons en outre montré que FRO2 et AHA2 étaient ubiquitinées, mais contrairement à IRT1, de façon indépendante de la concentration en métaux non ferreux. En utilisant des approches de génétique inverse, nous avons mis en évidence que HIR2 était impliquée dans le maintien de l'homéostasie du fer chez *Arabidopsis*. En effet, en absence de fer, les mutants *hir2* sont extrêmement chlorotiques et présentent des problèmes de développement à long terme, phénotype qui est fortement réduit grâce à l'ajout de fer. Malgré cette sensibilité à la carence en fer, nous avons montré que la protéine IRT1 est suraccumulée chez le mutant *hir2* dans ces conditions, et ceci de façon post-transcriptionnelle. Nous cherchons actuellement à déterminer comment HIR2 régule la dynamique et/ou la stabilité d'IRT1 dans la cellule. HIR2 pourrait assurer le recrutement d'IRT1 et plus généralement du complexe d'acquisition du fer décrit ci-dessus dans des microdomaines membranaires spécifiques, ce qui permettrai un contrôle spatial et temporal très précis de la machinerie d'acquisition du fer. D'autre part, nous avons également émis l'hypothèse que HIR2 pourrait être impliquée dans une voie d'endocytose d'IRT1 indépendante de la clathrine. Ce travail représente une des premières évidences du rôle des protéines des microdomaines membranaires dans la nutrition minérale chez les plantes.

Abstract

Iron is an essential nutrient for plant growth and development. In *Arabidopsis thaliana*, the transporter IRT1, which allows iron absorption through the epidermic cells of the root, is a major actor in iron nutrition. Bessides, IRT1 also transports the non-iron metals zinc (Zn), manganese (Mn) and cobalt (Co). These metals are considered as the secondary substrates of IRT1, and therefore this transporter is considered as poorly specific. Our laboratory has recently uncovered that these secondary substrates regulate IRT1 endocytosis. In order to uncover the different proteins that can be implicated in the traffic or in the regulation of IRT1 activity, we performed IRT1 immnopurification, followed by mass spectrometry analysis. This approach allowed us to produce a first interactome list of IRT1. Among the proteins that interact with IRT1, we isolated AHA2 and FRO2, both well known in the process of iron acquisition in *Arabidopsis*, and also a SPFH domain containing protein known as HIR2. Although it is known that HIR2 is contained in membrane microdomains in *Arabidopsis*, its function is still to be determined. Nevertheless, in the animal kingdom, SPFH domain containing proteins have been proposed as implicated in the formation of membrane microdomains. This is especially the case of the specific SPFH domain containing proteins known as Flotillins, which have the ability to mediate endocytosis in animals as in plants. After validation of the interaction between IRT1 and FRO2/AHA2/HIR2 by different complementary approaches, we microscopically analyzed the intracellular dynamics of these proteins. Our results suggest the existence of a protein complex that reunites the three major actors of iron homeostasis in *Arabidopsis*: IRT1, FRO2 and AHA2. We suspect that the main function of this complex is to optimize the process of iron absorption in the root. In spite of what is known for IRT1 and despite being part of a same complex, FRO2 and AHA2 are not massively endocytosed in response to a non-iron metal excess (Zn, Mn, Co). Furthermore, we have shown that FRO2 and AHA2 are ubiquitinated, although their ubiquitination is also independent of the concentration of the non-iron metals, unlike the ubiquitination of IRT1. Finally, using reverse genetic approaches, we have been able to show that HIR2 is implicated in the maintenance of the iron homeostasis. Indeed, *hir2* mutants are extremely sensitive to lack of Fe, even though they present posttranslational deregulations that result in the overaccumulation of the protein IRT1. We are currently trying to determine how HIR2 regulates the dynamics and/or the stability of IRT1 inside the cell. HIR2 could be assuring the recruiting of IRT1,or the recruitment of the

whole iron acquisition complex, into specific membrane microdomains. On the other hand, HIR2 could be implicated in a new pathway of internalization of IRT1, independent of clathrin.

Abbreviations

ABA: Abscisic Acid

Ade: Adenine

ACT: Actin

AHA2: *Arabidopsis* H^+-ATPase 2

Amp: Ampicillin

AMT: Ammonium transporter

AP2: Adaptor Protein Complex 2

ARF-GEF: ARF GDP/GTP exchange factor

ARF: ADP ribosylation factor

B: Boron

BFA: Brefeldin A

bHLH: Basic Helix-Loop-Helix

BOR1: Boron transporter 1

BRI1: Brassinosteroid Insensitive 1

BTS: BRUTUS

Ca: Calcium

CBR: Cytochrome B5 Reductase

CHC: Clathrin heavy chains

CLC: Clathrin light chains

CCP: Clathrin-coated pits

CCV: Clathrin-coated vesicle

Cd: Cadmium

CIPK11: CBL-Interacting Protein Kinase 11

CME: Clathrin mediated endocytosis

Co: Cobalt

Co-IP: co-Immunopurification

COP-II: Coat Protein Complex II

CSC: Cellulose synthase complex

DDM: n-Dodecyl β-D-maltoside

DIM: Detergent Insoluble Membranes

DMM: n-Dodecyl β-D-maltoside

DNA: Desoxyribonucleic acid

DNase: Deoxyribonuclease

DRM: Detergent Resistant membrane

DRP: Dynamin Related Proteins

DSM: Detergent Sensitive Membranes

DTT: Dithiothreitol

DUB: Deubiquitinating enzymes

E1: Ub:-activating enzyme

E2: Ub:-conjugating enzyme

E3: Ub: ligase

ECA1: Epsin-like Clathrin Adaptor 1

EDTA: Ethylenediaminetetraacetic acid

EE: Early endosome

EGFR: Epidermal Growth Factor Receptor

ER: Endoplasmic reticulum

ERAD: Endoplasmic Reticulum-Associated Degradation

ESCRT: Endosomal sorting complex required for transport

Fe: Iron

FPN1: Ferroportin 1

FIT: Fe-deficiency induced transcription factor

FLIM: Fluorescence Lifetime Imaging Microscopy

Flot: Flotillin

FLS2: Flagellin Sensing 2

FRD1: Ferric Reductase Defective 1

FRD3: Ferric Reductase Defective 3

FRET: Förster resonance energy transfer

FRO2: Ferric Chelate Reductase 2

FYVE: zinc finger domain named after FAB1, YOTB, VAC1 and EEA1

GFP: Green Fluorescent Protein

GO: Gene Ontogeny

GPI: Glycosylphosphatidylinositol

GUS: β-glucuronidase

Hygro: Hygromycin B

HIR: Hypersensitive Induced Reaction protein

HR: Hypersensitive Response

HRP: Horseradish Peroxidase

IDF: IRT1 Degradation Factor

IL: Intraluminal vesicle

IP: Immunoprecipitation

IRT1: Iron Regulated Transporter 1

K: lysine

Kana: Kanamycin

kDa: kilodalton

Ld: Liquid-disordered

LE: Late endosome

Leu: Leucine

Lo: Liquid-ordered

LRR: Leucine-Reach Repeat

LYK3: Lysin Motif Receptor-Like Kinase 3

MAE: Microdomain-associated endocytosis

MAMP: microbe-associated molecular pattern

Mn: Manganese

MP-AES : Microwave Plasma Atomic Emission Spectroscopy

MS: Murashige and Skoog medium

MVB: multivesicular bodies

NA: Nicotianamine

NIP: Nodulin26-like Intrinsic Protein

NRAMP1: Natural Resistance-Associated Macrophage Protein

O.D: Optical Density

PD: Plasmodesmata

PEN: Penetration

PHB: Prohibitin

PIC1: Permease In Chloroplast 1

PID: Proliferation, Ion and Death

PIP: Plasma membrane Intrinsic Protein

PM: plasma membrane

PMA2: Plasma Membrane ATPase 2

PVX: *Potato virus X*

OPT3: Oligopeptide transporter 3

ORF: Open Reading Frame

PALM: Photoactivated Localization Microscopy

PLV: ProteinA-LexA-VP16

PS: Phytosiderophores

PUB: Plant U-Box

PVDF: Polyvinylidene difluoride

PYE: POPEYE

qRT-PCR: quantitative RT-PCR

QTL: Quantitative Trait Locus

RALF: Rapid Alkalinisation Factor

RBOH: Respiratory Burst Oxidase Homologues

REM: Remorin

RNA: Ribonucleic acid

ROS: Reactive oxygen species

RT: Reverse transcription

RSV: Rice Stripe Virus

SDS: Sodium Dodecyl Sulfate

SNARE: Soluble N-ethylmaleimide-sensitive fusion protein attachment protein receptors

SNX: Sorting nexin

SOD: Superoxide dismutase

Spec: Spectinomycin

SPFH: Stomatin/Prohibitin/Flotillin/HflK/C

STED: Stimulated Emission Depletion

STORM: Stochastic Optical Reconstruction Microscopy

SUB: SUS bridge assay

SUS: Split-ubiquitin system

SYMREM: Symbiotic Remorin

SYP121: Syntaxin related protein 121

TCA: Trichloroacetic acid

TGN: Trans-Golgi network

TIRF(M): Total Internal Reflection Fluorescence (Microscope)

TM: Trans membrane domain

TMD: Ten Transmembrane Domains

TPC: TPLATE complex

Trp: Tryptophan

Ub: Ubiqutin

Ura: Uracil

VIT: Vacuolar Iron Transporter

VPS: Vacuolar Protein Sorting

WT: Wild Type

YSL2: Yellow Stripe-Like 2

ZIP: ZRT-IRT-like Protein

Zn: Zinc

Table of contents

Table of contents **1**

Chapter I **4**

Introduction **5**

I - Iron homeostasis, a vital process regulated at multiple levels in plants **5**

I.1 - Iron is essential for plant growth and development but in controlled amounts 5

I.2 - Iron uptake in plants 7

I.2.1 - Mechanism of iron acquisition 7

I.2.2 - IRT1 is a broad metal spectrum transporter 9

I.3 - The major actors of iron acquisition in *Arabidopsis* are co-expressed in a FIT-dependent manner under iron deficiency 10

I.3.1 - Expression territories of *IRT1*, *FRO2* and *AHA2* genes 10

I.3.2 - FIT, the master transcription factor involved in iron acquisition 11

I.4 - Fe transport and redistribution along the plant and subcellular distribution 12

I.4.1 - Iron transport across the root and redistribution 12

I.4.2 - Localization of iron inside the cell 16

II - Regulation of the three main actors implicated in Fe acquisition: AHA2, FRO2 and IRT1 proteins **19**

II.1 - Regulation of the intracellular protein trafficking 19

II.1.1 - The secretory pathway 19

II.1.2 - The endocytic pathway 21

II.1.2.1 - Generalities about the endocytic pathway: from the plasma membrane to the vacuole 21

II.1.2.2 - Endocytosis 23

II.1.2.2.1 - Clathrin mediated endocytosis 23

II.1.2.2.2 - Membrane microdomain-associated endocytosis 25

II.1.2.2.3 - Ubiquitination as a way to control endocytosis 26

II.1.3 - Polarity of nutrient transporters in the root 29

II.1.4 - Control of the intracellular trafficking of AHA2, FRO2 and IRT1 31

II.1.4.1 - A mobile AHA2 and a mysterious FRO2 31

II.1.4.2 - A very dynamic IRT1 32

II.2 - Regulation of the activity of the main actors of iron acquisition: good overview for AHA2, not so much for IRT1 and FRO2 35

II.2.1 - AHA2 35

II.2.2 - FRO2 36

II.2.3 - IRT1 36

III - Plant membrane microdomains: nature and functions 37
III.1 - The plasma membrane is a dynamic structure compartmentalized in microdomains 37
III.2 - Dissecting microdomains by biochemical and microscopy approaches 40
III.3 - Main families of membrane microdomain-associated proteins in plants 42
III.3.1 – Remorins 42
III.3.2 – The superfamily of SPFH domain containing proteins 43
III.3.2.1 – Generalities 43
III.3.2.2 – Flotillins 44
III.3.2.3 – HIR 45
III.4 - Biological functions of microdomain-associated proteins in plants 46
III.4.1 - Defence against pathogens 46
III.4.2 - Symbiotic response 47
III.4.3 - Hormonal signalling 48
IV – Context and objectives of the thesis 50

Chapter II 51

Results 53
I - IRT1 interactome in *Arabidopsis* root epidermal cells 53
II - Study of the interactions between IRT1 and FRO2/AHA2/HIR2 57
II.1 – FRO2 and AHA2 directly interact with IRT1 in a split-ubiquitin assay 57
II.2 - FRO2, AHA2 and HIR2 associate with IRT1, as revealed by co-immunopurifications in *Arabidopsis* roots 59
II.3 – Does a direct interaction between HIR2 and AHA2 allow the recruitment of IRT1 in HIR2-containing membrane microdomains? 63
III – Dynamics of the iron acquisition platform 66
III.1 - FRO2 and AHA2 are ubiquitinated in *Arabidopsis* root cells in a metal independent manner 66
III.1.1 – Probing the functionality of AHA2 fusion proteins by acidification assays 67
III.1.2 - FRO2 and AHA2 ubiquitination profiles in response to non-iron metal status 71
III.2 - Co-localization studies between IRT1 and FRO2/AHA2 in the root: Characterization of the dynamics of the Fe acquisition platform 74
IV – Role of HIR2 and membrane microdomains in the control of IRT1 and metal homeostasis 75
IV.1 – HIR2 and IRT1 localize in PM microdomains in root epidermal cells 75
IV.2 - HIR2 plays a role in Fe homeostasis 79
IV.2.1 – *hir2* mutants are hypersensitive to iron deficiency 79
IV.2.2 – IRT1 protein accumulation is disturbed in *hir2* mutants 82

IV.2.3 – The phenotype displayed by the *hir2-2* mutant under Fe starvation is not explained by a deregulation in the total metal content 84
V - Study of a putative role of flotillins in the control of IRT1 endocytosis and the impact on iron nutrition 86
Supplemental Data 90
Material and Methods 100
Chapter III 117
Discussion and Perspectives 118
I. IRT1 interactome: a new departure point in the study of the dynamics and the regulation of IRT1 and new insights in the iron acquisition process 118
II. IRT1, FRO2 and AHA2 form an iron-acquisition complex to optimize iron uptake at the epidermis of *Arabidopsis* roots. 121
III. HIR2 is a membrane microdomain-located protein that interacts with IRT1 and plays a role in Fe homeostasis 125
Bibliography 131

Chapter I

Introduction

Introduction

I - Iron homeostasis, a vital process regulated at multiple levels in plants

I.1 - Iron is essential for plant growth and development but in controlled amounts

Iron (Fe) is an essential and limiting nutrient for life. Fe can alternate between two oxidation states, ferrous (Fe^{2+}) and ferric (Fe^{3+}) iron, both being able to form coordinated complexes with oxygen, sulphur and nitrogen containing ligands (Guerinot and Yi, 1994; Yi and Guerinot, 1996; Flis *et al.,* 2016). Due to its redox properties Fe is a key component of electron transport chains involved in mitochondrial respiration and in photosynthesis (Thomine and Vert, 2013). In addition, Fe, as an essential cofactor for different metalloenzymes, participates in numerous biological functions such as nitrogen fixation, or in the synthesis of DNA, hormones and chlorophyll (Terry and Abadía, 1986; Briat and Lobrag, 1997; Steccanella *et al.,* 2015). Paradoxically, although being one of the most abundant elements in the Earth's crust, iron bioavailability to plants is often limited. Indeed, at neutral and alkaline pH and in aerobic conditions, most Fe is found as insoluble ferric oxides that are non-absorbable for plants (Palmer and Guerinot, 2009; Jeong *et al.,* 2017). Fe deficiency alters chlorophyll synthesis, which induces the appearance of leave interveinal chlorosis, and also disturbs electron transport in both photosystems I and II, impacting photosynthesis and compromising plant growth and development, which eventually leads to death (Guerinot and Yi, 1994; Yi and Guerinot, 1996; Briat *et al.,* 2015). On the other hand, iron overloading in plants due to specific conditions such as acidic and waterlogged soils induces toxicity. Indeed, free Fe^{2+} catalyses the production via the Fenton reaction of hydroxyl radicals that generate oxidative stress in the cells (Hendry and Brocklebank, 1985; Thomine and Vert, 2013). Due to the necessity/toxicity of Fe, the maintenance of plant iron homeostasis is tightly regulated by multiple mechanisms at the Fe acquisition, transport and storage levels.

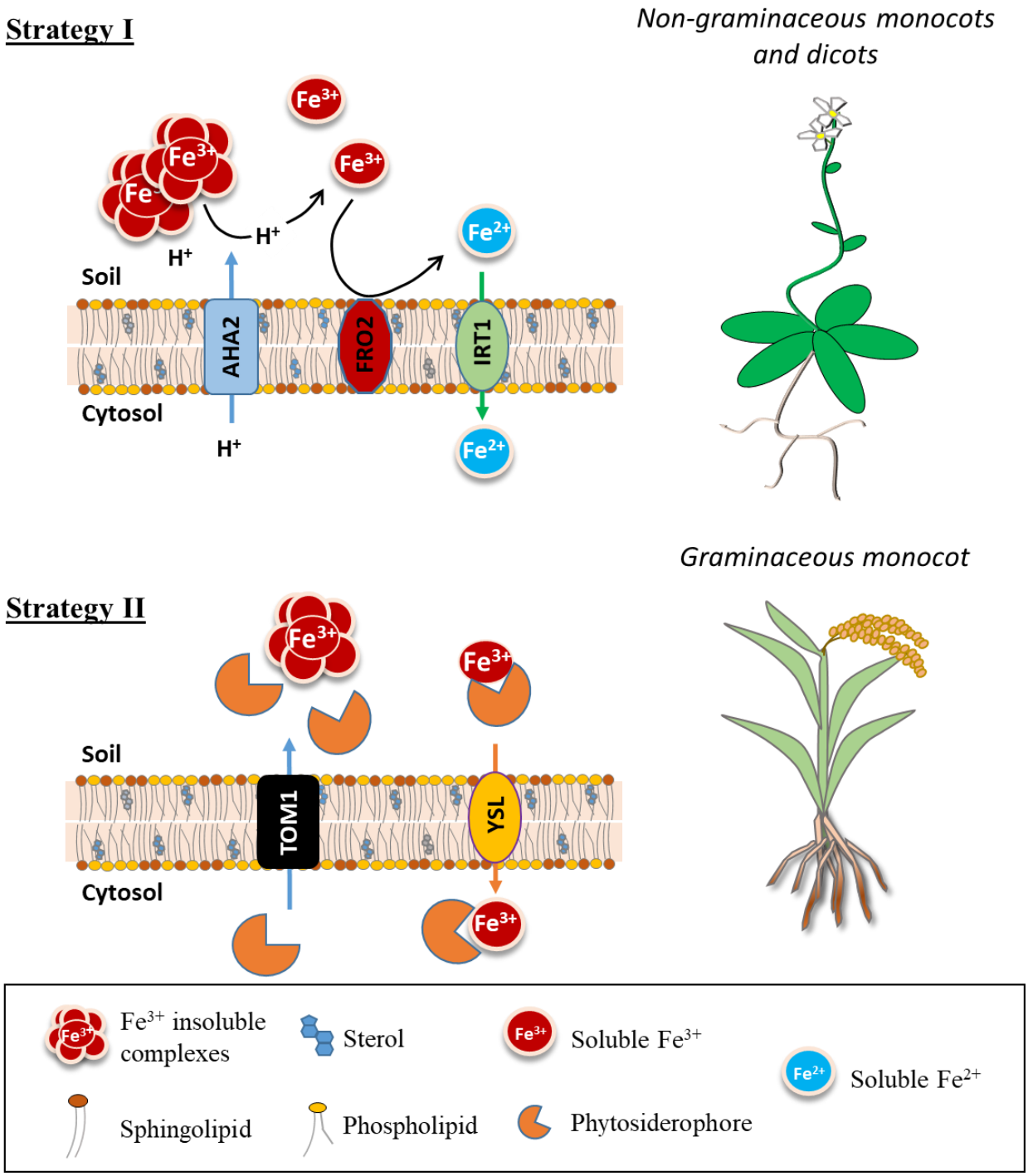

Figure 1. Different strategies for Fe acquisition in plants.
Iron absorption processes described in this figure occur in the epidermis of the root under iron limited conditions. During Strategy I, typical of non-graminaceous monocots and dicots, plants acidify the rhizosphere via proton extrusion mediated by the proton pump AHA2, thus allowing the solubilization of Fe^{3+} complexes. Then, solubilized Fe^{3+} is reduced to Fe^{2+} by the reductase FRO2 and finally Fe^{2+} is transported by IRT1 inside the cell. During Strategy II that occurs in graminaceous monocots, TOM1 protein liberates phytosiderophores in the rhizosphere, that chelate Fe^{3+}. Phytosiderophores-Fe^{3+} complexes are then directly uptaken by YSL transporters into epidermal cells.

I.2 - Iron uptake in plants

I.2.1 - Mechanism of iron acquisition

Plants have developed high affinity systems to cope up with low Fe availability in the soil and allow iron acquisition by the root using two different strategies (Marschner *et al.,* 1986) (Figure 1). Grasses evolved the chelation strategy or Strategy II in which Fe^{3+} chelators known as phytosiderophores (PS), which belong to the mugineic acid family, are first released into the soil by efflux transporters such as the Transporter of Mugineic acid family TOM1 in rice (Walker and Connolly, 2008; Nozoye *et al.*, 2011; Connorton *et al.*, 2017) . Then, PS-Fe^{3+} complexes are directly taken up by the root through the action of transporters from the Yellow Stripe (YS) family (Kobayashi and Nishizawa, 2012; Xiong *et al.,* 2013). Interestingly, grasses can also acquire Fe^{2+} from the soil in addition to PS-Fe^{3+} complexes (Ishimaru *et al.,* 2006).

In non-graminaceous plants, including *Arabidopsis thaliana*, iron absorption by root epidermal cells is a three-step process, called Strategy I, which combines Fe solubilisation through rhizosphere acidification, Fe reduction and uptake (Marschner and Römheld, 1994; Thomine and Vert, 2013). The major molecular actors implicated in this acidification-reduction-transport mechanism have been well identified in *Arabidopsis*. Under iron deficiency, ferric chelates are solubilized by local rhizosphere acidification via the release of protons by the *Arabidopsis* plasma membrane H^+-ATPase 2 (AHA2, also known as the Plasma Membrane ATPase PMA2) (Santi and Schmidt, 2009). Solubilized Fe^{3+} ions are then reduced to Fe^{2+} by the reductase Ferric Reduction Oxidase 2 (FRO2) (Robinson *et al.,* 1999) and, finally, transported into the cell by the iron transporter Iron Regulated Transporter 1 (IRT1) (Eide *et al.,* 1996; Vert *et al.,* 2002). In accordance to their essential role in iron acquisition, the *irt1* and *fro2* knock-out mutants named *irt1-1* and *ferric reductase defective-1* (*frd1*), respectively, accumulate low amount of iron, are extremely chlorotic and display severe growth defects in lack of Fe, which ultimately leads to death unless exogenous iron is provided (Yi and Guerinot, 1996; Robinson *et al.,* 1999; Vert *et al.,* 2002). Interestingly, during the Strategy I, the reduction of Fe^{3+} by FRO2 has been proposed to be the rate-limiting step in iron acquisition (Robinson *et al.,* 1999; Connolly *et al.,* 2003). Although twelve AHA isoforms are found in *Arabidopsis*, *aha* mutant analysis showed that rhizosphere acidification in response to Fe deficiency is mainly mediated by AHA2 (Santi and Schmidt, 2009). This acidification process is of first importance for plant iron uptake since the solubility of iron increases 1000-fold for every one unit drop in pH (Olsen *et al.,* 1981). Interestingly, orthologues of *AHA2*, *FRO2* and *IRT1* genes have been identified in multiple Strategy I species, suggesting a conserved

mechanism for iron acquisition (Cohen *et al.*, 2004; Tomasi *et al.*, 2013; Kobayashi *et al.*, 2014).

Recently, other actors of the *Arabidopsis* iron acquisition process have been identified such as the ATP-Binding Cassette G37 (ABCG37/PDR9) that is important for the export of coumarins in the rhizosphere under iron deficiency (Fourcroy *et al.*, 2014, Figure 2).

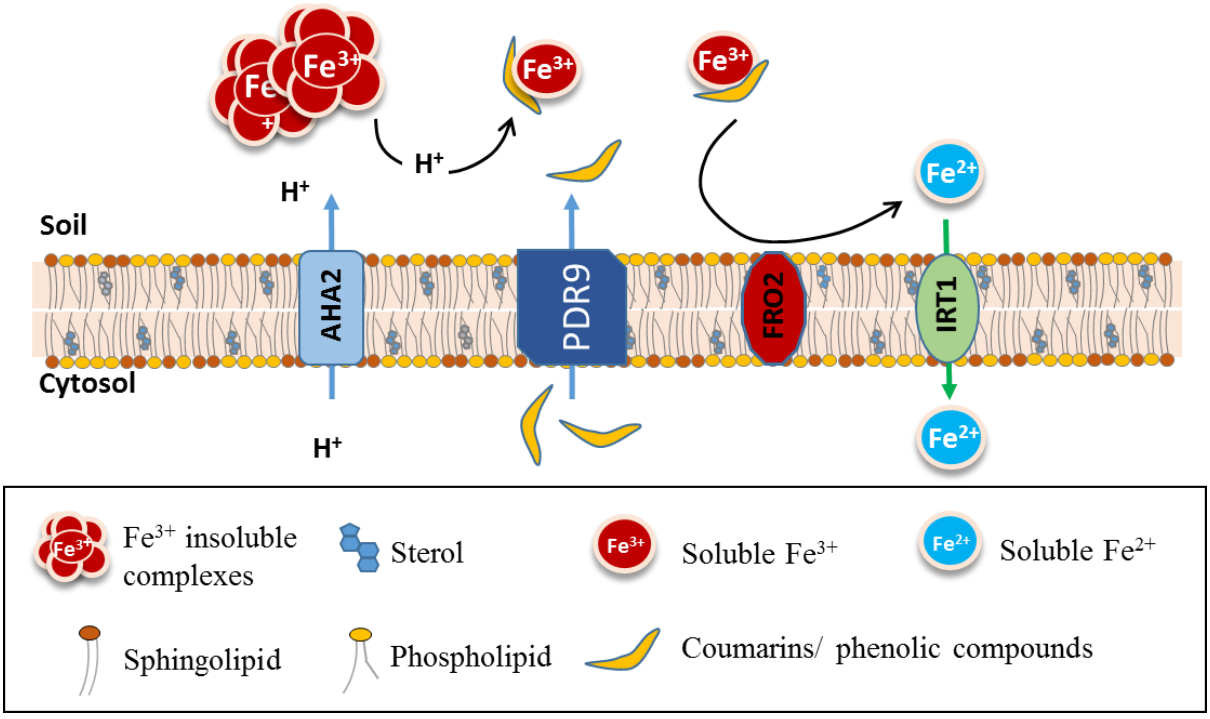

Figure 2. Possible mode of action of coumarins during Fe acquisition Strategy I.
The process described here complements the Fe acquisition mechanism described in Figure 1 and would be especially important in basic soils. According to the work of Fourcroy *et al.*(2016), PDR9 allows the release into the rhizosphere of coumarins and phenolic compounds that chelate Fe^{3+}, thus probably facilitating iron availability for FRO2 that will reduce Fe^{3+}. Finally, Fe^{2+} is uptaken by IRT1.

These excreted phenolic compounds, whose synthesis involves the Feruloyl-Coenzyme A 6'-Hydroxylase 1 (F6'H1) (Schmid *et al.*, 2014) and Cytochrome P450/CYP82C4 (Rajniak *et al.*, 2018), chelate Fe^{3+} and as a result were proposed to facilitate iron availability for FRO2 that generates Fe^{2+} subsequently transported by IRT1 (Fourcroy *et al.*, 2016). Recent work has shown that the production and secretion of coumarins by *Arabidopsis* roots were enhanced when iron availability was compromised by the high pH of the growth medium (Sisó-Terraza *et al.*, 2016). Therefore, coumarins may be of high importance for Fe acquisition in alkaline soils. Interestingly, the role of secreted coumarins in iron acquisition seems to be conserved in other plant species, as recently reported for *Nicotiana tabacum* (Lefèvre *et al.*, 2018). Indeed,

when the expression of *NtPDR3/NtABCG3* is prevented, the secretion of O-methylated coumarins into the rhizosphere is impaired leading to a hypersensitivity of tobacco transgenic plants to iron deficiency.

I.2.2 - IRT1 is a broad metal spectrum transporter

IRT1 belongs to the ZRT-IRT-like Protein (ZIP) family and was, with the zinc transporter Zinc-Regulated Transporter 1 (ZRT1) from *Saccharomyces cerevisiae*, the first member to be identified (Eide *et al.*, 1996; Gaither and J. Eide, 2001; Zhao and Eide, 2002). Importantly, IRT1 not only mediates high-affinity iron uptake, but also transports other divalent metals such as zinc (Zn), manganese (Mn), cobalt (Co) and cadmium (Cd) that constitute IRT1 secondary substrates (Rogers *et al.*, 2000; Vert *et al.*, 2001; Vert *et al.*, 2002). In this manuscript Zn, Mn and Co will be called the non-iron metals. Zn plays many different and important roles in the plant cell since it is the cofactor of more than 300 enzymes, including RNA polymerase, superoxide dismutase (SOD), alcohol dehydrogenase and carbonic anhydrase (Palmer and Guerinot, 2009). Among others, Mn is an essential component of the oxygen-evolving complex in photosystem II and is also a key cofactor of some SOD (Socha and Guerinot, 2014). Co, traditionally considered as an essential plant element, is nowadays considered as "beneficial" for plant growth, and only essential in legume plants, as *Rhizobium spp.* requires Co during nodulation, nitrogen fixation and leghemoglobin synthesis (White and Brown, 2010; Dalcorso *et al.*, 2014). Contrary to the other IRT1 secondary substrates, Cd has no physiological function and is highly toxic in plants, even in low amounts. (Zhao *et al.*, 2006; Fischer *et al.*, 2017). Although Zn and Mn are essential for plant cellular functioning, they are also toxic when present in excess. Interestingly, *Arabidopsis* transgenic lines over-expressing IRT1 under the control of the strong constitutive 35S promoter accumulate over 100-fold more Zn and Mn and also Co in roots compared to wild-type plants, whereas iron over-accumulation remains moderate in the same lines (Barberon *et al.*, 2011). The strong over-accumulation of non-iron metals in 35S::IRT1 transgenic lines induces oxidative stress and has detrimental effects on plant growth. Importantly this phenotype is reverted when plants are grown in the presence of low amounts of non-iron metals. The favoured transport of non-iron metals over iron by IRT1 is probably due to the fact that the uptake of Fe^{2+} by IRT1 requires the prior reduction of Fe^{3+} by FRO2, whose activity is limiting for iron uptake (Zelazny *et al.*, 2011). Altogether, these results show that the balance between iron and non-iron metals transported by IRT1 has to be tightly regulated to ensure optimal plant growth and development. So far, how metals are transported by IRT1 remains unknown, however site directed mutagenesis allowed to identify

some amino acid residues that are important for the selectivity of the transporter (Rogers *et al.*, 2000) as detailed hereafter in Chapter II.2.3.

I.3 - The major actors of iron acquisition in *Arabidopsis* are co-expressed in a FIT-dependent manner under iron deficiency

I.3.1 - Expression territories of *IRT1*, *FRO2* and *AHA2* genes

In *Arabidopsis*, iron acquisition via Strategy I occurs upon iron deficiency and, consistently, *IRT1*, *FRO2* and *AHA2* gene expression is activated under iron limited conditions (Colangelo and Guerinot, 2004; Brumbarova *et al.*, 2014). Promoter::β-glucuronidase (GUS) analysis and *in situ* hybridization showed that *IRT1* is expressed in root epidermal cells and, surprisingly, to a lower extent in flowers specifically in response to iron starvation (Vert *et al.*, 2002). Recently, IRT1 promoter was shown to be also active in root phloem companion cells and IRT1 expression in this cell type as well as in root epidermal cells is required for proper iron homeostasis (Marquès-Bueno *et al.*, 2016). Concerning the kinetics of *IRT1* expression, *IRT1* was shown to be actively transcribed within 24 h of exposure to Fe deficiency, followed by a maximal accumulation after three days of exposure to Fe deficiency (Connolly *et al.*, 2002). When plants are re-subjected to iron replete conditions, *IRT1* mRNA levels decrease rapidly. *FRO2* expression profile mirrors the one observed for *IRT1* since in situ hybridization and promoter::GUS analysis showed that *FRO2* is expressed in root epidermal cells and flowers under iron deficiency (Connolly *et al.*, 2003). In addition to perform iron uptake from the soil, IRT1 and FRO2 may be involved in the delivery of iron to developing pollen grains even though this hypothesis was never investigated. Expression of *IRT1* and *FRO2* genes was shown to be tightly co-regulated by a local perception of iron availability at the root level and through a systemic pathway involving a shoot-borne signal, in addition these two genes are diurnally co-expressed (Vert *et al.*, 2003). AHA2 appears to be the most abundant AHA isoform in *Arabidopsis* root and is expressed in epidermal cells, in the cortex and in phloem and xylem parenchyma cells (Santi and Schmidt, 2009; Haruta *et al.*, 2010; Fuglsang *et al.*, 2007). Contrary to *IRT1* and *FRO2* genes, *AHA2* is expressed under iron sufficient condition, however *AHA2* expression is increased by more than 3-fold in lack of iron (Santi and Schmidt, 2009). Comparatively, in iron deficient versus iron replete conditions, *IRT1* and *FRO2* expression is induced by 45 and 80 times, respectively. *AHA7* gene expression was also demonstrated to be upregulated by iron deficiency, however the function of AHA7 appears to be associated with

the development of root hairs and not with iron acquisition under iron limited conditions (Santi and Schmidt, 2009).

I.3.2 - FIT, the master transcription factor involved in iron acquisition

The basic Helix-Loop-Helix (bHLH) transcription factor FER-like Iron Deficiency-Induced Transcription Factor (FIT) is a key component of the Fe deficiency response, as such *fit* mutants are extremely chlorotic and die as seedlings under iron deficient condition (Colangelo and Guerinot, 2004). Initial microarray analysis showed that the expression of 179 genes was dependent on FIT (Colangelo and Guerinot, 2004) and recently the number of FIT-regulated genes was extended to 448 (Mai *et al.*, 2016). FIT is considered as a central hub in the induction of the iron deficiency response and importantly *IRT1*, *FRO2* and *AHA2* gene expression is regulated by FIT under iron limited conditions (Figure 3) (Colangelo and Guerinot, 2004; Ivanov *et al.*, 2012). Other components of the *Arabidopsis* iron acquisition machinery, such as *ABCG37/PDR9* gene, are also transcriptionally induced in response to iron deficiency in a FIT-dependent manner (Figure 3) (Rodríguez-Celma and Schmidt, 2013). As for *IRT1* and *FRO2*, *FIT* expression is induced in the outer cell layers of the root during Fe starvation, near the root tip and in upper root zones (Jakoby *et al.*, 2004; Wang *et al.*, 2007). Interestingly, FIT protein seems to be able to promote its own gene transcription (Figure 3)

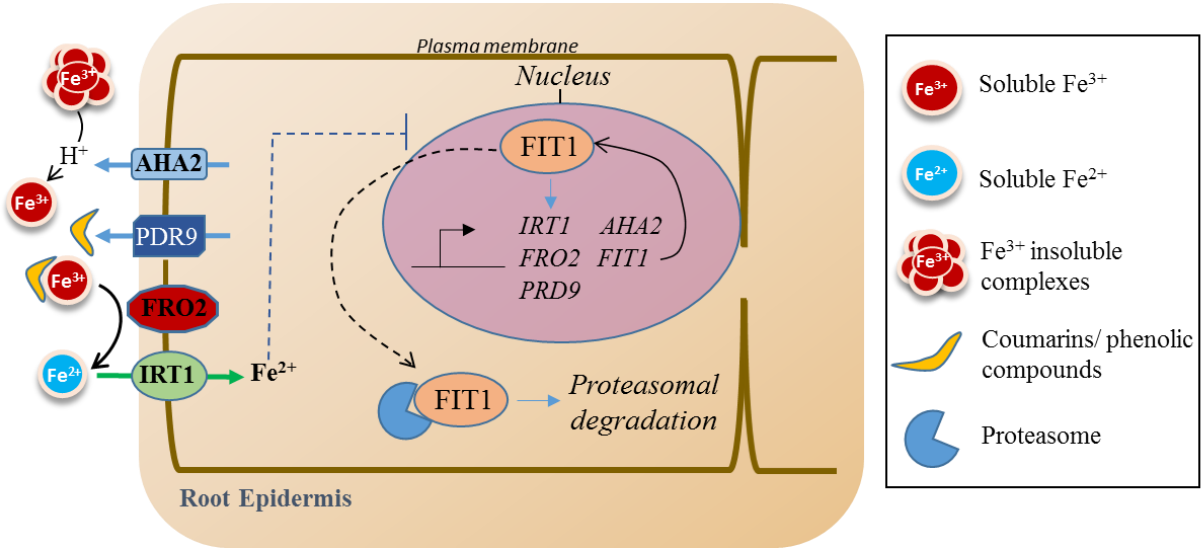

Figure 3. Transcriptional regulation of the genes involved in the iron acquisition under iron deficiency.
During Fe deficiency, the expression of the transcription factor FIT1 is induced. FIT then induces the transcription of the main genes involved in Fe uptake: *AHA2*, *FRO2*, *IRT1*, but also *PDR9*. FIT1 is degraded in the proteasome after inducing a round of transcription, which allows the newly synthetized FIT1 to restart the transcription of its target genes.

(Wang *et al.*, 2007; Brumbarova *et al.*, 2014). FIT regulation was extensively studied highlighting that FIT is highly controlled at the transcriptional and post-translational levels through the action of diverse positive and negative regulators, local and long-distance signals related to iron nutrition and the action of different hormones (Séguéla *et al.*, 2008; Maurer *et al.*, 2011; Matsuoka *et al.*, 2014; Yan Cui *et al.*, 2018). Interestingly, proteasome-mediated turnover of FIT is required for plant Fe deficiency responses, allowing the accumulation of an unstable pool of FIT that, after activation of target genes, will be degraded allowing freshly produced FIT to induce new transcription rounds of target genes (Figure 3) (Sivitz *et al.*, 2011). Very recently, FIT was demonstrated to be phosphorylated by the CBL-Interacting Protein Kinase 11 (CIPK11) in a calcium-dependent manner, shifting FIT from an inactive to an active form (Gratz *et al.*, 2019). To exert its function, FIT can form hetero-dimers with other iron-regulated transcription factors from the Ib subgroup of the bHLH family. Thus, *FRO2* and *IRT1* transcription was reported to be directly regulated by a complex of FIT/bHLH38 or FIT/bHLH39 (Yuan *et al.*, 2008). The two other transcription factors from the Ib subgroup, bHLH100 and bHLH101, were also shown to physically interact with FIT and were proposed to be involved in the process of Fe acquisition by regulating the expression of *FRO2* and *IRT1* genes (Wang *et al.*, 2013). However, these data are not in accordance with results obtained by another group showing that bHLH100 and bHLH101 do not regulate FIT target genes, suggesting that they play a non-redundant role with the two closely related transcription factors bHLH038 and bHLH039 (Svitz *et al.*, 2012). Although bHLH100 and bHLH101 are key regulators of iron-deficiency responses they would operate independently of the main regulator FIT (Sivitz *et al.*, 2012). Although they do not regulate the expression of the iron uptake genes, other transcription factors are important for the iron deficiency response in *Arabidopsis* such as the bHLH transcription factor named POPEYE (PYE) that is expressed in the pericycle in lack of iron (Long *et al.*, 2010). The expression of PYE is co-regulated with that of an E3-ubiquitin ligase called BRUTUS (BTS) which constitutes a negative regulator of the iron deficiency response (Long *et al.*, 2010; Hindt *et al.*, 2017; Kobayashi *et al.*, 2013).

I.4 - Fe transport and redistribution along the plant and subcellular distribution

I.4.1 - Iron transport across the root and redistribution

After being absorbed from the soil, iron is generally thought to be radially transported across the root via symplastic and apoplastic routes (Figure 4) (Palmer and Guerinot, 2009;

Jeong *et al.,* 2017). However, it was also hypothesized that iron may be transported from epidermal cells to underlying cortical cells via efflux transporters. As detailed later in this manuscript, IRT1 displays a polar localization in root epidermal cells and the loss of IRT1 polarity was shown to disturb iron homeostasis, probably because IRT1 works in this case against Fe efflux transporters, leading to radial transport defects within the root and, consequently, to impaired iron accumulation (Barberon *et al.,* 2014). This hypothesis is supported by studies based on dye-coupling approaches showing that differentiated *Arabidopsis* root epidermal cells and root hair cells are symplasmically isolated from cortical cells (Duckett *et al.,* 1994). Importantly, homologs of mammalian metal efflux transporters from the IREG/ferroportin family are found in *Arabidopsis* (Morrissey *et al.,* 2009; Schaaf *et al.,* 2006), however their role in iron exit from epidermal cells was not investigated so far. Further analysis will be required to precisely define the way iron is transported across the root and whether different pathways co-exist. It is important to note that since Fe is highly reactive, it will be bound to specific chelators or proteins in plant tissues to avoid the generation of oxidative stress. According to the redox potential and pH of the different plant compartments, the nature of these molecules will change during the process of transport, and iron will be found in different oxidative states as Fe^{2+} or Fe^{3+} complexes (Brumbarova and Bauer, 2009; Gayomba *et al.,* 2015; Jeong *et al.,* 2017). The pool of iron that may travel across the root via the apoplastic route could be remobilized into cortical and endodermal cells by the plasma membrane located Natural Resistance-Associated Macrophage Protein 1 (NRAMP1), a manganese transporter which also transports iron and whose expression is upregulated under Fe deficiency (Figure 4) (Curie *et al.,* 2000; Cailliatte *et al.,* 2010; Castaings *et al.,* 2016). At the endodermis level, the apoplastic transport of Fe but also water and other nutrients is stopped by the Casparian strip, a band of cell wall material with a high content of lignin with impermeable capabilities, moreover the coupled trans-cellular transport is limited at this point (Naseer *et al.,* 2012; Jeong *et al.,* 2017). Interestingly the deposition in the endodermal cell wall of suberin, a hydrophobic molecule that creates a diffusion barrier, can be modulated by mineral nutrition. Accordingly, the *irt1* mutant in which iron homeostasis is impaired presents a diminished suberization level at the endodermis, and part of its hypersensitive phenotype induced by a lack of Fe is alleviated when crossed with a suberin-less mutant, suggesting that the level of suberization is specifically responding to the Fe nutritional status and that plants may facilitate Fe uptake by decreasing suberin levels (Barberon *et al.,* 2016). Another way for nutrients to avoid the Casparian strip relays on the coordination of influx and efflux transporters, working coordinately to facilitate the transport towards the stele (Barberon, 2017).

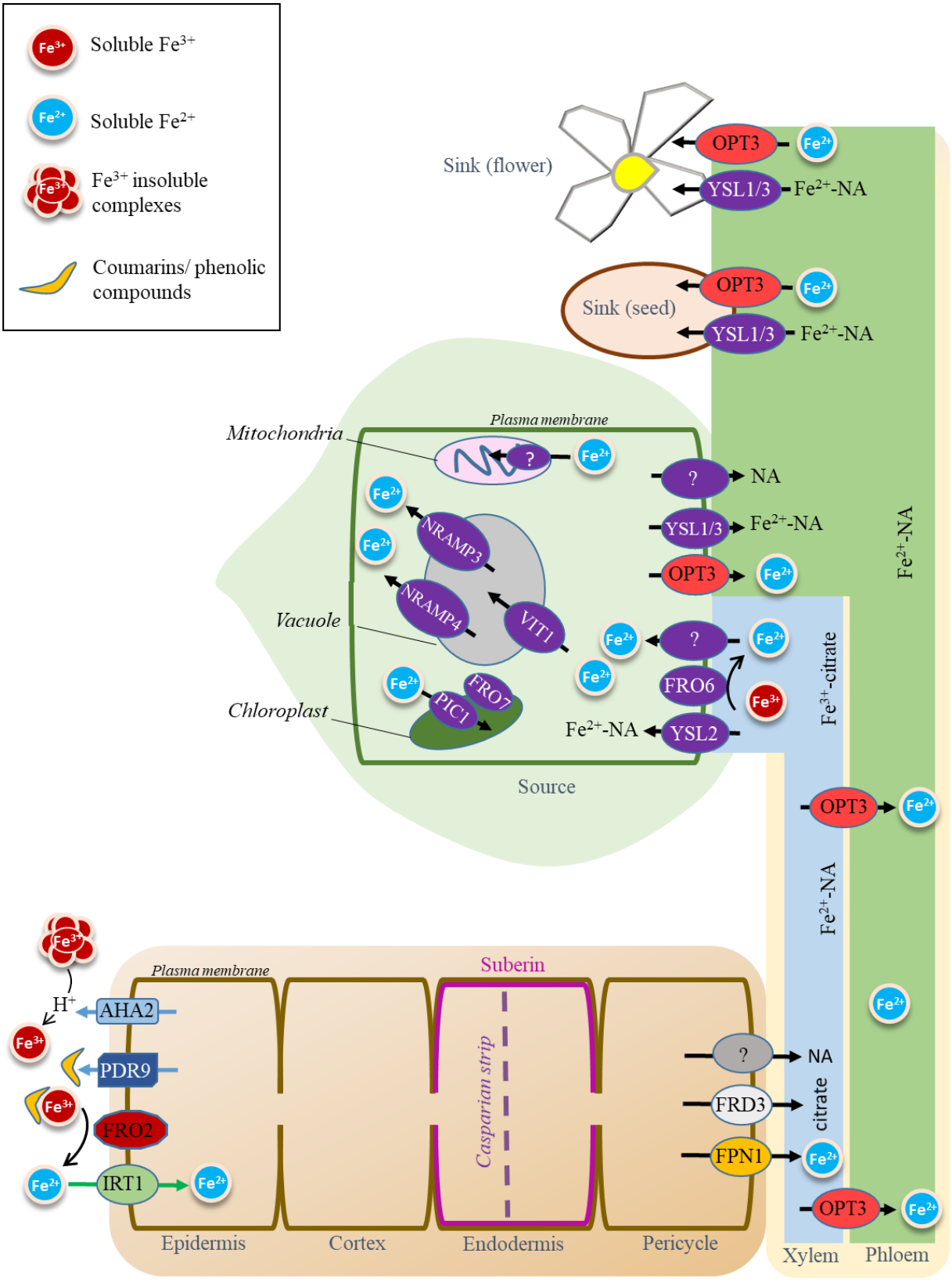
Soluble Fe3+
Soluble Fe2+
Fe3+ insoluble complexes
Coumarins/ phenolic compounds
Sink (flower)
OPT3
YSL1/3
Fe2+-NA
Sink (seed)
Mitochondria
Plasma membrane
Vacuole
Chloroplast
NRAMP3
NRAMP4
VIT1
PIC1
FRO7
FRO6
YSL2
NA
Fe3+-citrate
Source
Suberin
Casparian strip
AHA2
PDR9
FRO2
IRT1
FRD3
FPN1
citrate
Epidermis
Cortex
Endodermis
Pericycle
Xylem
Phloem

Figure 4. General overview of the process of Fe acquisition and redistribution in *Arabidopsis thaliana*.
Fe acquisition takes place in the epidermal cells of the root, as described in Figure 2. Then, Fe is probably radially transported across the root via symplastic and apoplastic routes. Once reaching the endodermis, the apoplastic Fe might be transported inside the cell. Furthermore, Fe nutritional status can influence suberin accumulation. In the pericycle, Fe is effluxed by FPN1 into the xylem where it travels complexed with citrate that is itself effluxed in the xylem by FRD3. Once in the leaves, Fe is probably reduced by FRO6 and uptaken inside the cell by an unknown transporter. A small proportion of Fe travels chelated to nicotianamine (NA) and is uptaken by YSL2 transporters in leaf cells. Once in the cytosol, Fe is transported inside chloroplasts and mitochondria, probably after a reduction mechanism. Fe excess can in turn be sequestered in the vacuole through the action of transporters such as VIT1. When needed, Fe can be remobilized from the vacuole by NRAMP3 and NRAMP4 transporters. OPT3 mediates the transport of Fe from xylem to phloem, where Fe travels complexed with NA. This transporter also removes Fe from old tissues and distributes it, together with YSL1 and YSL3 transporters, into sink tissues such as seeds and flowers.

However, iron influx and efflux transporters that would allow Fe to cross the endodermal cell layer remain unknown so far.

Once arriving to the pericycle of the root, iron is effluxed into the xylem through the action of the Ferroportin 1 (FPN1) transporter (Figure 4) (Morrissey *et al.*, 2009). In parallel, the Ferric Reductase Defective 3 (FRD3) transporter induces the efflux into the xylem of citrate that chelates iron which is then translocated to the shoots (Figure 4) (Durrett *et al.*, 2007). Iron probably travels as a tri-Fe^{3+}-tri-citrate complex, one of the main Fe compounds found in xylem sap of different plant species (Rellán-Álvarez *et al.*, 2010; Flis *et al.*, 2016). In accordance with the function of FRD3, *frd3* mutants are very chlorotic, present a constitutive induction of the iron deficiency response, accumulate less translocated Fe in leaves and present Fe accumulation in the root vasculature (Durrett *et al.*, 2007). As these defects are alleviated upon citrate addition in the growth media (Lahner *et al.*, 2003; Durrett *et al.*, 2007). Furthermore, FRD3 and citrate release in the apoplast were demonstrated to be important during reproductive stages, allowing pollen development, germination and early plant development (Roschzttardtz *et al.*, 2011). In addition to the transport of Fe-citrate complexes, translocation of iron in the xylem can also occur through the binding of Fe^{2+} to nicotianamine (NA) that belongs to the mugineic acid family (Curie *et al.*, 2009). If NA production is impaired, Fe remains attached to vascular bundles, consequently plants show interveinal chlorosis in young leaves, extreme reduction in plant yield and flower development defects that result in sterility (Klatte *et al.*, 2009). Interestingly NA also plays a role in the translocation of iron in the phloem (Figure 4) (Curie *et al.*, 2009). In *Arabidopsis*, Fe-NA complexes are distributed from the xylem to neighbouring

cells by the Yellow Stripe-Like 2 (YSL2) transporter which is expressed in many cell types in both roots and shoots (DiDonato *et al.*, 2004; Schaaf *et al.*, 2005). On the other hand, two other YSL named YSL1 and YSL3 seem to work redundantly in Fe-NA removal from senescent leaves into the phloem and in Fe-NA transport into the seeds (Figure 4). Besides YSL2, another plasma membrane transporter called Oligopeptide Transporter 3 (OPT3) is important for the translocation of Fe into sink tissues. However, contrary to YSL2, OPT3 is proposed to transport Fe^{2+} ions rather than chelated iron (Zhai *et al.*, 2014). Interestingly OPT3 expression is upregulated by Fe deficiency in the vasculature of seedlings and adult plants, in pollen, in minor veins of leaves and in stem nodes (Stacey *et al.*, 2002; Zhai *et al.*, 2014). Besides directly redistributing iron to developing tissues, OPT3 is also involved in Fe remobilization from old to young tissues and in Fe transfer from xylem to phloem, allowing long-distance transport of Fe in the plant (Figure 4) (Zhai *et al.*, 2014). Interestingly, *opt3-1* null mutant results in embryo lethality, but knockdown *opt3* mutants survive, giving rise to plants in which the Fe acquisition response is continuously induced, despite the fact that they over-accumulate Fe (Zhai *et al.*, 2014). How Fe^{3+}-chelates are able to enter the leaf cells remains unknown. However, as the ferric reductase FRO6, one of eight FRO family members, is expressed at high level in leaves it is possible that this protein mediates Fe reduction prior Fe uptake in this tissue (Figure 4) (Jain *et al.*, 2014). Accordingly to this hypothesis, the over-expression of AtFRO6 in transgenic tobacco enhances ferric chelate reductase activity in leaves, increasing plant tolerance to iron-deficiency (Li *et al.*, 2010).

I.4.2 - Localization of iron inside the cell

In plant cells, the quantitatively most important sites for iron use are chloroplasts and mitochondria, for instance chloroplast iron can represent 70% to 90% of cellular iron in mesophyll cells (Thomine and Vert, 2013). In these organelles, Fe forms complexes with ferritin proteins, which allows Fe storage, or associates with metalloproteins from electron transfer chains of two main prosthetic groups: Fe-S clusters and hemes (Briat *et al.*, 2007; Roschzttardtz *et al.*, 2013; Ortega-Rodes *et al.*, 2014). Ferritin form multimeric complexes composed of 24 subunits organized in a sphere shape, each complex can store up to 4.500 atoms of iron in its central cavity (Guerinot and Yi, 1994; Ravet *et al.*, 2009). By complexing iron, ferritins are important to avoid oxidative damages in the plant cell, importantly iron excess increases ferritin abundance (Reyt *et al.*, 2015). In *Arabidopsis*, iron import into the chloroplast was proposed to be performed by the Permease In Chloroplast 1 (PIC1) which is localized in the inner envelope of this organelle (Figure 4) (Duy *et al.*, 2007). PIC1 is able to complement

the growth defect of the Fe uptake-deficient yeast mutant *fet3fet4* and *PIC1* knock-out mutations result in dwarf plants with altered Fe homeostasis. Before being transported into the chloroplast, iron is thought to be first reduced, a step performed by the ferric reductase FRO7 which specifically localizes in the chloroplast (Figure 4) (Jeong *et al.*, 2008). Indeed, chloroplasts isolated from *fro7* loss-of-function mutants have significantly reduced Fe^{3+} reductase activity, reduced iron content and altered photosynthetic complexes.

Vacuolar storage of iron plays an essential role to maintain iron homeostasis in plant cells. In the storage vacuoles from endodermal cells of *Arabidopsis* embryo, imaging approaches revealed that iron is localized in globoids, a structure composed of phytate (Kim *et al.*, 2006; Roschzttardtz *et al.*, 2009). The main transporters allowing the entrance of iron into the vacuole are the tonoplast-localized Vacuolar Iron Transporter 1-like (VIT1) (Kim *et al.*, 2006) which is involved in Fe uptake in developing seeds and young plantlets and the IREG2/FPN2 protein (Morrissey *et al.*, 2009) that is involved in Fe vacuolar uptake in root epidermis and cortical cells. In turn, remobilization of Fe from vacuolar stocks is important for Fe homeostasis and is essential during germination to ensure the correct development of the young seedling, this step being performed by the tonoplastic proteins NRAMP3 and NRAMP4 (Figure 4) (Lanquar *et al.*, 2005). Indeed the growth of *nramp3 nramp4* double mutants is quickly arrested after germination unless the plants are complemented with either NRAMP3 or NRAMP4, or subjected to high concentrations of Fe, demonstrating their redundant role in Fe remobilization (Lanquar *et al.*, 2005). Interestingly, even in the presence of sufficient amount of external Fe, *IRT1* and *FRO2* genes are strongly upregulated in the *nramp3 nramp4* double mutant, showing that a failure to mobilize stored Fe during germination triggered Fe deficiency responses (Bastow *et al.*, 2018). Apart the germination step, NRAMP3 and NRAMP4 are also important for iron mobilization from the vacuole during later stages in the plant life (Lanquar *et al.*, 2005). Besides their role in iron efflux from the vacuole, NRAMP3 and NRAMP4 are also involved in Mn homeostasis by releasing this metal from the vacuole (Lanquar *et al.*, 2010).

In addition to be present in high quantity in chloroplasts, in mitochondria and in the vacuole, by combining complementary imaging approaches iron was also shown to accumulate in the nucleolus of *Arabidopsis* leaves and pea embryos (Hannetz Roschzttardtz *et al.*, 2011). However, the meaning of elevated concentration of iron in nucleolus remains unknown.

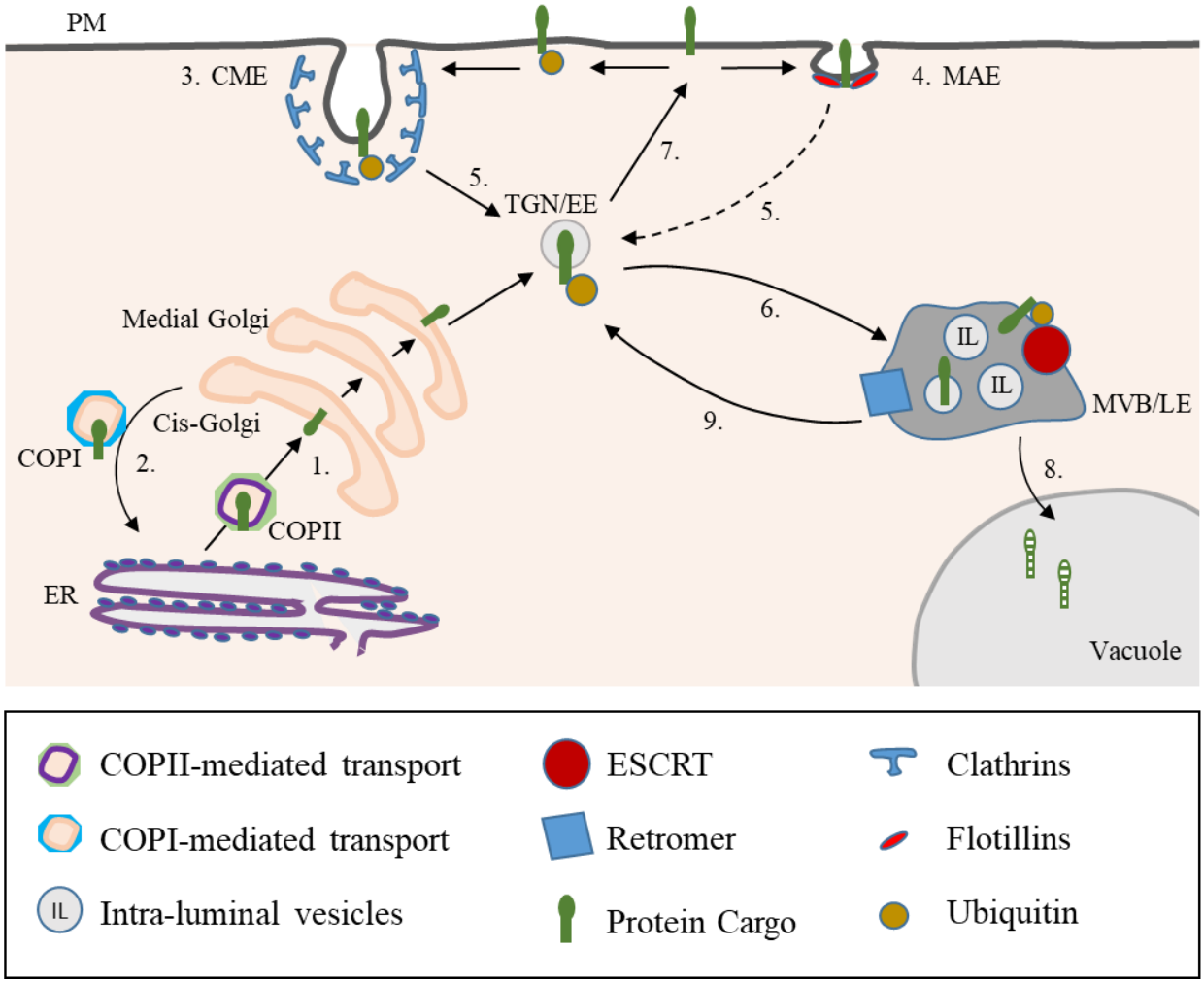

Figure 5. The secretory and endocytic pathways.
Newly synthetized proteins travel from the endoplasmic reticulum (ER) towards the cis-Golgi in COPII-coated vesicles (anterograde pathway) (1). A retrograde pathway, involving COPI vesicles, can transport cargo proteins from the Golgi towards the ER (2). After protein maturation through the different Golgi cisternae towards the Trans Golgi network (TGN/EE), the proteins are transported to the plasma membrane (PM). At the PM, cargo proteins can be internalized through clathrin-mediated endocytosis (CME), after the recognition of specific signals such as ubiquitin (3). Alternatively, PM proteins might undergo microdomain-associated endocytosis (MAE) (4). Afterwards, internalized proteins are targeted to the trans-Golgi network/early endosomes (TGN/EE) (5). At this step, endocytosed proteins can be targeted to multivesicular bodies/late endosomes (MVB/LE) (6) or recycled to the PM (7). Once in MVB/LE, ubiquitinated cargo proteins are recognized by the ESCRT machinery and sorted into intraluminal vesicles (IL) for further targeting to the vacuole and degradation (8). Alternatively, cargo proteins may be recycled to the TGN/EE thanks to the retromer complex (9).

II - Regulation of the three main actors implicated in Fe acquisition: AHA2, FRO2 and IRT1 proteins

The regulation of IRT1, FRO2 and AHA2 occurs at multiple levels and include a transcriptional control by iron availability of *IRT1*, *FRO2* and *AHA2* genes, as previously mentioned in this manuscript, but also post-translational controls of the corresponding proteins. Although our knowledge of the post-translational regulations of the three major actors of Fe acquisition is rather heterogeneous and, especially for FRO2, remains scarce, I will detail in the following section how the intracellular trafficking and/or the activity of these three proteins is controlled. Since my work was highly focused on the traffic and the endocytosis of membrane proteins inside the plant cell, using IRT1 as a model, I will first give an overview of the complexity of the different trafficking pathways and the way they are regulated. On the other hand, concerning the control of the activity *per se* of IRT1, AHA2 and FRO2, I decided to directly get into the heart of the matter by commenting what is specifically known about these proteins.

II.1 - Regulation of the intracellular protein trafficking

II.1.1 - The secretory pathway

The secretory pathway insures the delivery of newly synthetized proteins from the endoplasmic reticulum (ER) to the Golgi apparatus and their subsequent targeting to various destinations along the endomembrane system such as the plasma membrane (PM) or the tonoplast (Figure 5) (Bassham *et al.*, 2008; Pedrazzini *et al.*, 2013; Zelazny and Vert, 2014; Kim and Brandizzi, 2016). Exchange of proteins but also lipids between endomembrane compartments occurs through nucleation, scission and fusion of small transport vesicles (Hwang and Robinson, 2009).

Most lipids including sterols and ceramides are synthetized in the ER and transported via the secretory pathway towards the PM (Van Meer and Sprong, 2004). ER is also responsible for the synthesis, the folding, the disulfide bond formation and the oligomerization of proteins. In the case proteins are misfolded during these different steps, they are selected by the endoplasmic reticulum-associated degradation (ERAD) machinery and retrotranslocated into the cytosol for proteasome-mediated degradation (Vitale and Boston, 2008; Guerra and Callis, 2012; Zelazny and Vert, 2014). Functional proteins enter the anterograde pathway and are exported from the ER to the Golgi apparatus (Figure 5). This transport is mediated by specific vesicles coated and formed by the Coat Protein Complex II (COP-II) which is composed of

three cytosolic components: the GTPase Sar1, Sec23/Sec24 and Sec13/Sec31 heteromers (Zelazny and Vert, 2014; Chung *et al.,* 2016). Although the function of COPII complex was mainly investigated in yeast and mammals (Aridor, 2018), the COPII machinery is conserved in plants and several studies point to its role in protein exit from the ER (Mikosch *et al.,* 2006; Takagi *et al.,* 2013; Chung *et al.,* 2016). First Sar1 is activated by the membrane protein Sec12, a guanine nucleotide-exchange factor, and as a result Sar1-GTP inserts its amphipathic amino-terminal domain in the ER membrane leading to the binding of the protein and to the initiation of the membrane curvature (Lee *et al.,* 2005). Secondly, this initial deformation of the membrane is stabilized by the recruitment of Sec23/Sec24 heterodimer by Sar1-GTP, forming the pre-budding complex. Thirdly, after binding of cargo proteins, the pre-budding complexes are gathered together by the recruitment of Sec13/Sec31 heterotetramers that polymerize creating a lattice (Lederkremer *et al.,* 2001) responsible for the propagation of the membrane curvature initiated by Sar1, which finally creates the COPII vesicle. Recruitment of cargo proteins is mainly performed by the Sec24 subunit in yeast and mammmals but also in plants. Besides, diverse cargo binding sites recognizing a variety of ER sorting signals, such as diacidic motifs, were identified on Sec24 (Miller *et al.,* 2003; Mossessova *et al.,* 2003; Sieben *et al.,* 2008). Diacidic motifs are evolutionary conserved cytoplasmic motifs that correspond to the (D/E)x(D/E) sequence, with x representing any amino acid residue (Zelazny and Vert, 2014). In plants they were notably described to be important for the ER exit of diverse channels (Mikosch *et al.,* 2006; Zelazny *et al.,* 2009; Sorieul *et al.,* 2011). To maintain an equilibrium with COPII-mediated anterograde transport, a retrograde pathway is operated by vesicles coated with Coat Protein Complex I (COPI), also called coatomer, which allows the continual recycling of proteins and lipids from the Golgi apparatus to the ER (Brandizzi and Barlowe, 2013, Zelazny and Vert, 2014). COPI is composed of seven subunits (α, β, β′, γ, δ, ε, ζ) and was mostly studied in yeast and mammals. However, COPI homologue components are present in plants, which points to the conservation of function of such a complex, furthermore COPI-containing vesicles have been identified. Nevertheless the molecular function of the plant COPI machinery remains poorly studied (Contreras *et al.,* 2000; Pimpl *et al.,* 2000; Staehelin and Kang, 2008).

In plants, the Golgi apparatus is mainly in charge of sorting proteins toward other cellular compartments, such as the plasma membrane and the vacuole (Figure 5), previously enabling protein glycosylation. Besides, this organelle also participates in the synthesis and the assembly of cell wall components, such as the production of complex cell wall polysaccharides, while it also produces plasma membrane and tonoplast constituents, such as glycolipids

(Hawes, 2005, Zelazny and Vert, 2014). Finally, the Golgi apparatus also contributes to the synthesis of complex sphingolipids and to the transport of lipids (Klemm *et al.*, 2009). Although lipid transport was for long believed to be a counterpart necessary for protein transport and also needed to maintain membranes stability, nowadays it is well admitted that lipids are also active elements for correct cargo recruitment and membrane budding, fusion and fission (Van Meer and Sprong, 2004; Hammond and Balla, 2015). The Golgi apparatus is made of individual cisternae and is subdivided into the cis-, medial- and trans-Golgi (Figure 5) (Hwang and Robinson, 2009). Proteins arrive to the cis-Golgi from the ER, passing sequentially into the other two compartments, which makes this organelle polarized, finally reaching the trans-Golgi network (TGN), which exists as an independent organelle from the Golgi in plants (Brandizzi and Barlowe, 2013). Vesicles emitted from the TGN will finally fuse with the PM to deliver the cargo proteins. The process of vesicle fusion involves Soluble N-ethylmaleimide-sensitive fusion protein attachment protein receptors (SNARE). These proteins are classified as v-SNAREs, when present in the vesicle, or t-SNAREs, when present in the target membrane and interact when the vesicle reaches its destination membrane. In this way they will form a complex that will drive membrane fusion, and so allow cargo delivery (Kim and Brandizzi, 2012). Very interestingly, the work of Sutter *et al.* (2006) brought to light the role of SNARE proteins in controlling the delivery to the PM of some plant membrane proteins, such as the cation transporter KAT1, within specific membrane microdomains (See Introduction Chapter III.1 for microdomain definition). The distribution of KAT1 at the PM is highly dependent on the functionality of the syntaxin related protein (SYP121) SNARE in tobacco, while the expression of dominant negative forms of SYP121 does not affect delivery of other PM proteins such as the proton pump PMA2 (Sutter *et al.*, 2006). This result indicates that the specificity of the process of membrane tethering mediated by SNARE proteins depends, to a certain extent, on the identity of the cargo.

II.1.2 - The endocytic pathway

II.1.2.1 - Generalities about the endocytic pathway: from the plasma membrane to the vacuole

Proteins located at the PM can be internalized by clathrin-mediated endocytosis (CME), which is considered as the main endocytic route in plants, or by a clathrin-independent pathway involving membrane microdomains as detailed hereafter (Figure 5). Endocytosis can be constitutive to ensure PM protein turnover or induced in response to multiple stimuli, such as

environmental and metabolic cues, allowing for instance the rapid internalization of receptors, transporters and channels (Leborgne-Castel and Luu, 2009). After internalization from the plasma membrane, proteins first reach a compartment called early endosome (EE) which, as previously mentioned, coincides with the TGN in plants (Dettmer, 2006). As the TGN is also part of the secretory pathway, EE/TGN compartment was proposed to contain specialized subdomains with differentiated secretory and endocytic functions (Contento and Bassham, 2012), that have been shown to display specific lipid compositions (Wattelet-Boyer *et al.*, 2016). From EE/TGN, proteins can follow two pathways: they can be either recycled back to the PM or they can continue the endocytic pathway towards the vacuole for degradation (Figure 5). The recycling of cargo proteins involves ADP Ribosylation Factor-Guanine nucleotide Exchange Factors (ARF-GEF), such as GNOM, that activate ADP Ribosylation Factors (ARF) allowing them to localize to membranes and induce vesicle budding (Geldner *et al.*, 2003; Karandur *et al.*, 2017). The fungal toxin brefeldin A (BFA), which inhibits the activity of some ARF-GEF, impairs vesicular trafficking and recycling to the PM, resulting in the accumulation of endocytosed proteins in large cytosolic structures in plant roots called BFA bodies (Geldner *et al.*, 2003). Thus, BFA constitutes an interesting tool to study endocytosis and recycling in plants. As an alternative to recycling, endocytosed cargos can be targeted to multivesicular bodies (MVB), also known as late endosomes, that constitute an intermediate compartment before the vacuole where cargo degradation takes place (Figure 5). The Endosomal Sorting Complex Required for Transport (ESCRT) is an evolutionarily conserved multiprotein complex that promotes membrane deformation and scission towards the inner side of the MVB membrane, away from the cytosol. ESCRT ensures the capture and the sorting of ubiquitinated cargo proteins in intraluminal vesicles of the MVB for subsequent vacuolar targeting (Bassham *et al.*, 2008; Gao *et al.*, 2017; Yong Cui *et al.*, 2018). Ubiquitination, mentioned at this point as a cargo recognition signal for MVB sorting, is a post-translational modification corresponding to the covalent attachment of an ubiquitin (Ub), a 76-amino acid polypeptide, generally onto a lysine residue of a target protein (Romero-Barrios and Vert, 2018). Ubiquitination plays an essential role in plant endocytosis and its function will be detailed hereafter. After reaching the MVB, cargos can be also saved from degradation through the action of the retromer, a multiprotein complex which mediates cargo recycling from MVB back to the TGN (Jaillais *et al.*, 2007; Zelazny *et al.*, 2013). The retromer is formed of two subcomplexes: the core retromer, which is implicated in cargo selection and comprises the Vacuolar Protein Sorting (VPS) 26, VPS29 and VPS35 (Lucas *et al.*, 2016) and a dimer of Sorting Nexins (SNXs), which bind to phosphoinositide-containing endosomal membranes

(Cullen and Korswagen, 2011). Mutations occurring in different retromer subunits were shown to lead to abnormal protein distributions in the cell, leading to severe defects in auxin trafficking, nutrient uptake and suppression of effector triggered-immunity (Kleine-Vehn *et al.*, 2008; Ivanov *et al.*, 2014; Munch *et al.*, 2015).

II.1.2.2 - Endocytosis

II.1.2.2.1 - Clathrin mediated endocytosis

CME constitutes the main route of endocytosis in eukaryotic cells and in conjunction with the secretion system, it permits to regulate the subcellular localization of PM proteins, which allows them to properly perform their functions (Bitsikas *et al.*, 2014; Haucke and Kozlov, 2018). Several molecular actors of CME are conserved in plants, mammals and yeast such as some adaptor proteins, clathrin and dynamin-related proteins (Reynolds *et al.*, 2018), but interestingly other proteins involved in CME seem to be rather specific to plants as explained below. The whole CME process includes five steps allowing the internalization of cargo proteins in specific vesicles: nucleation, cargo selection, clathrin coat assembly, membrane scission and uncoating (McMahon and Boucrot, 2011).

The initiation process of CME, which occurs at specific spots of the PM named the clathrin-coated pits (CCP), is still a matter of debate (Fan *et al.*, 2015). In a first model, the nucleation of the nascent vesicle is thought to be achieved by the heterotetrameric Adaptor Protein complex 2 (AP2) that interacts with clathrin but also cargo proteins in plants (Fan *et al.*, 2013) whereas in a second model CCP pre-exist on the plasma membrane before the recruitment of AP2. In addition to AP2, the eight-core-component protein complex named TPLATE complex (TPC) is a plant essential CME adaptor that is not conserved in yeast, neither in animals (Van Damme *et al.*, 2011; Gadeyne *et al.*, 2014). TPC subunits were shown to physically interact with clathrin and AP2 subunits (Reynolds *et al.*, 2018). Interestingly, while *Arabidopsis* knock-out mutants for individual AP2 subunits remain viable, TPC subunit loss-of-function mutants exhibit pollen lethality, highlighting the crucial role played by TPC in plant endocytosis (Fan *et al.*, 2013; Gadeyne *et al.*, 2014). Although AP2 and TPC work together during CME (Zhang *et al.*, 2015), both adaptors do not answer in the same way in specific pharmacological and genetic studies. For example, in the presence of either salicylic acid or the pharmacological CME inhibitor tyrphostin A23, the association of AP2 to the membrane decreases, but this is not the case for TPC (Wang *et al.*, 2016). These results suggest that both adaptors may also have independent roles, to be addressed in the future. During CME, adaptors

connect the clathrin coat with specific phospholipids and confer also specificity for cargo recognition (Chen *et al.,* 2011; Baisa *et al.,* 2013). For example, tyrosine-based motifs YxxΦ, in which Φ is a bulky hydrophobic amino acid and x any amino acid, or dileucine motifs [DE]xxx[LIM] are recognized by the AP2 complex and are involved in protein internalization in animals (Traub, 2009; Kozik *et al.,* 2010). The function of tyrosine-based motifs is conserved in plants and they were demonstrated to interact with some AP2 subunits. Furthermore, mutation of YxxΦ motifs located in either the fungal pathogen sensor LeEix2 or the auxin efflux carrier PIN1 were shown to impair the internalization of these proteins from the PM (Bar and Avni, 2009; Sancho-Andrés *et al.,* 2016). Recently TPC was suggested to be involved, similarly to AP2, in the selection of cargo proteins during CME. Indeed two TPC subunits were demonstrated to physically interact with cellulose synthase complexes (CSC), although the determination of the motifs that allow the recognition of CSC by TPC remain to be determined (Sánchez-Rodríguez *et al.,* 2018). Importantly, in addition to motifs present in the sequence of membrane proteins, posttranslational modifications such as ubiquitination also play an essential role in protein internalization from the PM, as detailed hereafter.

Following the nucleation step and recruitment of the cargos to be internalized, the maturation of the vesicle requires clathrin coat assembly and the recruitment of additional endocytic accessory proteins (McMahon and Boucrot, 2011; Fan *et al.,* 2015). Clathrin is well evolutionary conserved and assembles in triskelia including three clathrin heavy chains (CHC) and three clathrin light chains (CLC) that will then oligomerize to form the clathrin cage thus increasing membrane curvature and inducing the formation of the clathrin-coated vesicles (CCV) (McMahon and Boucrot, 2011; Wang *et al.,* 2013; Mettlen *et al.,* 2018). The scission of the emerging CCV from the donor membrane is achieved by GTPases called dynamins that display the properties to induce the tubulation and the fission of membranes (Antonny *et al.,* 2016). In plants, Dynamin Related Proteins (DRP) from two subfamilies: DRP2 subfamily, that is similar to the metazoan dynamin and DRP1 subfamily that is plant specific. Both were shown to be important for CME (Fujimoto *et al.,* 2010; Fujimoto and Tsutsumi, 2014). After detachment of the CCV from the PM, the clathrin coat is removed by auxilins in animals, setting free a vesicle that is able to fuse with other endocytic compartments (Paez Valencia *et al.,* 2016). A recent study suggests that the function of auxilins is conserved in plants. Indeed, two putative homologs of auxilins from *Arabidopsis* called AUXILIN-LIKE 1 and AUXILIN-LIKE 2 were shown to interact with CLC and the over-expression of these two proteins inhibits endocytosis, likely by preventing clathrin recruitment to endocytic pits (Adamowski *et al.,* 2018).

II.1.2.2.2 - Membrane microdomain-associated endocytosis

Besides CME, another important pathway to internalize cargo proteins from the PM relies on membrane microdomains that are enriched in sphingolipids and sterols and that regroup specific sets of proteins as detailed hereafter in Introduction Chapter III.1. Microdomain-associated endocytosis (MAE) was first described in mammals and involves membrane microdomain-located proteins named flotillins (Meister and Tikkanen, 2014) (Figure 5). Notably, knock-down of mammalian Flotillin1 expression reduces the internalization from the PM of glycosylphosphatidylinositol (GPI)-linked proteins (Glebov *et al.*, 2005). Studies carried out in the animal field seem to accept that endosomes generated from MAE can also perform functions of recycling and remobilization of cargos for degradation (Liu *et al.*, 2005a; Solis *et al.*, 2013; Diaz-Rohrer *et al.*, 2014; Compeer *et al.*, 2018). In *Arabidopsis*, Flotillin1 (Flot1) was predominantly observed at the PM from which Flot1-positive vesicles budded and *co-localize*d with the endocytic tracer FM4-64 dye (Li *et al.*, 2012). Similarly to mammalian cells, *Arabidopsis* Flot1 was proposed to define a membrane microdomain-associated endocytic pathway (Li *et al.*, 2012; Daněk *et al.*, 2016). Flot1-labelled endosomes differ from the ones generated by CME in term of size and mobility. In *Arabidopsis*, further analysis showed that *Flot1* amiRNA transgenic lines display a decreased internalization from the PM of the brassinosteroid receptor Brassinosteroid Insensitive 1 (BRI1) (Wang *et al.*, 2015). Similarly, in the same study, BRI1 endocytosis was shown to be disturbed when the integrity of membrane microdomain was altered following pharmacological sterol depletion with methyl-β-cyclodextrin. In plants, proteins endocytosed, at least in part, through a MAE pathway have diverse functions and include among others the aquaporin Plasma membrane Intrinsic Protein 2;1 (PIP2;1) (Li *et al.*, 2011), the ammonium transporter AMT1;3 (Wang *et al.*, 2013) the immune receptor Flagellin Sensing 2 (FLS2) (Cui *et al.*, 2018) and the Respiratory burst oxidase homolog D (RbohD) (Hao *et al.*, 2014). So far, cargo proteins described as being retrieved from the PM by MAE are known to be also internalized in a clathrin-dependent manner in plants. Although the two pathways may co-exist it now emerges that the Flotillin/membrane microdomain-mediated endocytosis is favored in plants in response to specific stimuli including stress or hormonal signaling. Thus, upon brassinosteroid stimulation the co-localization between BRI1 and Flot1 increases and concomitantly the internalization of BRI1 through MAE is enhanced (Wang *et al.*, 2015). In addition, salt stress enhances the membrane microdomain-mediated endocytosis of *Arabidopsis* PIP2;1 that is mainly endocytosed in a clathrin-dependent manner in non-stressed conditions (Li *et al.*, 2011;

Luu *et al.*, 2012). Similarly, a salt stress stimulates the endocytosis of RbohD via membrane microdomains (Hao *et al.*, 2014). Biotic stress is also able to increase MAE in *Arabidopsis* cells as recently reported for FLS2 whose co-localization with Flot1 increases in response to the flagellin-derived peptide flg22, leading to an enhanced internalization of FLS2 through the membrane microdomain pathway (Cui *et al.*, 2018). In the context of the symbiotic process in *Medicago truncatula*, the bacterial Nod Factor was shown to increase the co-localization in membrane microdomains between a receptor that mediates bacterial infection called Lysin Motif Receptor-Like Kinase3 (LYK3) and Flotillin 4 (Flot4), however whether this relocalization mechanism is followed by LYK3 endocytosis in a Flot4-dependent manner remains to be determined (Haney *et al.*, 2011). Intriguingly, although microdomain-associated endocytosis was described for years in mammals and plants, the exact mechanisms involved in this pathway, including the recruitment of cargos to be endocytosed and the formation of the endocytic vesicle, remain to be determined (Meister and Tikkanen, 2014). The work performed by Frick *et al.* (2007) represents a first hint about the possible role of Flotillins in the generation of vesicles in specific microdomains. The authors showed that ectopic overexpression of Flotillins 1 and 2 induces their co-assembly to specific mammalian microdomains, which in turn induces membrane curvature, generating membrane buds towards the cytosol. Unfortunately, as their work is based on overexpression of GFP-tagged flotillins, it may not represent the dynamics of the endogenous proteins. In the future, it will be very important to address whether flotillins can structurally mediate cargo internalization and/or vesicle budding and to identify the machinery associated with MAE such as adaptor proteins.

II.1.2.2.3 - Ubiquitination as a way to control endocytosis

Ubiquitination is a key post-translational modification that is involved in endocytosis but also in other processes such as protein degradation in the proteasome or DNA damage response (Komander, 2009). Ubiquitination is a cascade process involving an ubiquitin-activating enzyme (E1), an ubiquitin-conjugating enzyme (E2) and an ubiquitin-protein ligase (E3) (Rotin and Kumar, 2009). First, in an ATP dependent reaction, E1 forms a thioester bond between a cysteine from its active site and the carboxyl terminus of the ubiquitin. Secondly, activated Ub is transferred to a cysteine residue in the active site of an E2. Finally, E2 may give ubiquitin directly to the protein substrate through an E3 from the RING family that acts as a scaffolding protein. Alternatively, Ub may be first transferred to an E3 from the HECT family before being linked to the substrate. This process results in the formation of an isopeptide bond, usually between the epsilon-amino group of the substrate lysine and the carboxyl group of the

last glycine from Ub (H., T., Kim *et al.,* 2007; Guerra and Callis, 2012; Romero-Barrios and Vert, 2018). E3-ubiquitin ligases play a key role in this multistep process as they recruit the target protein for ubiquitination and hence primarily dictate the specificity of the system. Target proteins can be modified with a single Ub molecule on one or several lysine residues, generating monoubiquitination and multi-monoubiquitination, respectively. Alternatively, as Ub contains itself seven lysines residues (K6, K11, K27, K29, K33, K48, K63), Ub molecules can be ligated to one another forming Ub chains (polyubiquitination) (Komander, 2009; Swatek and Komander, 2016). This process can quickly increase the levels of complexity of this post-translational mark, as the configuration of polyubiquitin chains can be very variable (H., T., Kim *et al.,* 2007). Importantly, ubiquitination is a reversible process since Ub moieties can be removed from the target proteins through the action of deubiquitinating enzymes (DUB) (Mevissen and Komander, 2017). One of the best-characterized functions of ubiquitination is to induce the degradation of cytosolic and nuclear proteins by the 26S proteasome, through K48-linked polyUb chains (Pickart and Fushman, 2004; Yadav *et al.,* 2016). On the other hand, monoUb and K63 polyUb were described to be involved in endocytosis and subsequent intracellular sorting (Mukhopadhyay and Riezman, 2007; Piper and Lehner, 2011). Ubiquitinated cargos are recognized by specific proteins carrying ubiquitin-binding domains that bind in a non-covalent way to the hydrophobic interaction surface of Ub (Dikic *et al.,* 2009; Piper *et al.,* 2016). In animals and yeast, ubiquitin binding domains are present in Epsins that allow the recruitment of ubiquitinated cargos for endocytosis. In *Arabidopsis*, Epsin homologs seem to be more implicated in vacuolar trafficking of soluble cargos (Polo *et al.,* 2002; Song *et al.,* 2006; Piper *et al.,* 2016). Epsin-like Clathrin Adaptor 1 (AtECA1) from *Arabidopsis*, is thought to act as an adaptor protein in clathrin coat assembly during cell plate formation. However, its specific cargo proteins have not been yet identified and AtECA1 does not contain any domain homologous to an ubiquitin-binding domain (Song *et al.,* 2012).

In yeast and mammals, ubiquitination occurs at various steps in endocytosis to control PM protein internalization and sorting into the MVB on their way to the vacuole/lysosome for degradation (Lauwers *et al.,* 2010). In particular, monoubiquitination was shown to be sufficient for endocytosis of the Ste2p yeast α-factor receptor and the Epidermal Growth Factor Receptor (EGFR) in mammals (Terrell *et al.,* 1998; Haglund *et al.,* 2003). Although monoubiquitination of some proteins is a sufficient signal for internalization, multi-monoubiquitination, or the presence of K63-linked polyUb chains generally increase the rate of such process, as observed for the Fur4 yeast uracil permease (Galan and Haguenauer-Tsapis, 1997; Blondel *et al.,* 2004). K63-linked polyUb chains emerged as being important during later

steps of endocytosis by controlling the sorting into the MVB. For instance, the Gap1 yeast amino-acid permease modified with a single K63-linked di-Ub chain is efficiently targeted to the vacuolar lumen whereas Gap1 monoubiquitinated on two distinct lysine residues fails to reach this compartment (Lauwers *et al.,* 2009). In plants, the first evidences for a role of ubiquitination in endocytosis came from studies on the root Boron transporter 1 (BOR1) (Kasai *et al.,* 2011) and IRT1 (Barberon *et al.,* 2011). Note that the role of ubiquitination in IRT1 intracellular dynamics will be discussed in a specific section hereafter. In the presence of boron excess, BOR1 is retrieved from the PM and is degraded to avoid a massive and detrimental boron uptake (Takano *et al.,* 2010). This mechanism is regulated through ubiquitination. Indeed, BOR1 is mono- and diubiquitinated in response to high boron concentration, which is crucial for the sorting of the transporter in MVB for subsequent targeting to the vacuole (Kasai *et al.,* 2011). Other environmental factors, such as bacterial infection, can induce the ubiquitination of PM proteins and their subsequent endocytosis. Thus, the immune receptor FLS2 is poly-ubiquitinated by the E3 ubiquitin ligases named Plant U-Box 12 (PUB12) and PUB13 in response to flagellin. This induces the endocytosis and the degradation of FLS2, resulting in an attenuation of immune signaling (Lu *et al.,* 2011). Poly-ubiquitination with K63 linkage was also demonstrated to be essential for BRI1 endocytosis in *Arabidopsis* (Martins *et al.,* 2015). Interestingly, a non-ubiquitinated version of BRI1 in which all the lysine residues were mutated to arginine residues ($BRI1_{K25R}$) is stabilized at the PM as shown by total internal reflection fluorescence (TIRF) microscopy. This suggests a direct role of ubiquitination in the step of BRI1 internalization from the cell surface (Martins *et al.,* 2015). However, given the fact that $BRI1_{K25R}$ internalization is not totally blocked combined with the absence of vacuolar targeting of this protein, it appears that BRI1 ubiquitination is also important for BRI1 sorting in later endocytic comportments and vacuolar delivery. In the same way as FLS2, BRI1 was demonstrated to be ubiquitinated by PUB12 and PUB13. Importantly, brassinosteroids are able to stimulate the interaction between BRI1 and these E3 ubiquitin ligases as well as BRI1 ubiquitination (Zhou *et al.,* 2018). In an original regulation mechanism, BRI1 phosphorylates PUB13 on a specific residue which results in an enhanced association between PUB13 and BRI1. K63 polyubiquitination of the auxin efflux carrier PIN2 was demonstrated to be essential for its vacuolar sorting in *Arabidopsis* and on a physiological point of view for auxin distribution in root meristems (Leitner *et al.,* 2012). As observed in yeast and mammals, K63 polyubiquitination of membrane proteins in plants clearly emerges as a key regulation of endocytosis.

II.1.3 - Polarity of nutrient transporters in the root

Some membrane proteins are not uniformly distributed at the cell surface, but rather organized in an asymmetric fashion according to a specific cellular axis and they are, thus, designed as polar PM proteins. This property allows them to perform specific physiological functions in root cells. In this way, root cell proteins can exhibit apico-basal polarity, when proteins are distributed at either the apical or the basal domain, corresponding to PM regions facing the shoot and the root tip, respectively (Grunewald and Friml, 2010; Grebe, 2010). PIN proteins constitute the prototype for the apico-basal polarization of membrane proteins and the importance of PIN polarity for auxin transport was extensively studied in the past (Dettmer and Friml, 2011; Luschnig and Vert, 2014; Norman, 2016). Although PINs represent an excellent model to study the establishment and the role of PM protein polarity, I believe that the description of PIN polarity is rather out of the scope of my thesis. Therefore, I decided to focus on the polarity of nutrient transporters in plant roots.

In the radial axis of the root, the terms *outer domain* and *inner domain* refer to PM regions oriented towards the surface of the root and the vasculature, respectively. This outer/inner polarity was reported for root nutrient transporters and channels. Such is the case of the *Arabidopsis* boric acid channel Nodulin26-like Intrinsic Protein5;1 (NIP5;1) that localizes in the outer domain of the PM in root epidermal cells and the boron exporter BOR1, present in the inner cell domain of the root endodermis and also found in other cell types (Takano *et al.,* 2010; Wang *et al.,* 2017). It is currently assumed that the fact that both transporters maintain an opposite pattern of polarity is able to facilitate boron transcellular transport, from the rhizosphere to the vascular tissue of the root. Accordingly; the boric acid channel OsNIP3;1 and OsBOR1, a close orthologue of AtBOR1, may facilitate boron transport throughout the root in rice (Fuji *et al.,* 2009). Interestingly, the *Arabidopsis* boron exporter BOR4 displays the same polarity as NIP5;1 at the outer domain of the PM in root epidermal cells, however BOR4 mediates the extrusion of boron from the root to prevent boron toxicity (Miwa *et al.,* 2007). In rice, the transport of silicon across the root was also shown to require the polarity of specific transporters, namely the Low silicon rice1 (Lsi1) silicon influx channel and the Low silicon rice2 (Lsi2) silicon exporter that are localized to the outer PM domain and the inner PM domain of the same root cells, respectively (Ma *et al.,* 2006; Ma *et al.,* 2007). An increasing number of PM proteins have been described to be polar such as proteins from the Pleiotropic Drug Resistance family, including PDR9 which is localized at the outer PM domain of root epidermal cells (Łangowski *et al.,* 2010; Nakamura and Grebe, 2018).

PIN proteins have been traditionally used as models to study the mechanisms behind the creation and maintenance of protein polarity in plant cells. However, nutrient transporters are also very interesting models to study the establishment of cell polarity in plants (Zelazny and Vert, 2014; Nakamura and Grebe, 2018). So far nutrient transporter polarity was demonstrated to be achieved and maintained by polar secretion and endocytic/recycling process. Early studies proposed that the polarity of some nutrient transporter, such as BOR4, maybe directly achieved by polar secretion (Łangowski *et al.,* 2010). More recently this notion was reinforced when the exocyst complex was shown to be implicated in the control of NIP5;1 but also PDR8/Penetration3 (PEN3) polarity. The exocyst is a vesicle tethering octameric complex which facilitates a first contact between secretory vesicles and target membranes (Žárský *et al.,* 2013). Indeed, the EXO84b exocyst subunit *co-localize*d with NIP5;1 and PEN3 at the outer PM domain of root epidermal cells and NIP5;1 and PEN3 localization and polarity were severely disturbed in *exo84b* mutants (Mao *et al.,* 2016). Interestingly, mutant analysis revealed that Actin7 (ACT7) is required for correct polar EXO84b distribution at the outer PM domain (Mao *et al.,* 2016). In addition to targeted secretion, endocytic/recycling processes were also demonstrated to be important for nutrient transporter polarity. Indeed, loss of AP2 clathrin adapter function impairs NIP5;1 polar localization suggesting that NIP5;1 polarity is maintained by clathrin-mediated endocytosis. In addition, NIP5;1 phosphorylation on threonine residues located in specific N-terminal threonine-proline-glycine repetitions is required for proper NIP5;1 endocytosis and polarity (Wang *et al.,* 2017). The role of CME in the establishment of BOR1 polarity at the inner PM domain was recently highlighted by two different studies. First, BOR1 protein was demonstrated to interact with the AP2 complex and mutants for different AP2 subunits were shown to display defects in localization and endocytosis of BOR1, showing that AP2-dependent endocytosis is involved in the polar localization of BOR1 (Yoshinari *et al.,* 2019). Secondly, DRP1A was shown to co-localize with BOR1 at the PM and was important to mediate the CME of BOR1 and to maintain its polarity. Indeed, Geiger

the expression of dominant negative forms of DRP1A, or the absence of DRP1A in loss-of-function mutants, resulted in the inhibition of BOR1 endocytosis and the loss of the polar localization of this transporter (Yoshinari *et al.,* 2016). A post-endocytic recycling-based mechanism implying tyrosine motifs was also proposed to be involved in the polar localization of BOR1 to the inner PM domain (Takano *et al.,* 2010). Indeed, mutation in tyrosine-based sorting signals in BOR1 altered the polar localization of BOR1 without changing its internalization rate from the PM. The authors proposed that the inhibition of a polar targeting

pathway due to tyrosine mutations might have resulted in nonpolar recycling and thus nonpolar distribution of BOR1 (Takano *et al.*, 2010). In conclusion it appears that the establishment of the polar localization of nutrient transports in plant root is a complex process that probably relies on multiple mechanisms based on polar secretion and endocytosis/recycling.

II.1.4 - Control of the intracellular trafficking of AHA2, FRO2 and IRT1

II.1.4.1 - A mobile AHA2 and a mysterious FRO2

The proton pump AHA2 inserts in membranes thanks to the presence of ten transmembrane domains (TMD) (Falhof *et al.*, 2016). Membrane fractionation analysis combined with immunodetections revealed that AHA2 is highly present in the PM but is also detected in the secretory pathway including the ER and the Golgi apparatus (DeWitt *et al.*, 1996). Which structural determinants allow AHA2 to reach the PM remain to be identified. However, some domains of other H^+-ATPase were demonstrated to be important for their trafficking such as the nucleotide binding domain from the large loop of the *Nicotiana plumbaginifolia* PMA4 protein that is essential for PM targeting (Lefebvre, 2004). Very few data are available concerning the trafficking and the endocytosis of AHA2 since this protein is often used as a PM marker but is rarely studied per se. However, AHA2 was shown to accumulate in BFA bodies in *Arabidopsis* root cells, suggesting that endocytosed AHA2 can be recycled to the PM (Martiniere *et al.*, 2019). In addition, dim light conditions were reported to result in AHA2 accumulation in unknown cytoplasmic compartments of root cells even though the protein is also observed at the PM (Haruta *et al.*, 2018). However, whether this process reflects endocytic events remains to be determined.

FRO2 is a membrane protein containing eight predicted TMD and a large soluble cytoplasmic domain (Schagerlöf *et al.*, 2006). Although FRO2 is supposed to be present at the PM of root epidermal cells in *Arabidopsis* to reduce Fe^{3+}, this localization was never experimentally proven since attempts to generate FRO2 antibodies were unsuccessful (Connolly *et al.*, 2003) and because no functional fluorescent fusion of FRO2 exists. This problematic hampered the study of FRO2 intracellular dynamics. Interestingly, proteomic analyses identified FRO2 and also AHA2, as being part of the *Arabidopsis* ubiquitinome (Kim *et al.*, 2013; Johnson and Vert, 2016; Walton *et al.*, 2016), nevertheless the significance of the putative ubiquitination of FRO2 and AHA2 remains totally unknown.

II.1.4.2 - A very dynamic IRT1

For several years, our laboratory has been interested in IRT1 protein dynamics in the cell and in its role in the maintenance of metal homeostasis in *Arabidopsis*. Initially, immunolocalizations performed on *Arabidopsis* roots with a specific anti-IRT1 antibody revealed that IRT1 was localized in early endosomes in epidermal cells and rapidly cycled between this compartment and the PM to perform metal absorption (Barberon *et al.*, 2011). IRT1 internalization from the PM requires, at least in part, CME since IRT1 was stabilized at the cell surface when CME is disturbed using dominant negative clathrin hub (Barberon et al 2014). In addition, IRT1 intracellular dynamic is dependent on its multi-monoubiquitination on lysine residues located in the large cytosolic loop of IRT1 (K154 and K179). Indeed an $IRT1_{K154RK179R}$ mutant version that is partially impaired in ubiquitination is no more internalized from the PM (Barberon *et al.*, 2011). Importantly, IRT1 was the first plant PM protein, concomitantly with BOR1, to be demonstrated to undergo ubiquitin-dependent endocytosis. From a biological point of view, transgenic plants expressing mutant versions of IRT1 for the lysine residues are severely affected, due to uncontrolled non-iron metal (Zn, Mn, Co) uptake generating oxidative stress. Thus, limiting the pool of IRT1 at the PM by ubiquitin-dependent endocytosis was proposed as a protective mechanism to limit the absorption of readily available non-iron metals over iron, whose reduction by FRO2 is limiting for iron uptake (Zelazny *et al.*, 2011). IRT1 ubiquitination was proposed to be achieved by the IRT1 Degradation Factor1 (IDF1) E3 ubiquitin ligase since *idf1* loss-of-function mutants showed delayed degradation of IRT1 associated with impaired ubiquitination (Shin *et al.*, 2013).

Interestingly, IRT1 is localized in a polar manner in root epidermal cells and accumulates at the outer PM domain, facing the rhizosphere, as demonstrated by immunolocalization (Barberon *et al.*, 2014) or using a functional translational fusion of IRT1 (IRT1-mCitrine) expressed under the control of *IRT1* promoter in *irt1-1* mutant (Dubeaux *et al.*, 2018). IRT1 polarity is probably established independently of CME and ubiquitin-dependent endocytosis since $IRT1_{K154RK179R}$ or IRT1 expressed in a genetic background impaired in clathrin function still accumulate at the outer PM domain of root epidermal cells (Barberon *et al.*, 2014). However, searching for IRT1-interacting proteins led to the identification of FYVE1/FREE1 as an important actor of the maintenance of IRT1 polarity. FYVE1/FREE1 overexpression leads to an apolar localization of IRT1 in epidermal cells, which was shown to increase plant sensitivity to iron starvation while decreasing the uptake of IRT1 metal substrates (Barberon *et al.*, 2014). These results suggest that the polarization of

IRT1 is critical for proper radial transport of IRT1 metal substrates toward the vasculature. FYVE1/FREE1 associates with the membrane of the MVB and was subsequently demonstrated to directly bind ubiquitin and to be incorporated in subunit I of the ESCRT complex (Gao *et al.*, 2014). The reason why FYVE1/FREE1 overexpression induces an apolar localization of IRT1 to the PM instead of enhancing its targeting to the vacuole remains unclear and will have to be addressed in the future (Zelazny and Vert, 2015). Another important factor involved in IRT1 trafficking is the *Arabidopsis* retromer component Sorting Nexin 1 (SNX1). SNX1 partially co-localizes with IRT1 in endosomes and a *snx1* knock-out mutant displays hypersensitivity to iron deficiency and shows enhanced degradation of IRT1 (Ivanov *et al.*, 2014). Since retromer components are known to be involved in the retrograde transport of cargo proteins (Heucken and Ivanov, 2017), SNX1 likely allows the recycling of internalized IRT1 to prevent its premature degradation .

Although IRT1 subcellular localization is not controlled by the availability of Fe, the primary substrate of IRT1, non-iron metal substrates of IRT1 (Zn, Mn and Co) were shown to control IRT1 endocytosis (Barberon *et al.*, 2011; Barberon *et al.*, 2014). In the presence of physiological concentrations of non-iron metals, the IRT1-mCitrine fusion protein is localized in early endosomes and in the PM of root epidermal cells in a polar manner (Figure 6, -Fe + Metals). However, in the presence of an excess of non-iron metals (Figure 6, -Fe +++ Metals), IRT1-mCitrine is targeted to late endosomes and then to the vacuole for degradation whereas it is exclusively located at the PM in absence of non-iron metals (Dubeaux *et al.*, 2018). The metal-mediated endocytosis of IRT1 was investigated in detail, which allowed to identify different determinants/actors involved in this process. First, the excess of non-iron metals is directly sensed by IRT1 through the binding of these metals to four histidine residues located in the large cytosolic loop of IRT1. Indeed, mutation of these histidine residues into alanines ($IRT1_{4HA}$) abolished the capacity of IRT1 to bind non-iron metals and $IRT1_{4HA}$-mCitrine expressing plants failed to retrieve IRT1 from the PM in root epidermal cells resulting in a hyper-accumulation of non-iron metals, which is deleterious for the plant. Secondly, metal-loaded IRT1 was proposed to recruit the CIPK23 kinase that in turn phosphorylates IRT1. In the *cipk23* loss-of-function mutant, IRT1 is no more endocytosed in response to non-iron metal excess and, consequently, this mutant is hypersensitive to these metals. Thirdly, the CIPK23-dependent phosphorylation of IRT1 enhances the recruitment of IDF1 that induces the K63 poly-ubiquitination of IRT1, promoting IRT1 endocytosis and subsequent degradation. Importantly, IRT1 phosphorylation is not only important for IRT1 ubiquitination, but also constitutes per se a signal required for endosomal sorting and vacuolar degradation of IRT1.

According to these data IRT1 was proposed to be a transceptor displaying transporter and receptor hybrid functions (Dubeaux *et al.*, 2018). From a physiological point of view, the metal-mediated endocytosis and degradation of IRT1 allow to limit the accumulation in *Arabidopsis* of highly reactive non-iron metals under iron-limited conditions.

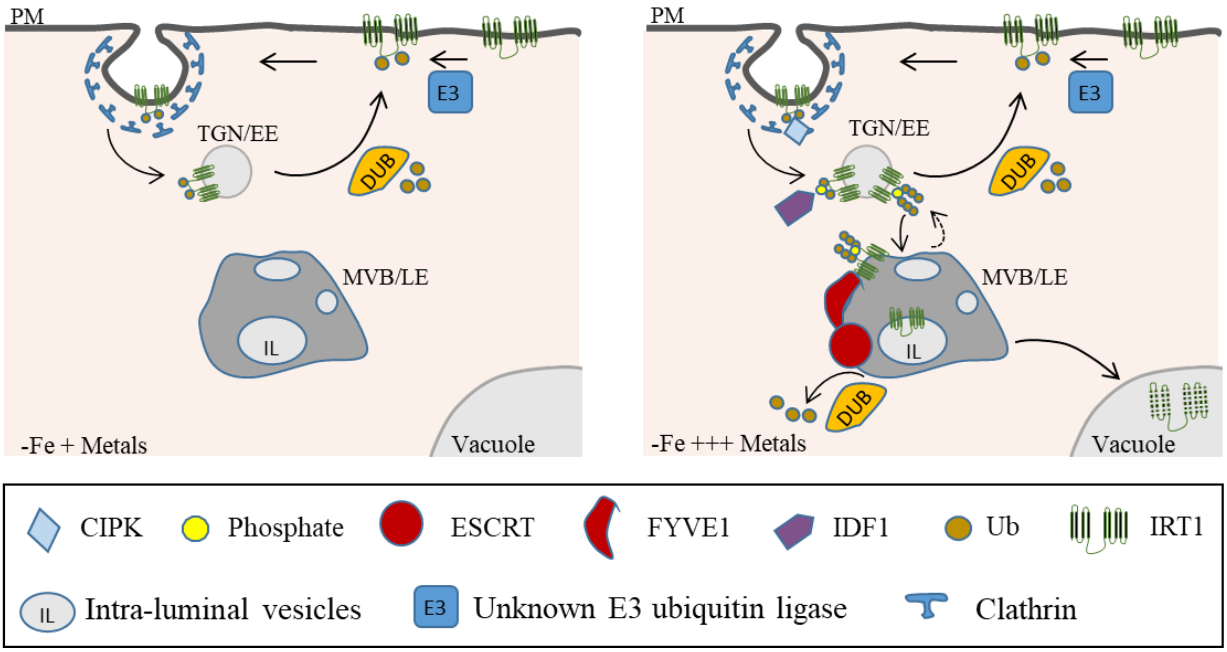

Figure 6. IRT1 is endocytosed and degraded in response to non-iron metal excess. During Fe limitation and in the presence of physiological concentrations of non-iron metals (-Fe + Metals), IRT1 is localized in the PM and in the TGN/EE compartment of root epidermal cells. IRT1 internalization from the PM is achieved through its multi-monoubiquitination by an unknown E3 ligase. From TGN/EE, IRT1 is able to be recycled to the PM, probably through the action of an unknown deubiquitinase (DUB). On the contrary, upon Fe limitation and in the presence of an excess of non-iron metals (-Fe +++ Metals), the elevated level of these metals is directly sensed by IRT1 thanks to direct non-iron metal binding to histidine residues located in the large cytosolic loop of IRT1. Metal-loaded IRT1 is then phosphorylated by CIPK23, triggering two different outcomes: (1) IRT1 phosphorylation enhances the recruitment of the IDF1 E3 Ub ligase that catalyzes the extension of monoUb moieties into K63 polyUb chains on IRT1, (2) phosphorylation also directly impacts the sorting of IRT1. Indeed, the decoration of IRT1 with both phosphate groups and K63 polyUb chains is necessary for IRT1 efficient sorting towards MVB/LE and for vacuolar degradation. The FYVE1 protein that interacts with IRT1 and is a component of the ESCRT complex likely plays a role in this sorting mechanisms in MVB/LE. The endocytosis and degradation of IRT1 under -Fe +++ Metals conditions allows to protect the plant against the toxicity of non-iron metals, by impairing their uptake. Adapted from Dubeaux et al., 2018.

II.2 - Regulation of the activity of the main actors of iron acquisition: good overview for AHA2, not so much for IRT1 and FRO2

II.2.1 - AHA2

As previously mentioned, Fe solubility increases 1000 fold with the decrease of only one pH unit in the rhizosphere. Therefore, AHA2-mediated acidification is of great importance during Fe acquisition, and this process must be tightly regulated. Electron cryo-microscopy analysis of two-dimensional crystals of AHA2 revealed that the protein probably contains three distinct domains of equal size, although probably differently regulated (Jahn *et al.*, 2001). C-terminal parts of AHA proteins are known to specifically possess autoinhibitory domains with the capacity to regulate their enzymatic activity (Palmgren *et al.*, 1991) and phosphorylation seems in general to be a major post-translational modification involved in the regulation of AHA2 activity. Indeed, phosphorylation of Thr-947 generates a binding site for 14-3-3 proteins, which in turn activates AHA2 and other H^+-ATPases (Fuglsang *et al.*, 1999; Yuan *et al.*, 2017). On the other hand, phosphorylation of the Ser-931 in the C-terminal part of AHA2, mediated by the Protein Kinase SOS2-like 5 (PKS5) protein kinase, inhibits AHA2 interaction with 14-3-3 activating proteins (Fuglsang *et al.*, 1999; Fuglsang *et al.*, 2007). Interestingly, PKS5 can also interact with calcium (Ca^{2+}) binding proteins (Fuglsang *et al.*, 2007). As high extracellular pH, together with Fe deficiency (Gratz *et al.*, 2019) can increase Ca^{2+} cytosolic concentrations, it is possible that part of AHA2 regulations depends on Ca^{2+} signalling pathways (Fuglsang *et al.*, 2007). Besides, sucrose, auxin, and small peptides were identified as triggers of AHA2 phosphorylation (Niittylä *et al.*, 2007; Haruta *et al.*, 2014; Barbez *et al.*, 2017). Interestingly, AHA responses to auxin signalling seem to require the mediation of PM receptor-like kinase Feronia (Barbez *et al.*, 2017). Intriguingly, previous phosphoproteome measurements demonstrated that specific interactions between Feronia and the secreted peptide Rapid Alkalinisation Factor (RALF) could mediate the phosphorylation of AHA2 at Ser-899, resulting in the inhibition of H^+ transport activities (Haruta *et al.*, 2014). The same Ser-899 modification occurs during bacterial attack, upon detection of bacterial flagellin by FLS2, accompanied by a concomitant increase in apoplastic alkalization (Nühse *et al.*, 2007).

When activated, different ATPases have been shown to be able to oligomerize, forming dimers, which sometimes is considered as an activation mechanism in itself (Lopez *et al.*, 2000; Sarabipour and Hristova, 2016). In the case of H^+-ATPases, their activation can convert dimers into hexamers (Kanczewska *et al.*, 2005). Indeed the association of the *Nicotiana*

plumbaginifolia PMA2 dimers with 14-3-3 proteins was reported as a trigger for the association of PMA2 proteins into complexes of six phosphorylated units, in hexameric structures which include 14-3-3 proteins (Duby and Boutry, 2009), where 14-3-3 polypeptides could be implicated in hexamer stabilization (Kanczewska *et al.*, 2005).

Concerning the regulation of AHA in relationship with Fe acquisition, a recent work showed that Cytochrome B5 Reductase 1 (CBR1) seemed to be involved in the stimulation of the activity of AHA proteins activity during Fe starvation (Oh *et al.*, 2016). Although the exact mechanism remains unknown, *Arabidopsis* CBR1-overexpressing lines presented higher levels of unsaturated fatty acids than WT plants which was correlated with an increase in AHA activity and rhizosphere acidification. This result suggested that the lipid environment may regulate AHA activity. In accordance with these results, the binding of unsaturated fatty acids to the C-terminal part of AHA was then shown to result in the subsequent activation of these proteins (Han *et al.*, 2017).

II.2.2 - FRO2

FRO2 belongs to the Flavocytochrome b family of metalloreductases. These ferric chelate reductases are evolutionary related to the core flavocytochrome b subunit of a group of human superoxide generating NADPH oxidases (Schagerlöf *et al.*, 2006; Jain *et al.*, 2014). These proteins are able to transfer electrons from cytosolic donors to single electron acceptors situated in the other side of membranes. To this purpose they contain FAD domains, haem groups, and four conserved histidine residues (Robinson *et al.*, 1999). So far, how *Arabidopsis* FRO2 activity is regulated remains totally unknown. In animals few data are available concerning the regulation of Flavocytochrome b proteins. The human flavocytochrome b_{558} contains the subunit gp91phox which is functionally related to FRO2. Interestingly, it has been observed that phosphorylation could be at the base of the control of the activity of gp91phox (Raad *et al.*, 2009). Strikingly, in the context of Fe acquisition, although FRO2 constitutive overexpression improved the plant tolerance to mild Fe deficiency, 35S::FRO2 *Arabidopsis* transgenic lines only presented enhanced ferric reductase activity when subjected to lack of Fe (Connolly *et al.*, 2003), suggesting the existence of a putative post-transcriptional or post-translational regulation of FRO2, although this hypothesis was never verified afterwards.

II.2.3 - IRT1

IRT1 is one of the best characterized ZIP transporters in plants but, despite of this, little is known about the regulation of its activity. However, the selectivity of IRT1 regarding the

transport of its different metal substrates was investigated by specific amino acid substitutions followed by functional complementation tests in different yeast mutants affected in metal transport (Rogers *et al.*, 2000). It appeared that the replacement of the glutamic acid residue at position 103 by alanine increased the substrate specificity of IRT1 by selectively eliminating its ability to transport zinc. In the same way, substitutions of the aspartic acid residues from positions 100 and 136 with alanine abolished iron and manganese transport, which suggested that the transport of these two metals may be mechanistically inseparable. Interestingly, two of the three mutations that are able to change IRT1 specificity are localized in a single extracellular loop located between transmembrane regions II and III (Fig 8A). Extracellular loops of other ZIP proteins were shown to be essential for substrate selectivity and substrate sensing. In the case of the mammalian ZIP4, the external loop between the second and third TMD is required for endocytosis of ZIP4 in response to low micromolar concentrations of Zn (Chun *et al.*, 2019). Furthermore, structural studies made in the large extracellular domain of the human ZIP4 revealed the existence of conserved subdomains that are probably involved in dimerization (Zhang *et al.*, 2016), indicating that such a process could be a way of regulation of other ZIP proteins such as IRT1. Indeed, the human ZIP13 had been previously reported as being able to form homodimers (Bin *et al.*, 2011).

III - Plant membrane microdomains: nature and functions

III.1 - The plasma membrane is a dynamic structure compartmentalized in microdomains

The plasma membrane is composed of a lipid bilayer and proteins and is involved in basic and varied functions for cell survival such as cellular transport, communication with the internal and external media and signalling (Van Meer *et al.*, 2009; Gronnier *et al.*, 2018). To accomplish these functions, the PM must provide cell stability while allowing rapid adaptation to intracellular and extracellular changes. This compromise is accomplished by maintaining the structure of the PM while organizing different sub-regions of different sizes and functions (Van Meer *et al.*, 2009; Gronnier *et al.*, 2018). Intrinsically, the lipidic composition of the membranes can be actively modified, which contributes to increase the rigidity of the membranes, which also hampers the free diffusion of proteins (Grunewald and Friml, 2010; Gronnier *et al.*, 2018; Mamode Cassim *et al.*, 2019). From a structural point of view, phospholipids, sphingolipids and sterols give shape to the PM. Phospholipids are the major components of membranes and, because of their high abundance and amphipathic structure, they serve as the structural matrix

of cellular membranes (Nakamura, 2017). From a molecular point of view, phospholipids contain two hydrophobic fatty acyl groups and a hydrophilic polar head group attached to a glycerol backbone. This structure allows them to spontaneously form bilayers in aqueous environments, where the hydrophilic heads face the aqueous environment at each surface of the bilayer and the hydrophobic tails are shielded from the water in the interior (Alberts *et al.*, 2002). The next category of structural lipids are the sphingolipids. These molecules, in turn, are composed of a backbone made of sphingosine and linked by an amid bound to a fatty acid, forming ceramides, their basic and common structural units (Coskun and Simons, 2011). Three main components define the structure of sphingolipids: a polar head, a fatty acyl chain, and a long-chain amino-alcohol base. According to the nature of these three components, the structure of sphingolipids can be very diverse, giving rise to different classes of sphingolipids in plants. Sterols, in turn, are isoprenoids formed by a cylcopentaperhydrophenantren, with only one hydroxyl group attached to one of its rings. They are mostly non-polar lipids. While animals and yeast incorporate only one kind of sterol, plants are able to produce multiple sterol species. They can be more or less saturated, branched or linear, and the number and position of the double bonds in the cycle differ among the different phytosterols (Furt *et al.*, 2010). Once incorporated into membranes, the hydrophobic core of sterols interacts with the chains of phospholipids and sphingolipids, although the interaction between sphingolipids and sterols are entropically more favourable (Huang and Feigenson, 1999; Ali *et al.*, 2018). In addition to lipids, most of the biological membranes contain also up to 50% of proteins by weight in their composition (Cooper, 2000). Interestingly, lipids and proteins can locally regulate their special distribution in a reciprocal manner, thanks to the establishment of different biophysical and thermodynamic interactions (Quinn, 2010; Corradi *et al.*, 2018). On the one hand, the interaction between proteins and lipids is so tight, such as in the case of protein transmembrane domains, that proteins can modify the behaviour of the surrounding lipids. For example, proteins can decrease the lipidic diffusion rate in the nearby area, which impacts the segregation of membrane components (Macháň and Hof, 2010; Trimble and Grinstein, 2015). On the other hand, lipids present self-assembly properties that can lead to the aggregation of specific sets of proteins (Cacas *et al.*, 2012).

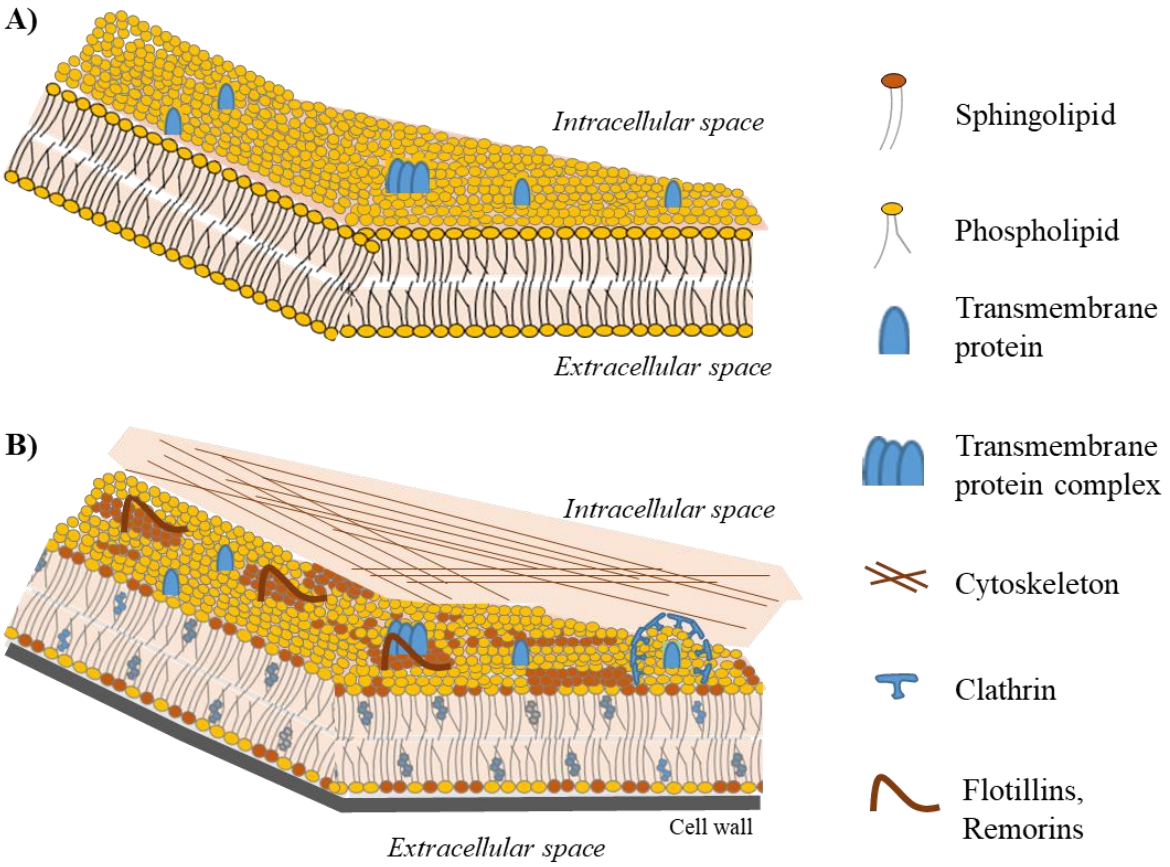

<u>Figure 7.</u> The plasma membrane as a dynamic structure compartmentalized in microdomains.

(A) Representation of the plasma membrane according to the two-dimensional continuum fluid model of Singer and Nicolson (1972). This model presents membranes as lipid bilayers in which proteins are either embedded or attached. The phospholipids of the mosaic structure are predominantly arranged as an interrupted bilayer, arranged so that their polar groups are in contact with the aqueous phase. A small portion of the lipids are more intimately associated with the integral proteins. **(B)** Representation of the plasma membrane as a compartmentalized structure. Here, the lipid bilayer interacts closely with the cell wall and with the cytoskeleton underneath, in a three dimensional model. The biological membranes have the ability to concentrate and cluster different processes in individualized and coexisting microdomains. These domains are enriched in sterols, sphingolipids and specific proteins and can be efficiently regulated.

From the point of view of membrane organization, the presence of unsaturated acyl chains in phospholipids is thought to produce kicks in the hydrocarbon chains, impeding a tight packaging between lipids. Lipids with an opposite nature, presenting long and saturated fatty acid chains, such as sphingolipids (Brown, 1998), can be tightly packed, presenting as a result slow mobility which in biological membranes defines the appearance of liquid order domains (Lo). In these domains, there is a prevalence of sphingolipids and sterols over phospholipids regarding membrane lipid composition. However, according to the degree of lipid condensation and the degree of lateral diffusion, both influenced by external factors such as temperature and pressure, more disorganized states arise. As a result, the biological membranes behave like liquid-like structures in either liquid-ordered (Lo) or liquid-disordered (Ld) phases. Interestingly, both organization levels can coexist in a given biological membrane (García-Sáez and Schwille, 2010; Cacas *et al.*, 2012), which results in the dynamic assembly of specific lipids and proteins into Lo phases or Ld phases. This situation enables the emergence of higher orders of membrane compartmentalization, known as microdomains that corresponds to micro and nanoscale associations of specific lipids and proteins, with a predominant enrichment in sterols and sphingolipids. Taking these considerations into account, nowadays biological membranes are still thermodynamically described as according to the model of Singer and Nicolson (1972) (Figure 7A). This model presents membranes as lipid bilayers in which proteins are either imbibed or attached. However, in opposition to the original model, the membrane is no longer regarded as a lipid bilayer where proteins and lipids freely diffuse in a random manner, but as a highly compartmentalized surface. The biological membranes have the ability to concentrate and cluster different processes in individualized and coexisting spots, which are efficiently regulated spatially and temporally, a process that in plants, involves the participation of the cytoskeleton (as in animal cells) and the cell wall (Figure 7B) (Langhorst *et al.*, 2007; Malinsky *et al.*, 2013; Lv *et al.*, 2017).

III.2 - Dissecting microdomains by biochemical and microscopy approaches

The amphipathic structure of detergents, their capacity to form micelles and their conic shape allow the direct incorporation of detergents into membranes promoting their solubilisation (Cassim *et al.*, 2018). Interestingly, the highly ordered structure of microdomains makes them insoluble to non-ionic detergents, such as Triton X-100, in cold, compared to Ld regions of the PM (Mongrand *et al.*, 2004; Laude and Prior, 2004; Lefebvre *et al.*, 2007). Consequently, these membrane regions tend to remain as detergent resistant membranes

(DRM) also called detergent insoluble membranes (DIMs). As a result, the preparation of DIM followed for instance by lipid composition analysis or proteomic analysis allowing to determine the nature of the associated proteins, is commonly used to study membrane microdomains in plants (Borner *et al.*, 2005; Konrad and Ott, 2015). DIM preparation may generate artificial structures that do not exist as such in living cells (Tanner *et al.*, 2011) and the detection of two different proteins in DIM fractions does not provide evidence that both proteins *co-localize* in intact plasma membranes. Besides, detergent-to-protein ratios have to be taken in consideration since the different plant tissues and membranes may require different ratios for proper DIM extraction, and maladjustments would induce errors in the determination of microdomain composition (Delaunay *et al.*, 2007). For these reasons the existence of microdomains has been often call into question in the past. Therefore, imaging has revealed as a powerful and complementary technique to study microdomains in vivo, permitting to validate the biochemical evidences obtained by DIM preparations.

Although in this thesis "microdomain" is used as a general term, these specific membrane domains can be indeed classified according to their size, as determined by microscopy analysis, in microdomains when they are in the micrometer scale or in nanodomains which size varies from 10 to 100 nm (Jacobson *et al.*, 2007). Due to the different sizes and the spatiotemporal dynamics of the different microdomain structures, the spatial and temporal resolution limits of the microscope often impair the proper characterization of micro and nanodomains. Fortunately, recent advances in light microscopy methods seem to successfully overcome these issues. For example, different microdomains have already been studied by using (TIRFM) (Asanov *et al.*, 2010; Li *et al.*, 2012; Jarsch *et al.*, 2014). About temporal resolution, the utilization of spinning-disk microscopy is also of great use when studying microdomains. In contrast to classical confocal microscopy, the spinning disk manages to illuminate the whole region of observation in a simultaneous way. This characteristic allows to reduce the acquisition time of the image and hence it reduces the phototoxicity, which successfully allows the identification of microdomains and the study of their dynamics (Haney and Long, 2010; Haney *et al.*, 2011). For the moment, different super-resolution techniques emerge and/or start being applied to the plant field, such as Photoactivated Localization Microscopy (PALM), Stochastic Optical Reconstruction Microscopy (STORM), Structured Illumination Microscopy (SIM), and Stimulated Emission Depletion (STED). They are all capable of resolving structures below the diffraction limit of light and today constitute important techniques to further decipher microdomains structure and regulation (Truong-Quang and Lenne, 2014; Wang *et al.*, 2018). As these super-resolution techniques were not applied during my thesis, their characteristics

will not be hereby discussed. The analysis of the protein composition of DIM prepared from different plant species and tissues as well as microscopy approaches allowed to identify specific proteins that appear systematically associated with membrane microdomains and consequently are considered as microdomain markers. These proteins include the remorin family proteins and the superfamily of Stomatin/Prohibitin/Flotillin/HflK/C (SPFH) domain-containing proteins whose characteristics are presented hereafter. Remorins and SPFH domain-containing proteins studied so far are exclusively present, or at least enriched, in PM DIM fractions and they display a punctate distribution at the PM, typical of microdomain associated proteins, when analyzed by microscopy technics (Mongrand *et al.*, 2004; Browman *et al.*, 2007; Jarsch *et al.*, 2014). Their association with sterol compartments can be assessed by the use of sterol depletion drugs, such as methyl-beta-cyclodextrin, and genetic tools, such as *Arabidopsis* mutants impaired in sterol production. Under sterol depletion, these proteins are no longer found in DIMs, but in detergent sensitive membranes (DSMs); and the clustered distribution that they present under the microscope changes to random patterns (Raffaele *et al.*, 2009; Tapken and Murphy, 2015).

Biochemical approaches allowed the identification of multiple proteins with diverse functions including channels, transporters or receptors that, although not being permanent residents of microdomains, can be nonetheless recruited to microdomains during specific cell responses (Dart, 2010; Keinath *et al.*, 2010; Truong-Quang and Lenne, 2014). In plants, for instance, AHA2 was found in DIMs but also in DSMs and possess the ability to interact with specific microdomain-located proteins (Borner *et al.*, 2005; Raffaele *et al.*, 2009; Lv *et al.*, 2017). In other cases, the recent advances in microscopy have been able to determine punctate distribution patters for proteins that had never been observed as microdomain components before. Some of these proteins will be discuss hereafter. Based on the huge diversity of proteins identified by proteomic analysis in DIM it is tempting to speculate that the cellular mechanisms described as being controlled by membrane microdomains are totally underestimated today.

III.3 - Main families of membrane microdomain-associated proteins in plants

III.3.1 – Remorins

Remorins (REMs) are a multigene family that comprises 16 members in the genome of *Arabidopsis thaliana* and constitute, so far, the best-characterized nanodomain markers (Raffaele *et al.*, 2007). REMs are divided into six phylogenetically distinguishable groups

according to their very variable N-terminal regions. Remorins were notably shown to accumulate in the PM lining the plasmodesmata (PD), a membranous channel that ensures a cytoplasmic communication between adjacent cells and is important during development and plant defense reactions (Raffaele *et al.*, 2009; Grison *et al.*, 2015; Sager and Lee, 2014). All remorins possess a REM-C-terminal anchor (CA) corresponding to a lipid-binding motif that confers membrane nanodomain organization (Gronnier *et al.*, 2017). Interestingly, remorins also share the so called "remorin signature", a highly conserved coiled-coil domain in the remorin C-terminal region (Raffaele *et al.*, 2007). This domain seems to be the structural components that allows remorin oligomerization by facilitating remorin assembly into coiled-coil trimers and permitting subsequent trimer-trimer interactions. Such associations seem to enable their further assembly into long filaments and their recruitment to the inner leaflet of the membrane, which eventually could result in the organization of specific nanodomains at the membrane (Bariola *et al.*, 2004; Martinez *et al.*, 2019). Another important feature of remorins is their possibility to be modified by S-acylation. For instance S-acylation of *Medicago truncatula* Symbiotic Remorin 1 (SYMREM1) was demonstrated to be sufficient to anchor the protein in the PM although this post-translational modification is not sufficient to mediate a microdomain sub-localization (Konrad *et al.*, 2014). Furthermore, different works reported the regulation of the localization of REMs by phosphorylation (Benschop *et al.*, 2007; Marín and Ott, 2012). In *Arabidopsis*, AtREM1.2 and AtREM1.3 are phosphorylated in the presence of the resistance to *P. syringae pv. maculicola* 1 protein (RPM1) and triggered in the presence of microbe-associated molecular pattern (MAMPs) (Benschop *et al.*, 2007; Widjaja *et al.*, 2009). Therefore, phosphorylation may activate different signalization cascades upon stimuli recognition e.g. during defense responses. This possibility opens new perspectives related to the regulation of these proteins.

III.3.2 – The superfamily of SPFH domain containing proteins

III.3.2.1 – Generalities

The SPFH domain, also known as prohibitin homology (PHB) domain or Band_7 domain, defines a protein superfamily that regroups proteins with different functions, but evolutionary conserved from prokaryotes to eukaryotes (Rivera-Milla *et al.*, 2006; Bach and Bramkamp, 2013). The importance of SPFH domain-containing proteins is supported by the fact that they emerged independently in different kingdoms (Rivera-Milla *et al.*, 2006). In

animals, the association of these proteins with microdomains is, in multiple cases, sterol dependent and specific lipidations of SPFH domain-containing proteins, e.g. myristoylation and S-acylation, are important for their adhesion to the cytosolic layer of the PM (Konrad and Ott, 2015). According to their localization and their function SPFH domain-containing proteins are regrouped in different sub-families, which in plants comprise: flotillins, stomatins, prohibitins, erlins and the Hypersensitive Induced Reaction proteins (HIRs). Interestingly, contrary to other SPFH domain-containing proteins, HIRs are specific to plants (Daněk *et al.*, 2016). Generally, very little is known about the function of plant SPFH domain-containing proteins whereas animal homologs are better characterized. In the case of erlins, so far these proteins have been poorly characterized in plants, and only one erlin was identified in *Arabidopsis* (At2g03510). Expressed during all developmental stages and in mostly all the tissues, the protein is predicted to localize at the membrane of the ER and possibly other internal membranes such as in the Golgi apparatus (Schmid *et al.*, 2005; Nikolovski *et al.*, 2012; Parsons *et al.*, 2012). In the case of prohibitins and stomatins, these proteins are part of mitochondrial membranes, where they participate in the assembly of protein complexes such as respiratory complex I and the 2-oxoglutarate dehydrogenase (Gehl and Sweetlove, 2014; Piechota *et al.*, 2015). As my PhD project was focused on PM proteins and plant adaptation to environmental conditions, I will focus my description on flotillins and HIRs.

III.3.2.2 – Flotillins

The *Arabidopsis* genome contains 3 different *flotillin* genes: *Flot1* (At5g25250), *Flot2* (At5g25260) and *Flot3* (At5g64870) (Daněk *et al.*, 2016). The whole SPFH domain situated in the N-terminal part of human flotillins was shown to account for the proper localization of these proteins to the PM and endosomal compartments (Langhorst *et al.*, 2008). Furthermore, the S-acylated and myristoylated residues that are present also in the N-terminal part of animal flotillins are essential for the accumulation of these proteins in sterol-enriched membrane fractions (Morrow *et al.*, 2002; Liu *et al.*, 2005). Interestingly, as described in Daněk *et al.* (2016), plant flotillins lack S-acylation or myristoylation predicted sites, but possess putative Cholesterol Recognition/interaction Amino acid Consensus sequences, or CRAC/CARC motifs. As these motifs are involved in protein-sterol interaction and sterol recognition, they may facilitate the recruitment of plant flotillins to PM sterol-enriched microdomains. Besides, sterol depletion seems to decrease *Arabidopsis* Flot1 diffusion coefficients, while in parallel, knocking-down *Flot1* seems to affect sterol internalization, but further scientific evidences are

still needed (Li *et al.*, 2011; Li *et al.*, 2012). Another particularity of flotillins is the presence of coiled-coiled structures in the C-terminal part of these proteins, that facilitate flotillin oligomerization in animals (Solis *et al.*, 2007). Despite of this, flotillin oligomerization is not well understood in plants. As described in Introduction Chapter II.1.2.2.2, flotillins are involved in microdomain-associated endocytosis, and so these particularities will not be further addressed in this section.

Although in *Arabidopsis*, only Flot1 was proposed to be involved in microdomain-associated endocytosis so far, Flot2 and Flot3, the functions of which remain unknown, are probably involved in intracellular trafficking since they interact with proteins involved in endocytosis and vesicular trafficking such as ESCRT proteins, SNAREs, the exocyst and Rab-GTPases (Daněk *et al.*, 2016).

III.3.2.3 – HIR

HIR are SPFH domain-containing proteins that are exclusive to plants (Di *et al.*, 2010). They are also members of the Proliferation, Ion and Death (PID) superfamily, as they were first described as being able to induce, when over-expressed, spontaneous hypersensitive lesions in leaves of *Capsicum annuum*, rice, and wheat (Zhou *et al.*, 2010; Choi *et al.*, 2010; Duan *et al.*, 2013). The genome of *Arabidopsis* contains four different *HIR* genes (denominated as in Qi *et al.*, 2011): *HIR1 (*At1g69840), which is expressed in all plant tissues (Lv *et al.*, 2017), *HIR2 (*At3g01290) whose highest expression levels are registered in leaves and roots (Daněk *et al.*, 2016)., and finally *HIR3* (At5g51570) and *HIR4 (*At5g62740), which are expressed in all organs to a certain extent, and mostly in reproductive tissues and seeds (Daněk *et al.*, 2016). The presence of putative myristoylation and S-acylation sites in HIRs probably facilitates their association with the PM, their main subcellular location, although some HIR proteins have been found in the tonoplast in rice (Zhou *et al.*, 2010), or in endosomes in pepper (Choi *et al.*, 2013). Interestingly, the cytoskeleton, and specially the microtubules, were shown to control the lateral mobility of HIR1 in *Arabidopsis* and facilitating the oligomerization of the protein (Lv *et al.*, 2017). Indeed, *Arabidopsis* HIR proteins were previously shown to form homo and hetero-oligomers (Qi *et al.*, 2011), however the role of HIR oligomerization remains unclear so far. Interestingly, by forming multimeric complexes and binding to sterols, animal SPFH domain-containing proteins were proposed to actively participate in the formation of membrane microdomains (Browman *et al.*, 2007). Whether the formation of HIR complexes may act in a similar manner by recruiting specific lipids and hence allowing the formation of particular membrane microdomains remains to be determined.

III.4 - Biological functions of microdomain-associated proteins in plants

III.4.1 - Defence against pathogens

Different microdomain-associated proteins were shown to play an important role in plant defence against pathogens. Thus, the Solanaceae remorins localized in plasmodesmata were described to impair the movement of the *Potato virus X* (PVX) (Raffaele *et al.,* 2009). Indeed remorins could physically interact with the movement protein Triple Gene Block Protein1 (TGBp1) from PVX and remorin overexpression was demonstrated to impair the cell-to-cell movement of PVX, thus limiting viral spreading in plants. Interestingly, deletions of the REM-CA domain from *Solanum tuberosum* Remorin from Group 1, Homolog 3 (StREM1.3) resulted in the loss of StREM1.3 PM localization, which impaired movement restriction over PVX (Perraki *et al.,* 2012). Furthermore, it was recently observed in *Arabidopsis* that the intrinsically disordered N-terminal domain of REM1.3 can be phosphorylated by a Calcium-dependent Protein Kinase 3 (AtCPK3) in response to virus infection (Perraki *et al.,* 2018). REM1.3 phosphorylation is required for its PM nanodomain localization which is essential to reduce the mobility of the virus by regulating the callose deposition at plasmodesmata. The fact that remorins are important defence lines against virus is strengthened by the occurrence of specific pathogen strategies to counter remorin defence responses. Indeed it was recently uncovered that Rice Stripe Virus (RSV) can interfere with the S-acylation of *Nicotiana benthamiana* REM1, affecting its targeting to PM microdomains. As a result, NbREM1 is subjected to autophagic degradation, which facilitates disease progression (Fu *et al.,* 2018).

HIR proteins also were found of great importance during plant defence against pathogens. A first evidence of the participation of HIRs in immune responses comes from their transcriptional activation upon pathogen attack or in presence of pathogen elicitors such as flg22 and chitin Daněk *et al.* (2016). From a molecular point of view, some HIR proteins are able to interact with Leucine-Reach Repeat proteins (LRR), a protein superfamily that provides pathogen recognition, triggering the immune response. Indeed, Jung and Hwang (2007) and Zhou *et al*. (2009) revealed, using a yeast-two-hybrid assay, an interaction between LRR1 and HIR1 homologs from rice and pepper. Interestingly, the overexpression of a pepper HIR protein (CaHIR1) in *Arabidopsis* increased the resistance to *Pseudomonas syringae* (Jung and Hwang, 2007; Jung *et al.,* 2008). Furthermore, *in planta* interaction studies highlighted that *Arabidopsis* HIR1 and HIR2 can associate with the immune receptor RPS2 (Qi *et al.,* 2011). RPS2 is a nucleotide-binding-LRR subclass protein having the ability to respond to the bacterial effector

AvrRpt2 by activating effector-triggered immunity that culminates in an hypersensitive response (HR) (Day *et al.*, 2005). Importantly several *Arabidopsis hir* knock-out mutants, including *hir2-1*, were shown to display compromised resistance to *Pseudomonas syringae*. On the other hand, over-expression of HIR1 and HIR2 in *Arabidopsis* transgenic line reduced the growth of this bacteria (Qi *et al.*, 2011). Although HIR proteins appear to be important for the RPS2-mediated defence against pathogen, the underlying mechanism remains unknown so far. Interestingly the proteome associated with plant DIM is modified during pathogen infection, suggesting that infection modulates the localization of a pool of proteins in PM microdomains. For instance the plant immune receptor FLS2 was shown to shift from DSM to DIM after flagellin treatment, suggesting that FLS2 might be recruited in membrane microdomains (Keinath *et al.*, 2010). Further ultra-resolution microscopy approaches demonstrated that FLS2 can be found in specific clusters at the PM, co-localizing with remorins in nanodomains (Bücherl *et al.*, 2017) Exposure of *Arabidopsis* culture cells to different microbial elicitors of the immune response is accompanied by kinase activation, consequent Ca^{2+} influx and the activation of the Respiratory Burst Oxidase Homologues (RBOH) NADPH oxidase that drives Reactive Oxygen Species (ROS) bursts in response to pathogens (Sandor *et al.*, 2016). ROS activation indeed, seems a necessary condition that lead to an increase in PM order. These results not only seed light on the importance of a microdomain organization against pathogen attacks, but also highlight how different kinds of microdomain-protein associations related to a single biological function (e.g. pathogen defense) may coexist. This situation increases the levels of complexity of such responses at the same time that it confirms microdomains as important signaling platforms for plant immunity.

III.4.2 - Symbiotic response

Remorins and flotillins were shown to participate in the establishment of symbiosis between nodule plants and nitrogen-fixing bacteria. In *Medicago truncatula*, flotillin-like genes are more abundant than in *Arabidopsis* since a total of seven genes was identified (Haney and Long, 2010). Among these different *flotillin* genes two are especially upregulated during early phases of nodulation: *Flot2* and *Flot4* (Haney and Long, 2010). Flot2 and Flot4 proteins were observed in PM microdomains and, interestingly, upon rhizobial inoculation, Flot4 uniquely accumulates in the tip of elongating root hairs and was proposed to be involved in polar growth of the infection threads. Importantly, the silencing of *Flot* 2, 3 and 4 results in a significant decrease of the nodulation capabilities of *Medicago truncatula*, accompanied by changes in root and nodule morphology. More precisely, the silencing of Flot2 and Flot4 results in a

decrease number of infection threats that permit bacterial entrance into the plant tissues. As previously explained in Introduction Chapter II.1.2.2.2, the *Medicago truncatula* LYK3 protein, a receptor mediating symbiotic bacterial infections at the root surface, is localized in PM microdomains (Haney *et al.*, 2011). Interestingly, upon symbiont inoculation, the dynamics of LYK3 changes since it becomes less mobile and tends to *co-localize* with Flot4 (Haney *et al.*, 2011) (see below). Similarly to *Flot2* and *Flot4*, the transcription of a specific remorin, *MtREM2.2* gene, is actively transcribed during the first phases of the establishment of the bacterial symbiosis (Lefebvre *et al.*, 2010). Indeed, RNA interference of *MtREM2.2* resulted in nodulation disorders similar to those observed when *Flot* are silenced. For this reason, the contribution of remorins to the establishment of the symbiotic process resulted initially quite elusive, as its functions seemeed to slightly overlap with the ones described for flotillins. Nevertheless, MtREM2.2 was shown to interact with LYK3 and it was proposed to act as scaffolding protein (Lefebvre *et al.*, 2010). Recent work has been able to show that the incorporation of LYK3 into nanodomains requires Flot4 and SYMREM1 (Liang *et al.*, 2018). These data provide enough evidence of a collaborative association between remorins and flotillins during the establishment of the symbiosis. In the work presented by Liang *et al.*, (2018), the authors showed that Flot4 forms the initial core structure of the microdomain, but upon symbiotic infection, the subsequent physical interaction of SYMREM1 with LYK3 stabilize the activated receptors in Flot4 specific nanodomains. This allows the progression of the infection thread towards the root cortex (Liang *et al.*, 2018).

Recently, the contribution of PM microdomain-associated proteins in the symbiotic interaction occurring during soybean nodulation was investigated (Qiao and Libault, 2017; Qiao *et al.*, 2017). Transcriptomic analyses brought forward the participation to the symbiotic interaction of three specific genes that were highly expressed in soybean nodules: Glyma.05G029800, Glyma.06G065600, and Glyma.13G065000. All of them code for SPFH domain-containing proteins and two of the closest orthologs of Glyma.13G065000 and Glyma.05G029800 respectively in *Arabidopsis* are the proteins HIR1 and HIR4 (Qiao and Libault, 2017). Although how HIR proteins may participate in symbiosis remains unknown, such data highlighted possible new roles of HIR proteins to be addressed in the future.

III.4.3 - Hormonal signalling

The study of the role of membrane microdomains in hormone response is just emerging and notably concern the regulation of the brassinosteroid signalling. Brassinosteroids are plant hormones known to regulate very different developmental and physiological responses,

including cell elongation and root growth (Saini *et al.*, 2015). As described in Introduction Chapter II.1.2.2.2, although the brassinosteroid receptor BRI1 is mainly internalized by CME (Jaillais and Vert, 2016), the work of Wang *et al.* (2015) brought forward the contribution of microdomains in BRI1 internalization. These results are very interesting and advance promising discoveries in the field of study of the brassinosteroid responses, however further research is needed to establish the biological importance of this BRI1 internalization pathway. Apart microdomain-associated endocytosis, the localization of BRI1 in defined PM microdomains is probably important for the specificity of the brassinosteroid signalling. Indeed, the spatial separation of BRI1 and the immune receptor FLS2 in distinct PM microdomains was proposed to allow these proteins to achieve different biological processes, while employing common downstream signalling components (Bücherl *et al.*, 2017).

On the contrary, the contribution of microdomains in the regulation of the drought stress responses mediated by the phytohormone abscisic acid (ABA) is better understood from a molecular point of view. In this context, ABA perception *via* the ABA receptor RCAR1/PYL9 [regulatory components of ABA receptor 1/PYR1 (pyrabactin resistance 1)-like protein 9] initiates a cascade that results in the phosphorylation and consequent activation of the anion channel SLAH3 situated in the PM of guard cells, a process mediated by the specific calcium dependent kinase CPK21 (Geiger *et al.*, 2012). Ultimately, the activation of SLAH3 contributes to chloride and nitrate release from guard cells, which in turn initiates stomatal closure. Interestingly, CPK21 is found in DIM from *Arabidopsis thaliana* mesophyll cells; and different signalling components of the draught response are, at least transitionally, associated with AtREM1.3-labelled nanodomains. In parallel, the expression of SLAH3 and CPK21 in previously infiltrated *Nicotiana benthamiana* leaves, demonstrated that the proportion of SLAH3 in DIM fractions increases when CPK21 is co-expressed, which indicates a microdomain preferential localization of activated forms of SLAH3 over inactivated forms of this transporter (Demir *et al*., 2013). Consequently, the authors suggest that the phytohormone ABA affects SLAH3 function by controlling the membrane localization of the anion channel and its activating kinase. Still, the molecular changes that allow microdomain recruitment of these specific proteins remins to be uncovered, as well as the possible contribution of remorins to the process of recruitment and/or the activation of CPK21 and SLAH3.

IV – Context and objectives of the thesis

IRT1 is responsible for iron uptake in *Arabidopsis thaliana*. Hence, our understanding of this transporter is the cornerstone of the study of plant iron acquisition, which is an important process for the introduction of Fe into terrestrial food chains. Although IRT1 regulation has been studied for years, only a handful of proteins are nowadays known to participate in the regulation of this transporter, as detailed in the introduction. With the aim of discovering new proteins involved in IRT1 dynamics/activity or working in concert with IRT1, our laboratory performed co-immunopurification of IRT1 combined with mass spectrometry analyses to identify IRT1 interactors. Different putative IRT1-interacting proteins related to either trafficking process or Fe nutrition were isolated. From these candidates, the ferric reductase FRO2 and the proton pump AHA2 appeared as particularly interesting regarding the process of Fe acquisition. Indeed, both are already known to act in concert with IRT1 in the acidification-reduction-transport strategy for iron uptake in *Arabidopsis thaliana*. Besides, a third candidate, the SPFH-domain containing protein HIR2, called our attention. The putative interaction between IRT1 and HIR2 suggested a possible contribution of membrane microdomains in the control of IRT1, which had never been uncovered before.

Therefore, during my thesis, I aimed to: a) Characterize the association of IRT1 with FRO2 and AHA2 in the process of Fe acquisition and explore the possibility that these proteins form an "iron acquisition complex", allowing the optimization of iron uptake in *Arabidopsis*. b) Uncover the role of HIR2 and membrane microdomains in the process of Fe acquisition, by characterizing HIR2 contribution in the intracellular dynamics of IRT1.

Our interest in discovering the role of HIR2-containing microdomains in Fe acquisition, led us to establish a collaboration with the laboratory of Jan Martinec, from the Institute of Experimental Botany, in Prague. One of their work research axes focuses on the characterization of flotillins and HIR proteins in plants. In a candidate approach, we tried to uncover a possible involvement of flotillins in IRT1 endocytosis and more generally in the process of Fe nutrition. A large part of this work is still in process and will be discussed separately.

Chapter II

Results

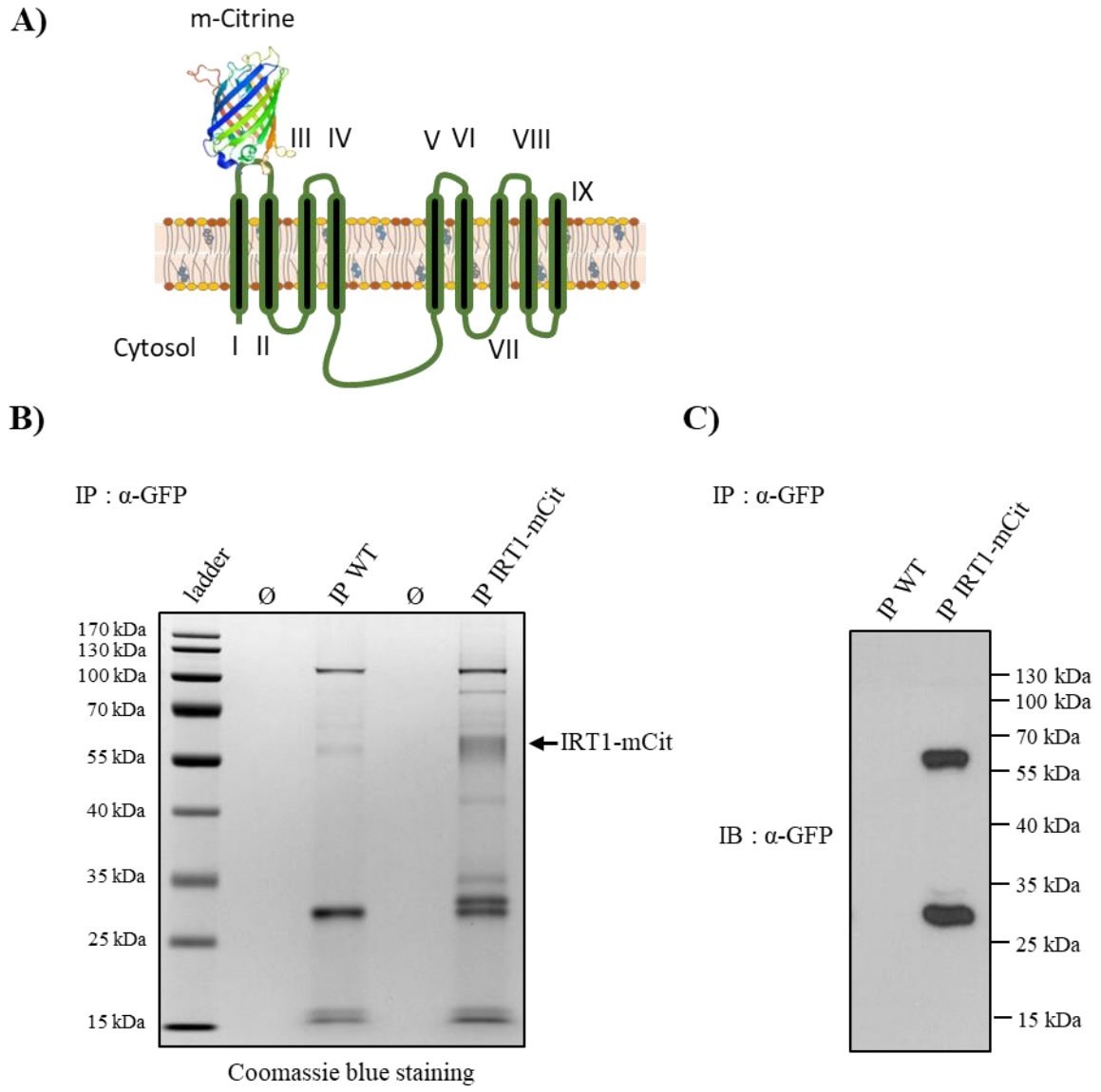

<u>Figure 8.</u> Immunopurification of IRT1-mCitrine and the associated proteins.

(A) Schematic representation of the functional IRT1-mCitrine fusion protein. I to IX refer to the different transmembrane regions of IRT1 from the N-terminal to the C-terminal part. The mCitrine was introduced in the first extra-cytosolic loop (Dubeaux *et al.,* 2018). **(B)** Immunopurifications (IP) of IRT1-mCitrine were performed with anti-GFP antibodies coupled to magnetic microbeads on solubilized protein extract from wild type (WT) and *irt1-1*/IRT1 ::IRT1-mCitrine plant roots. Immunopurified proteins were then stained with coomassie blue. **(C)** Immunoblotting (IB) with anti-GFP antibodies was performed on a part of WT and IRT1-mCitrine immunopurified fractions as prepared in (B). The upper band corresponds to IRT1-mCitrine full length (63 kDa) whereas the lower band corresponds to a cleavage product of IRT1-mCitrine.

Results

I - IRT1 interactome in *Arabidopsis* root epidermal cells

Although this IRT1 interactome was established before the beginning of my thesis, I believe it is very interesting to comment it, moreover I am first author in a manuscript which includes these data. To identify proteins interacting with IRT1 in root epidermal cells, IRT1-mCitrine fusion protein expressed under the control of *IRT1* promoter in *irt1-1* mutant was immunopurified and proteins co-purified with IRT1 were identified by mass spectrometry. IRT1-mCitrine protein, in which the mCitrine fluorescent tag, derived from the GFP, was introduced in the first extracellular loop of IRT1 between transmembrane domains I and II (Figure 8A), is functional since it complements *irt1-1* growth defects and chlorosis (Dubeaux *et al.*, 2018). Briefly, IRT1-mCitrine transmembrane protein was solubilized from root extracts with a soft non-ionic detergent n-Dodecyl β-D-maltoside (DDM) to preserve the interactions between IRT1 and its partners. Then, IRT1-mCitrine and the associated proteins were immunopurified with anti-GFP antibodies coupled to magnetic microbeads. The same procedure was performed on DDM-solubilized proteins from wild type plant (WT) roots as a negative control. Immunoprecipitated proteins from IRT1-mCitrine and WT plants were separated by SDS-PAGE (Figures 8B and 8C) and analyzed by mass spectrometry. Proteins were considered as IRT1 interactors when they were specifically identified in IRT1-mCitrine immunopurified fraction with at least two different peptides. This approach allowed the identification of 142 putative IRT1 interactors (supplemental Table 1). Among them 31 were found in the two independent experiments that were performed and 111 were found in one experiment or the other. Concerning the molecular functions of IRT1 interactors, Gene Ontology annotation (http://www.pantherdb.org/) reveals that the majority of assigned accessions correspond to catalytic activity (50%) followed by binding and transport activities (20% and 11%, respectively) (supplemental Figure 2 A). In terms of biological process, 34% and 33% of IRT1-interacting proteins are associated with cellular and metabolic process respectively, 9% are linked to localization or response to stimulus (supplemental Figure 2 B). Since the control of IRT1 trafficking is of the utmost importance in the regulation of this transporter we specifically looked for IRT1-interactingproteins that are linked to the secretory or endocytic pathways (supplemental Table 2). Clathrin was found as putatively interacting with IRT1, which is in accordance with previous results showing that IRT1 can undergo

Table 1. Compilation and brief description of the main proteins found in mass spectrometry analyses as putative IRT1 interactors related to this project. This selection includes candidates known to work together with IRT1 in the process of Fe uptake, and candidates belonging to the SPFH superfamily, whose participation in Fe nutrition has never been uncovered. Number of total peptides refers to the total number of peptides that were found in each one of the two independent mass spectrometry analyses that were carried out.

			N° of unique peptides			
Accession	**Protein name**	**Protein size (kDa)**	**Experiment 1**	**Experiment 2**	**Number of transmembrane domains**	**Subcellular localization**
AT4G30190	H(+)-ATPase 2	104	5	13	10	plasma membrane
AT3G01290	Hypersensitive induced reaction 2	31	5	12	0	plasma membrane
AT1G01580	Ferric reduction oxidase 2	82		3	11	plasma membrane
AT5G62740	Hypersensitive induced reaction 4	31		2	0	plasma membrane
AT2G03510	SPFH/Band 7/PHB domain-containing membrane-associated protein family	41	3	8	1	endoplasmic reticulum

The number of transmembrane domains present in each protein was obtained thanks to the datebase AramTMCon (http://aramemnon.uni-koeln.de). The subcellular localization of each protein was investigated in SUBACon (http://suba.plantenergy.uwa.edu.au).

clathrin-mediated endocytosis (Barberon *et al.*, 2011; Barberon *et al.*, 2014). Interestingly SEC13a and SEC31b proteins were identified as IRT1-putative interactors suggesting a role of coat protein complex II (COPII) machinery in the export of IRT1 from the endoplasmic reticulum (ER) to the Golgi apparatus. Reversely, IRT1 probably also undergoes retrograde transport from the Golgi to the ER since it interacts with components of COPI vesicles (Supplemental Tables 1 and 2).

Another very interesting group of IRT1 interactors are proteins linked to the *Arabidopsis* metal homeostasis such as iron transporters from the VIT family (Yamada et al., 2013) or the Pleiotropic drug resistance 8 / Penetration 3 protein that was proposed to act as a cadmium extrusion pump (D.,-Y., Kim *et al.*, 2007) (Supplemental Tables 1 and 2). Recently, coumarins, that are excreted in the rhizosphere, were shown to be important for iron acquisition in an IRT1-dependent manner as detailed in the introduction of this thesis. Interestingly, Feruloyl-Coenzyme A 6'-Hydroxylase 1 (F6'H1) (Schmid et al., 2014) and Cytochrome P450/CYP82C4 (Rajniak *et al.*, 2018), both involved in coumarin biosynthesis, were identified as a putative IRT1-interacting protein (Supplemental Tables 1 and 2). As mentioned in the section "Context and objectives of the thesis", FRO2 and AHA2, which act in concert with IRT1 in the acidification-reduction-transport strategy for iron uptake, were identified as part of IRT1 interactome (Table 1). During my PhD, I characterized the interaction between IRT1 and these two major actors of iron acquisition. Among the putative interactors of IRT1, we identified several proteins with SPFH domains (Table 1), notably HIR2 and HIR4, and also a SPFH-domain containing protein of unknown function (AT2G03510). From these three proteins, HIR2 seemed to be the most suited candidate to focus our analyses. On the one hand, HIR2 is known to be present at the plasma membrane, as mentioned in the Introduction, which makes this protein a good candidate to interact with IRT1. On the other hand, the protein appeared highly represented in both mass spectrometry analyses performed, unlike HIR4. *At2g03510* gene was identified as a marker in a quantitative trait locus (QTL) analysis for zinc hyper-accumulation in *Arabidopsis halleri.* Moreover, this gene shows significant high levels of expression in roots of this Zn accumulator species (Filatov *et al.*, 2006; Filatov *et al*., 2007). Despite of this, the corresponding protein is annotated as being the only erlin described to date in *Arabidopsis.* Therefore, this protein is expected to localize in the endoplasmic reticulum and is thus less likely involved in a direct way in the process of Fe uptake *per se*. At present, the number of IRT1 interactors controlling the subcellular localization of this transporter is very succinct and a possible participation of membrane microdomain-located proteins in the control of IRT1 and metal nutrition has never been addressed. Thus, we decided to further characterize

the interaction between HIR2 and IRT1 and the contribution of HIR2 to the process of Fe uptake.

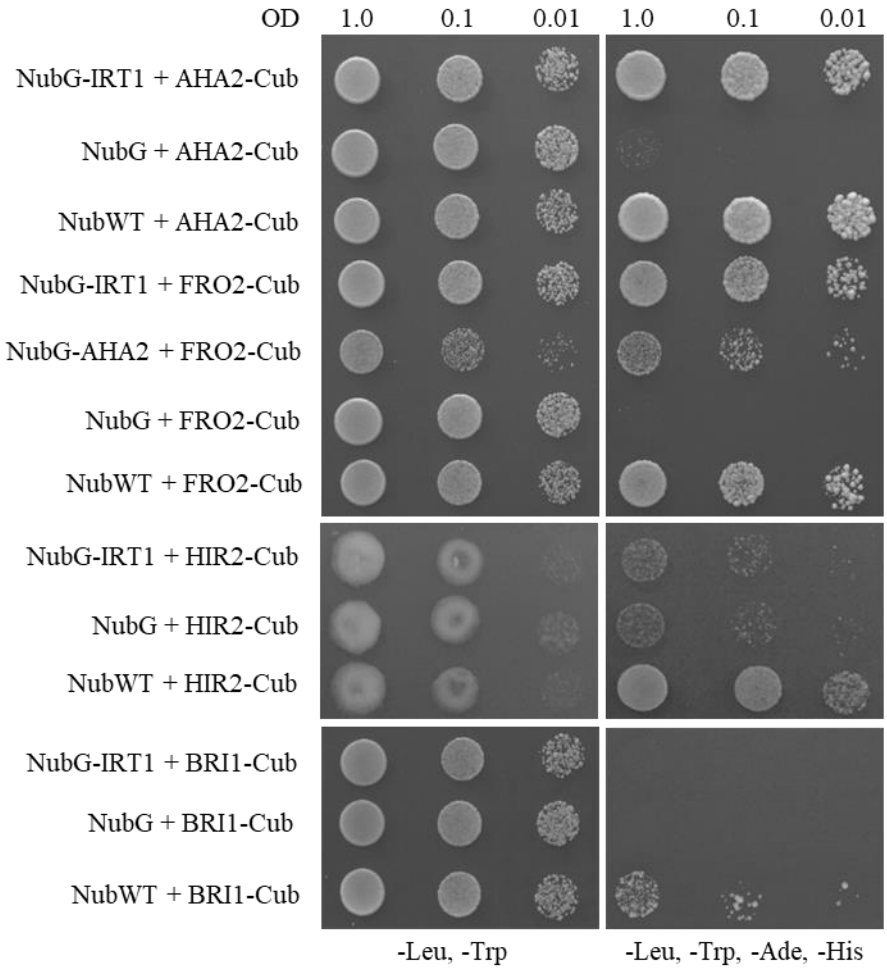

<u>Figure 9.</u> IRT1 interacts with FRO2 and AHA2 in a split-ubiquitin assay.
Yeasts co-expressing Cub fusion proteins with NubG fusion proteins or NubG (negative control of interaction) or NubWT (positive control of interaction) were spotted in serial dilutions on a synthetic medium without Leu and Trp (control medium) or without Leu, Trp, His, Ade (selective medium). Yeast growth on control and selective medium was recorded after 24h and 48h, respectively. Besides internal negative interaction tests performed by co-expressing Cub fusion proteins with NubG, an additional negative control was introduced in this assay by co-expressing NubG-IRT1 and BRI1-Cub. OD: optical density. The interaction test was performed in triplicates, a representative example is hereby shown.

II - Study of the interactions between IRT1 and FRO2/AHA2/HIR2

II.1 – FRO2 and AHA2 directly interact with IRT1 in a split-ubiquitin assay

To verify the interaction between IRT1 and AHA2/FRO2/HIR2, we first took advantage of the split-ubiquitin system that allows to detect direct interactions between membrane proteins in yeast and was successfully used in the past to investigate protein interactions with IRT1 (Shin *et al.*, 2013b; Dubeaux *et al.*, 2018). IRT1 fused to the mutated N-terminal half of ubiquitin (NubG) that is unable to spontaneously reassemble with the C-terminal part of ubiquitin (Cub), was co-expressed in yeast with AHA2, FRO2 or HIR2 fused to Cub linked to the chimeric transcription factor ProteinA-LexA-VP16 (PLV) (Figure 9). On a non-selective medium (-Leu -Trp), all the transformed yeasts grew normally showing that the expression of the different fusion proteins does not induce toxicity (Figure 9, left panels). Physical interactions between IRT1 and AHA2/FRO2 were then tested through the ability to rescue yeast growth on a selective medium (-Leu -Trp -Ade -His) (Figure 9, right panels). Yeasts co-expressing NubG-IRT1 with AHA2-Cub or FRO2-Cub grew on a selective medium, similarly to the respective positive controls NubWT + AHA2-Cub/FRO2-Cub, whereas no growth was observed for the respective negative controls NubG + AHA2-Cub/FRO2-Cub. This result indicates that IRT1 directly interacts with AHA2 and FRO2. As an additional negative control for split-ubiquitin, NubG-IRT1 was co-expressed with a transmembrane protein that is probably not linked to IRT1, the brassinosteroid receptor BRI1, fused to Cub. Whereas yeast co-expressing NubWT with BRI1-Cub (positive control of interaction) grew on a selective medium, no growth was observed when BRI1 and IRT1 were co-expressed, indicating that these two proteins do not interact. Interestingly, our split-ubiquitin assay also revealed that the two IRT1 interactants AHA2 and FRO2, expressed as NubG and Cub fusions, respectively, could physically interact (Figure 9). Unfortunately, the split-ubiquitin assay did not allow us to reveal a direct interaction between IRT1 and HIR2 (Figure 9). Indeed, yeasts co-expressing NubG-IRT1 and HIR2-Cub grew as the negative control (NubG + HIR2-Cub), in which a slight autoactivation took place. This result may imply that the interaction between IRT1 and HIR2 could be indirect.

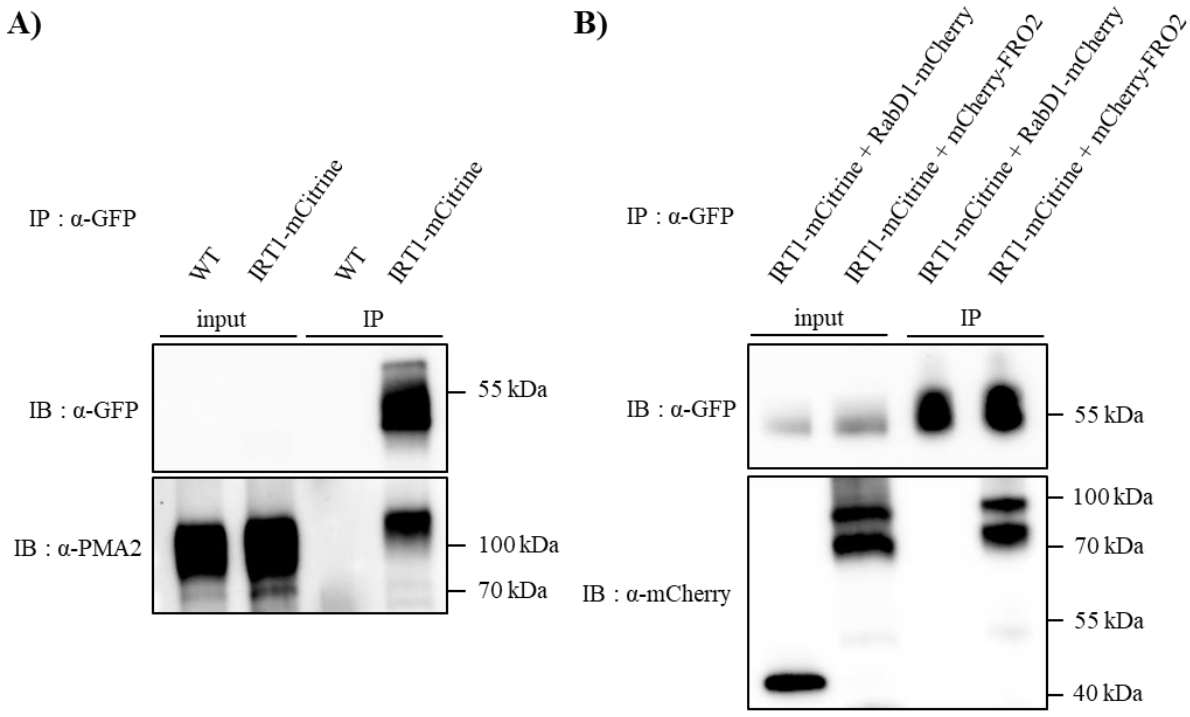

Figure 10. FRO2 and AHA2 are part of an IRT1-protein complex in *Arabidopsis* root cells as revealed by co-immuopurifications.

(A) Endogenous AHA2 is likely co-immunopurified with IRT1-mCitrine. Immunoprecipitations (IP) were performed using anti-GFP antibodies on solubilized root protein extracts from *irt1-1*/IRT1::IRT1-mCitrine and wild-type plants (negative control). Inputs and IP fractions were subjected to immunoblotting (IB) with anti-GFP (top) and anti-PMA2 antibodies (bottom). **(B)** mCherry-FRO2 is co-immunopurified with IRT1-mCitrine. IP were performed using anti-GFP antibodies on solubilized root protein extracts from *irt1-1*/IRT1::IRT1-mCitrine plants co-expressing FRO2::mCherry-FRO2 or UBQ10::RabD1-mCherry, this protein co-localizing with IRT1 in endosomes (negative control). Inputs and IP fractions were subjected to IB with anti-GFP (top) and anti- mCherry antibodies (bottom). Note that mCherry-FRO2 migrates at the expected size (bottom band) but also at a higher molecular weight (top band) that may correspond to post-translationally modified mCherry-FRO2. In (A) and (B), plants were firstly grown on MS/2 medium containing 50 µM Fe-EDTA and then transferred on a -Fe + Metals medium supplemented with 300 µM of the iron chelator Ferrozine. The interaction test was performed in triplicates, a representative example is hereby shown. Expected protein sizes: AHA2: 108 kDa, mCherryFRO2: 110 kDa, IRT1-mCitrine: 64 kDa, RabD1-mCherry: 51 kDa.

II.2 - FRO2, AHA2 and HIR2 associate with IRT1, as revealed by co-immunopurifications in *Arabidopsis* roots

After having investigated interactions between IRT1 and AHA2/FRO2/HIR2 in a heterologous system, we then decided to confirm our previous observations in *Arabidopsis* roots by performing co-immunopurifications (co-IP) combined with immunodetections. To analyze the interaction between IRT1-mCitrine and endogenous AHA2, we used a previously described antibody raised against Plasma Membrane H^+-ATPase 2 (PMA2) from *Nicotiana plumbaginifolia* that also recognizes *Arabidopsis* AHA proteins. An immunoblot performed with the anti-PMA2 antibody on a protein extract from yeast transformed with a vector allowing the expression of AHA2, showed a strong signal around 100 kDa. This specific band is not observed for the negative control, showing that the anti-PMA2 antibody effectively recognizes *Arabidopsis* AHA2 isoform (Figure 15B). For the interaction test, IRT1-mCitrine expressed under the control of *IRT1* promoter in the roots of the corresponding transgenic line was first immunopurified (Figure 10A). As a negative control, the same purification procedure was performed on roots from wild type plants (WT). Then, the immunopurified fractions were probed with the anti-PMA2 antibodies. A strong signal around 100 kDa was detected for the IRT1-mCitrine immunopurified fraction whereas no signal was observed for the negative control (Figure 10A). Although this signal could correspond to other AHA isoforms than AHA2, due to a lack of specificity of the anti-PMA2 antibodies and since it is difficult to discriminate between the close molecular weights of AHA proteins, this result suggests that endogenous AHA2 likely associates with IRT1 in root epidermal cells. The existence of an IRT1-AHA2 complex is strengthened by the split-ubiquitin test described previously and will be discussed hereafter.

Since no antibody raised against FRO2 was available, we decided to generate for the first time a functional translational fusion of FRO2 expressed under the control of *FRO2* promoter in the previously described *fro2* mutant named *frd1-1* (Robinson *et al.*, 1999). To do so, the mCherry fluorescent protein was fused to the C-terminal end or the N-terminal part of FRO2, generating FRO2-mCherry and mCherry-FRO2 fusions, respectively. While being properly expressed in plants, FRO2-mCherry is not functional since it does not allow to restore the dwarfism and the hyper chlorotic phenotype of *frd1-1* under iron deficiency (data not shown). However, the expression of mCherry-FRO2 fully restored the developmental defects and the chlorosis of *frd1-1* mutant in lack of iron, showing that mCherry-FRO2 fusion protein is functional (Figure 11B and 11C). Interestingly, mCherry-FRO2 accumulates specifically in the

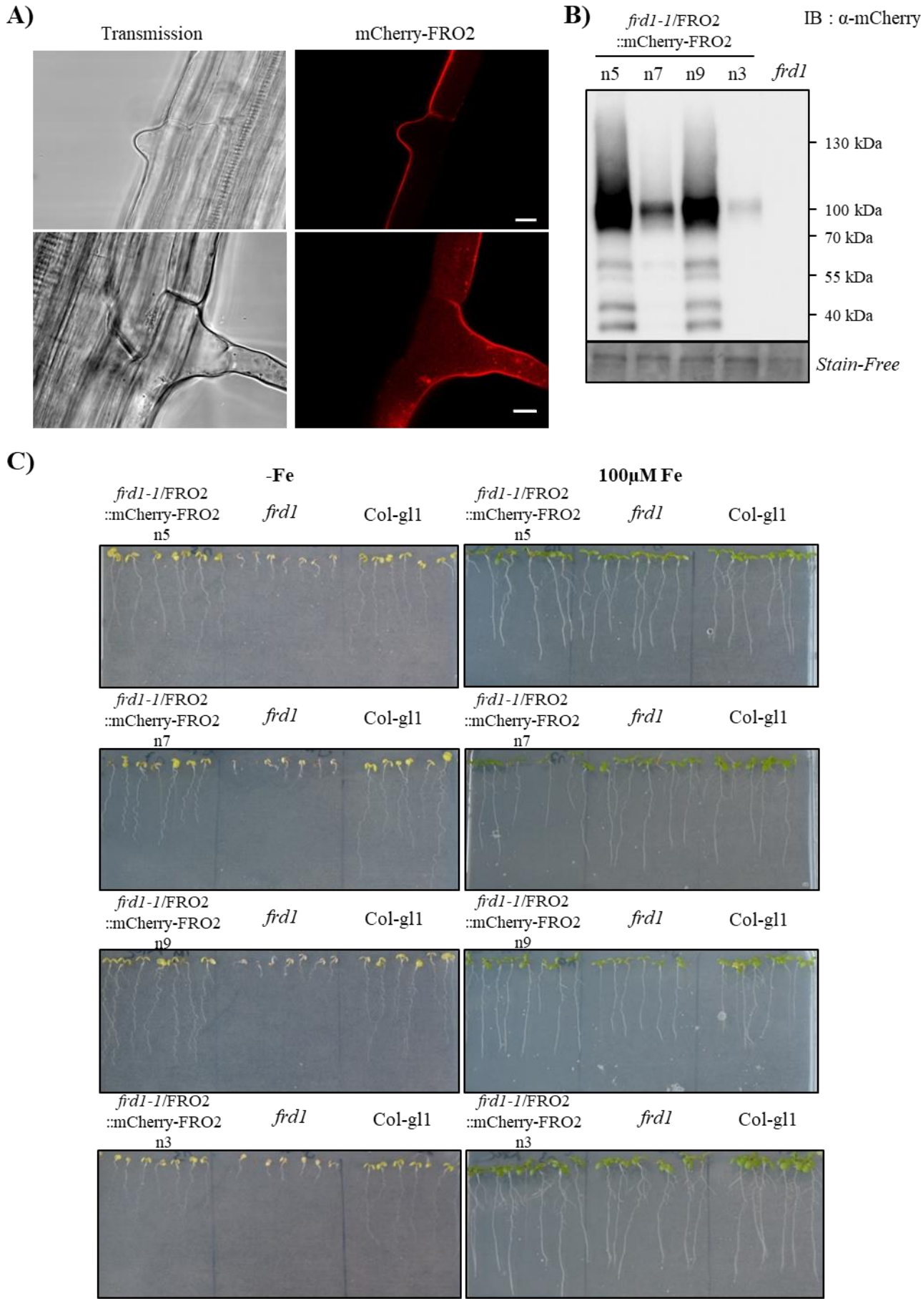
A)
Transmission
mCherry-FRO2
B)
frd1-1/FRO2
::mCherry-FRO2
IB : α-mCherry
n5
n7
n9
n3
frd1
130 kDa
100 kDa
70 kDa
55 kDa
40 kDa
Stain-Free
C)
-Fe
100µM Fe
frd1-1/FRO2
::mCherry-FRO2
n5
frd1
Col-gl1
frd1-1/FRO2
::mCherry-FRO2
n7
frd1
Col-gl1
frd1-1/FRO2
::mCherry-FRO2
n9
frd1
Col-gl1
frd1-1/FRO2
::mCherry-FRO2
n3
frd1
Col-gl1

Figure 11. Expression of mCherry-FRO2 complements the *frd1-1* mutant phenotype in lack of iron.

(A) Confocal microscopy analysis of mCherry-FRO2 localization in the differentiated part of a root from *frd1-1*/FRO2::mCherry-FRO2 plant (line n9) grown in absence of iron and in presence of physiological levels of non-iron metals. Note that mCherry-FRO2 is specifically expressed in root epidermal cells where it localizes at the PM in a polar fashion facing the medium, as well as in intracellular compartments. Scale bars = 10 µm. **(B)** Expression of mCherry-FRO2 protein in *frd1-1*/FRO2::mCherry-FRO2 transgenic lines n3, n5, n7 and n9 grown as in (A) was revealed by performing an anti-mCherry immunoblot on root microsomal protein extracts. *frd1-1* mutant was used as a negative control. Stain-Free Imaging Technology was used to make a loading control. **(C)** Complementation test of *frd1-1* mutant. Wild type plants (Columbia gl1), *frd1-1* mutant and four independent *frd1-1*/FRO2::mCherry-FRO2 transgenic lines (n3, n5, n7 and n9) were grown 11 days on MS/2 medium in absence of iron (-Fe) or in presence of 100µM Fe-EDTA (+Fe). In both cases media contained physiological levels of non-iron metals. PM= Plasma Membrane.

epidermis of the root, where it distributes at the PM and in some internal vesicles (Figure 11A). To analyze the interaction between FRO2 and IRT1 in *Arabidopsis* roots by co-IP, transgenic lines co-expressing mCherry-FRO2 and IRT1-mCitrine under the control of their respective endogenous promoters were generated. The laboratory had also previously generated a transgenic line co-expressing IRT1-mCitrine and RabD1-mCherry, this latter co-localizing with IRT1 in endosomes, that was used for a negative control (Supplementary Figure 2). Our results showed that mCherry-FRO2 was efficiently co-immunopurified with IRT1-mCitrine whereas RAbD1-mCherry was not, proving that FRO2 and IRT1 form a protein complex in root epidermal cells (Figure 10B). To go further, we investigated the interaction between mCherry-FRO2 and endogenous AHA2 in *Arabidopsis* roots. For this purpose, mCherry-FRO2 expressed under the control of *FRO2* promoter was immunopurified from root protein extracts of the corresponding transgenic line and in parallel the purification procedure was performed on roots from WT plants (negative control). An immunoblot performed with anti-PMA2 antibodies on immunopurified fractions revealed that AHA2 is likely co-immunopurified with mCherry-FRO2, whereas no signal was detected for the negative control (Figure 12). Although the same considerations about the specificity of the antibody used to detect AHA2 should be kept in mind, this result reinforces the notion of a FRO2-AHA2 interaction that was also detected by split-ubiquitin (Figure 9). These combined analyses provide evidences that IRT1, FRO2 and AHA2 can interact with each other in *Arabidopsis* root epidermal cells, probably in a direct manner, which led us to propose that IRT1, AHA2 and FRO2 could constitute an iron acquisition complex.

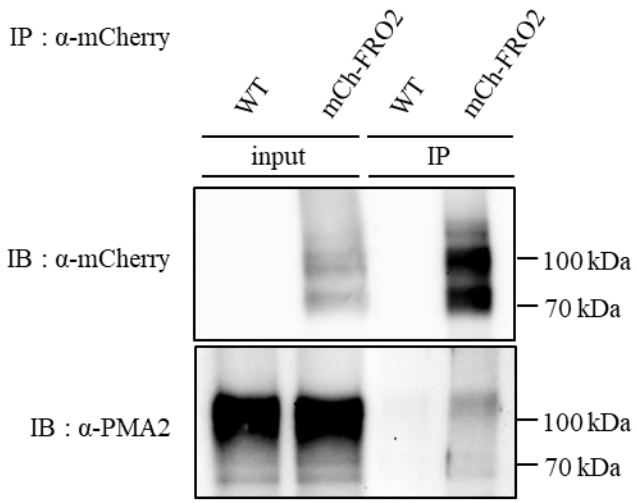

Figure 12. FRO2 and AHA2 likely interact in *Arabidopsis* root cells.
Immunoprecipitation (IP) was performed using anti-mCherry antibodies on solubilized root protein extracts from *frd1-1*/FRO2::mCherry-FRO2 and wild-type plants (negative control) first grown on MS/2 medium containing 50 µM Fe-EDTA and then transferred on a -Fe + Metals medium supplemented with 300 µM of the iron chelator Ferrozine. Inputs and IP fractions were subjected to immunoblotting (IB) with anti-mCherry (top) and anti-PMA2 antibodies (bottom). The interaction test was performed in triplicates, a representative example is hereby shown. Expected protein sizes: AHA2: 108 kDa, mCherryFRO2: 110 kDa.

The interaction between IRT1 and HIR2 was also investigated in *Arabidopsis* roots by performing co-IP combined with immunodetections (Figure 13). IRT1-mCitrine expressed under the control of *IRT1* promoter was immunopurified from root protein extracts and the same purification protocol was performed on WT plant roots (negative control). Immunopurified fractions were then probed with an anti-HIR antibody (see Material and Methods) (Qi *et al.*, 2011). A signal at the expected molecular weight of HIR proteins was detected for IRT1-mCitrine immunopurified fraction whereas no signal was observed for the negative control (Figure 13A). Thus, some endogenous HIR proteins are able to form a complex with IRT1. To specifically investigate the interaction between IRT1 and HIR2 isoform, co-immunopurifications were performed on protein extracts from roots of *Arabidopsis* transgenic lines co-expressing IRT1-mCitrine and HIR2-mCherry or RabD1-mCherry (negative control) (Figure 13B). It is important to mention that HIR2-mCherry fusion protein is functional as detailed hereafter (Figure 23). Our results showed that HIR2-mCherry was co-purified with I RT1-mCitrine whereas RAbD1-mCherry was not, proving that HIR2 and IRT1 can associate among a protein complex in root cells.

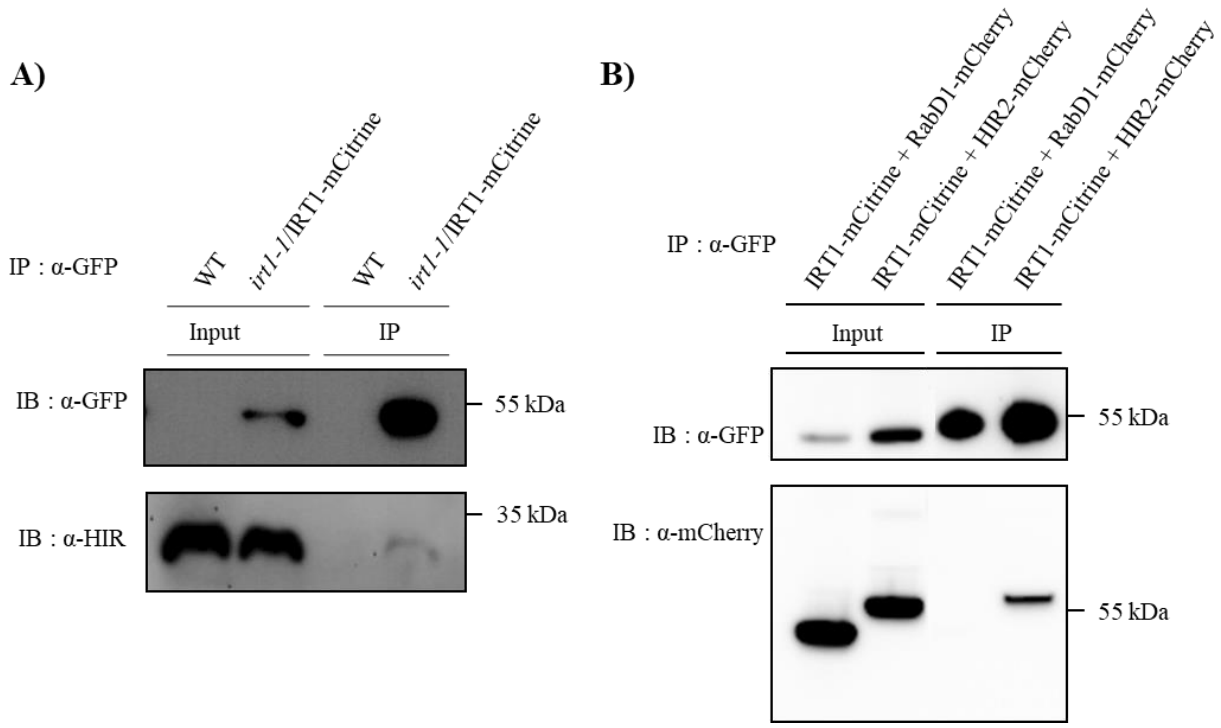

Figure 13. HIR2 is able to interact with IRT1 in *Arabidopsis* root cells as revealed by co-immuopurifications.

(A) Endogenous HIR proteins are co-immunopurified with IRT1-mCitrine. Immunoprecipitations (IP) were performed using anti-GFP antibodies on solubilized root protein extracts from *irt1-1*/IRT1::IRT1-mCitrine and wild-type plants (negative control). Inputs and IP fractions were subjected to immunoblotting (IB) with anti-GFP (top) and anti-endogenous HIR antibodies (bottom). **(B)** HIR2-mCherry is co-immunopurified with IRT1-mCitrine. IP were performed using anti-GFP antibodies on solubilized root protein extracts from *irt1-1*/IRT1::IRT1-mCitrine plants co-expressing 35S::HIR2-mCherry or UBQ10::RabD1-mCherry, the later co-localizing with IRT1 in endosomes (negative control). Inputs and IP fractions were subjected to IB with anti-GFP (top) and anti-mCherry antibodies (bottom). In (A) and (B), plants were firstly grown on MS/2 medium containing 50 µM Fe-EDTA and then transferred on a -Fe + Metals medium supplemented with 300 µM of the iron chelator Ferrozine. The interaction test was performed in triplicates, a representative example is hereby shown. Expected protein sizes: HIR2: 31 kDa, HIR2-mCherry: 60 kDa, IRT1-mCitrine: 64 kDa, RabD1-mCherry: 51 kDa.

II.3 – Does a direct interaction between HIR2 and AHA2 allow the recruitment of IRT1 in HIR2-containing membrane microdomains?

Although we were unable to reveal a direct interaction between HIR2 and IRT1, we investigated whether the two other members of the putative iron acquisition complex, FRO2 and AHA2, could directly interact with HIR2 in a split-ubiquitin assay (Figure 14). Yeast co-

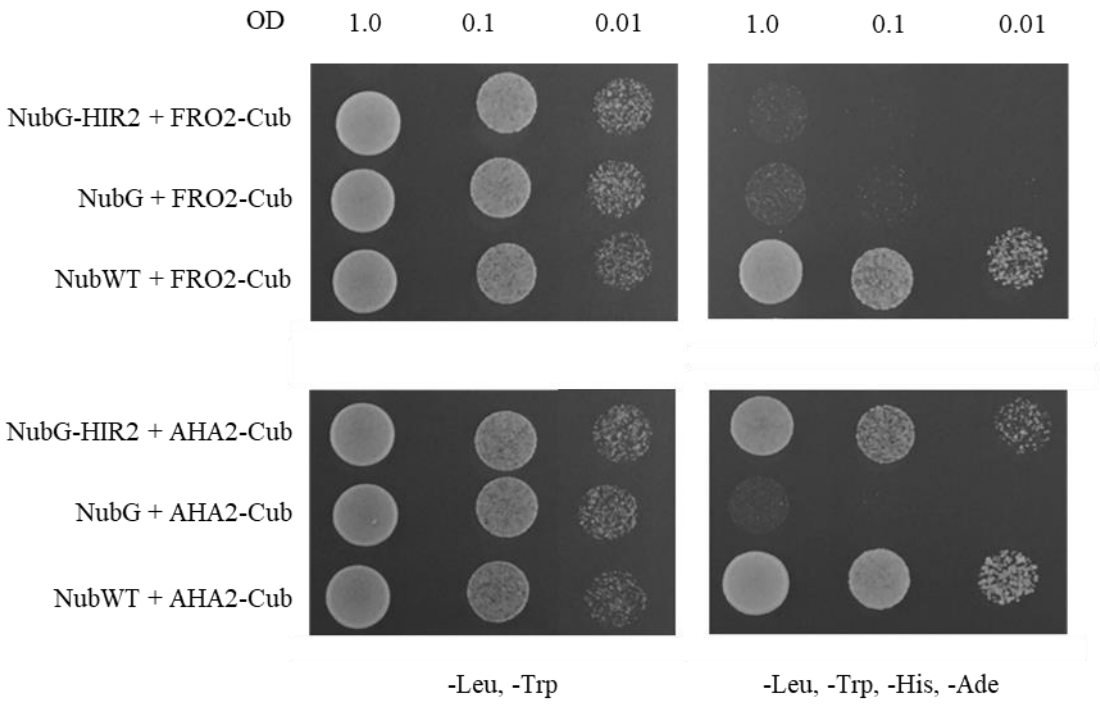

Figure 14. HIR2 interacts with AHA2 but not with FRO2 in a split-ubiquitin assay.
Yeasts co-expressing Cub fusion proteins with NubG fusion proteins or NubG (negative control of interaction) or NubWT (positive control of interaction) were spotted in serial dilutions on a synthetic medium without Leu and Trp (control medium) or without Leu, Trp, His, Ade (selective medium). Yeast growth on control and selective medium was recorded after 24h and 48h, respectively. OD: optical density. The interaction test was performed in triplicates, a representative example is hereby shown.

expressing NubG-HIR2 with FRO2-Cub did not grow on a selective medium, similarly to the negative control NubG + FRO2-Cub, whereas yeast growth was recorded for the positive control NubWT + FRO2-Cub. This implies that FRO2 and HIR2 do not interact in this test. In plant cells, we cannot exclude that FRO2 may interact in a non-direct manner with HIR2, but further experiments will be required to investigate this possibility. Interestingly, in the split-ubiquitin assay, yeast co-expressing NubG-HIR2 and AHA2-Cub were able to grow on a selective medium as observed for the positive control NubWT + AHA2-Cub, whereas no growth was observed for the negative control (Figure 14). This result shows that HIR2 and AHA2 are able to directly interact in this system.

As AHA2 is able to directly interact with both IRT1 and HIR2 we wondered whether AHA2 could create a "link" between IRT1 and HIR2 facilitating their interaction. To test this hypothesis, we performed a split-ubiquitin bridge (SUB) assay which allows the detection of

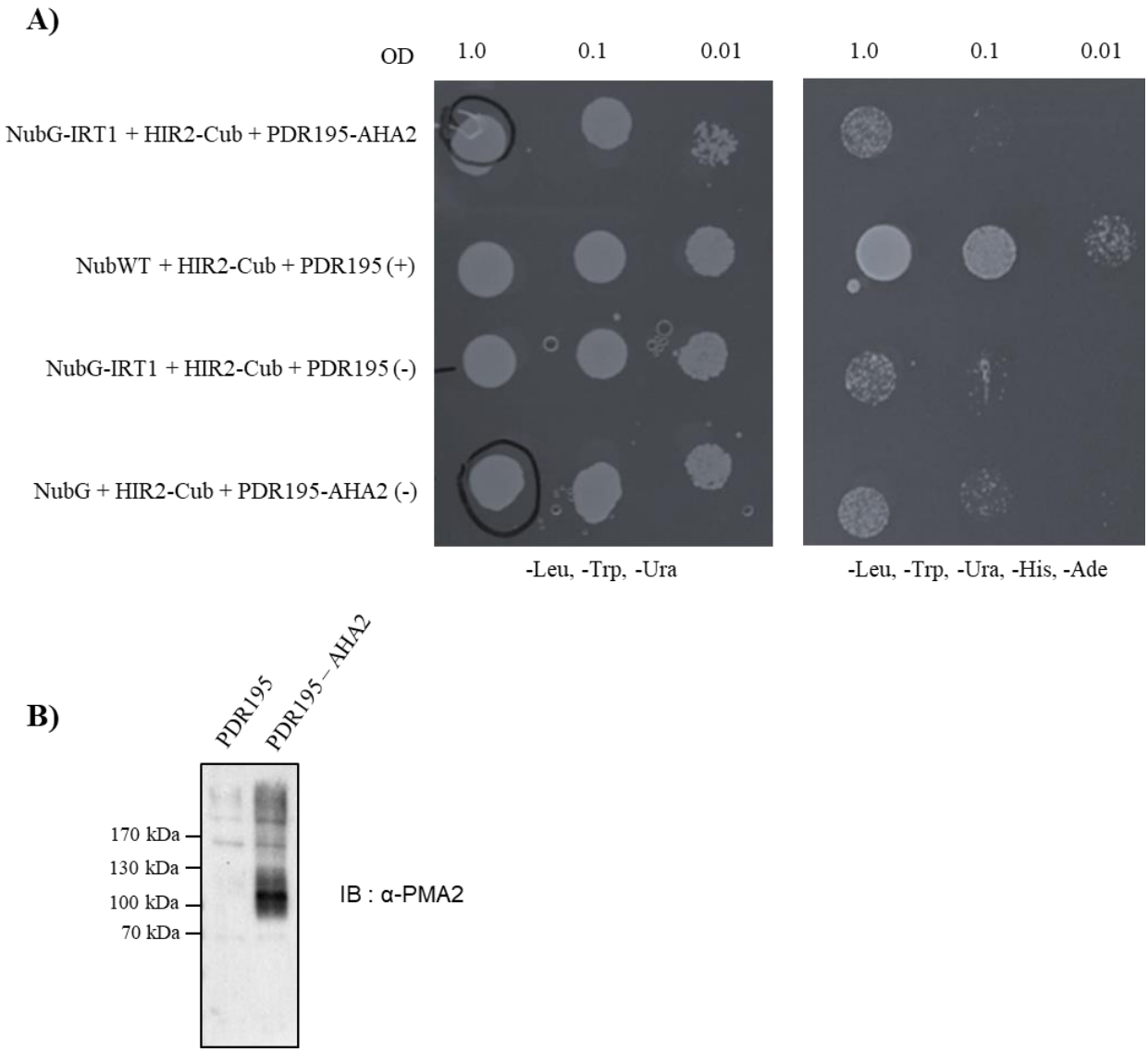

<u>Figure 15.</u> AHA2 does not mediate the interaction link between HIR2 and IRT1 in a split-ubiquitin-bridge assay.

(A) To perform the split ubiquitin-bridge assay, yeast was co-transformed with HIR2-Cub construct, NubG-IRT1 constructions and PDR195-AHA2 vector that allows the expression of a non-tagged version of AHA2. As a positive control (+), yeast was co-transformed with the following constructs: HIR2-Cub, NubWT and the empty PDR195 vector. As negative controls (-), yeasts were co-transformed with the following constructions: HIR2-Cub, NubG-IRT1 and the empty PDR195 vector or HIR2-Cub, NubG and PDR195-AHA2. Yeast were spotted in serial dilutions on a synthetic medium without Leu, Trp and Ura (control medium) or without Leu, Trp, Ura, His and Ade (selective medium). Yeast growth on control and selective medium was recorded after 24h and 48h, respectively. **(B)** Anti-PMA2 immunoblot performed on a protein extract from yeast co-transformed with HIR2-Cub, NubG-IRT1 and PDR195-AHA2 constructs revealed a strong specific signal at around 100 kDa, showing that AHA2 is indeed expressed (PDR195-AHA2 line). A protein extract from yeast co-transformed with HIR2-Cub, NubG-IRT1 and the empty PDR195 vector was used as negative control ("PDR195" line).

trimeric protein interactions based on the split-ubiquitin technique (Grefen, 2014). To perform this test, we co-expressed HIR2-Cub with NubG-IRT1 and a non-tagged version of AHA2 from a PDR195-AHA2 construct (Figure 15A). If AHA2 is able to bring in close proximity HIR2 and IRT1, it may lead to the reconstitution of the full ubiquitin molecule, permitting yeast growth on a minimal media. Yeast co-expressing HIR2-Cub + NubG-IRT1 + AHA2 weakly grew on the selective medium similarly to the two negative controls we performed, whereas for the positive control (HIR2-Cub + NubWT + the PDR195 empty vector) a clear growth was observed (Figure 15A). We decided to verify that the absence of interaction between HIR2 and IRT1 was not due to a lack of expression of AHA2. To do so, an immunoblot with the anti-PMA2 antibodies previously described was performed on total protein extract from yeast, previously co-transformed with HIR2-Cub + NubG-IRT1 + PDR195-AHA2. This immunoblot revealed that AHA2 was indeed strongly accumulated (Figure 15B). According to these results, AHA2 may not be the "element" that allows the interaction between IRT1 and HIR2. However, we cannot exclude that the huge size/molecular weight of AHA2 (~108 kDa) may sterically hamper the association of the two halves of ubiquitin carried by HIR2 and IRT1, even if AHA2 could indeed help HIR2 and IRT1 to interact in the same complex. Other experiments will be needed to determine whether AHA2 may be the protein required to "link" HIR2 and IRT1, as commented in the Discussion of this thesis.

III – Dynamics of the iron acquisition platform

III.1 - FRO2 and AHA2 are ubiquitinated in *Arabidopsis* root cells in a metal independent manner

Upon an excess of non-iron metal substrates IRT1 ubiquitination increases considerably, leading to the endocytosis and the degradation of IRT1 in the vacuole (Dubeaux *et al.*, 2018). Interestingly, proteomic analyses allowed the identification of AHA2 and FRO2 as part of the *Arabidopsis* ubiquitinome (Kim *et al.*, 2013; Johnson and Vert, 2016; Walton *et al.*, 2016). Since AHA2 and FRO2 belong to an IRT1-containing protein complex, we wondered whether ubiquitination of these proteins could be co-regulated by the availability of non-iron metals. The analysis of protein ubiquitination profile is usually performed by immunopurifying the protein of interest followed by immunodetection of the ubiquitinated forms of the protein. During this approach it is useful to work with a tagged version of the query protein to optimize its immunopurification. We already mentioned that the mCherry-FRO2 protein is functional, then we aimed at creating a functional fusion of AHA2 by fusing its C-terminus to a fluorescent

protein, the GFP or the mCherry. We decided to create C-terminal tagged AHA2 proteins because several studies reported C-terminal fusions of AHA or PMA proteins as being functional, in plants as in yeast (Lefebvre, 2004; Sutter *et al.*, 2007; Martiniere *et al.*, 2012; Fajardo-Somera *et al.*, 2013). However, we wanted to verify that our AHA2-GFP/mCherry fusions proteins were effectively functional as described below.

III.1.1 – Probing the functionality of AHA2 fusion proteins by acidification assays

To investigate the functionality of our AHA2 C-terminal tagged proteins, the acidification capacities of transgenic lines expressing AHA2-GFP under the control of the *35S* promoter were compared to those of WT plants (Col-0). Note that a *35S::AHA2-GFP* T3 homozygous line was obtained in the laboratory before I started my PhD. An anti-GFP immunoblot performed root microsomal fractions revealed that AHA2-GFP is properly expressed this line (Figure 16A). Moreover, microscopy analysis on this transgenic line showed that AHA2-GFP is mainly localized at the PM in root cells (Figure 16B). A way of testing the acidification capacity of plants, notably root-induced acidification, consists in the introduction inside the growth medium of bromocresol purple that displays a purple color at basic pH and turns yellow upon acidification. This technique was successfully used by Santi and Schmidt (2009) to identify which AHA proteins were responsible for the rhizosphere acidification during the Fe acquisition process. Bromocresol purple assays was also successfully used when testing the acidification capabilities of different *Arabidopsis* mutants affected in Fe uptake (Long *et al.*, 2010; Oh *et al.*, 2016). As mentioned in the introduction lack of Fe induces AHA2-mediated acidification. AHA2-GFP expression being controlled by a constitutive promoter, we reasoned that if the construction was functional, high proton extrusion in Col-0/ 35S::AHA2-GFP plants should be independent of Fe conditions, unlike for wild type plants and the knock-out-mutant for *AHA2* (*aha2)*. For this reason, these different plant lines were first grown for 10 days in Fe 50 µM and transferred afterwards to 50 µM Fe + bromocresol media at a slightly basic pH (6.5). In parallel, we subjected the same lines to lack of Fe conditions during the bromocresol treatments (MS/2 media pH (6.5) + bromocresol purple). We expected that in lack of Fe the acidification activity of Col-0 plants would increase, resembling the acidification phenotype of the AHA2 overexpressor, and unlike *aha2* plants.

Surprisingly, differences among genotypes resulted scarce and variable (Figure 16C), and the *aha2* mutant was not impaired in acidification capabilities. Interestingly, acidification was clearly reduced when the plants were not submitted to Fe deficiency, as any real change in

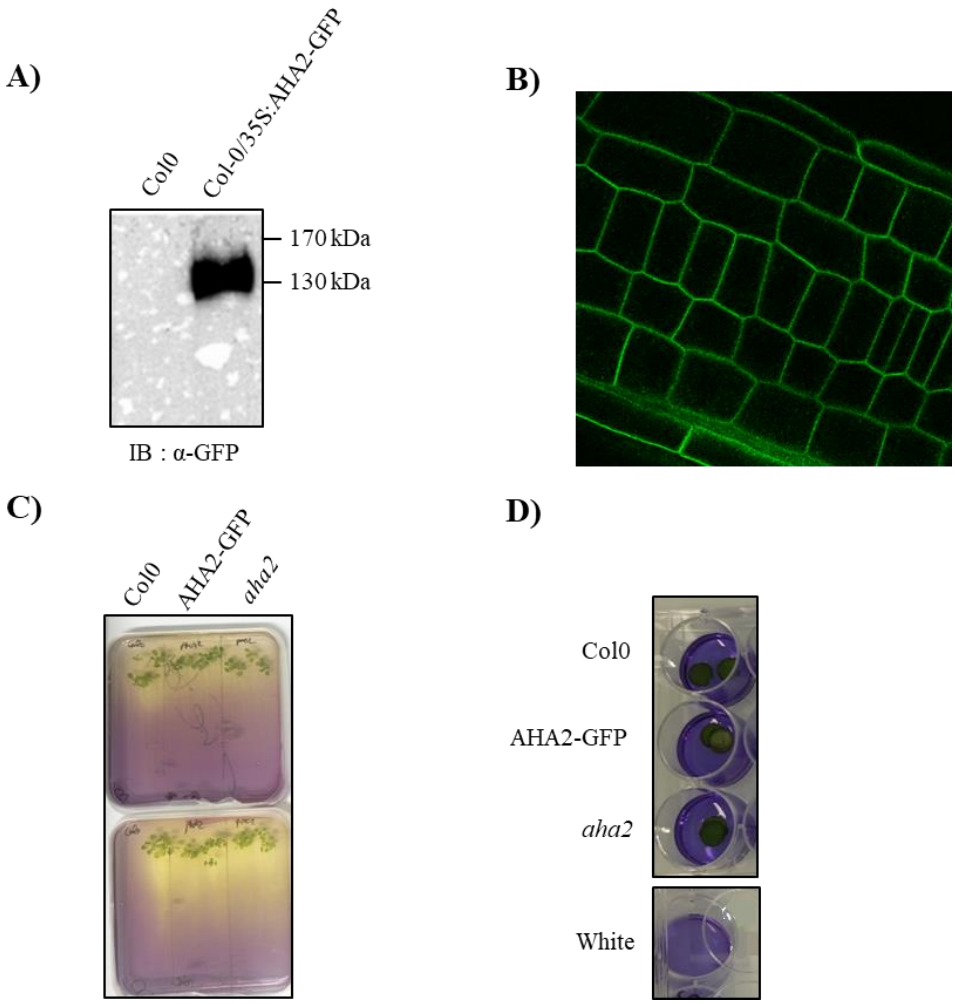

<u>Figure 16.</u> Study of the functionality of AHA2 C-terminal tagged proteins by performing acidification tests.

(A) Anti-GFP immunoblot performed on a protein microsomal fraction from roots of a Col-0/35S::AHA2-GFP T3 homozygous line revealed AHA2-GFP protein accumulation. A protein microsomal fraction from roots of a Col-0 was used as a negative control. **(B)** Confocal microscopy analysis of AHA2-GFP localization in the same transgenic line as in (A). Plants were grown for 11 days in -Fe + Metal condition before observation. Scale bar = 10 µm. **(C)** A representative acidification assay showing the rhizosphere acidification (yellow color) induced by the roots of different plants: Col-0 (1), Col-0/35S::AHA2-GFP (2) and *aha2* knock-out mutant (3). Plants were grown 7 days in the presence of 50 µM Fe and then transferred 4 days to a –Fe MS/2 medium (pH6.5) containing 0.005% bromocresol purple before observation. Pictures of two different Petri dishes corresponding to repetitions of the same acidification test show the heterogeneity inside an experiment as well as the absence of difference in term of acidification between the roots of the different tested genotypes. **(D)** A representative liquid acidification assay performed on *Nicotiana benthamiana* leaf disks expressing different fusion proteins. 1, 2 and 3 refer to the different constructions used for tobacco infiltrations: (1) 35S::AHA2Δ66-GFP, (2) 35S::AHA2Δ66-mCherry, (3) 35S::GFP. An extra well containing the reactive, but no leaf disk served as a blank. Leaf disks were subjected to a 5 hours incubation in liquid MS/2 (pH 7.6) supplemented with 0.005% bromocresol purple. Afterward, acidification of the medium was recorded by measuring OD at 590 nm.

agar coloration took place (result not shown). Given the small reproducibility of the acidification phenotype in between plates, observed within the same experiment, we concluded that bromocresol assays onto agar plates was not enough sensitive to reveal acidification phenotypes in our case. Moreover, the overexpression of AHA2-GFP was not sufficient to increase root-mediated acidification. Even if AHA2-GFP is expressed in a constitutive manner under the control of the strong *35S* promoter, the fact that AHA protein activity is tightly regulated (see Introduction Chapter II.2.1) made us hypothesize that our gain of function strategy in term of acidification might be unsuccessful. Therefore, we decided to test the incidence of the fusion of a tag in the C-terminal part of a constitutive active AHA2 protein lacking the 66 last amino acids and named AHA2Δ66. This type of AHA2 truncated versions that are hyperactive were described by (Regenberg *et al.*, 1995). At the moment, we are generating *Arabidopsis* transgenic lines carrying the *35S::AHA2Δ66-GFP/mCherry* cassettes. In the meantime, we tried to transiently express these constructions in *Nicotiana benthamiana* plants. As a negative control, plants were infiltrated with a *35S::GFP* construct, as the expression of a cytosolic GFP should not induce acidification. Two days after transfection, after verifying protein expression by microscopy, leaf disks were cut and incubated in liquid MS/2 medium supplemented with 0.005 % bromocresol purple and subjected to agitation (Figure 16D). After 4 h, 6 h, 12 h and 24 h, liquid media was recovered. To measure the acidification of the medium by leaf disks, net proton flux was quantified by reading the optical density of the media at 590 nm, which is the wavelength of absorption of the unprotonated form of the bromocresol purple dye, as described for roots by Santi and Schmidt (2009). Despite of our efforts, we were not able to measure differences in term of acidification between leaf disks expressing AHA2Δ66 fusion proteins and the negative control (GFP) (result not shown). Apart this liquid colorimetric assay, we also attempted to directly measure medium acidification by removing the leaves and directly measuring the pH of the MS/2 media with a pH meter, no bromocresol was added in this case. In this case we were not able either to detect pH differences between leaves transformed with the control construction or with the different AHA2 constructions. Due to the lack of successful results, we decided to await to get *Arabidopsis* T3 homozygous lines carrying the *35S::AHA2Δ66-mCherry* and *35S::AHA2Δ66-GFP* constructions in order to perform acidification experiments.

Although we did not yet establish that AHA2-GFP/mCherry proteins efficiently transport protons, we decided to continue our analysis using these fusion proteins since, as mentioned above, this type of fusions were successfully used in the past. In addition, AHA2-GFP seems to be correctly folded since it was properly targeted to the PM and was not observed

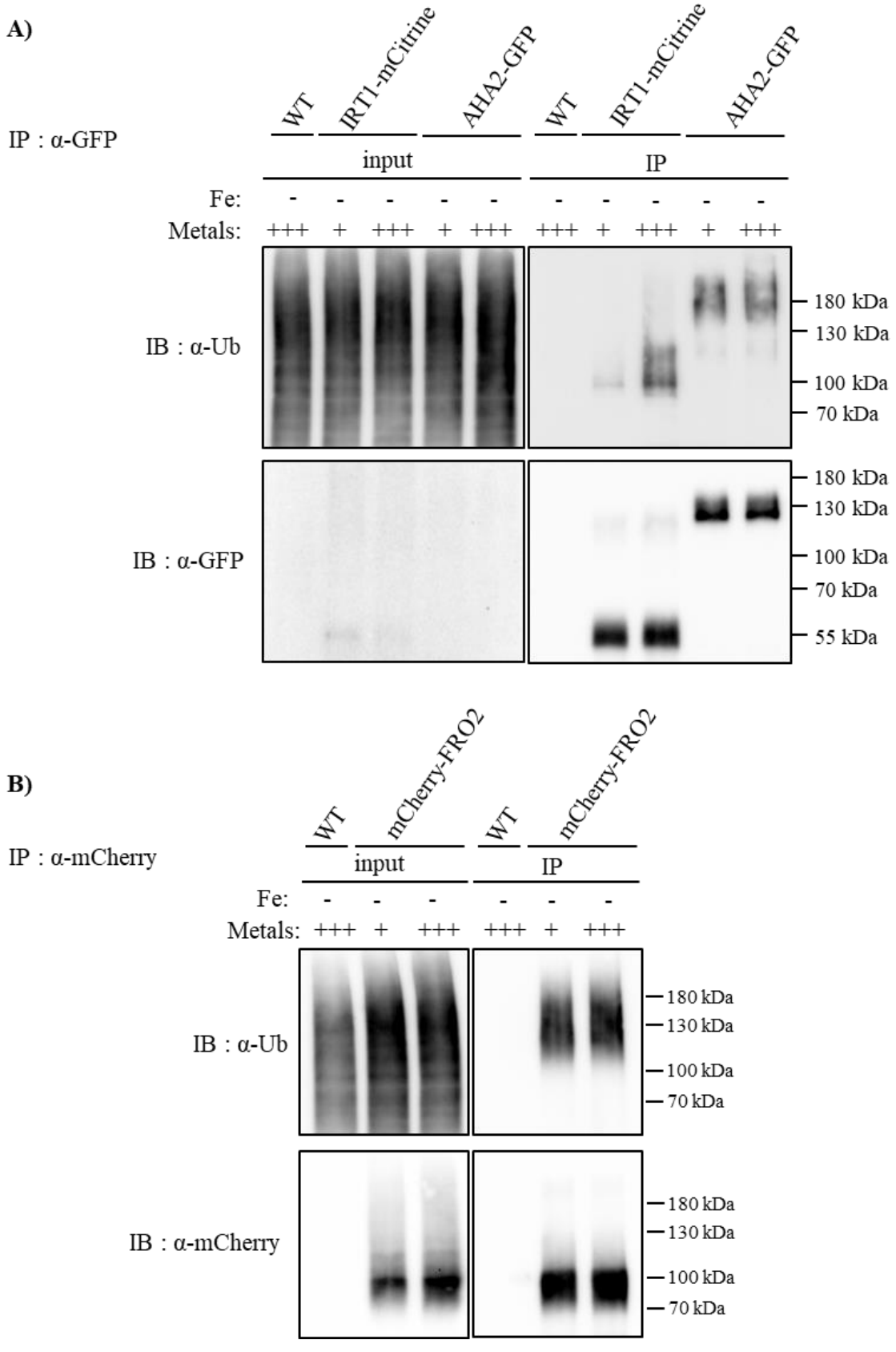
A)
IP : α-GFP
WT
IRT1-mCitrine
AHA2-GFP
WT
IRT1-mCitrine
AHA2-GFP
input
IP
Fe:
Metals:
IB : α-Ub
IB : α-GFP
180 kDa
130 kDa
100 kDa
70 kDa
55 kDa
B)
IP : α-mCherry
WT
mCherry-FRO2
WT
mCherry-FRO2
input
IP
Fe:
Metals:
IB : α-Ub
IB : α-mCherry
180 kDa
130 kDa
100 kDa
70 kDa

<u>Figure 17.</u> FRO2 and AHA2 are ubiquitinated in *Arabidopsis* root cells in a metal independent manner.
Immunoprecipitations (IP) were performed using anti-GFP antibodies on solubilized root protein extracts from wild-type (WT), *irt1-1*/IRT1::IRT1-mCitrine and Col0/35S::AHA2-GFP plants **(A)** or using anti-mCherry antibodies on solubilized root protein extracts from WT and *frd1*/FRO2::mCherry-FRO2 plants **(B)**. Inputs and IP fractions were subjected to immunoblotting (IB) with anti-Ub antibody (P4D1) (A and B, top), anti-GFP (A, bottom) or anti-mCherry antibodies (B, bottom). Plants grown in iron deficient condition were subjected to physiological level of non-iron metals (+) or to an excess of these metals (+++) for 2 hours. WT plants were used as negative controls for IP.

in the ER (Figure 16B), where misfolded proteins are often retained. This choice will be commented in the discussion.

III.1.2 - FRO2 and AHA2 ubiquitination profiles in response to non-iron metal status

As mentioned above, we aimed at analyzing whether the ubiquitination of FRO2 and AHA2 could be regulated by the availability of non-iron metals, as previously observed for their interacting partner IRT1. First, we determined whether AHA2 and FRO2 are ubiquitinated in vivo by performing IP of AHA2-GFP and mCherry-FRO2 expressed in *Arabidopsis* roots, followed by the immunodetection of ubiquitination with P4D1 general anti-ubiquitin antibodies. In the presence of physiological concentrations of non-iron metals (+), AHA2-GFP and mCherry-FRO2 immunopurified fractions probed with P4D1 antibodies showed high-molecular-weight smears that are typical of ubiquitinated proteins as observed for IRT1-mCitrine used as a positive control (Figure 17A and B). Note that no signal was detected when the immunopurified fractions of the different negative controls, corresponding to IP performed on protein extracts from WT plant roots, were probed with the P4D1 antibodies. As expected, after short non-iron metal excess treatment (+++), immunopurified IRT1-mCitrine was much more ubiquitinated than in standard conditions (Figure 17A), however the pool of ubiquitinated AHA2-GFP and mCherry-FRO2 remained unchanged (Figure 17A and B). Hence, although AHA2, FRO2 and IRT1 belong to the same complex involved in a common mechanism i.e. iron acquisition, ubiquitination of these proteins is differently regulated by metal availability.

A)

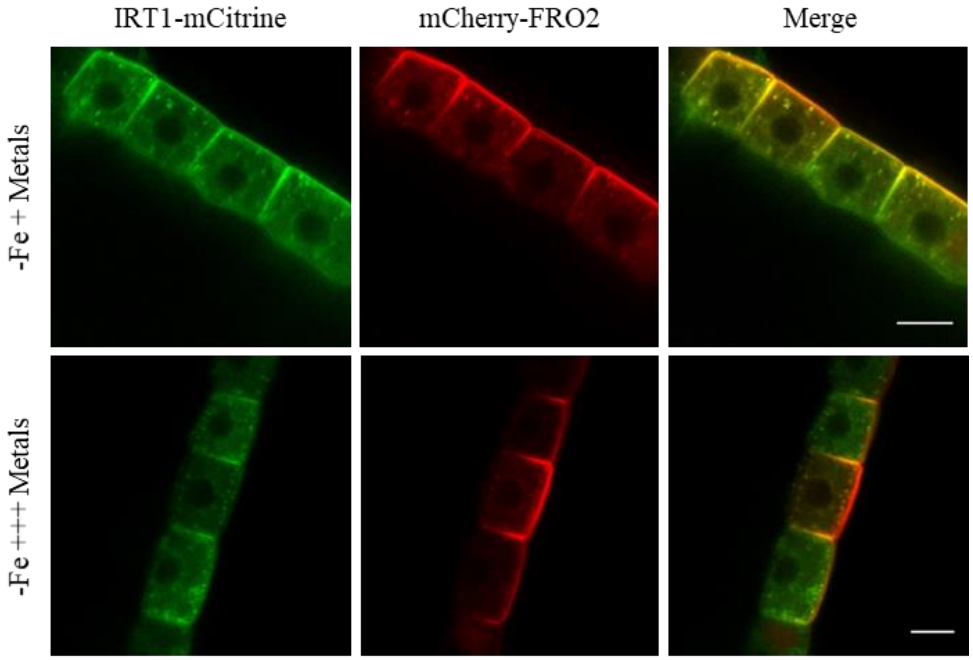
IRT1-mCitrine
mCherry-FRO2
Merge
-Fe + Metals
-Fe +++ Metals

B)

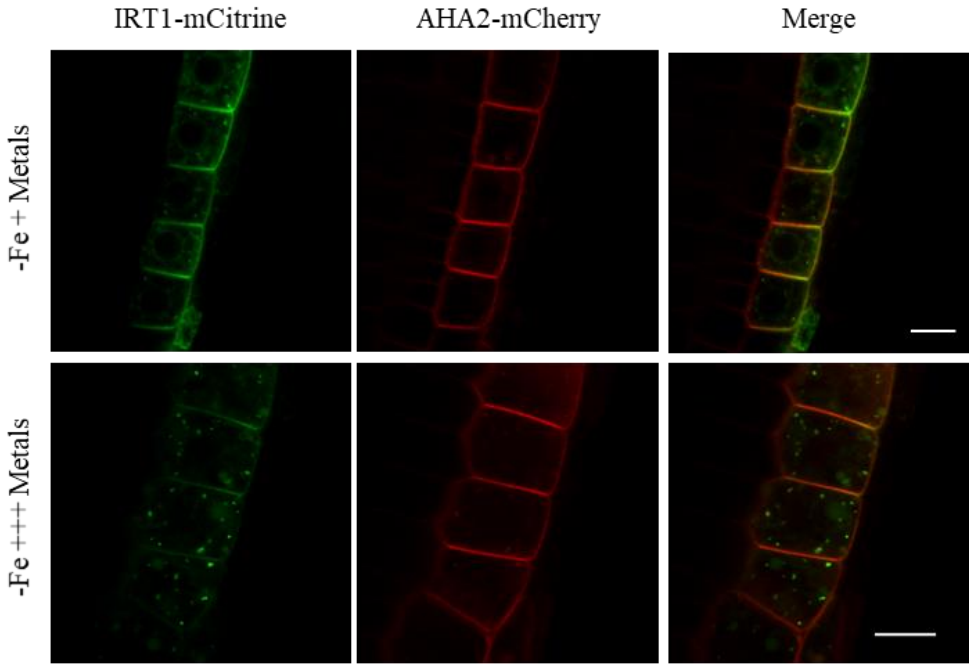
IRT1-mCitrine
AHA2-mCherry
Merge
-Fe + Metals
-Fe +++ Metals

C)

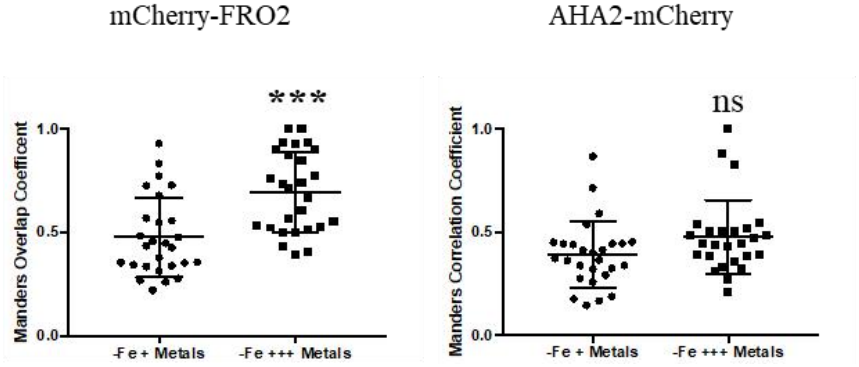
mCherry-FRO2
AHA2-mCherry
***
ns
Manders Overlap Coefficent
Manders Correlation Coefficient
1.0
0.5
0.0
-Fe + Metals
-Fe +++ Metals

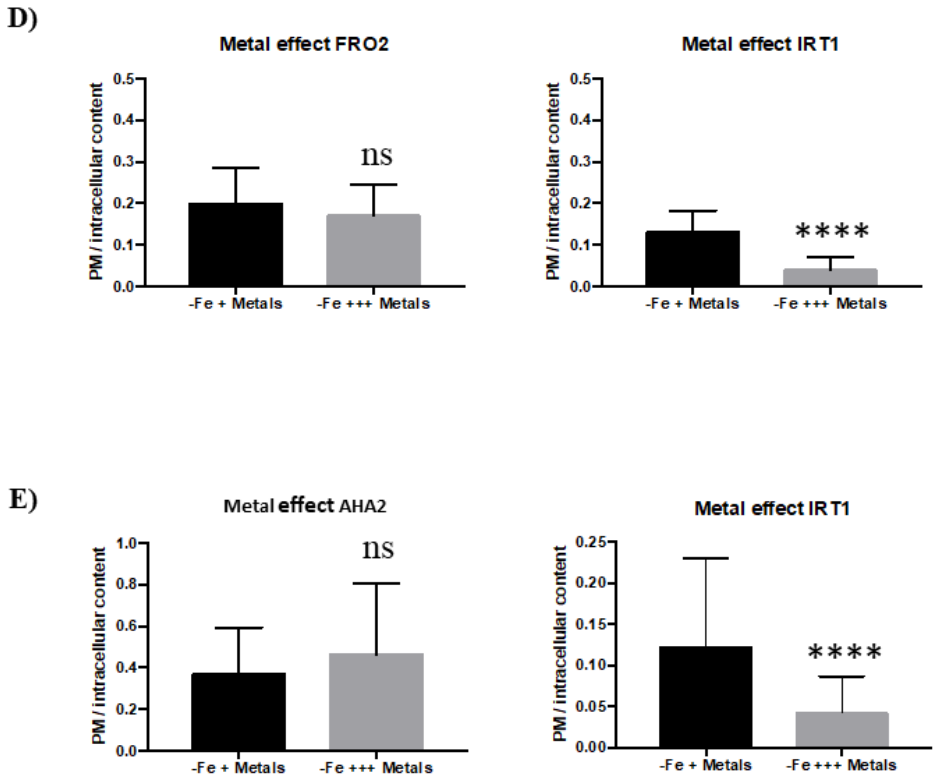

<u>Figure 18.</u> The endocytosis of IRT1 and FRO2/AHA2 is differently regulated by non-iron metals in root epidermal cells.

Confocal microscopy analyses of *irt1-1/*IRT1::IRT1-mCitrine plants co-expressing mCherry-FRO2 under the control of *IRT1* promoter **(A)** or AHA2-mCherry under the control of *IRT1* promoter **(B)**. Plants grown in iron deficient condition were subjected to physiological level of non-iron metals (-Fe + Metals) or to an excess of these metals (-Fe +++ Metals) for 2 hours. Scale bars = 10 µm. **(C)** Quantification of the colocalization of mCherry-FRO2 and AHA2-mCherry signals with IRT1-mCitrine fluorescence in endosomes from experiments performed as in (A) and (B) Mander's overlap coefficient for mCherry-FRO2 is 0.48 in –Fe + Metals and 0.69 in –Fe +++ Metals. Mander's overlap coefficient for AHA2-mCherry is 0.48 in –Fe + Metals and 0.47 in –Fe +++ Metals. **(D)** Ratio of plasma membrane to intracellular fluorescence signal intensities for IRT1-mCitrine and mCherry-FRO2 from experiments performed as in (A). **(E)** Ratio of plasma membrane to intracellular fluorescence signal intensities for IRT1-mCitrine and mCherry-FRO2 from experiments performed as in (B). The whole volume of the epidermal cells was accounted for the results. Graphs represent mean +- SEM. Three independent replicates were carried out with a total number of 27 cells. Significant differences between treatments in mean fluorescence levels are marked with an asterisk (Two tailed unpaired t-test was conducted, P< 0.005).

III.2 - Co-localization studies between IRT1 and FRO2/AHA2 in the root: Characterization of the dynamics of the Fe acquisition platform

Although the intracellular dynamics of IRT1 and AHA2 were previously independently investigated (Barberon *et al.*, 2011; Dubeaux *et al.*, 2018; Haruta *et al.*, 2018), FRO2 subcellular distribution has never been determined so far. Moreover, it reminds unknown where in root cells IRT1 *co-localize*s with FRO2 and AHA2. Thus, we decided to investigate the respective localization of IRT1-mCitrine and FRO2 / AHA2 expressed as mCherry fusion proteins. For this study, we focused on the root tip epidermal cells which are well suited to analyze the precise localization of PM proteins and where IRT1 metal-triggered endocytosis was previously characterized (Dubeaux *et al*., 2018). In addition, the effect of non-iron metal status on FRO2 and AHA2 dynamics was analyzed, using IRT1 as a reference. When IRT1-mCitrine and mCherry-FRO2 were co-expressed under the control of *IRT1* and *FRO2* promoters, respectively, the two proteins accumulated in the epidermis of the differentiated zone of the root (result not shown). However, we failed to find a time frame for which IRT1 and FRO2 were both present at the root tip. To circumvent this problem and to be able to analyze IRT1 and FRO2 intracellular dynamics at the root tip, IRT1-mCitrine and mCherry-FRO2 were both expressed under the control of *IRT1* promoter. For the same purpose, AHA2-mCherry was also expressed under the control of *IRT1* promoter. In the presence of physiological amounts of non-iron metals (-Fe + Metals) mCherry-FRO2 was present at the plasma membrane in a polar fashion facing the medium, as observed for IRT1-mCitrine (Figure 18A). FRO2 was also observed in numerous intracellular vesicles highly co-localizing with IRT1, as determined by quantification (Figure 18C) (Mander's overlap coefficient of 0.48). These vesicles correspond to early endosomes since IRT1 constitutes a marker of these compartments in such metal conditions (Dubeaux *et al.*, 2018). Contrary to IRT1 and FRO2, AHA2-mCherry displayed a non-polar plasma membrane localization in epidermal cells in the same metal conditions and was also found in few endosomes co-labelled with IRT1-mCitrine (Mander's overlap coefficient of 0.39) (Figure 18B and C). The intracellular dynamics of FRO2 and AHA2 was then investigated after a short term metal excess treatment (-Fe +++ Metals) that triggers IRT1 endocytosis and its subsequent degradation. Upon non-iron metal excess, IRT1-mCitrine was depleted from the cell surface and accumulated in late endosomes (Figure 18A and B) whereas mCherry-FRO2 and AHA2-mCherry were mostly detected at the plasma membrane (Figure 18A and B respectively) even though they were also found to co-localize

with IRT1-mCitrine in few late endosomes. To obtain quantitative information concerning this phenomenon, the ratio of plasma membrane to intracellular fluorescence signal intensities was measured for the three fusion proteins in presence of physiological non-iron metal provision or in presence of an excess of these metals. As previously reported (Dubeaux *et al.*, 2018), this PM/intracellular ratio highly decreased for IRT1-mCitrine in response to non-iron metal excess (Figure 18D and E), whereas in the case of mCherry-FRO2 and AHA2-mCherry, no significant difference in this ratio was observed (Figure 18D and E respectively). Thus, contrary to IRT1, FRO2 and AHA2 are not massively endocytosed in response to non-iron metal excess. However, the level of co-localization between FRO2 and IRT1 in endosomes significantly increased with non-iron metal excess compared to control conditions (Figure 18C) (Mander's coefficient of 0.69), suggesting a minor effect of non-iron metal status on FRO2 endocytosis. On the other hand, the co-localization between IRT1 and AHA2 in endosomes was not significantly modified by non-iron metals (Figure 18C) (Mander's coefficient of 0.47).

IV – Role of HIR2 and membrane microdomains in the control of IRT1 and metal homeostasis

IV.1 – HIR2 and IRT1 localize in PM microdomains in root epidermal cells

When I started this work, data concerning HIR2 were really scarce and notably the expression pattern of HIR2 in *Arabidopsis* as well as its subcellular localization remained unknown. Therefore, we decided to express a HIR2-mCherry functional fusion (see Figure 23) under the control of *HIR2* promoter in a *hir2* knock-out mutant isolated in the laboratory and named *hir2-2* (see hereafter). Confocal microscopy analysis revealed that in this transgenic line, HIR2-mCherry was specifically present in the epidermis of the differentiated zone of the root, including root hairs, whereas at the root tip HIR2 was only found in the lateral root cap (Figures 19A and B). In all cases HIR2-mCherry was mostly localized at the PM although, in some cells, the protein was observed in scarce intracellular compartments. The preferential localization of HIR2 in the PM of root epidermal cells suggests that most of the IRT1-HIR2 interactions should occur at the PM level. Importantly, as suggested by transcriptomic data (Dinneny *et al.*, 2008), *HIR2* promoter does not seem to be regulated by iron status. So far, the expression pattern of HIR2 in the aerial part of *Arabidopsis* has not been investigated.

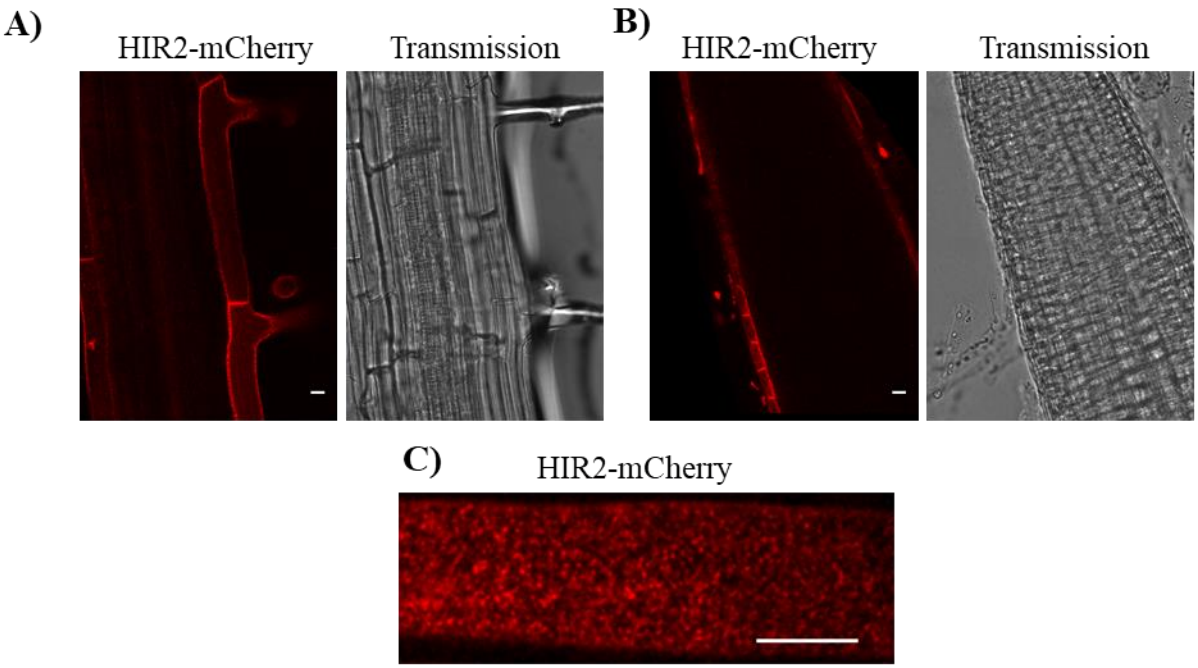

<u>Figure 19.</u> HIR2 specifically accumulates in root epidermal cells and in the lateral root cap, at the plasma membrane level.
Confocal microscopy analysis performed on *hir2-2/*HIR2::HIR2-mCherry transgenic lines in the differentiated zone of the root **(A)** at the root tip **(B)** and spinning disk confocal acquisitions performed at the surface of the root epidermis of the same transgenic line **(C)**. Plants were grown in –Fe + Metals conditions for 11 days before observation. These observations apply to at least three independent lines. Scale bar = 10 µm.

To determine whether HIR2 but also IRT1 are clustered in PM membrane microdomains, we performed spinning-disk confocal microscopy at the very surface of roots from *Arabidopsis* transgenic lines expressing fluorescent versions of HIR2 and IRT1. In early experiments, we expressed a HIR2-GFP fusion under the control of the *35S* promoter. As a negative control of microdomain localization, we decided to use the Low Temperature Induced protein 6b (LTi6b) fused to GFP (GFP-LTi6b), since this protein is located in the PM but is not known to be present in microdomains. Both proteins, GFP-LTi6b and IRT1-mCitrine, were also expressed under a 35S promoter. In this way, we revealed that HIR2 displayed a punctate distribution at the cellular surfaces which confirmed that HIR2 is present in restricted membrane microdomains in *Arabidopsis* root epidermal cells (Figure 20B). This observation complements the information obtained by another research group that identified HIR2 as a protein enriched in DIM preparations from *Arabidopsis* roots (Qi *et al.*, 2011). Contrary to HIR2-mCherry and as expected, GFP-LTI6b is homogeneously distributed at the PM level, showing that this protein is not recruited in specific membrane microdomains (Figure 20A). Interestingly, we revealed

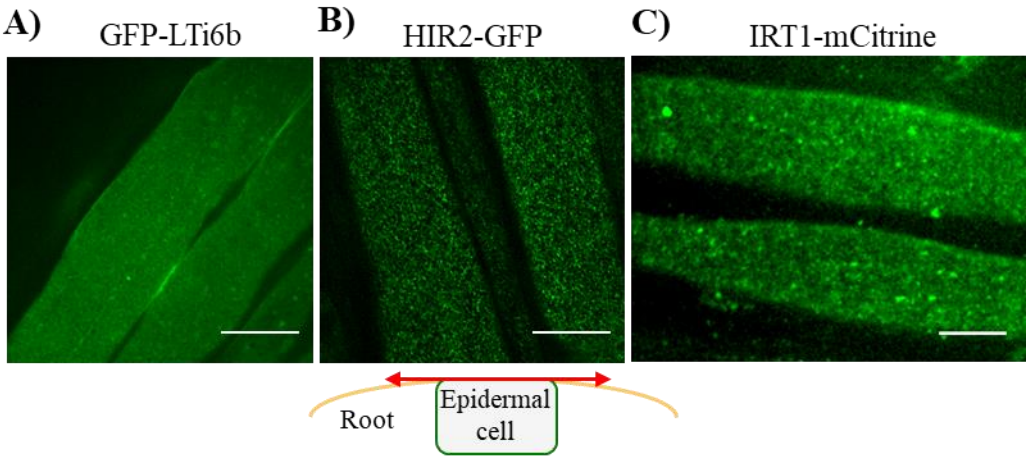

Figure 20. HIR2 and IRT1 proteins are localized in plasma membrane microdomains of root epidermal cells.
Spinning-disk confocal acquisitions performed at the surface of the root epidermis of different transgenic lines: **(A)** Col-0/35S::GFP-LTi6b, **(B)** Col-0/35S::HIR2-GFP, **(C)** Col-0/35S::IRT1-mCitrine. HIR2 and IRT1 present a punctate distribution at the PM level while LTi6B, used as a negative control for membrane microdomain localization, presents a very homogenous distribution. Some endosomes (brighter and bigger dots) are observed in IRT1-mCitrine expressing plants in (C). Plants were grown for 7 days in -Fe + Metal conditions before observation. Scale bar = 10µm.

that IRT1 can also be clustered in small areas of the PM likely corresponding to microdomains (Figure 20C). However, IRT1-mCitrine did not displayed a membrane microdomain localization in all the root epidermal cells that we analyzed. This intriguing result may be due to the fact that IRT1 is not an obligatory PM microdomain-recruited protein. Additionally, although we used a strong *35S* promoter, the expression level of IRT1-mCitrine was rather low and changed from one cell to another. Thus, it appeared that the detection of IRT1-Citrine in PM microdomains was more difficult in cells expressing low amount of the fluorescent protein.

To go further and try to determine whether IRT1 and HIR2 co-localized in the same PM microdomains, we performed co-localization analysis using transgenic plants co-expressing IRT1-mCitrine and HIR2-mCherry. Membrane microdomains have already been proposed as specific platforms, capable of recruiting different proteins implicated in plant immune signaling (Qi and Katagiri, 2012; Introduction Chapter 3). One of our hypotheses is that IRT1 may be recruited in membrane microdomains by interacting with HIR2 that would act as a scaffolding protein, allowing the formation of a putative iron acquisition protein platform. Besides, although so far IRT1 endocytosis was demonstrated to be clathrin-dependent (Barberon *et al.*, 2014), there are also specific membrane microdomains that are able to induce microdomain-associated endocytosis (MAE) (Introduction Chapter II.1.2.2.2), a pathway that can be

stimulated by environmental factors. As the molecular functions of HIR2 are still poorly understood, a participation of HIR2 in IRT1 endocytosis could not be disregarded. To explore both possibilities, plants were subjected to either lack of Fe, either to lack of Fe in an excess of non-iron metals, condition that triggers IRT1 depletion from the PM.

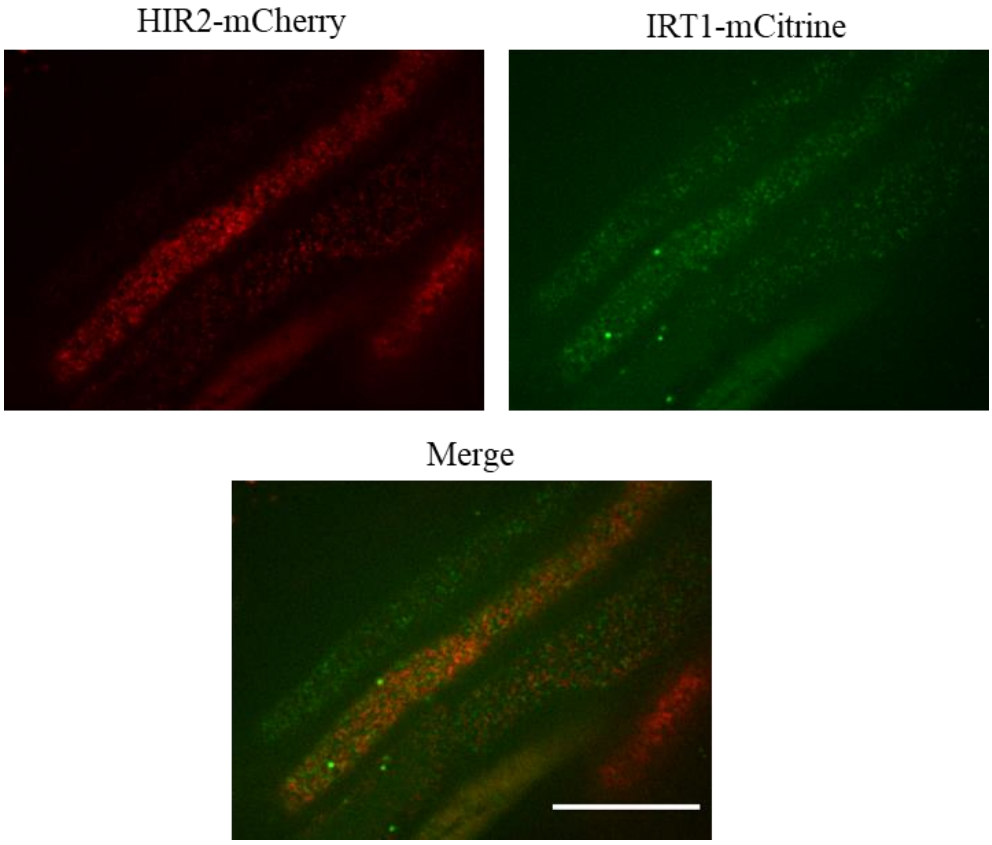

Figure 21. Membrane microdomains labelled by HIR2 and IRT1 proteins seem to be distinct.
Spinning-disk confocal acquisitions performed at the surface of the root epidermis of Col-0/35S::IRT1-mCitrine plants co-expressing HIR2-mCherry under the control of *HIR2* promoter. Plants were grown 7 days in -Fe + Metal conditions before observation. Scale bar = 10 µm.

In order to detect enough IRT1-mCitrine at the PM, avoiding incidental effect of non-iron metal nutrition on IRT1 levels, we decided to use transgenic lines expressing IRT1-mCitrine under the control of the *35S* promoter. The 35S::IRT1-mCitrine line had already been successfully used to characterize the non-iron metal-mediated endocytosis of IRT1 (Dubeaux *et al.*, 2018). Therefore, we performed co-localization analysis using transgenic plants co-expressing IRT1-mCitrine and HIR2-mCherry. In order to avoid possible silencing due to the presence of two *35S* promoters, HIR2-mCherry was expressed under the control of *HIR2*

promoter. Microscopy analysis had confirmed that HIR2-mCherry expressed under the control of *HIR2* promoter is correctly located in PM microdomains in root epidermal cells (Figure 19C). Then, the IRT1-mCitrine/HIR2-mCherry co-expressing plants were challenged with physiological concentrations of non-iron metals or with an excess of non-iron metals, always in absence of iron. Unfortunately, we were not able to detect a co-localization between IRT1 and HIR2, independently of the non-iron metal status employed. When the plants were exposed to physiological concentrations of non-iron metals, we could observe a punctate pattern disposition of IRT1 and HIR2, but in distinct microdomains, and no co-localization in endosomes (Figure 21). Challenging the plants with non-iron metal excess resulted in the same distinct puncta pattern observed for both proteins. Furthermore, the treatment did not affect the internalization of HIR2, that reminded stable at the PM (result not shown).

To summarize, we showed that HIR2 expressed under the control of *HIR2* promoter specifically accumulates in epidermal cells of the *Arabidopsis* root. Consequently, HIR2 and IRT1 share the same tissue specific localization. Microscopy analysis revealed that HIR2 is localized in PM microdomains. In the case of IRT1, the protein can be observed in PM microdomains, but not systematically. Although IRT1 and HIR2 can interact among a protein complex, so far, we failed to observe IRT1 and HIR2 in common PM microdomains.

IV.2 - HIR2 plays a role in Fe homeostasis

IV.2.1 – *hir2* mutants are hypersensitive to iron deficiency

Since HIR2 interacts with IRT1, a key component of the iron uptake machinery in *Arabidopsis*, we decided to study a putative role of HIR2 in metal homeostasis. For this purpose, we performed reverse genetic approaches by analyzing the phenotype of *hir2* loss-of-function mutants under different iron status. Before I started my thesis, preliminary analysis performed in our laboratory suggested that the *hir2-1* mutant, published as being a knock-out mutant of *HIR2* (Qi *et al.*, 2011), was more chlorotic than WT plants (Col-0) when grown in the absence of iron, whereas *hir2-1* behaved as WT plants in presence of sufficient amount of iron (Supplementary Figure 3). Then our group isolated a second allelic variant of *hir2* (SALK_124393C), that was named *hir2-2* and that was assigned as a loss-of-function mutant, because *HIR2* transcript was no more detected in this mutant (Figure 22A). Since the phenotype of *hir2-2* in lack of iron appeared to be more pronounced and robust than for *hir2-1* mutant, we decided to first characterize in detail the *hir2-2* mutant.

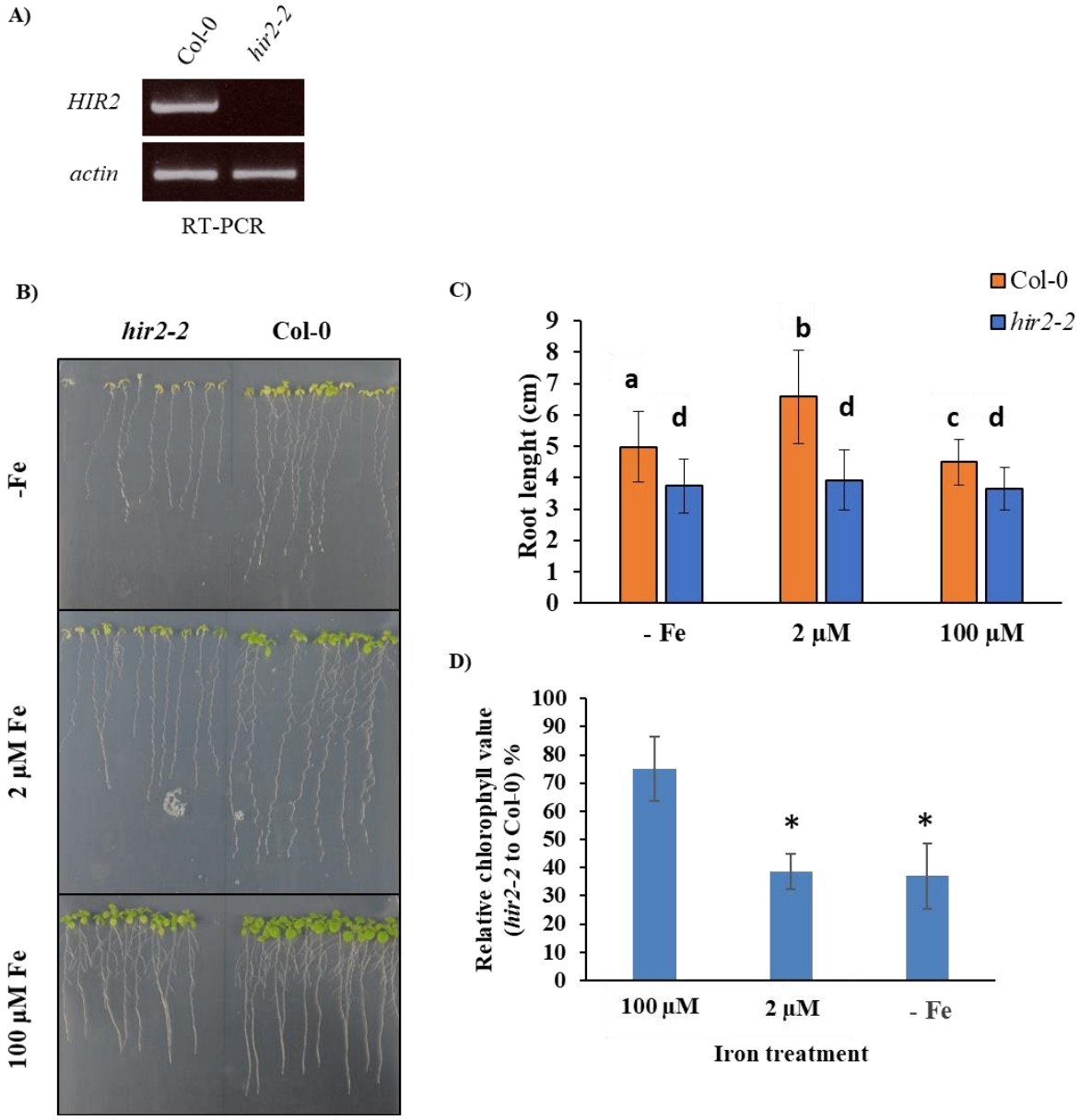

Figure 22. The *hir2-2* mutant presents an hypersensitivity to iron deficiency compared to WT plants.

(A) RT-PCR analysis showed that *HIR2* transcript do not accumulate any more in *hir2-2* mutant compared to Col-0 plants (WT), revealing *hir2-2* as a knock-out mutant. **(B)** Phenotypical analysis of *hir2-2* mutant upon different iron status. Col-0 and *hir2-2* mutant plants were grown for 14 days on MS/2 medium in lack of Fe (-Fe), in presence of low Fe concentrations (2 µM Fe-EDTA) or in Fe replete conditions (100 µM-Fe-EDTA). **(C)** The average length of the primary root of Col-0 and *hir2-2* mutant grown as in (B) was measured. Different letters indicate significant growth differences between the two genotypes exposed to a same metal condition and also statistical differences registered within a same genotype exposed to different metal conditions (One-way ANOVA, Tukey's post-test, $P < 0.05$). Error bars represent the ±SD, n=3-4 biological replicates (each made of23 to 34 plants). **(D)** The total chlorophyll contents of the aerial parts of plants grown as in (B) were measured. Graphs show relative chlorophyll content (*hir2-2 versus* of Col-0). Error bars represent the ±SD, n = 3-4 biological replicates, each composed of two technical replicates, each one made of a pull of approximately 30 plantlets. The asterisks indicate statistically significant differences in chlorophyll accumulation as determined by one-way ANOVA (Tukey's post-test, $P < 0.05$).

To do so, we decided to grow the *hir2-2* mutant and Col-0 WT plants on different media containing increasing iron concentrations. More precisely, the plants were subjected to total lack of Fe (-Fe), to low Fe conditions (2 µM Fe) and to Fe replete conditions (100 µM Fe). As seen in Figure 22B, the *hir2-2* mutant grew quite similarly to WT plants in Fe replete conditions. On the contrary, Fe depletion greatly affected the development of *hir2-2* compared to Col-0 plants, moreover, *hir2-2* appeared highly chlorotic and seemed to present shorter primary roots. Therefore, we decided to further quantify these two parameters, that are typical phenotypic markers of the Fe deficiency response (as described in Introduction Chapter I.1). The length of Col-0 primary root tended to vary according to the different Fe treatments and its growth seemed stimulated by the presence of low Fe conditions (Figure 22C). On the contrary, the length of *hir2-2* primary root remained constant, independently of the treatments (Figure 22C). The measurement of plant chlorophyll contents revealed major differences between *hir2-2* and WT plants and, hence, was probably the most relevant parameter to detect iron homeostasis defects in the context of this study (Figure 22D). Indeed, in lack of Fe, *hir2-2* mutant presented a decrease of approximately 64 % in the total chlorophyll content of leaves in comparison to WT plants. A similar phenotype was observed in low iron condition (2 µM Fe). On the contrary, when subjected to 100 µM Fe, *hir2-2* mutant accumulated an important quantity of chlorophyll yet in smaller amounts than WT plants (Figure 22D). These results suggest that the iron homeostasis is impaired in *hir2-2* mutant, highlighting, to my knowledge for the first time, the role of a membrane microdomain protein in plant metal nutrition.

In addition, we performed complementation tests by expressing HIR2-mCherry protein under the control of the *35S* promoter in *hir2-2* mutant. Expression of HIR2-mCherry allowed to partially revert the phenotype of *hir2-2* mutant plants under iron deficiency. Indeed *hir2-2*/35S:: HIR2-mCherry transgenic lines were greener and displayed longer roots than *hir2-2* in these conditions, even though they do not behave as WT plants (Figure 23). This result suggests that the mutation in *HIR2* gene is indeed responsible for the phenotype observed for *hir2-2* under iron deficiency. One explanation for the partial complementation we observed is that HIR2-mCherry is not fully functional. Another possibility is that the *35S* promoter, that is not epidermis specific, is not really appropriate to perform this complementation test. To try to fully complement the *hir2-2* mutant phenotype, we decided to introduce a genomic fragment containing *HIR2* gene and its promoter (2.700 bp in total) in the genome of *hir2-2.* This work is in progress.

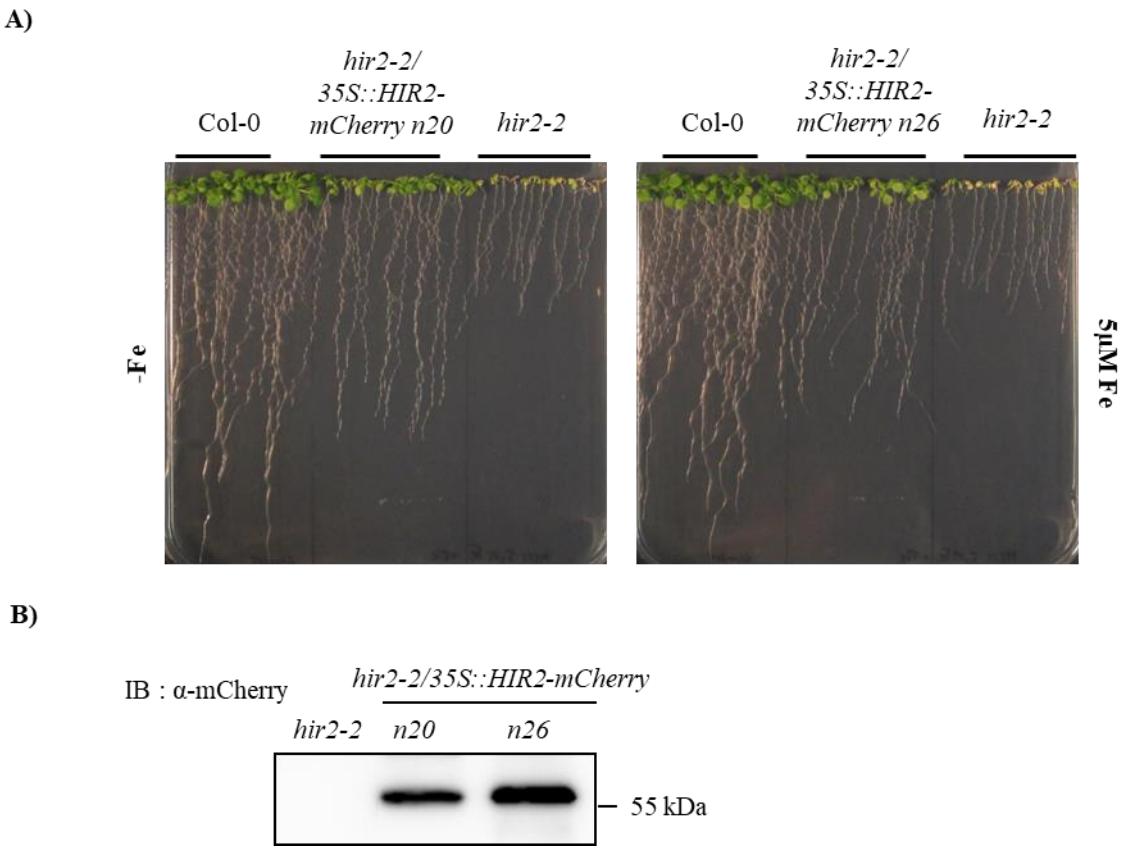

Figure 23. Expression of HIR2-mCherry complements the phenotype displayed by *hir2-2* mutant under iron limited conditions.
(A) The *hir2-2* mutant, *hir2-2/*35S::HIR2-mCherry transgenic lines (n20 and n26) and Col-0 plants were grown 11 days on MS/2 in low iron conditions. **(B)** Immunoblot with an anti-mCherry antibody performed on root protein extracts from *hir2-2/*35S::HIR2-mCherry transgenic lines showed HIR2-mCherry accumulation. A root protein extract from *hir2-2* mutant was used as a negative control.

IV.2.2 – IRT1 protein accumulation is disturbed in *hir2* mutants

We wondered whether the hypersensitivity of *hir2* mutants to Fe starvation may result from a possible deregulation of IRT1 protein accumulation. Interestingly, initial immunoblot analysis performed on root protein extracts with an antibody raised against endogenous IRT1 revealed that IRT1 protein was over-accumulated in *hir2-1* mutants compared to WT plants under iron deficiency (Supplemental figure 3). During my thesis, I obtained similar results by comparing IRT1 protein accumulation in *hir2-2* and WT plants (Figure 24), but the difference in IRT1 content was even more pronounced than between *hir2-1* and WT plants. We cannot exclude that between the two series of experiments, separated by about one year, our non-iron conditions were slightly different, which may explain the difference observed between *hir2-1*

and *hir2-2* mutants. Quantification of the IRT1 signals of several immunoblots allowed to establish that IRT1 protein was on average 6 times more abundant in *hir2-2* mutant compared to WT plants. RT-qPCR analysis performed on RNA extracted from the roots of *hir2-2* and WT plants grown in the same iron deficient conditions showed that *IRT1* transcript accumulation remained nearly unchanged between both genotypes. Therefore, the over-accumulation of IRT1 protein in *hir2-2* mutant is likely due to a post-transcriptional mechanism, this idea being strengthen by the fact that IRT1 and HIR2 proteins interact. This result suggests that the "turn-over"/degradation of IRT1 may be affected in absence of HIR2 and, as developed in the Discussion section, one hypothesis is that IRT1 endocytosis might be disturbed in the context of the *hir2-2* mutant. Although Flot1 protein is known to be involved in microdomain-associated endocytosis (Li *et al.*, 2012), whether other members from the *Arabidopsis* SPFH domain-containing protein family, such as HIR, are involved in the same process has never been addressed so far.

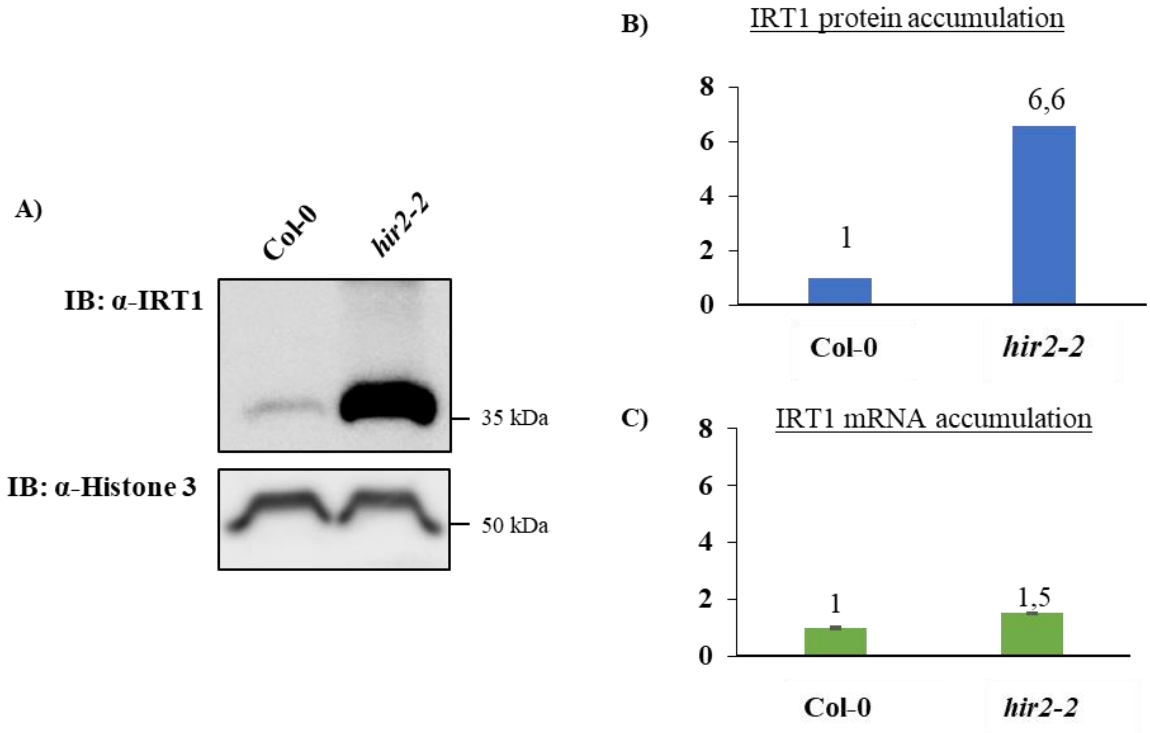

Figure 24. IRT1 protein over-accumulates in the roots of *hir2-2* mutant in lack of Fe.
(A) Anti-IRT1 and anti-Histone 3 (loading control) immunoblots were performed on root protein extracts from *hir2-2* and Col-0 plants grown on MS/2 medium in low iron conditions (2 µM Fe-EDTA) as presented in Figure 21B. **(B)** Quantification of the levels of IRT1 protein accumulation visualized in (A), using Col-0 as a reference. **(C)** Relative *IRT1* transcript accumulation measured by RT-qPCR performed on mRNA extracted from the roots of *hir2-2* and Col-0 plants grown as in (A). *EF1α* gene was used as a reference. Two technical replicates were performed. Error bars represent relative standard deviation. Note that 4 biological repetitions were performed and for each repetition an immunoblot and RT-qPCR were done. A representative analysis is presented in this figure.

IV.2.3 – The phenotype displayed by the *hir2-2* mutant under Fe starvation is not explained by a deregulation in the total metal content

The very chlorotic phenotype displayed by *hir2-2* mutant under Fe starvation may be explained by two different hypotheses. First, as *hir2-2* over-accumulates IRT1 protein, the secondary substrates of IRT1 (Zn, Mn, Co) present in the media may be preferentially and highly uptaken in conditions of lack of Fe. The uptake of these non-iron metals by IRT1 is not dependent of a prior step of reduction, unlike for Fe, therefore their absorption is favored over the possible Fe traces. As non-iron metals are toxic when present in excess, the phenotype observed in *hir2-2* mutant may therefore be due to a toxicity caused by a massive uptake of these metals. Secondly, in *hir2-2* mutant, IRT1 may be mislocalized outside of specific PM microdomains if we assume that HIR2 is important to recruit IRT1 in such domains. In this context and since it was demonstrated that the lipidic environment surrounding a membrane protein can greatly influence its activity (Oh *et al.*, 2016), IRT1 may be present in large amount but remain inactive due to an inappropriate lipid context. According to this hypothesis, a significant decrease in the content of all the substrates of IRT1 (Fe, Zn, Mn and Co) would be expected in *hir2-2* mutant, explaining why these plants are hypersensitive to iron deficiency.

To shed light about these two hypotheses, we measured and compared the total content in Zn, Mn and Fe in leaves from Col-0 and *hir2-2* mutant plants. Co measurement was not performed because, at the concentration used in the media, this metal does not produce great physiological outputs, neither triggers IRT1 internalization contrary to Zn and Mn (Dubeaux *et al.*, 2018). Before metal quantifications, Col-0 and *hir2-2* plants were grown in the same metal regimes we previously used, i.e. -Fe, 2 µM Fe, 100 µM Fe. We also subjected the plants to a condition where Fe is lacking but in presence of an excess of non-iron metals (-Fe +++ Metals). Considering our first hypothesis, we expected that in this condition, the amount of IRT1 secondary substrates uptaken by *hir2-2* would be higher than in the other conditions.

As previously described, lack of Fe or 2 µM Fe induced a stronger chlorosis in *hir2-2* mutant compared to WT plants (result not shown). This phenotype was exacerbated in both genotypes when lack of Fe was accompanied by an excess of non-iron metals (-Fe +++ Metals) and reverted upon sufficient Fe addition (100 µM Fe + Metals) (result not shown). The metal content analysis measured in plant leaves properly reflected the metal conditions to which the plants were subjected. Thus, conditions of 100 µM Fe resulted in leaves that were highly charged in Fe, for the mutant and for WT plants (Figure 25A). In the same way, plant exposure

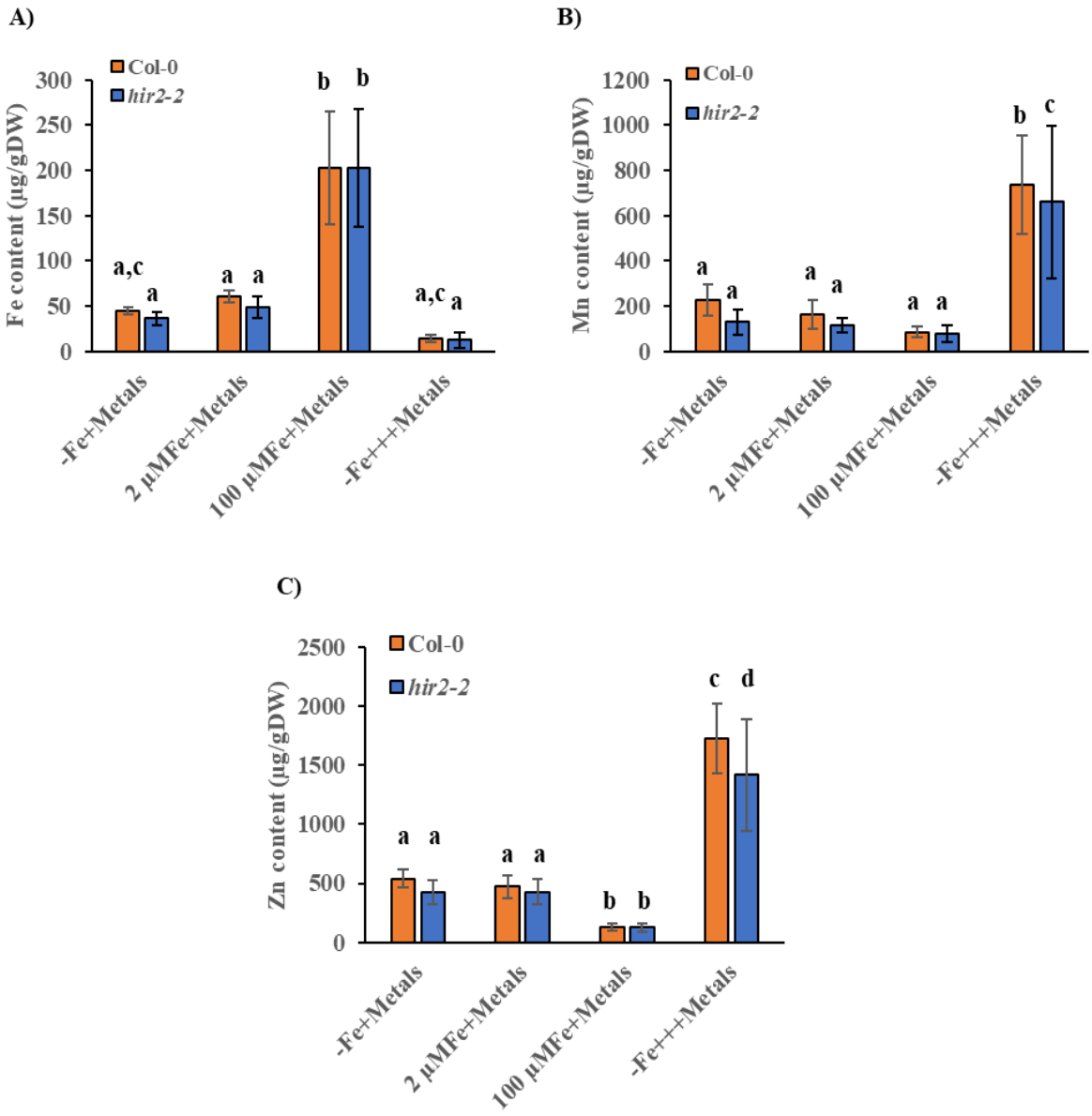

<u>Figure 25.</u> *hir2-2* mutant and Col-0 plants display similar metal accumulation profiles in leaves.

Fe, Mn and Zn contents inside the leaves of *hir2-2* mutants and Col-0 plants subjected to different metal growth conditions for 8 days: lack of Fe accompanied by non-iron metal excess (-Fe +++ Metals), physiological concentrations of non-iron metals combined with a lack of Fe (-Fe + Metals), with low Fe conditions (2 µM Fe + Metals) or with Fe replete conditions (100 µM Fe + Metals). The average metal content in the different genotypes according to treatments was measured by Microwave Plasma Atomic Emission Spectroscopy (MP-AES) and here represented with one graph per metal. Statistical differences between the average of metal accumulation were calculated by one-way ANOVA. Error bars represent the ±SD, n = 4 biological replicates (each with three technical repetitions). Different letters indicate that metal contents were statistically different by Tukey's post-test ($P < 0.05$) between genotypes, within a given growth condition, and within a same genotype subjected to different growth conditions.

to non-iron metal excess resulted in high accumulations of Zn and Mn in the leaves of the plants (Figure 25B and C). Nevertheless, whatever the metal that was quantified and the growth conditions, we did not detect significant differences in term of metal accumulation between *hir2-2* mutant and WT plants (Figure 25). The only exception, was registered when plants were exposed to –Fe +++ Metals conditions. In this case, Col-0 plants presented slightly more Mn and Zn than *hir2-2* mutant plants in a significant way (Figure 25B and C), although both genotypes accumulated equal amounts of Fe (Figure 25A). In –Fe + Metals and 2 µM Fe + Metals conditions, we noticed that *hir2-2* mutant presented a slight tendency, although non-significant, to accumulate less Fe, Zn and Mn than WT plants (Figure 25). Altogether, these results invalidated the two hypotheses we formulated.

V - Study of a putative role of flotillins in the control of IRT1 endocytosis and the impact on iron nutrition

In plants, membrane proteins can be internalized from the PM via a clathrin-independent pathway involving membrane microdomains containing the Flot1 protein (Li et al., 2012, Wang et al., 2015, Introduction Chapter 2). As described above, our results suggest that microdomains play an important role in the maintenance of metal homeostasis and we hypothesized that this mechanism might be mediated by the regulation of IRT1 endocytosis. Beyond the study of HIR2 protein described so far, we tried to determine whether flotillins, which possess a SPFH domain like HIR2, could be involved in the control of IRT1 intracellular dynamics. In *Arabidopsis thaliana* there are three flotillin proteins that have a high identity rate between them (as mentioned in Introduction Chapter 3): Flot1, Flot2 and Flot3. Although the function of the Flot2 and Flot3 proteins remains unknown, they are probably involved in intracellular trafficking since they interact with proteins involved in endocytosis and vesicular trafficking (https://associomics.dpb.carnegiescience.edu/Associomics/Home.html). During my thesis, we initiated a collaboration with the team of Professor Jan Martinec of the Institute of Experimental Botany, Czech Academy of Sciences, Prague, Czech Republic, who has an excellent expertise concerning plant SPFH domain-containing proteins and more particularly flotillins. This collaborative project, in which I was involved, was funded by a PHC Barrande (https://www.campusfrance.org/fr/barrande). This is an ongoing project that includes two main axes of research: the study of the possible role of flotillins in the intracellular dynamics of IRT1 and a possible physiological impact on metal nutrition in *Arabidopsis thaliana*. Below, I present

some results we obtained in collaboration with Michal Danek, a PhD student from Jan Martinec's laboratory.

In order to decipher a possible role of flotillins in Fe nutrition, we initiated a phenotypic study of *flot1*, *flot2*, and *flot3* loss-of-function mutants, available in the laboratory of Jan Martinec, that were subjected to Fe-sufficient or Fe-deficient conditions. Preliminary results showed that the *flot1* and *flot3* mutants presented shorter roots than WT plants in lack of iron, which is a hallmark of hypersensitivity to Fe deficiency, this situation was reverted upon sufficient Fe addition. On the other hand, *flot2* mutant behaved as WT plants under iron deficient conditions. Since this experiment was performed in duplicates so far, I decided to wait for three biological repetitions before making conclusions and presenting quantification graphs. Moreover, the chlorophyll and metal contents of *flot* mutants and WT plants will have to be compared.

In the case where IRT1 undergoes flotillin-mediated endocytosis, IRT1 might interact with flotillins. To test this possibility, we performed a split-ubiquitin test in which NubG-IRT1 was co-expressed in yeast with Flot1, Flot2 and Flot3 Cub fusions. Although yeast co-expressing Flot-Cub fusions with NubWT (positive control) grew on a selective medium, co-expression of NubG-IRT1 with the 3 Flot-Cub fusions did not allow yeast to grow on the same medium, as observed for the 3 negative controls (NubG + Flot-Cub fusions) (figure 26). Thus, IRT1 does not directly interacts with Flotillins in this system. However, since yeast membrane microdomains are different in composition from plant microdomains, we cannot account to what extent differences in membrane composition may limit the split-ubiquitin approach when testing microdomain associated proteins. In addition, as observed for IRT1-HIR2, we cannot exclude that indirect interactions between IRT1 and Flotillins may occur in plants.

To determine whether flotillins might be involved in certain endocytosis mechanisms of IRT1, we decided to perform co-location analyzes at the root tip of *Arabidopsis* between IRT1 and flotillins. To do so, we first generated transgenic lines constitutively co-expressing IRT1-mCitrine with mCherry tagged versions of either Flot1, Flot2 or Flot3 proteins. Flot1-associated endocytosis was demonstrated to be stimulated by environmental factors. As previously explained in the Introduction (Chapter 3), salt stress enhanced the membrane microdomain-mediated endocytosis of the *Arabidopsis* aquaporin PIP2;1 that is mainly endocytosed in a clathrin-dependent manner in non-stressed conditions (Li *et al.*, 2011). Therefore, in the context of this project and in addition to standard conditions, we decided to investigate whether an excess of non-iron metals, that is stressful for plants, had an impact on a possible co-localization between Flotillins and IRT1 in PM membrane microdomains.

Spinning-disk microscopy revealed that IRT1-mCitrine and the three Flot-mCherry proteins clustered in distinct PM microdomains in root epidermal cells under iron deficiency and in presence of physiological amounts of non-iron metals (Figure 27A, C and D). In addition, an excess of non-iron metals did not induce a co-localization between IRT1-mCitrine and Flot-mCherry proteins in membrane microdomains (result not shown). Although Flot2-mCherry and Flot3-mCherry were only located at the PM, Flot1-mCherry was also detected in endosomes as previously described, however whatever the non-iron metal status, IRT1-mCitrine did not co-localize with Flot1-mCherry in this population of endosomes (Figure 27B).

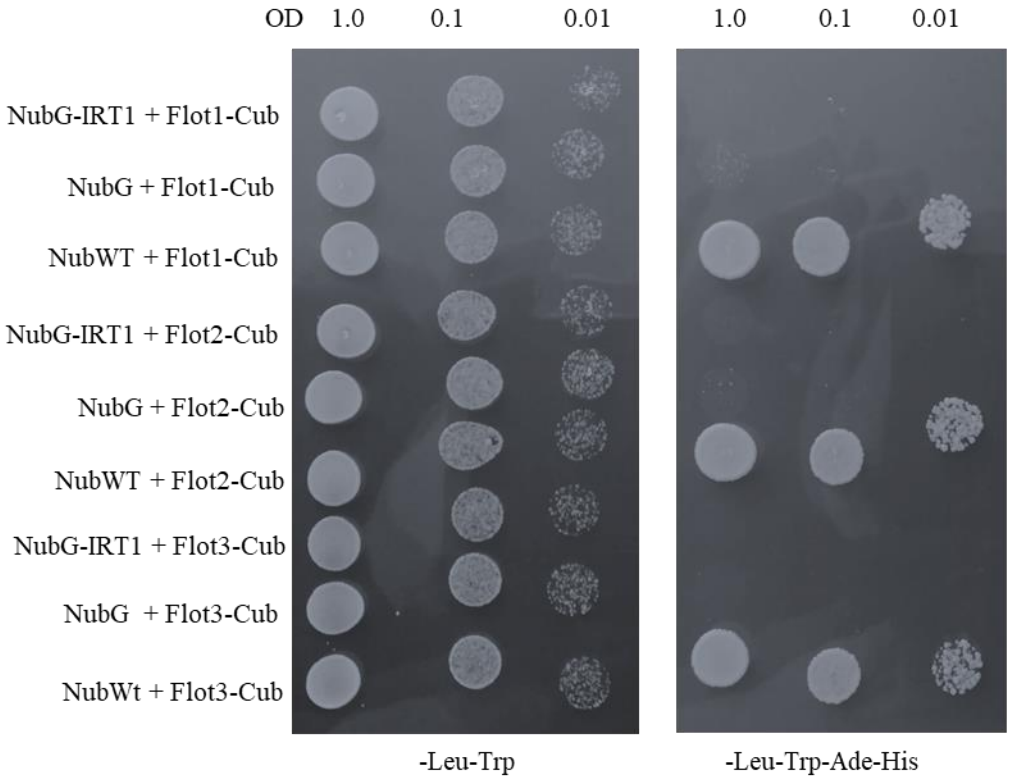

<u>Figure 26.</u> Flot1, Flot2 and Flot3 do not interact with IRT1 in split-ubiquitin assay.
Yeasts co-expressing Cub fusion proteins with NubG fusion proteins or NubG (negative control of interaction) or NubWT (positive control of interaction) were spotted in serial dilutions on a synthetic medium without Leu and Trp (control medium) or without Leu, Trp, His, Ade (selective medium). Yeast growth on control and selective medium was recorded after 24h and 48h, respectively. OD: optical density.

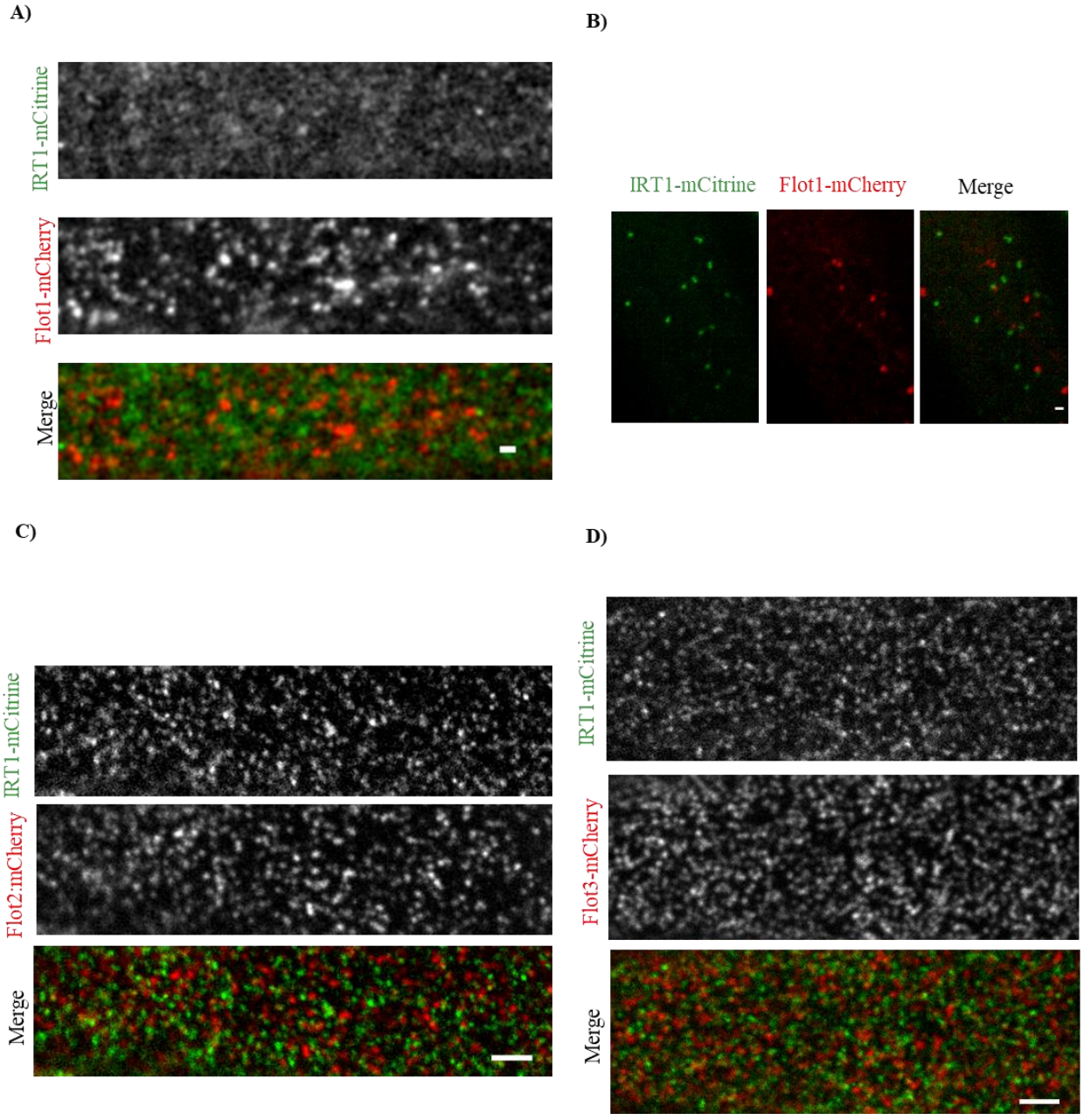

<u>Figure 27</u>. IRT1 does not *co-localize* with Flot1, Flot2 or Flot3 in plasma membrane microdomains.

Spinning-disk microscopy analysis performed on the roots of Col-0/35S::IRT1-mCitrine plants co-expressing 35S::Flot1-mCherry **(A and B)**, 35S::Flot2-mCherry **(C)** or 35S::Flot3-mCherry **(D)**. For (A), (C) and (D), images were acquired at the very surface of root epidermal cells allowing the visualization of PM microdomains, whereas for (B) the acquisition was performed inside the cell revealing distinct IRT1-mCitrine and Flot1-mCherry labeled endosomes. Plants were grown in lack of Fe and in presence of physiological concentrations of non-iron metals during 7 days. Scale bars 2 µm.

Supplemental Data

Supplemental table 1. Compilation and brief description of the proteins found in mass spectrometry analyses as putative IRT1 interactors. Number of total peptides refers to the total number of peptides that were found in each one of the two independent mass spectrometry analyses that were carried out. The number of transmembrane domains present in each protein was obtained thanks to the datebase AramTMCon (http://aramemnon.uni-koeln.de). The subcellular localization of each protein was investigated in SUBACon (http://suba.plantenergy.uwa.edu.au).

			Number of unique peptides			
Accession	**Protein name**	**Protein size (kDa)**	**Experiment 1**	**Experiment 2**	**Number of transmembrane domains**	**Subcellular localization**
AT3G15950	Endoplasmic reticulum body component NAI2	85	3	27	0	endoplasmic reticulum
AT3G11130	Clathrin heavy chain	193	7	24	0	plasma membrane
AT1G21750	Protein disulfide isomerase 5	56	6	16	0	endoplasmic reticulum
AT4G30190	H(+)-ATPase 2	104	5	13	10	plasma membrane
AT1G04820	Tubulin alpha-4 chain	50	6	6	0	cytosol
AT3G01290	Hypersensitive induced reaction 2	31	5	12	0	plasma membrane
AT2G03510	SPFH/Band 7/PHB domain-containing membrane-associated protein family	41	3	8	1	endoplasmic reticulum
AT5G27540	MIRO-related GTP-ase 1	72	4	21	1	mitochondrion
AT1G78900	Vacuolar ATP synthase subunit A	69	3	10	0	vacuole/golgi
AT2G20580	26S Proteasome regulatory subunit S2 1A	98	6	8	2	cytosol/nucleus
AT4G34200	Phosphoglycerate dehydrogenase 1	63	5	8	0	plastid
AT1G79920	Heat shock protein 70 family protein	92	3	4	0	golgi
AT5G17330	Glutamate decarboxylase 1	57	4	5	0	cytosol
AT2G32730	26S proteasome regulatory complex RPN2	109	3	2	1	nucleus/cytosol
AT4G02930	GTP binding Elongation factor Tu family protein	49	4	7	0	mitochondrion

AT1G09640	Translation elongation factor EF1B	47	6	7	0	cytosol
AT3G17390	Methionine adenosyltransferase 4	43	3	5	0	nucleus/plasma membrane
AT3G06850	Dark Inducible 3	53	6	4	0	mitochondrion
AT2G20140	AAA-type ATPase family protein	49	2	3	0	nucleus/cytosol
AT3G52930	Aldolase superfamily protein	39	2	3	0	cytosol
AT4G13940	S-adenosyl-L-homocysteine hydrolase 1	53	6	3	0	cytosol
AT3G29360	UDP-glucose 6-dehydrogenase family protein	53	4	3	0	extracellular
AT1G57720	Translation elongation factor EF1B	46	3	3	0	cytosol
AT5G23540	Mov34/MPN/PAD-1 family protein	34	2	3	0	nucleus/cytosol
AT5G09900	Regulatory particle non-ATPase subunit 5A	51	3	2	0	nucleus/cytosol
AT1G54000	GDSL Lipase-like protein 22	43	2	2	0	vacuole
AT1G29310	SecY protein transport family protein	52	2	2	10	golgi
AT4G31940	Cytochrome P450	59	3	2	2	endoplasmic reticulum
AT1G10670	ATP-citrate lyase A-1	47	2	2	0	cytosol
AT1G22410	Class-II DAHP synthetase family protein	58	3	2	0	plastid
AT3G04120	GAPC1 glyceraldehyde-3-phosphate dehydrogenase C subunit 1	37	6	11	0	nucleus/cytosol
AT2G36530	Low expression of osmotically responsive gene 2	48	7		0	cytosol
AT4G24190	Heat shock protein 90.7	94	7		0	endoplasmic reticulum
AT5G09810	Actin 7	42	4		0	cytosol
AT5G19510	Translation elongation factor EF1B/ribosomal protein S6 family protein	24	4		0	cytosol
AT3G19820	DWARF1 / DIMINUTO	65	4		1	endoplasmic reticulum
AT5G55070	Dihydrolipoamide succinyltransferase	50	3		0	mitochondrion
AT1G79920	Heat shock protein 70 family protein	92	3		0	golgi
AT1G53750	Regulatory particle triple-A 1A	48	3		0	nucleus/cytosol

AT3G14990	Class I glutamine amidotransferase-like superfamily protein	42	2		0	golgi
AT5G19760	Mitochondrial substrate carrier family protein	32	2		2	mitochondrion
AT2G20140	AAA-type ATPase family protein	49	2		0	nucleus/cytosol
AT3G13610	Feruloyl-Coenzyme A 6’-Hydroxylase 1 (F6'H1)	41	2		0	peroxisome
AT3G57010	Calcium-dependent phosphotriesterase superfamily protein	42	2		1	endoplasmic reticulum
AT3G48930	OB-fold-like protein	18	2		0	cytosol
AT4G33650	Dynamin-related protein 3A	90	2		0	mitochondrion
AT2G33210	Heat shock protein 60-2	62	2		0	mitochondrion
AT1G70770	Protein of unknown function DUF2359	67	2		1	endoplasmic reticulum
AT1G79930	Heat shock protein 91	92		25	0	cytosol
AT1G09080	Binding Protein 3 (BIP3)	75		13	1	endoplasmic reticulum
AT4G27860	Vacuolar iron transporter (VIT) family protein	68		11	5	vacuole
AT1G77510	Protein disulfide isomerase 6	56		10	0	endoplasmic reticulum
AT5G56000	Heat shock protein 90.4	80		9	0	cytosol
AT5G24290	Vacuolar iron transporter (VIT) family protein	61		8	4	vacuole
AT2G46750	L -Gulono-1,4-Lactone Oxidase 2	65		8	0	extracellular
AT1G22300	14-3-3 Epsilon	29		7	0	cytosol
AT1G35160	14-3-3 Phi	30		7	0	cytosol
AT3G01280	Voltage dependent anion channel 1	29		7	0	mitochondrion
AT5G56030	Heat shock protein 81.2	80		7	0	cytosol/nucleus
AT3G63460	SEC31b	120		6	0	golgi
AT3G62360	Carbohydrate-binding-like fold	133		5	1	endoplasmic reticulum
AT1G73260	Kunitz trypsin inhibitor 1	24		5	0	extracellular
AT1G06950	Translocon at the inner envelope membrane of chloroplasts 110	112		5	3	plastid
AT2G01530	MLP-like protein 329	18		5	0	cytosol

AT3G13930	Dihydrolipoamide acetyltransferase	58		5	0	mitochondrion
AT3G51660	Tautomerase	12		4	0	peroxisome
AT5G10450	14-3-3 Lambda	28		4	0	cytosol
AT2G30490	Cinnamate-4-hydroxylase	58		4	1	endoplasmic reticulum
AT5G61790	Calnexin 1	60		4	1	endoplasmic reticulum
AT1G20260	Vacuolar ATP synthase subunit B1	54		4	0	vacuole
AT1G70850	MLP-like protein 34	36		4	0	cytosol
AT1G59870	Pleiotropic drug resistance 8 / Penetration 3	165		4	14	plasma membrane
AT3G20380	TRAF-like family protein	43		4	0	extracellular
AT4G28470	26S proteasome regulatory subunit S2 1B	98		4	4	cytosol/nucleus
AT1G79550	Phosphoglycerate kinase 3	42		4	0	cytosol
AT5G43010	Regulatory particle triple-A ATPase 4A	45		4	0	cytosol/nucleus
AT5G60660	Plasma membrane intrinsic protein 2;4	31		3	6	plasma membrane
AT1G01580	Ferric reduction oxidase 2	82		3	11	plasma membrane
AT2G37040	Phenylalanine ammonia lyase 1	79		3	0	cytosol
AT2G37170	Plasma membrane intrinsic protein 2;1	30		3	6	plasma membrane
AT1G07920	GTP binding Elongation factor Tu family protein	50		3	0	cytosol
AT1G78570	Rhamnose biosynthesis 1	75		3	0	cytosol
AT2G38040	Acetyl Co-enzyme a carboxylase carboxyltransferase alpha subunit	85		3	0	plastid
AT1G65720	Unknown protein	20		3	1	extracellular
AT1G50200	ACD Alanyl-tRNA synthetase	110		3	0	mitochondrion
AT1G71220	UDP-glucose:glycoprotein glucosyltransferases	182		3	0	endoplasmic reticulum
AT3G46740	Translocon at the outer envelope membrane of chloroplasts 75-III	89		3	0	plastid
AT4G18800	RAB GTPase homolog A1D	24		3	0	golgi
AT4G20850	Tripeptidyl peptidase	152		3	0	plastid
AT4G21150	Ribophorin II family protein	75		3	3	endoplasmic reticulum

AT5G54500	Flavodoxin-like quinone reductase 1	22		3	0	plasma membrane
AT1G20200	Embryo defective 2719	56		3	0	cytosol/nucleus
AT1G30230	Elongation factor 1B beta	25		3	0	cytosol
AT1G47128	Responsive to dehydration 21	51		3	0	extracellular
AT4G09000	General regulatory factor 1	30		3	0	cytosol
AT5G15090	Voltage dependent anion channel 3	29		3	0	mitochondrion
AT1G45201	Triacylglycerol lipase-like 1	55		3	3	golgi
AT5G19990	Regulatory particle triple-A ATPase 6A	47		3	0	cytosol/nucleus
AT1G11910	Aspartic proteinase A1	55		3	0	vacuole
AT1G55020	Lipoxygenase 1	98		2	0	golgi
AT1G62020	Coatomer alpha subunit	137		2	0	cytosol
AT4G31480	Coatomer beta subunit	106		2	1	cytosol
AT4G08850	Leucine-rich repeat receptor-like protein kinase family protein	115		2	2	plasma membrane
AT2G45960	Plasma membrane intrinsic protein 1;2	31		2	6	plasma membrane
AT5G11560	Catalytics	109		2	1	endoplasmic reticulum
AT2G21660	Glycine rich protein 7	17		2	0	nucleus
AT5G20010	RAS-related nuclear protein-1	25		2	0	cytosol
AT1G18270	Ketose-bisphosphate aldolase class-II family protein	147		2	0	cytosol
AT3G61430	Plasma membrane intrinsic protein 1;1	31		2	6	plasma membrane
AT4G17530	RAB GTPase homolog 1C	22		2	0	cytosol
AT1G07890	Ascorbate peroxidase 1	28		2	0	cytosol
AT1G22520	Domain of unknown function (DUF543)	20		2	1	mitochondrion
AT1G24510	TCP-1/cpn60 chaperonin family protein	59		2	0	cytosol
AT1G49240	Actin 8	42		2	0	cytosol
AT3G02780	Isopentenyl pyrophosphate:dimethylallyl pyrophosphate isomerase 2	33		2	0	plastid
AT3G44330	M28 Zn-peptidase nicastrin	62		2	1	endoplasmic reticulum
AT4G37910	Mitochondrial heat shock protein 70-1	73		2	0	mitochondrion

AT5G05010	Clathrin adaptor complexes medium subunit family protein	58		2	0	golgi
AT5G25780	Eukaryotic translation initiation factor 3B-2	82		2	0	cytosol
AT5G14040	Phosphate transporter 3;1	40		2	2	mitochondrion
AT3G26440	Transmembrane protein (DUF707)	45		2	1	golgi
AT5G41670	6-phosphogluconate dehydrogenase 3	53		2	0	mitochondrion
AT2G21390	Coatomer, alpha subunit	136		2	0	cytosol
AT5G07440	Glutamate dehydrogenase 2	45		2	0	mitochondrion
AT2G33040	Gamma subunit of Mt ATP synthase	35		2	0	mitochondrion
AT4G26910	Dihydrolipoamide succinyltransferase	50		2	0	mitochondrion
AT3G44110	DNAJ homologue 3	46		2	0	nucleus
AT1G78300	14-3-3 Omega	29		2	0	cytosol
AT3G02520	General regulatory factor 7	30		2	0	plasma membrane/cytosol
AT1G18070	Translation elongation factor EF1A	59		2	0	cytosol
AT5G44340	Tubulin beta chain 4	50		2	0	cytosol
AT5G43060	Granulin repeat cysteine protease family protein	51		2	0	extracellular
AT1G35620	Protein disulfide isomerase 8	50		2	1	endoplasmic reticulum
AT3G09820	Adenosine kinase 1	38		2	0	cytosol
AT1G53240	Mitochondrial malate dehydrogenase 1	36		2	0	mitochondrion
AT1G74020	Strictosidine synthase 2	35		2	0	vacuole
AT2G30050	SEC13a	33		2	0	cytosol/nucleus
AT2G32080	Purin-rich alpha 1	32		2	0	golgi
AT2G32920	Protein disulfide isomerase 9	48		2	0	endoplasmic reticulum
AT2G40010	Ribosomal protein L10 family protein	34		2	0	cytosol
AT3G42050	Vacuolar ATP synthase subunit H family protein	50		2	0	golgi/vacuole
AT5G62740	Hypersensitive induced reaction 4	31		2	0	plasma membrane

A)

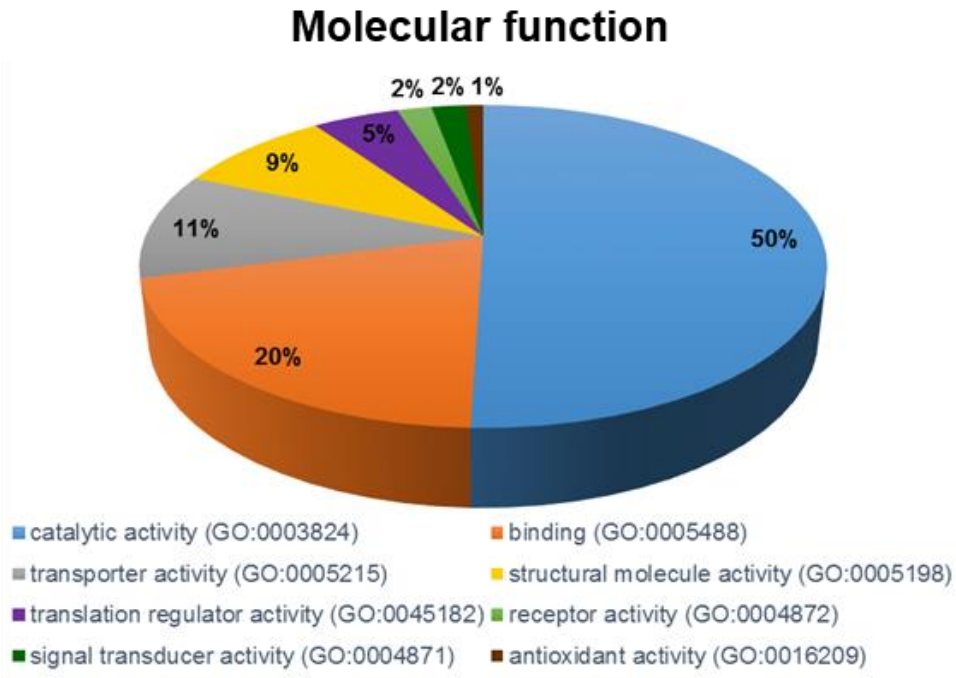

B)

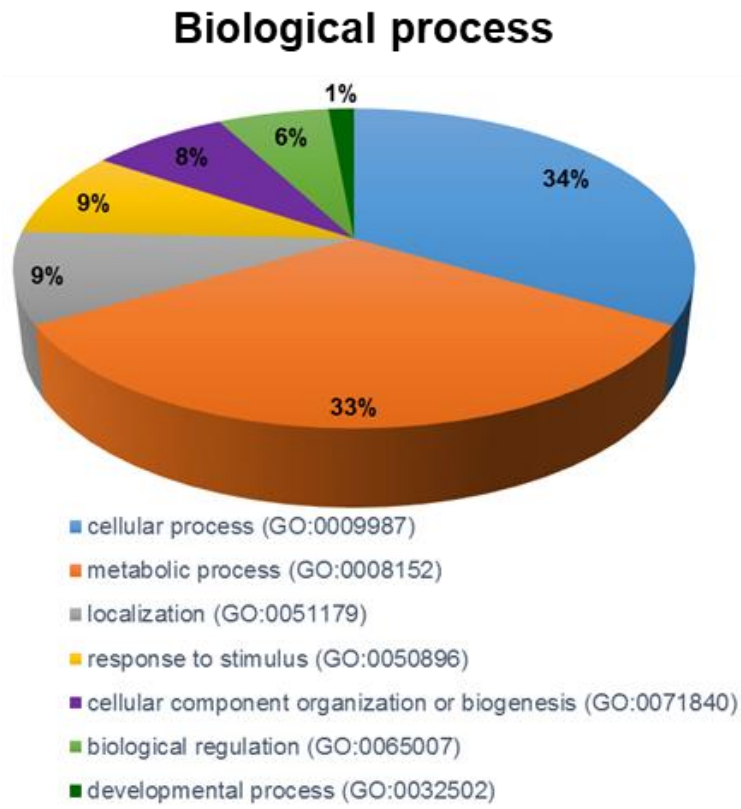

Supplemental Figure 1. Characteristics of IRT1 interactome. (A) Molecular function of IRT1 interactors and **(B)** the biological process in which these proteins are involved were classified using Gene Ontology annotation (http://www.pantherdb.org/).

<u>Supplemental Table 2.</u> IRT1 interactants involved in intracellular trafficking or metal homeostasis.
This table was created using Gene Ontogeny (GO) annotations from The *Arabidopsis* Information resource (TAIR) (https://www.*Arabidopsis*.org).

	Accession	Protein name
Intracellular trafficking	AT3G11130	Clathrin heavy chain
	AT1G04820	Tubulin alpha-4 chain
	AT1G29310	SecY protein transport family protein
	AT5G09810	Actin 7
	AT4G33650	Dynamin-related protein 3A
	AT3G63460	SEC31b, COPII component
	AT4G18800	RAB GTPase homolog A1D
	AT1G62020	Coatomer alpha subunit, COPI component
	AT4G31480	Coatomer beta subunit, COPI component
	AT4G17530	RAB GTPase homolog 1C
	AT1G49240	Actin 8
	AT5G05010	Clathrin adaptor complexes medium subunit family protein
	AT2G21390	Coatomer, alpha subunit, COPI component
	AT5G44340	Tubulin beta chain 4
	AT2G30050	SEC13a, COPII component
Metal homeostasis	AT4G30190	H(+)-ATPase 2
	AT4G31940	Cytochrome P450
	AT3G13610	Feruloyl-Coenzyme A 6’-Hydroxylase 1 (F6'H1)
	AT4G27860	Vacuolar iron transporter (VIT) family protein
	AT5G24290	Vacuolar iron transporter (VIT) family protein
	AT2G01530	MLP-like protein 329
	AT1G59870	Pleiotropic drug resistance 8 / Penetration 3
	AT1G01580	Ferric Reduction Oxidase 2
	AT1G07890	Ascorbate peroxidase 1

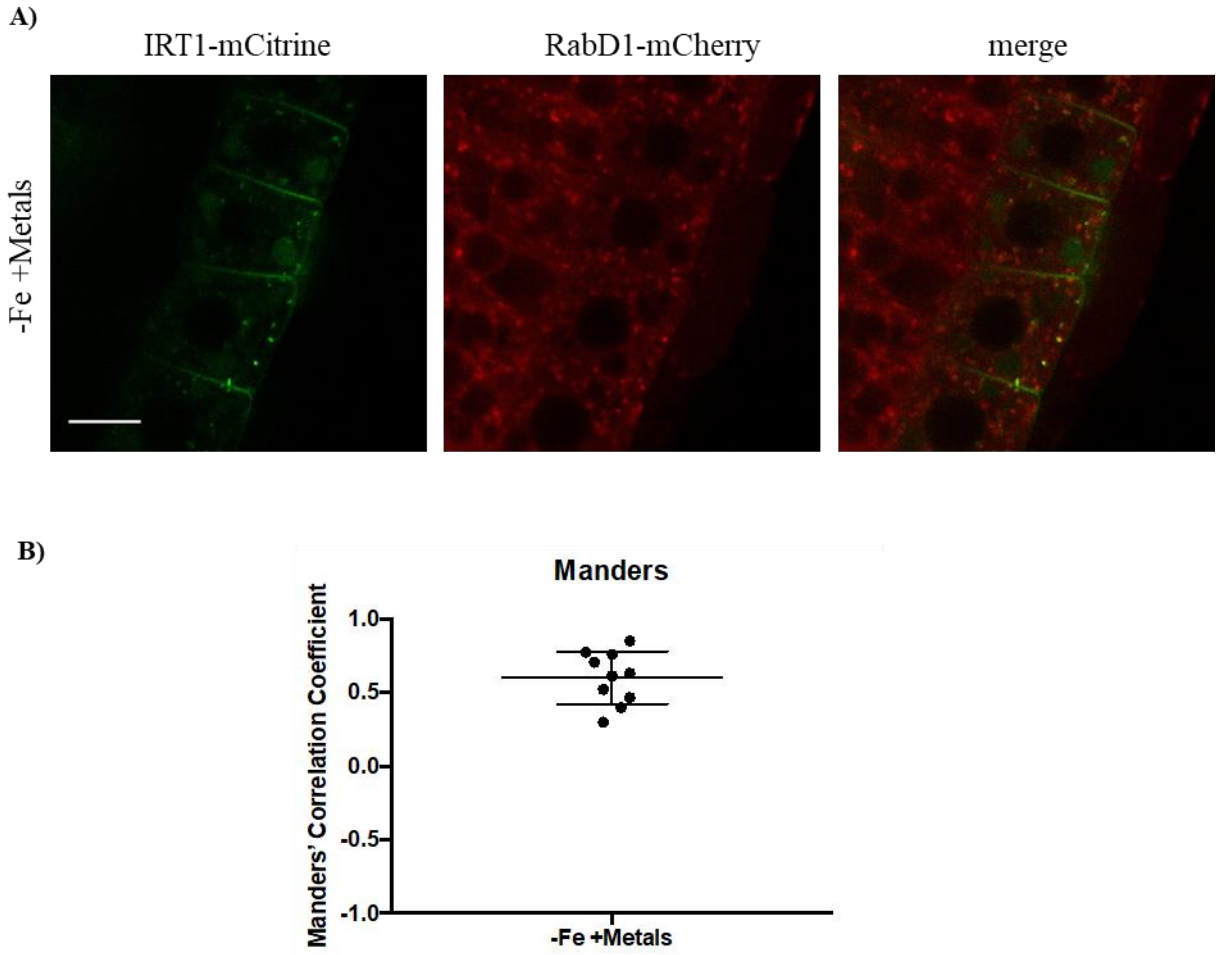

<u>Supplemental Figure 2.</u> IRT1 co-localizes with the early endosomal marker RabD1
(A) Confocal microscopy analyses of *irt1-1*/IRT1::IRT1-mCitrine transgenic line crossed with the Wave Line number 25 expressing RabD1-mCherry fusion protein under the control of Ubi10 promoter (Geldner et al., 2009). Plants were grown in iron deficient condition for 11 days before visualization. Scale bars = 10 µm. **(B)** Quantification of the co-localizationbetween IRT1-mCitrine and RabD1-mCherry. Mander's overlap coefficient of 0.6.

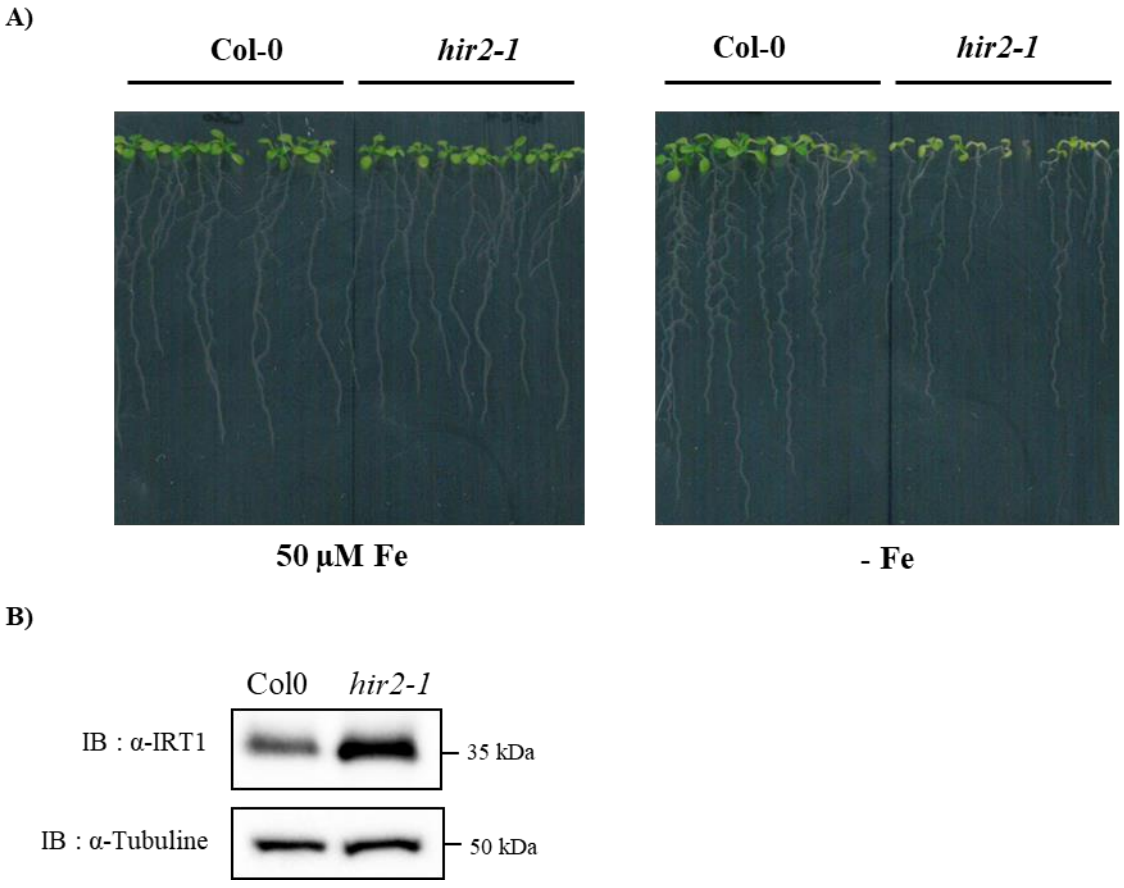

<u>Supplemental Figure 3.</u> The *hir2-1* mutant is hypersensitive to a lack of iron compared to WT plants and over-accumulates IRT1 protein.

(A) The *hir2-1* mutant*,* described in Qi et al. (2011) and WT plants (Col-0) were grown during 14 days on MS/2 medium in absence of Fe (-Fe) or in presence of sufficient amount of Fe (50 µM-Fe-EDTA). **(B)** Total proteins were extracted from the roots of plants grown in lack of Fe as in (A) and were then subjected to immunodetections with an anti-IRT1 antibody or with an anti-tubulin antibody (loading control). Analysis were performed in triplicates and a representative immunoblot is shown.

Material and Methods

Plant material and growth conditions

Arabidopsis thaliana wild type plants (Col-0, Col-gl1,Ws and Ws-4), the *fro2* loss-of-function mutant named *frd1-1* (Yi and Guerinot, 1996), the previously described *irt1-1*/IRT1::IRT1-mCitrine and Col0/35S::IRT1-mCitrine lines (Dubeaux *et al.*, 2018), the different flotillins loss-of-function mutants *flot1, flot2, flot3* (respectively SALK_203966C, FLAG_352D08 and SALK_143325C, kindly provided by Jan Martinec), the *aha2* loss-of-function mutant (SALK_022010), *HIR2* loss-of-function mutants *hir2-1* (SALK_092306) (Qi *et al.*, 2011) and *hir2-2* (SALK_124393C) which was isolated in our laboratory (See Table 1 for genetic backgrounds of the mutants) and the various transgenic plants generated in this study were vertically grown in sterile conditions at 21ºC with 16 h light/8 h dark cycles, using half-strength Murashige and Skoog (MS/2) medium (Murashige and Skoog, 1962). MS/2 contained 1% sucrose, 1% agar and different concentrations of non-Fe IRT1 metal substrates (Fe, Zn, Mn, Co). Hence, depending on the experiment (see below), plants were grown in the absence of iron to induce the iron-deficiency response and in the presence of physiological concentrations of IRT1 secondary substrates Zn, Mn and Co (-Fe +Metals) or in the presence of an excess of these metals (-Fe +++Metals) which corresponds to a 10-fold concentration of Zn, Mn and Co, using the MS/2 medium as a reference (Dubeaux *et al.*, 2018). On the other hand, plants may also grow in iron replete conditions by using MS/2 medium containing 50 µM or 100 µM Fe-EDTA and physiological concentrations of the non-iron metals Zn, Mn and Co (+Fe).

For immunopurifications followed by mass spectrometry analyses, *irt1-1*/IRT1::IRT1-mCitrine transgenic lines and Ws wild-type plants, used as a negative control, were initially grown for 9 days on MS/2 medium containing 50 µM Fe-EDTA, then transferred for 5 days onto a -Fe +Metals medium to induce IRT1-mCitrine expression and finally subjected to a -Fe +++ Metals treatment for 48 h. To confirm the interactions between IRT1, FRO2, AHA2 and HIR2 by co-immunopurifications, the various genotypes were grown for 11 days on MS/2 medium containing 50 µM Fe-EDTA, and then transferred for 4 days on a -Fe +Metals medium supplemented with 300 µM of the iron chelator named Ferrozine [3-(2-pyridyl)-5,6-diphenyl-1,2,4-triazine sulfonate] to ensure a rapid and strong expression of genes under the control of *IRT1* and *FRO2* promoters.

To analyze mCherry-FRO2, AHA2-GFP and IRT1-mCitrine ubiquitination profiles, the appropriate transgenic lines as well as wild type plants used as negative controls were grown for 11 days on -Fe +Metals solid medium. Then, plants were transferred for 2 h in -Fe +Metals (control) or –Fe +++Metals liquid medium as previously described (Dubeaux *et al.*, 2018).

For microscopy analysis, transgenic lines expressing IRT1/AHA2/FRO2 fusion proteins under the control of *IRT1* promoter, were first grown for 11 days on a -Fe +Metals medium to ensure protein expression. Then, to investigate the effect of non-iron metals on the subcellular localization of the fusion proteins, plants were subjected for 2 h to a -Fe + Metals (control) or -Fe +++ Metals liquid treatments. The localization of mCherry-FRO2 and HIR2-mCherry fusion proteins expressed in *frd1-1*/FRO2::mCherry-FRO2 and *hir2-2*/HIR2::HIR2-mCherry transgenic lines, respectively, was analyzed in plants grown during 11 days in -Fe + Metals condition. Transgenic lines expressing IRT1-mCitrine under the control of the 35S promotor were grown for 7 days in -Fe +Metals condition before imaging.

For mCherry-FRO2 functionality test followed by protein extraction, *frd1-1*/FRO2::mCherry-FRO2 transgenic lines, *frd1-1* mutant and Col-gl1 wild-type plants were grown for 11 days on MS/2 lacking iron (-Fe +Metals) or supplemented with 100 µM Fe-EDTA (control conditions).

For phenotypic analysis, *hir2-2* mutant and Col-0 plants (control) were grown for 14 days in the absence of iron, in the presence of low amount of iron (2 µM Fe-EDTA) or in iron replete condition (100 µM Fe-EDTA, control condition) each time with physiological concentrations of non-iron metals. The resulting material was used to perform immunoblots on root protein extracts, RNA extractions from roots and measurement of chlorophyll content in leaves. For metal content measurements in *hir2-2* mutant and Col-0 leaves, plants were grown using the same media as for phenotypic analysis but for 8 days, in addition plants were also grown in the presence of an excess of non-iron metals (-Fe +++Metals). For HIR2-mCherry functionality test, *hir2-2*/35S::HIR2-mCherry transgenic lines, *hir2*-2 mutant and Col-0 plants were grown for 14 days in the presence of low amount of iron (2 µM Fe-EDTA) or in iron replete condition (100 µM Fe-EDTA, control condition) each time with physiological concentrations of non-iron metals. Roots from iron-starved transgenic lines and *hir2-2* (negative control) were collected to analyze HIR2-mCherry protein accumulation by immunoblot as detailed below.

For plant cultures in the greenhouse, *Arabidopsis thaliana* and *Nicotiana benthamiana* were grown at 21°C and 24°C, respectively, under long day conditions.

Constructions and generation of *Arabidopsis* transgenic lines

To perform complementation assays of the *hir2-2* mutant, a *HIR2* genomic fragment of 2.700 bp (*HIR2g*) containing *HIR2* coding sequence and *HIR2* promoter was amplified from Col-0 genomic DNA using high-fidelity Phusion polymerase (Thermo Scientific) and the primers listed in Table 3. *HIR2g* was subsequently introduced by NotI restriction inside the PMLBART vector, that confers resistance to Basta in plants.

All the other constructions generated during this work were obtained using MultiSite Gateway® Three-Fragment Vector Construction kits (Life Technologies), according to the specifications of the manufacturer. Thus, open reading frames (ORF) of *FRO2*, *AHA2*, *HIR2*, *LTi6b* and *mCherry* were amplified with the high-fidelity Phusion polymerase (Thermo Scientific) from *Arabidopsis* Col-0 cDNA using the primers listed in Table 3. In addition, to create a hyperactive form of AHA2 protein, a truncated version of *AHA2* lacking the 66 last codons and called *AHA2Δ66* was also generated (Regenberg *et al.*, 1995).

Depending on the final use, the stop codon of the different ORF was conserved or not (see Table 4). Amplified DNA were then cloned in Invitrogen entry vectors, either pDONR 221 (when aiming C-terminal fusion) or pDONR P2RP3 (when aiming N-terminal fusion). *FRO2* promoter corresponding to a sequence of 1,845 pb upstream of the *FRO2* start codon and *HIR2* promoter corresponding to a sequence of 1,241 pb upstream of the *HIR2* start codon were amplified from *Arabidopsis thaliana* genomic DNA with primers described in Table 3 and cloned into pDONR P4P1R plasmid. All the entry vectors generated during this thesis are listed in Table 4. Entry vectors carrying the IRT1, PIN2 and 35S promoters (pDONR.P4P1R-IRT1/PIN2/35S) or the GFP and the mCherry coding sequence allowing C-terminal fusions (pDONR P2RP3-GFP/mCherry) were previously described (Marquès-Bueno *et al.*, 2016; Dubeaux *et al.*, 2018).

Final destination vectors for expression in plants were obtained by multisite Gateway® recombination using the entry vectors described above and the pH7m34GW (hygromycin resistance in plants) and pK7m34GW (kanamycin resistance in plants) destinations plasmids used for mCherry and GFP fusions, respectively. The final vectors generated during this thesis and allowing the expression of the proteins of interest fused to different tags under the control of specific promoters are listed in Table 4 and the respective primers are enlisted in Table 3. As part of a collaboration with the team of Jan Martinec from the Institute of Experimental Botany in Prague, Czech Republic, genetic constructions named pGreen0029.35S::Flot1/Flot2/Flot3-mCherry and allowing the constitutive expression in plants

of these three flotillins fused to the mCherry were generated by Michal Danek, a Czech PhD student participating in the project (Table 4) .

After verification by sequencing, the final constructions were introduced in *Agrobacterium tumefaciens* strain AGL0. In the case of pGreen0029.35S::Flot1/Flot2/Flot3-mCherry vectors, AGL0 was co-tranformed with the pSOUP plasmid. *Arabidopsis thaliana* was then transformed following the floral dip protocol described in Clough and Bent, 1998 to generate the different transgenic lines that are described in Table 5.

During this work two crosses were also performed: *irt1-1*/IRT1::IRT1-mCitrine transgenic line was crossed with the Wave Line number 25 expressing RabD1-mCherry fusion protein under the control of Ubi10 promoter (Geldner *et al.,* 2009) and Col-0/35S::IRT1-mCitrine line was crossed with the *hir2-2* mutant.

Transient expression of proteins in *Nicotiana benthamiana*

Agrobacterium tumefaciens strain AGL0 was transformed with the constructions of interest and grown in LB medium containing the required antibiotics for 16 h at 28°C. In parallel a culture of the *Agrobacterium* strain C58 containing the p19 vector coding the p19 viral-encoded suppressor of gene silencing was also performed. Co-expression of p19 with a protein of interest allows to enhance the expression of the latter in *Nicotiana benthamiana,* (Voinnet *et al.,* 2003). Then, AGL0 strains carrying the vectors of interest were mixed with C58p19 strain, after centrifugation at 3,000 *g* for 10 min, the pellet of *Agrobacterium* was resuspended in infiltration media (10 mM MES KOH pH 5.6, 10 mM $MgCl_2$, 150 µM acetosyringone). The final OD_{600} for AGL0 strains and C58p19 were 0.6 and 0.3, respectively. After 2 h of incubation at 21°C, *Agrobacterium* suspensions were used to infiltrate 21 day-old *N.benthamiana* leaves. After 48 h, leaves expressing the proteins of interest were collected for subsequent experiments.

Metal extraction and analysis

Plants were grown as describe above. The aerial parts of plants belonging to the same genotype and grown in a same metal condition were cut and pooled together, collected with plastic forceps and washed in 10 mM EDTA pH 5.5. After rinsing twice with milliQ water, tissues were dried for at least 48 h at 70ºC. Afterwards, dry tissues were weighted and transferred into 15 ml tube containing 500 µl of H_2O_2 and 1 ml of HNO_3. Total tissue digestion was achieved by heating the samples in a thermoblock (ED36 LabTech) in three steps: first 100ºC for 60 min, secondly 120ºC for 360 min, thirdly 80ºC for 60 min. After digestion, milliQ

water was added to the extracts to reach a final volume of 4 ml. The metal concentrations were measured by Microwave Plasma Atomic Emission Spectroscopy (MP-AES) (Agilent 4200 MP-AES) and expressed as µg of metal per mg of dry mass tissue.

Immunopurifications

Immunopurifications (IP) were performed on approximatively 500 mg of *Arabidopsis* roots, mostly as previously described (Dubeaux *et al.*, 2018). Briefly, for IRT1-mCitrine IP followed by mass spectrometry, for co-IP analysis between IRT1-mCitrine and mCherry-FRO2/HIR2-mCherry, as well as for co-IP analysis between mCherry-FRO2 and endogenous AHA2, roots grinded in liquid nitrogen were resuspended in IRT1 solubilization buffer (50 mM Tris-HCl pH 7.4, 150 mM NaCl, 5 mM EDTA, 1% n-Dodecyl β-D-maltoside (DDM) and plant specific protease inhibitors (Sigma-Aldrich), using 300 µl of buffer per 100 mg of tissue. For co-IP analysis between IRT1-mCitrine and endogenous AHA2, grinded roots were resuspended in RIPA buffer (50 mM Tris-HCl (pH 7.5), 150 mM NaCl, 0.5% sodium deoxycholate, 1% IGEPAL®CA-630, 0.1% SDS and plant specific protease inhibitors (Sigma-Aldrich)) using 300 µl of RIPA per 100 mg of tissue. After two successive centrifugations at 3,800 *g* for 10 min at 4 °C, the resultant supernatants were collected and solubilization of membrane proteins was continued for 1 h 30 min at 4 °C on a rotating wheel. Samples were then centrifuged at 100,000 *g* for 1 h at 4 °C to remove unsolubilized material and supernatants containing solubilized proteins were recovered for IPs. GFP and mCitrine fusion proteins were immunopurified using µMACS GFP isolation kit (Miltenyi Biotec) while IP of mCherry fusion proteins was performed using RFP-Trap®_MA magnetic beads (Chromotek), following the instructions of the manufacturers. Before elution, four-five washes were performed with IRT1 solubilization buffer or RIPA buffer depending on the immunopurification type.

To analyze the ubiquitination profile of AHA2-GFP and IRT1-mCitrine, the solubilization of fusion proteins as well as the IP procedure were exactly performed as previously described (Dubeaux *et al.*, 2018). The same protocol was used for mCherry-FRO2 except that the protein was immunopurified with RFP-Trap® MA magnetic beads (Chromotek).

Mass spectrometry analysis

For sample preparation, proteins from each eluate were separated by SDS-PAGE in order to fractionate the protein samples into 2 or 3 fractions, including proteins from 10 to 63

kDa and above 63 kDa, respectively, to exclude abundant contaminating IRT1-mCitrine protein at 63 kDa. After Coomassie Blue staining, each gel fraction was cut in bands and subjected to in-gel trypsin digestion with the Progest robot (Genomic Solutions) using standard conditions including reduction and alkylation as described previously (Blanchet *et al.*, 2014). Tryptic peptides extracted from the different bands of each gel fraction were pooled, vacuum dried and resuspended in 0.1% (v/v) formic acid prior to nanoLC-MS/MS mass spectrometry analyzes. The same cutting pattern of the SDS-PAGE lane was performed for each eluate.

Tryptic peptides from the two or three SDS-PAGE fractions from each eluate were analyzed separately by nanoLC-MS/MS with the Triple-TOF 4600 mass spectrometer (ABSciex) coupled to the nanoRSLC ultra performance liquid chromatography (UPLC) system (Thermo Scientific) equipped with a trap column (Acclaim PepMap100C18, 75 µmi.d.× 2 cm, 3 µm) and an analytical column (Acclaim PepMapRSLCC18, 75 µmi.d.× 50 cm, 2 µm, 100 Å). Peptides were loaded at 5 µl/min with 0.05% TFA in 5% acetonitrile and peptides separation was performed at a flow rate of 300nl/min with a 5 to 35% solvent B gradient in 40 min. Solvent A was 0.1% formic acid in water, and solvent B was 0.1% formic acid in 100% acetonitrile. NanoLC-MS/MS experiments were conducted in a Data Dependent acquisition method by selecting the 20 most intense precursors for CID fragmentation with Q1 quadrupole set at low resolution for better sensitivity.

Protein identification was performed by processing raw data with MS Data Converter software (AB Sciex) for generating .mgf data files and protein identification were performed using the MASCOT search engine (Matrix science, London, UK) against the Swissprot and TAIR10 databases with carbamidomethylation of cysteines set as fixed modification, oxidation of methionines as variable modifications. Peptide and fragment tolerance were respectively set at 20 ppm and 0.05 Da. Results were analyzed with Scaffold 3.6.5 software (Proteome Software). Proteins were validated when identified with at least two unique peptides and 95 % probability levels for both peptides and proteins.

Extraction of root total proteins and immunoblots

Total proteins were extracted from around 100 mg of roots grinded in liquid nitrogen and directly resuspended in 2X SDS sample buffer (300 µl of buffer per 100 mg of tissue). Samples were heated at 65°C during 10 min, centrifuged 10 min at 20,000 *g* and finally supernatants were collected and directly used for SDS-PAGE.

Immunoblot analysis were performed as previously described (Barberon *et al.*, 2011). The efficiency of protein transfer on polyvinylidene difluoride (PVDF) membrane was verified

using the Stain-Free Imaging Technology (Bio-Rad). Immunodetection of GFP and mCitrine fusion proteins was performed using an anti-GFP antibody conjugated to horseradish peroxidase (HRP) (Miltenyi Biotec 130-091-833, 1/5,000). mCherry fusion proteins were monitored with a rabbit anti-DsRed antibody (Clontech 632496, 1/5,000). Immunodetection of endogenous IRT1 protein was performed using an affinity-purified antipeptide IRT1 antibody diluted 1/3,000 (Séguéla *et al.*, 2008). Endogenous AHA2 protein was immunodetected with the rabbit anti-PMA2 (W1C) antibody diluted 1/15,000 (Morsomme *et al.*, 1998). Ubiquitin modifications were detected with the P4D1 mouse anti-ubiquitin antibody (Millipore 05-944, 1/4,000). Anti-HIR antibody that recognizes HIR1, HIR2 and HIR4 isoforms was diluted 1/3,000 (Qi *et al.*, 2011). Loading controls were obtained by using anti-Histone3 antibody (Active Motif # 39763, 1/6,000), or anti-α tubulin antibody (Sigma-Aldrich T5168, 1/5,000). Depending on the primary antibody, the anti-rabbit IgG (Bio-Rad 170-6515) or the anti-mouse IgG (Bio-Rad 172-1011) secondary antibodies both coupled to HRP and diluted 1/20,000 were used. Detection of HRP chemiluminescence was performed using SuperSignal West Dura Extended Duration Substrate (Thermo Scientific) in a Chemidoc Touch Imaging system (Bio-Rad).

Preparation of microsomal fraction

Plant roots were grinded in liquid nitrogen and resuspended in microsomal extraction buffer (500 mM sucrose, 50mM HEPES, 5mM EDTA, pH 7.4 and plant specific protease inhibitors (Sigma-Aldrich)), using 300 µl of buffer per 100 mg of tissue. Cell debris were removed by two successive centrifugations at 3,800 *g* for 10 min at 4 ºC. Then the supernatant was collected and centrifuged at 100,000 *g* for 1 h at 4 ºC allowing to recover a pellet corresponding to microsomes. The microsomal fraction was then resuspended in 2X SDS sample buffer, heated at 65ºC for 10 min before SDS-PAGE analysis.

Constructions and split-ubiquitin assay

To generate split-ubiquitin vectors using the Gateway® technology, specific entry vectors were first created by cloning the *FRO2* ORF (Open Reading Frame) without the stop codon, the *AHA2* ORF, the *HIR2* ORF and the *IRT1* ORF with their stop codons into the pDONR 221 (Table 6). To amplify these different ORF we used the primers enlisted in Table 3 (see primer names followed by "stop"). The flotillins ORFs *FLOT1, FLOT2, FLOT3* without stop were introduced in pMetYC-Dest vectors. In addition we used the pDONR 221-BRI1 without the stop codon which was previously generated (Martins *et al.*, 2015) and the pDONR

221-AHA2 and pDONR 221-HIR2 without stop codons that were created in this study and were also used to generate plant expression vectors as mentioned above. To create final split-ubiquitin plasmids, *FRO2*, *AHA2*, *HIR2*, *FLOT1*, *FLOT2*, *FLOT3* and *BRI1* ORFs without the stop codons were inserted into pMetYC-DEST destination vector (Hachez *et al.*, 2014) to produce the constructs FRO2-Cub-PLV, AHA2-Cub-PLV, HIR2-Cub-PLV, FLOT1-Cub-PLV FLOT2-Cub-PLV, FLOT3-Cub-PLV and BRI1-Cub-PLV, where Cub corresponds to the C-terminal part of ubiquitin and PLV to a chimeric transcription factor named ProteinA-LexA-VP16 (Table 6). The expression of Cub-PLV fusions is under the control of the *met25* promoter that is repressed by methionine. *IRT1*, *AHA2* and *HIR2* ORFs carrying their stop codons were cloned into the pNX35-DEST destination vector to generate the NubG-IRT1, NubG-AHA2 and NubG-HIR2 fusions expressed under the control of the constitutive *ADH* promoter (Table 6). NubG corresponds to the mutated N-terminal part of ubiquitin that is unable to spontaneously reassemble with the C-terminal part of ubiquitin. The physical interaction between two membrane proteins fused to NubG and Cub-PLV can force the reassembly of the two parts of ubiquitin. The reconstituted ubiquitin molecule is then cleaved by yeast de-ubiquitinases allowing the release of the PLV transcription factor that will enter into the nucleus and induce the expression of reporter genes such as *ADE2* and *HIS3* (Grefen, 2014). The wild-type ubiquitin N-terminal fragment (NubWT), expressed under the control of the *ADH* promoter from the pNubWT-Xgate vector, can spontaneously reassemble with Cub and thus was used as a positive control of interaction in our split-ubiquitin assay. On the other hand, the NubG fragment expressed by the non-recombined pNX35-DEST vector was used as a negative control of interaction (Hachez *et al.*, 2014).

Split-ubiquitin assay was performed as previously described (Dubeaux *et al.*, 2018). Briefly, THY.AP4 yeast strain (MATa ; ade2-, his3-, leu2-, trp1-, ura3- ; lexA::ADE2, lexA::HIS3, LexA::lacZ) was co-transformed with the Nub and Cub constructs of interest and co-transformed cells were selected on SD medium lacking Leu and Trp. Then, yeasts co-expressing Cub-PLV fusion proteins with NubG fusion proteins or NubG (negative control of interaction) or NubWT (positive control of interaction) were dropped in serial dilutions (O.D. 1, 0.1, 0.01) onto SD medium without Leu and Trp (control medium) or onto SD medium lacking Leu, Trp, His, Ade (selective medium) supplemented with 500 µM methionine (250 µM methionine for IRT1/BRI1 interaction test) to repress the expression of the Cub-PLV fusion proteins. Yeast growth on control and selective medium was recorded after 24 h and 48 h at 30°C, respectively. Besides internal negative interaction tests performed by co-expressing Cub-

PLV fusion proteins with NubG, co-expression of NubG-IRT1 and BRI1-Cub-PLV was used as an additional negative control.

The split-ubiquitin bridge assay

To allow for the expression in yeast of a non-tagged version of AHA2 under the control of the constitutive *PMA1* promoter, the pDONR 221-AHA2 with stop was recombined into the pDR195GW destination vector, that contains a uracil synthesis gene, using the Gateway technology (Table 6). To investigate whether AHA2 is able to create a bridge between IRT1 and HIR2 proteins, a split-ubiquitin bridge assay (Grefen, 2014) was performed by co-expressing NubG-IRT1, HIR2-Cub-PLV and AHA2 in THY.AP4 cells. As negative controls, yeasts were co-transformed with NubG-IRT1 and HIR2-Cub-PLV constructs and the pDR195 empty vector, in parallel yeasts were also co-transformed with HIR2-Cub-PLV and pDR195-AHA2 constructs and the non-recombined pNX35-DEST vector which allows for the expression of NubG. As a positive control, THY.AP4 cells were co-transformed with the HIR2-Cub-PLV construct, the pDR195 empty vector and the pNubWT-Xgate vector allowing for the expression of NubWT.

Yeast protein extraction

Yeast culture of 10 ml ($O.D_{600}$ 1) was centrifuged at 3,200 x *g* for 5 min at room temperature and pelleted cells were frozen in liquid nitrogen until needed. Cells were then re-suspended in 300 µl of 20% (w/v) trichloroacetic acid (TCA) and 100 µl of glass beads (diameter 1.25 to 1.55 mm) was added. Cells were disrupted by vortexing 3 times for 1 min. Between each cycle, tubes were kept on ice for 1 min. After centrifugation at 2,300 x *g* for 10 min at 4 °C, the supernatant was removed and pellets were re-suspended in 100 µl 2X buffer (450 mM TrisHCl pH 8.8, 15 % glycerol, 1% SDS, 2 mM EDTA and 0.5 % bromophenol blue) containing 100 mM DTT. Samples were denatured at 65 ºC for 10 min, and cell debris were pelleted by centrifugation at 14,000 *g* for 5 min at 4 °C. The supernatant corresponding to total proteins was collected and used for SDS-PAGE.

Acidification assays

Arabidopsis thaliana root acidification assays:

In order to observe root acidification capabilities of different *Arabidopsis* lines a

colorimetric acidification assay requiring bromocresol purple were performed. The bromocresol purple is a pH indicator which changes colour from yellow at low pH (pH 5.7) to violet at high pH (above pH 6.8). In a first test, performed as described in Oh *et al.*, 2016, plants were seeded on MS/2 medium (pH 5.7) containing 50 µM Fe-EDTA. After 10 days, the plantlets were transferred onto iron free MS/2 medium (pH 6.5) containing 0.005% bromocresol purple (Sigma-Aldrich) and let to grow for 4 days before observing acidification around the root, indicated by a colour change of the medium from purple to yellow. In parallel, as a control, a batch of plants was transferred to MS/2 medium (pH 6.5) containing 50 µM Fe-EDTA and 0.005 % bromocresol purple. As lack of Fe induces rhizosphere acidification, we expect that plants transferred from +Fe to +Fe conditions will present slight acidification phenotypes, with the exception of Col0/35S::AHA2-GFP. As here AHA2 is under the control of a constitutive promoter, high levels of acidification, even in +Fe conditions should be expected if the fusion results functional. Note that for all the acidification assays MS/2 medium contains physiological concentration of non-iron metals.

Nicotiana benthamiana acidification assays:

Two days after transfection (see the section transient expression of proteins in *Nicotiana benthamiana*) leaf disks of 7 mm diameter were cut and incubated in liquid MS/2 (pH 7.6 as described for liquid bromocresol assays in Oh *et al.*, 2016) without sucrose, in MS/2 containing 0.005 % bromocresol purple, under agitation. The unprotonated form of the dye has an optical density wavelength of absorption at 590 nm. Therefore, net proton flux was measured by reading the optical density at 590 nm after 4 h, 6 h, 12 h and 24 h, treatment in liquid. Apart the colorimetric assay described so far, medium acidification by leaf disks was directly measured with a pHmeter. Only leaves from an equivalent growth stage were compared with one another.

Measurement of leaf chlorophyll contents

For chlorophyll extraction, *Arabidopsis* leaves were finely ground in liquid nitrogen, and pigments were extracted by addition of 1ml of acetone per 35 mg of fresh tissue. After vortexing for 30 s, tubes were incubated on a wheel, at 4 ºC, in darkness for 1 h 30 min. After removing cell debris by centrifugation at 20,000 *g* for 15 min at 4°C, the absorbance at 661.6 nm and 644.8 nm of the resulting pigment extracts was spectrophotometrically determined (Thermo Scientific Evolution™ 201). The concentrations of chlorophyll a and b were determined according to the equations described in Lichtenthaler and Buschmann (2001):

$c_a(\mu g/ml) = 11.24A_{661.6} - 2.04A_{644.8}$

$c_b(\mu g/ml) = 20.13A_{644.8} - 4.19A_{661.6}$

$c_{a+b}(\mu g/ml) = 7.05A_{661.6} + 18.09A_{644.8}$

Root length analyses

Primary root length was measured from plants that grew vertically *in vitro* (see the section Plant material and growth conditions). The plates were scanned, and root lengths were measured from pictures using Fiji image software (http://fiji.sc/).

RNA extractions and RTqPCR analysis

Total RNA extractions from Col-0 and *hir2-2* plant roots were performed using TRIzol™ reagent (Qiagen) as indicated by the manufacturer. DNA was removed from all RNA samples using rDNase treatment (MACHEREY-NAGEL). RNA integrity was then verified by agarose gel electrophoresis. Reverse transcription was performed on 0.5 µg of total RNA with RT Revert Aid Reverse Transcriptase (Thermo Scientific) and oligo$(dT)_{18}$ according to specifications of the manufacturer. The resulting cDNA was diluted 1/10 in milliQ water and used for qPCR analysis using the reactive SYBR™ Green I (Roche), in a LightCycler® 96 (Roche). The amplification program was as following: one cycle of pre-incubation at 95°C for 300 sec, followed by 40 cycles of amplification including 3 steps (95°C 15 sec, 60°C 15 sec, 72°C 15 sec), followed by a melting step in which a dissociation curve is obtained (95°C 10 sec, 65°C 30 sec, 95°C 1 sec). *EDF1α* gene was used as reference gene to normalize the results, as previously used in Dubeaux *et al.* (2018). The primers were design using Primer3 software (http://primer3.ut.ee/) and are listed in Table 3. Relative gene expression was calculated by considering primer efficiencies (E) for the target gene and the control gene (ref), using the method described in Pfaffl (2001) and the following equation:

$$\text{Ratio} = (E_{\text{target}})^{\Delta CP_{\text{target}}\,(\text{control-sample})} / (E_{\text{ref}})^{\Delta CP_{\text{ref}}\,(\text{control-sample})}$$

A total of three biological replicates from three independent phenotypic analysis (each one containing a pool of 25-30 plantlets roots per genotype) were performed.

Confocal microscopy

Standard confocal microscopy analysis was performed with a Leica SP8 upright confocal laser scanning microscope. For mCitrine and mCherry imaging, the 514 nm and 561 nm lasers were used, respectively. Before observation, plants were mounted in water or in MS/2 liquid medium containing the proper metal composition (-Fe +Metals or –Fe +++ Metals). Detection settings were kept constant within experiments. For quantifications, z-stacks encompassing the whole cell volume were imaged and then subjected to maximum projection. Quantifications of co-localization in endosome populations were performed in Fiji (http://fiji.sc/), using maximum intensity projections and the plugging coloc2. The ratios of PM over intracellular relative signal content were obtained by selecting whole cell and intracellular content mean fluorescence with ImageJ. A total of three independent experiments were carried out for each one of the co-localization assays, where a total number of 27 cells were analyzed. Representative images are shown.

The spinning disk images were obtained with an Inverted-Microscope Eclipse-Ti-E (Nikon) and images were recorded with a Prime 95B™ Scientific CMOS (sCMOS) camera (Photometrics). For GFP/mCitrine and mCherry imaging, the 488 nm and 561 nm lasers were used, respectively. A dual-band dichroic mirror (491/561 nm, Chroma) was used and band-pass filters of 525/45 nm and 607/36nm (Semrock) allowing the detection of GFP/mCitrine and mCherry, respectively.

Statistical analyses

The different statistical analyses mentioned in the legends were performed using the software GraphPad Prism.

Table 2. List of the genetic backgrounds that carry the mutated *IRT1, HIR2, FRD1,FLOT1, FLOT2, FLOT3, AHA2*

Genetic Background	**Mutant**
Ws	*irt1-1*
Col-0	*hir2-2*
Col-gl1	*frd1-1*
Col-0	*flot1*
Ws-4	*flot2*
Col-0	*flot3*
Col-0	*aha2*

Table 3. List of primers used during this work

NAME	SEQUENCE (5'-3')
HIR2g.F	ATTGCGGCCGCTTCACCAGCATGCAACCAC
HIR2g.R	ATTGCGGCCGCTGATTGAGATGGGCTTCATTTTAG
attB2r.FRO2.F	GGGGACAGCTTTCTTGTACAAAGTGGCTATGGAGATCGAAAAAAGCAATAAC
attB3.FRO2.R	GGGGACAACTTTGTATAATAAAGTTGTCACCAGCTGAAACTGATAGATTC
attB2r.LTI6b.F	GGGGACAGCTTTCTTGTACAAAGTGGCTATGAGTACAGCCACTTTCGTA
attB3.LTI6b stop.R	GGGGACAACTTTGTATAATAAAGTTGTCACTTGGTGATGATATAAAGA
AHA2.F	GGGGACAAGTTTGTACAAAAAAGCAGGCTTCACCATGTCGAGTCTCGAAGATATC
AHA2.R	GGGGACCACTTTGTACAAGAAAGCTGGGTACACAGTGTAGTGACTGGGAG
AHA2Δ66.R	GGGGACCACTTTGTACAAGAAAGCTGGGTAAAGTGTCCTTTGAGCAAGTG
AHA2 stop.R	GGGGACCACTTTGTACAAGAAAGCTGGGTACTACACAGTGTAGTGACTGGGAG
FRO2.F	GGGGACAAGTTTGTACAAAAAAGCAGGCTTCACCATGGAGATCGAAAAAAGCAATAAC
FRO2.R	GGGGACCACTTTGTACAAGAAAGCTGGGTACCAGCTGAAACTGATAGATTC
IRT1.F	GGGGACAAGTTTGTACAAAAAAGCAGGCTCCATGGCTTCAAATTCAGCACTTC
IRT1 stop.R	GGGGACCACTTTGTACAAGAAAGCTGGGTATTAAGCCCATTTGGCGATAATC
HIR2.F	GGGGACAAGTTTGTACAAAAAAGCAGGCTTCACCATGGGGAATCTTTTCTGTTGC
HIR2.R	GGGGACCACTTTGTACAAGAAAGCTGGGTAGGAGGCATTGTTGGCCTGTA
HIR2 stop.R	GGGGACCACTTTGTACAAGAAAGCTGGGTATTAGGAGGCATTGTTGGCCTGTA
attB4.promoFRO2.F	GGGGACAACTTTGTATAGAAAAGTTGCCTTTATTGACCTCTAGGAGGAC
attB1r.promoFRO2.R	GGGGACTGCTTTTTTGTACAAACTTGCCCTCTCTTTCCTCTCAGGATTTC
attB4.promoHIR2.F	GGGGACAACTTTGTATAGAAAAGTTGCGCTTCACCAGCATGCAACCAC
attB1r.promoHIR2.R	GGGGACTGCTTTTTTGTACAAACTTGCTATTCTGAACAAGAAGCAAGAAG
attB1.mCherry.F	GGGGACAAGTTTGTACAAAAAAGCAGGCTTCACCATGGTGAGCAAGGGCGAGGAGG
attB2.mCherry.R	GGGGACCACTTTGTACAAGAAAGCTGGGTACTTGTACAGCTCGTCCATGC
ACT2.F	GCCCAGAAGTCTTGTTCCAG
ACT2.R	TCATACTCGGCCTTGGAGAT
EF1a qPCR.F	GTCGATTCTGGAAAGTCGAC
EF1a qPCR.R	AATGTCAATGGTGATACCACGC
IRT1 qPCR.F	CGGTTGGACTTCTAAATGC
IRT1 qPCR.R	CGATAATCGACATTCCACCG
attB2r.GFP.F	(Marquès-Bueno *et al.*, 2016)
attB3.GFP.R	(Marquès-Bueno *et al.*, 2016)

Table 4. Different plant constructs used during the development of this work. The table shows the different entry vectors, destination vectors and the final constructs, and the availability of this material at the beginning of the project

pDONR P4P1R	pDONR 221	pDONR P2RP3	Destination vector	Bacterial Resistance	Plant Resistance	Final Construct	Availability
promoter FRO2	mCherry ORF without stop	FRO2 ORF with stop	pH7m34GW	Spec	Hygro	pHy/pFRO2::mCherry-FRO2	Available at the beginning of the thesis
promoter FRO2	FRO2 ORF without stop	mCherry ORF with stop	pH7m34GW	Spec	Hygro	pHy/pFRO2::FRO2-mCherry	Available at the beginning of the thesis
promoter 35S	mCherry ORF without stop	FRO2 ORF with stop	pH7m34GW	Spec	Hygro	pHy/35S::mCherry-FRO2	Available at the beginning of the thesis
promoter 35S	FRO2 ORF without stop	mCherry ORF with stop	pH7m34GW	Spec	Hygro	pHy/35S::FRO2-mCherry	Available at the beginning of the thesis
promoter IRT1	mCherry ORF without stop	FRO2 ORF with stop	pH7m34GW	Spec	Hygro	pHy/pIRT1::mCherry-FRO2	Generated during the thesis
promoter IRT1	FRO2 ORF without stop	mCherry ORF with stop	pH7m34GW	Spec	Hygro	pHy/pIRT1::FRO2-mCherry	Available at the beginning of the thesis
promoter IRT1	AHA2 ORF without stop	mCherry ORF with stop	pH7m34GW	Spec	Hygro	pHy/pIRT1::AHA2-mCherry	Generated during the thesis
promoter 35S	AHA2 ORF without stop	mCherry ORF with stop	pH7m34GW	Spec	Hygro	pHy/35S::AHA2-mCherry	Available at the beginning of the thesis
promoter 35S	AHA2 ORF without stop	GFP ORF with stop	pK7m34GW	Spec	Kana	pKan/35S::AHA2-GFP	Available at the beginning of the thesis
promoter 35S	AHA2Δ66 ORF without stop	mCherry ORF with stop	pH7m34GW	Spec	Hygro	pHy/35S::AHA2Δ66-mCherry	Generated during the thesis
promoter 35S	AHA2Δ66 ORF without stop	GFP ORF with stop	pK7m34GW	Spec	Kana	pKan/35S::AHA2Δ66-GFP	Generated during the thesis
promoter HIR2	HIR2 ORF without stop	mCherry ORF with stop	pH7m34GW	Spec	Hygro	pHy/pHIR2::HIR2-mCherry	Generated during the thesis
promoter 35S	HIR2 ORF without stop	mCherry ORF with stop	pH7m34GW	Spec	Hygro	pHy/35S::HIR2-mCherry	Available at the beginning of the thesis
promoter 35S	mCherry ORF without stop	LTi6b ORF with stop	pH7m34GW	Spec	Hygro	pHy/35S::mCherry-LTi6b	Available at the beginning of the thesis
promoter 35S	HIR2 ORF without stop	GFP ORF with stop	pK7m34GW	Spec	Kana	pKan/35S::HIR2-GFP	Available at the beginning of the thesis
promoter PIN2	mCherry ORF without stop	FRO2 ORF with stop	pH7m34GW	Spec	Hygro	pHy/pPIN2::mCherry-FRO2	Generated during the thesis
promoter PIN2	FRO2 ORF without stop	mCherry ORF with stop	pH7m34GW	Spec	Hygro	pHy/pPIN2::FRO2-mCherry	Generated during the thesis
promoter PIN2	AHA2 ORF without stop	mCherry ORF with stop	pH7m34GW	Spec	Hygro	pHy/pPIN2::AHA2-mCherry	Generated during the thesis
promoter PIN2	HIR2 ORF without stop	mCherry ORF with stop	pH7m34GW	Spec	Hygro	pHy/pPIN2::HIR2-mCherry	Generated during the thesis
				Kana	Kana	pGreen0029.35S::Flot1-mCherry	Generated during the thesis in Jan Martinec's lab
				Kana	Kana	pGreen0029.35S::Flot2-mCherry	Generated during the thesis in Jan Martinec's lab
				Kana	Kana	pGreen0029.35S::Flot3-mCherry	Generated during the thesis in Jan Martinec's lab

Table 5. List of the different genotypes that were used during this work, and the constructs with which they were transformed. The last column also shows the availability of the line at the beginning of this work

Genotype of transgenic line transformed	**Constructs used for the transformation**	**T0 availability at the beginning of the thesis**
irt1-1/pIRT1::IRT1-mCitrine	pIRT1::mCherry-FRO2	No
irt1-1/pIRT1::IRT1-mCitrine	pIRT1::AHA2-mCherry	No
irt1-1/pIRT1::IRT1-mCitrine	35S::HIR2-mCherry	Yes
irt1-1/pIRT1::IRT1-mCitrine	pHIR2::HIR2-mCherry	Yes
irt1-1/pIRT1::IRT1-mCitrine	35S::mCherry-LTi6b	Yes
irt1-1/pIRT1::IRT1-mCitrine	pIRT1::FRO2-mCherry	Yes
irt1-1/pIRT1::IRT1-mCitrine	35::FRO2-mCherry	Yes
Col-0/35S::IRT1-mCitrine	35S::FLOT1-mCherry	No
frd1-1	pFRO2-mCherry-FRO2	No
frd1-1	pFRO2-FRO2-mCherry	Yes
frd1-1	35S::mCherry-FRO2	No
hir2-2	pHIR2::HIR2-mCherry	No
hir2-2	35S::HIR2-mCherry	Yes
hir2-2	HIR2g	No
Col-0/35S::AHA2-GFP	pFRO2-mCherry-FRO2	No
Col-0/35S::AHA2-GFP	35S::mCherry-LTi6b	No
Col-0	35S::HIR2-GFP	yes
Col-0	pPIN2::mCherry-FRO2	No
Col-0	pPIN2::FRO2-mCherry	No
Col-0	pPIN2::HIR2-mCherry	No
Col-0	pPIN2::AHA2-mCherry	No
Col-0/pPIN2::IRT1-mCitrine	pPIN2::mCherry-FRO2	No
Col-0/pPIN2::IRT1-mCitrine	pPIN2::FRO2-mCherry	No
Col-0/pPIN2::IRT1-mCitrine	pPIN2::HIR2-mCherry	No
Col-0/pPIN2::IRT1-mCitrine	pPIN2::AHA2-mCherry	No
Col-0/35S::IRT1-mCitrine	pPIN2::mCherry-FRO2	No
Col-0/35S::IRT1-mCitrine	pPIN2::FRO2-mCherry	No
Col-0/35S::IRT1-mCitrine	pPIN2::HIR2-mCherry	No
Col-0/35S::IRT1-mCitrine	pPIN2::AHA2-mCherry	No
irt1-1/pIRT1::IRT1-mCitrine	RabD1	Yes
Ws	pIRT1-mCherry-FRO2	No
irt1-1/pIRT1::IRT1-mCitrine	pIRT1-mCherry-FRO2	No
Col-0	35S::AHA2Δ66-GFP	No
Col-0	35S::AHA2Δ66-mCherry	No

Table 6. Entry clones, destination vectors and final vectors used during the Split-ubiquitin assays and their availability at the beginning of this work

Entry clone	Destination Vector	Bacterial Resistance	Selection marker in yeast	Final fusion / vector	Availability
pDONR 221-BRI1 ORF without stop	pMetYC-DEST	Amp	LEU2	BRI1-Cub-PLV	Available at the beginning of the thesis
pDONR 221-FRO2 ORF without stop	pMetYC-DEST	Amp	LEU2	FRO2-Cub-PLV	Available at the beginning of the thesis
pDONR 221-AHA2 ORF without stop	pMetYC-DEST	Amp	LEU2	AHA2-Cub-PLV	Available at the beginning of the thesis
pDONR 221-HIR2 ORF without stop	pMetYC-DEST	Amp	LEU2	HIR2-Cub-PLV	Available at the beginning of the thesis
pDONR 221-AHA2 ORF with stop	pNX35-DEST	Amp	TRP0	NubG-PMA2	Available at the beginning of the thesis
pDONR 221-HIR2 ORF with stop	pNX35-DEST	Amp	TRP1	NubG-HIR2	Available at the beginning of the thesis
pDONR 221-IRT1 ORF with stop	pNX35-DEST	Amp	LEU1	NubG-IRT1	Available at the beginning of the thesis
pDONR 221-AHA2 ORF with stop	pDR195GW	Amp	URA3	pDR195-AHA2 ORF with stop	Generated during the thesis
pENTR3C-Flot1 ORF without stop	pMetYC-DEST	Amp	LEU2	Flot1-Cub-PLV	Generated during the thesis
pENTR3C-Flot2 ORF without stop	pMetYC-DEST	Amp	LEU2	Flot2-Cub-PLV	Generated during the thesis
pENTR3C-Flot3 ORF without stop	pMetYC-DEST	Amp	LEU2	Flot3-Cub-PLV	Generated during the thesis

Chapter III

Discussion and Perspectives

Discussion and Perspectives

I. IRT1 interactome: a new departure point in the study of the dynamics and the regulation of IRT1 and new insights in the iron acquisition process

Iron acquisition is essential for plant growth and development. The fact that IRT1 is the main Fe acquisition transporter in root epidermal cells in *Arabidopsis* attracted the focus of the scientific community, leading to the discovery of very complex transcriptional regulations that lead to *IRT1* transcription in the context of Fe deficiency (Brumbarova *et al.*, 2014). In addition to Fe, IRT1 allows the uptake of non-iron metals, namely Zn, Mn and Co. All these metals are essential for plants, but are toxic when present in excess. Therefore, IRT1 protein must be tightly regulated to maintain metal homeostasis and to ensure plant optimal growth. Although IRT1 has been studied for years (Zelazny and Vert, 2015; Dubeaux *et al.*, 2018), only a handful of proteins were identified as IRT1 regulators, such as FYVE1, SNX1, IDF1 and CIPK23, which mainly control IRT1 intracellular localization (Shin *et al.*, 2013; Barberon *et al.*, 2014; Ivanov *et al.*, 2014; Dubeaux *et al.*, 2018). To better understand how IRT1 is regulated, we searched for IRT1 interactors by performing immunopurification of the functional IRT1-mCitrine fusion protein coupled to mass spectrometry analysis to identify the co-purified proteins. Such approach has the great advantage to reveal physiologically relevant protein-protein interactions in plant cells and was successfully used in the past to identify proteins that interacts with channels and receptors (Karlova *et al.*, 2006; Bellati *et al.*, 2016).

Among 142 proteins putatively interacting with IRT1, we defined a group of proteins related to the intracellular trafficking and including clathrin, tubulin and actin (Supplemental Table 2). An association between clathrin and IRT1 is in agreement with the previously reported clathrin-mediated internalization of IRT1 from the PM (Barberon *et al*., 2014). The co-IP technic does not allow to determine whether two proteins directly interact or not, however it is likely that the interaction between IRT1 and clathrin is mediated by an unknown adaptor protein. So far the role of actin and tubulin in IRT1 dynamics has never been investigated, however since these proteins are known to be involved in plant endocytosis (Fan *et al.*, 2015) their presence in the IRT1-interactome opens interesting perspectives. Two small G proteins from the Rab class, RAB GTPase homolog A1D and RAB GTPase homolog 1C, were also found as putative interactors of IRT1 (Supplemental Table 2). Although the role of these two

proteins in intracellular trafficking has never been investigated, similar Rab proteins were described to act in plant endocytic pathways (Qi and Zheng, 2013). Intriguingly, the IDF1 E3 ubiquitin ligase and the CIPK23 kinase were not found in our IRT1 interactome, although their function in controlling IRT1 endocytosis was previously demonstrated, as well as their capacity to interact with IRT1 (Shin *et al.*, 2013; Dubeaux *et al.*, 2018). However, IDF1 and CIPK23 interactions with IRT1 were revealed by split-ubiquitin and yeast-two hybrid targeted approaches, respectively. Given the functions of IDF1 and CIPK23, their interactions with IRT1 are probably very transient and may be lost during the co-IP procedure, contrary to the split-ubiquitin and yeast-two hybrid systems where these associations would be stabilized (Xing *et al.*, 2016). Until now, studies of IRT1 trafficking mainly described endocytic mechanisms and how IRT1 travels along the secretory pathway remained unknown. Interestingly, the IRT1 interactome brought to light for the first time interactions between proteins involved in the secretory pathway and IRT1. Thus, several components of the COPII machinery appeared as IRT1 putative interactors, suggesting a role of COPII in the recruitment and the transport of IRT1 from the ER to the Golgi apparatus (Supplemental Table 2). Membrane proteins exit the ER via the recognition by the COPII machinery of specific cytoplasmic export motifs, such as diacidic motifs corresponding to (D/E)x(D/E), with x representing any amino acid residue (Zelazny *et al.*, 2009). A diacidic motif (EDD) located in the large cytosolic loop of IRT1 at the position 180 may be involved in the packaging of IRT1 in COPII vesicles and its export from the ER, even if it remains to be experimentally determined.

Besides IRT1 interactors linked to the intracellular trafficking, proteins involved in metal homeostasis constitute a very interesting group of candidates (Supplemental Table 2). Recently coumarins, that are excreted in the rhizosphere by PDR9, were demonstrated to be important for *Arabidopsis* iron acquisition by chelating Fe^{3+} and as a result facilitating iron availability for FRO2, as commented in the Introduction Chapter I (see also Figure 2). Intriguingly, IRT1 putatively interacts with F6'H1 and Cytochrome P450/CYP82C4 that are both involved in coumarin biosynthesis (Schmid *et al.*, 2014; Rajniak *et al.*, 2018). Nevertheless, the meaning of these interactions remains unclear notably because PDR9 was not identified as interacting with IRT1. However, the solubilization of PDR9, a large transmembrane protein, may not be optimal in the conditions we used for the co-IP and other approaches will be necessary to determine whether the PDR9 and IRT1 could work in concert among a common protein complex. Interestingly, FRO2 and AHA2, which act with IRT1 in

the acidification-reduction-transport strategy for iron acquisition, were found as interacting with IRT1, as detailed below.

Interestingly, several SPFH-domain containing proteins were identified as putatively interacting with IRT1, namely HIR2, HIR4 and AT2G03510, this latter being the only *Arabidopsis* erlin. The interaction between IRT1 and proteins from this family highlighted the possibility that membrane microdomains contribute to the regulation of IRT1. The role of HIR2 in the control of IRT1 was investigated in detail. The presence of HIR4 in IRT1 interactome may suggest a role of this protein in IRT1 regulation and since HIR proteins are known to oligomerize, IRT1, HIR2 and HIR4 may be present in a common protein complex. As previously mentioned, although AT2G03510 appears to be related to Zn homeostasis and metal hyperaccumulation, its contribution to these processes is far from being understood. Since AT2G03510 is predicted to be located in the ER (Daněk *et al.*, 2016), it suggests that IRT1 may be present in ER membrane microdomains, in addition to PM microdomains. In the future it will be interesting to first confirm the interaction between IRT1 and AT2G03510 and then to determine the molecular outcome of this interaction.

It is important to comment some limitations about the approach of co-immunopurifications coupled to mass spectrometry we performed in this work. First, during this analysis, wild type plants were used as a negative control and, although similar controls were previously reported (Karlova *et al.*, 2006; Bu *et al.*, 2017), they are probably not optimal. In the future, to strengthen our results, the use of transgenic lines expressing the cytosolic mCitrine or a modified mCitrine anchored in the plasma membrane may constitute a better negative control, allowing to exclude proteins putatively interacting with the mCitrine and not with IRT1. Secondly, co-IP followed by mass spectrometry analyses experiments are usually performed in triplicates. In this work, only two independent experiments were performed. To strengthen our IRT1 interactome, it would be interesting to perform in the future an additional experiment. However, it is worth noting that although some interactors are not detected in all replicates, they may constitute anyway interesting candidates. In this study, it is illustrated by the case for FRO2 that was isolated in one experiment on two.

II. IRT1, FRO2 and AHA2 form an iron-acquisition complex to optimize iron uptake at the epidermis of *Arabidopsis* roots.

Using co-IP analysis followed by immunodetections, we confirmed that IRT1 associates with FRO2 and AHA2 proteins in *Arabidopsis* root epidermal cells under iron deficient conditions (Figure 10). In addition, AHA2 was found to co-purify with FRO2 (Figure 12). Importantly, physical interactions between IRT1, FRO2 and AHA2 are probably direct as revealed by a split-ubiquitin assay (Figure 9). According to these results, we proposed that IRT1, FRO2 and AHA2 may constitute a specialized iron-acquisition platform. As mentioned in the results, the interactions between IRT1/FRO2 and AHA2 were revealed in *Arabidopsis* using anti-*Nicotiana plumbaginifolia* PMA2 antibodies that indeed recognize *Arabidopis* AHA2, as confirmed by immunodetecting AHA2 expressed in yeast. When this anti-PMA2 antibodies were used to probe a protein extract from the *Arabidopsis aha2* knock-out mutant, signals corresponding to AHA proteins were detected (result not shown), showing that other AHA proteins than AHA2 are recognized by these antibodies. Indeed, the mass spectrometry analyses performed on IRT1 co-immunopurified fractions identified peptides specific to AHA2 isoform, but also peptides common to AHA2 and other AHA proteins, mostly AHA1. However, no peptide specific to other AHA proteins than AHA2 were found. Therefore, although in our co-IP analysis other AHA proteins besides AHA2 may interact with IRT1 or FRO2, the signal obtained may probably correspond to specifically AHA2, the isoform that chiefly mediates rhizosphere acidification in lack of Fe (Santi and Schmidt, 2009). We attempted to reveal interactions between IRT1/FRO2 and AHA2-GFP/mCherry fusion proteins, but for an unknown reason this approach resulted unsuccessful. However, our split-ubiquitin assay unambiguously showed that AHA2 interacts with IRT1 and FRO2, moreover co-IP analysis combined with mass-spectrometry analysis revealed AHA2, and none of the other 11 AHA proteins, specifically interacts with IRT1. For these reasons, we believe that the interactions between AHA2 and IRT1/FRO2 are specific. Although being only a supposition, the absence of interaction detected between IRT1/FRO2 and AHA2-GFP/mCherry may be due to a partial functionality of AHA2 fusion proteins, although this type of C-terminal-tagged AHA/PMA proteins were previously shown to be, at least in part, functional. Despite our multiple efforts, we were unable to show, using acidification tests, that our AHA2-GFP/mCherry fusions expressed in plants were active. As previously mentioned, since the activity of AHA is highly regulated, notably by their C-terminus that act as negative regulators, the accumulation of AHA

proteins may not obligatory correlate with an increase in proton pump activity. For this reason, C-terminus deleted AHA2 proteins, that were shown to be constitutively active (Regenberg *et al.*, 1995), were fused to fluorophores and soon their activity will be investigated to determine the impact of the C-terminal fusion on AHA2 properties. Nonetheless, AHA2-GFP and AHA2-mCherry are properly synthetized and correctly targeted to the PM and endosomes in root cells (Figures 16A and B). In addition, AHA2-GFP can be efficiently post-translationally modified by ubiquitination (Figure 17). These results made us think that these fusion proteins are likely functional.

Due to the restrictive expression of IRT1 and FRO2 in the epidermal cells of the root (Barberon *et al.,* 2014 and Figure 11A) the iron acquisition platform probably only exists in this cell type, although AHA2 expression appears ubiquitous in the root (Haruta *et al.*, 2018). Microscopy analysis revealed that FRO2 was localized at the outer polar domain of the PM in root epidermal cells (Figure 11A and 18), similarly to IRT1. The polarity of FRO2 had not been addressed so far, due to the difficulties to obtain proper antibodies against FRO2, or functional FRO2 fluorescent fusion proteins. The co-polarity between FRO2 and IRT1 in the outer polar domain of the PM highlight the specificity of their functions achieved at the interface between the root surface and the rhizosphere. In the future, it will be interesting to determine whether the polarity of IRT1 and FRO2 is established by common mechanisms, for instance by investigating the role of FYVE1 protein on FRO2 polarity. Contrary to IRT1 and FRO2, the distribution of AHA2 in the PM of root epidermal cells was homogenous (Figure 18), suggesting that AHA2 does not obligatory associate with FRO2 and IRT1 since they are excluded from the inner polar domain of the PM. This result is in accordance with the function of AHA2 that is not restricted to iron acquisition (Yuan *et al.*, 2017; Hoffmann *et al.*, n.d.; Pacifici *et al.*, 2018). Interestingly, we showed that IRT1 not only co-localized with FRO2 and AHA2 at the PM, but also in endosomes (Figure 18). Although our interaction tests do not provide information about where the interactions between IRT1, FRO2 and AHA2 occur, the subcellular localization of these proteins point to the PM and endosomes as putative sites of interaction. In the future, Förster resonance energy transfer-fluorescence lifetime imaging microscopy (FRET-FLIM), which allows to detect protein-protein interactions in living plant cells with a high spatial and temporal resolution (Zelazny *et al.*, 2007) may reveal where IRT1 interacts with FRO2 and AHA2 in the cell. Unfortunately, this technique could not be used during this work, because it requires the presence of fluorescent tags in the cytosolic domains of the protein to be tested and in the case of IRT1-mCitrine, the mCitrine is located in an extracellular loop of IRT1 to preserve its functionality (Dubeaux *et al.*, 2018, Figure 8A).

Therefore, another functional fusion of IRT1, with the fluorophore located on the cytosolic face, will have first to be generated.

IRT1 intracellular dynamics is regulated by ubiquitination, notably, in response to non-iron metal excess, IRT1 is highly ubiquitinated which induces its endocytosis and its degradation in the vacuole. Therefore, we decided to uncover whether FRO2 and AHA2, which interact with IRT1 among an iron acquisition complex, may undergo a similar process. We demonstrated that AHA2 and FRO2 are also ubiquitinated but, interestingly, FRO2 and AHA2 ubiquitination does not change in response to non-iron metal excess (Figure 17). Whether FRO2 and AHA2 ubiquitination is a constitutive process or is regulated by environmental cues remains to be determined. We also characterized the response of AHA2 and FRO2 to non-iron metal excess in terms of subcellular localization. Interestingly, contrary to IRT1, non-iron metal excess does not induce a massive internalization of FRO2 and AHA2 from the PM in root epidermal cells (Figure 18). Numerous studies performed in plants and yeast highlighted that ubiquitin-mediated endocytosis of transporters can be directly regulated by their substrates (Gitan and Eide, 2000; Kasai *et al.*, 2011; Dubeaux *et al.*, 2018). Although FRO2 and AHA2 form a complex with IRT1, their catalytic activities are totally different from the one of IRT1 and non-iron metals do not constitute substrates. Thus, it is not surprising that their intracellular trafficking, as well as their ubiquitination, as described above, are not strongly and directly impacted by IRT1 secondary substrates. However, concerning FRO2 response to non-iron metals, some fine mechanisms may exist since FRO2 was shown to more co-localize with IRT1 in endosomes in response to non-iron metal excess, suggesting a possible increase of FRO2 internalization from the PM in these conditions (Figure 18). Since this phenomenon is subtle and because FRO2 ubiquitination does not increase upon non-iron metal excess, this observation may correspond to FRO2 protein that is passively internalized by interacting with IRT1. To test this hypothesis, it would be interesting to assess if the increased FRO2 internalization upon non-iron metal excess is maintained in the absence of IRT1 or in conditions where IRT1 is no longer internalized. To do so, we expressed the mCherrry-FRO2 protein in *irt1-1* mutant and in a transgenic line where the $IRT1_{2KR}$-mCitrine mutated protein, which is unable to be internalized due to the absence of ubiquitination, is expressed in *irt1-1*. The localization of FRO2 as well as its response to non-iron metal excess inside both genetic backgrounds will be addressed in the future. To go further, it would be also very interesting to analyze the co-endocytosis of FRO2 and IRT1 by performing TIRF microscopy that allows the study of internalization processes occurring at the PM with a high spatial and temporal resolution (Johnson and Vert, 2017). Intriguingly, contrary to FRO2, we did not find AHA2 as

being more *co-localized* with IRT1 in endosomes in response to non-iron metal excess. This may imply that AHA2 and IRT1 dissociate before IRT1 internalization from the PM, even if it remains to be demonstrated.

Our work shed new light on the co-regulation of *IRT1*, *FRO2* and *AHA2* genes whose expression is induced under iron deficiency. Indeed the existence of a complex gathering IRT1, FRO2 and AHA2 requires the presence of all the partners in the same cell type at the same time. Besides *AHA2*, *AHA7* gene expression is upregulated in response to low iron showing that this H^+-ATPase also participates in the iron deficiency response, however mutant analysis revealed that rhizosphere acidification is chiefly mediated by AHA2 in lack of iron (Santi and Schmidt, 2009). As previously mentioned, we did not isolate AHA7 in IRT1 interactome and out of the 12 members of the *Arabidopsis* AHA family, only AHA2 was specifically co-purified with IRT1 during the mass spectrometry analyses, showing the specificity of this interaction and reinforcing the importance of AHA2 in iron acquisition. As presented in the Introduction (Chapter I), Fe is a very abundant element in the rhizosphere, but scarcely bioavailable. During the iron acquisition process, local rhizosphere acidification by the root is essential to increase iron availability. Indeed iron solubility increases 1000-fold for every one unit drop in pH (Olsen *et al.*, 1981). Moreover, the presence of oxygen in the soil probably induces the constant re-oxidation of Fe^{2+}, produced by FRO2, to Fe^{3+} that is not transported by IRT1. Thus, we propose that the close proximity between IRT1, FRO2 and AHA2 gathered among a common protein complex create a local environment in the rhizosphere, in term of pH and Fe^{2+} concentration, which promotes an optimal acquisition of iron (Figure 28). This original mechanism provides new insights in our understanding of the control of iron uptake in plant roots, which may have agronomic outcomes. To fully validate our model, it would be very interesting in the future to be able to disturb the assembly of the Fe acquisition protein complex and analyse the impact in term of iron acquisition. To this purpose, we might generate IRT1, FRO2 or AHA2 mutated proteins that are still active but that cannot interact anymore with the other components of the complex. However, this constitutes a long-term approach.

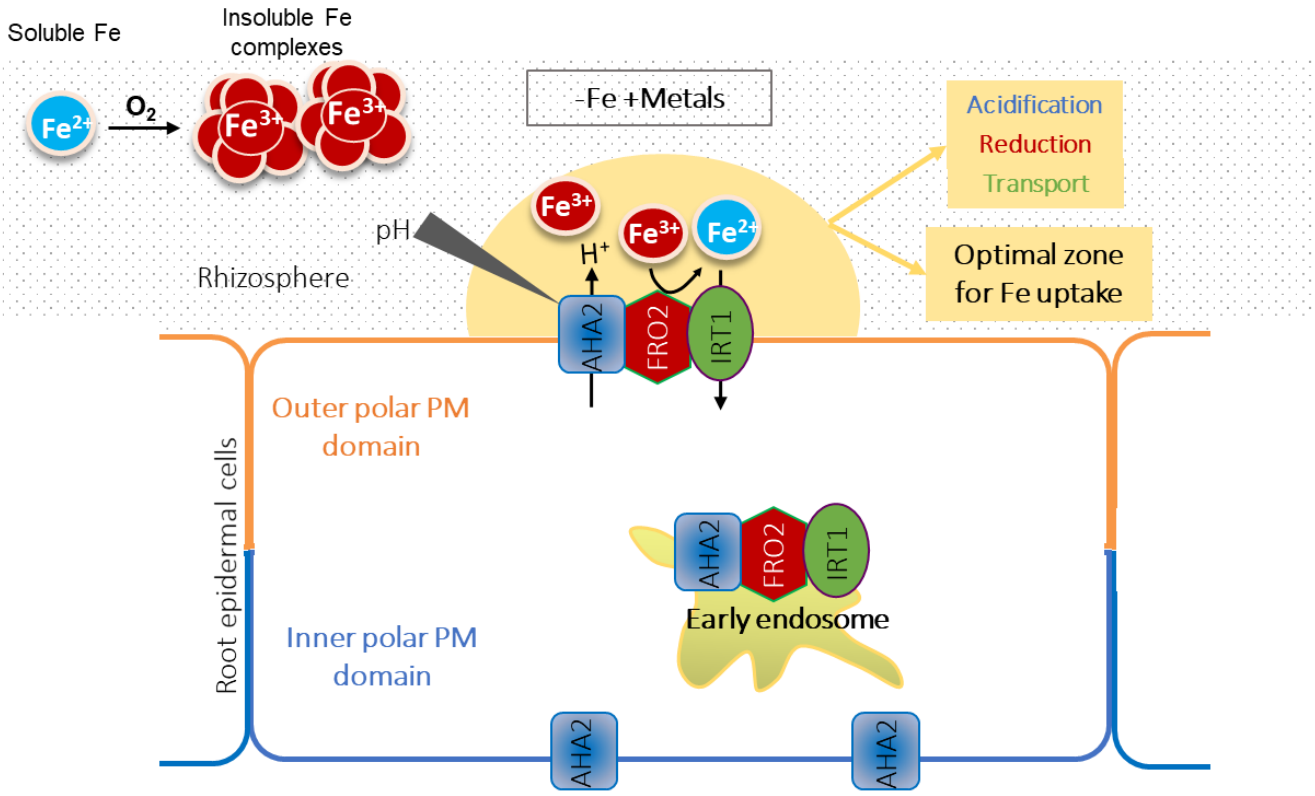

<u>Figure 28.</u> Tentative model for the functioning of the iron acquisition complex
IRT1, FRO2 and AHA2 proteins interact at the outer polar plasma membrane (PM) domain of root epidermal cells to form a specialized complex which optimizes iron acquisition by creating a local environment with low pH and high Fe^{2+} concentration. Outside this optimal zone for iron acquisition, we propose that Fe^{2+} is constantly re-oxidized to Fe^{3+} ,which in turn forms insoluble iron complexes. In addition to be plasma membrane localized, the iron acquisition complex is also probably present in early endosomes, reflecting endocytic events of the complex. Note that contrary to IRT1 and FRO2, AHA2 is distributed at both plasma membrane polar domains. This model depicts the localization of IRT1, FRO2 and AHA2 in the absence of iron and in the presence of physiological amounts of non-iron metals (–Fe +Metals).

III. HIR2 is a membrane microdomain-located protein that interacts with IRT1 and plays a role in Fe homeostasis

By performing co-IP analysis followed by immunodetections, we confirmed that IRT1 associates with HIR2 among a protein complex in *Arabidopsis* root epidermal cells (Figure 13), however, the interaction between IRT1 and HIR2 is probably indirect as evidenced by the split-ubiquitin test we performed (Figures 9). The fact that the interaction between these two proteins seems indirect, made us hypothesize that another member of the Fe acquisition platform may

create a linkage between IRT1 and HIR2. Indeed, a split-ubiquitin analysis revealed that HIR2 directly interacts with AHA2 (Figure 14), this latter being able to interact with IRT1 too. However, in a variant of the split-ubiquitin assay that allows to test trimeric interactions, we failed to show that AHA2 mediates an interaction between IRT1 and HIR2 (Figure 15). As previously mentioned in the results, it could be due to the large size of AHA2 protein that would impair ubiquitin reconstruction even though AHA2 indeed facilitates the interaction between IRT1 and HIR2. In the future, further investigations should be performed in *Arabidopsis*. For instance, it will be interesting to determine whether HIR2 is co-immunopurified with IRT1 in the absence of AHA2 in *aha2* mutant background. Besides, it would be also interesting to investigate the effect of AHA2 deletion on the formation of the Fe acquisition complex. Although AHA2 may indirectly allow the recruitment of IRT1 in membrane microdomains containing HIR2, another unknown protein found in IRT1 interactome may also perform this function. Interestingly, AHA2 was recently proposed to interact with another HIR isoform, HIR1, in the context of the response against pathogens (Lv et al., 2017). Thus, AHA2-HIR interaction is not restricted to iron uptake process.

Microscopy analysis revealed that HIR2 is specifically targeted to the PM of the root epidermis, where it distributes in a dotted disposition pattern typical of microdomain-located proteins (Figure 19 and 20). Interestingly, IRT1 can adopt this punctate distribution at the PM in epidermal cells showing that this transporter can indeed localize in membrane microdomains (Figure 20). However, IRT1 can be also homogeneously distributed at the cell surface, showing that IRT1 is probably not an obligatory membrane microdomain protein. Despite our efforts, we failed to visualize HIR2 and IRT1 in common PM microdomains using spinning-disk microscopy (Figure 21). This is really intriguing since IRT1 and HIR2 proteins are able to associate and it constitutes a real issue in our understanding of the regulation of IRT1 by HIR2. As stated in the Introduction, preparation and analysis of detergent-insoluble membranes (DIM) constitute a biochemical way to study membrane microdomains. HIR2 but also AHA2 were previously shown to be associated with DIM (Borner et *al*., 2005; Qi et *al*., 2011). In addition to the microscopy analyses described above, biochemical approaches will be performed in the future to show that IRT1 is also present in DIM prepared from *Arabidopsis* roots and to determine in which proportion. It will also be interesting to perform the same approach for FRO2, which interacts with IRT1 among the iron acquisition complex. Interestingly, the work of Tan *et al.*, (2017) provided first biochemical evidences that IRT1 from *Malus xiaojinesis* (MxIRT1) is present in plant DIM.

To study the role of HIR2 in iron homeostasis, we initiated reverse genetic approaches by analysing the phenotype of *hir2* loss-of-function mutants, *hir2-1* and *hir2-2*, under different metal status. Before I started my thesis, preliminary data performed in our laboratory suggested that *hir2-1* mutant was more chlorotic than WT plants under iron deficiency, suggesting a default in iron homeostasis (Supplemental Figure 3). I confirmed this result by characterizing in detail the phenotype of *hir2-2* mutant under different iron regimes. Notably, we measured a huge decrease in chlorophyll content in *hir2-2* mutant compared to WT plants under iron deficiency (Figure 22). The hyper-chlorosis of *hir2-2* mutant was strongly reverted by the addition of sufficient amounts of Fe. Interestingly, expression of the HIR2-mCherry fusion protein partially reversed the chlorosis of *hir2-2* mutant in the absence of iron (Figure 23). These results suggest that iron homeostasis is disturbed in *hir2* mutants and show for the first time, to our knowledge, the role of a membrane microdomain protein in plant metal nutrition. To go further, it will be important to fully complement the phenotype of *hir2-2* mutant by introducing a *HIR2* genomic fragment, as described in the results. In addition, similar deep phenotypical analysis will be performed on *hir2-1* mutant. Intriguingly, under iron replete conditions, *hir2-2* mutant contains slightly less chlorophyll than WT plants. Moreover, in the same standard conditions, *hir2-2* displays shorter primary roots than WT plants. These observations are in accordance with the fact that HIR2 performs other functions unrelated to Fe nutrition, such as the mediation of the pathogen defence response (Qi *et al.*, 2011). To go further in the study of the role of HIR proteins in metal homeostasis, it will be interesting to investigate the function of other HIR isoforms, such as HIR4 that putatively interacts with IRT1 protein, as previously mentioned. The phenotype of *hir4* knock-out mutants will be analyzed in response to iron deprivation. More importantly, the double *hir-2 hir-4* mutant will be generated to possibly reveal an even more dramatic phenotype in iron limited conditions in comparison to single mutants. The hypersensitive phenotype displayed by *hir2* mutants when exposed to a lack of Fe, together with the interaction between HIR2 and IRT1 proteins, made us wonder whether IRT1 protein level was deregulated in the absence of HIR2. Surprisingly, despite the strong chlorosis displayed by *hir2* mutants, IRT1 protein over-accumulated in the roots of *hir2-1* and *hir2-2* compared to WT plants in low iron conditions (Supplemental figure 3 and Figure 24). Although IRT1 protein accumulated more than six times in the roots of *hir2-2* compared to Col-0, the amount of *IRT1* transcript varied very little between both genotypes (Figures 24B and C), suggesting a post-transcriptional regulation of IRT1. As stated below, IRT1 endocytosis and degradation could be affected in *hir2* mutants, which may explain IRT1 over-accumulation.

During my thesis, to try to understand why the *hir2-2* mutant was hypersensitive to iron deficiency, we formulated two hypotheses. In a first hypothesis, the over-accumulation of IRT1 in *hir2-2* mutant could favour, in low iron conditions, the entrance of the non-iron metal substrates of IRT1 (Zn, Mn and Co) since these metals do not need a reduction step to be uptaken. A huge accumulation of toxic non-iron metals might have explained the hyper chlorosis of *hir2-2* mutant. In a second hypothesis, in the absence of HIR2, IRT1 may be present in large amount but mis-localized outside of specific PM membrane microdomains or elsewghere in the cell, which may decrease or inhibit IRT1 activity due to a different lipid context. In this case, we expected that *hir2-2* mutant would be unable to acquire any IRT1 metal substrates (Fe, Zn, Mn and Co), explaining why the metal homeostasis was disturbed. To evaluate both possibilities we compared the leaf metal contents in *hir2-2* mutant and WT plants. Surprisingly, we found that both genotypes accumulated very similar amounts of Fe, Mn and Zn, whatever the growth conditions (Figure 25). This result invalidated our two hypothesis since the pool of IRT1 present in *hir2-2* appeared to be functional and because *hir2-2* mutant did not accumulate more non-iron metals than WT plants in leaves. Normally, a metallic unbalance in the root of *Arabidopsis*, motivated by the exposure of the plant to different metal regimes, results into a measurable metal unbalance in the shoot (Viehweger, 2014). Nonetheless, in order to fully characterize *hir2-2* mutant, it will be of extreme importance to compare the metal accumulation profile in roots from *hir2-2* and WT plants, which may reveal some differences. Even if the total metal accumulation is not impacted in *hir2-2*, it is possible that the metal repartition in different tissues or cellular compartments is disturbed in this mutant. Therefore, we planned to compare the localization of the iron pool in *hir2-2* mutant and in WT plants, using the Perls/DAB staining combined with microscopy (Roschzttardtz *et al*., 2009), to try to highlight possible deregulation in *hir2-2*. Now, it clearly appears that further information must be gathered about the metal nutritional status of *hir2-2* mutants before we can completely reject one of our initial hypotheses. It is important to consider that, in addition to a role in the control of IRT1, HIR2 may also modulate the activity of other metal transporters in *Arabidopsis*. As a result, the phenotype of *hir2-2* mutant under iron deficiency might result from several defaults in metal transport.

How HIR2 regulates IRT1 at the molecular level remains unknown. However, according to the functions performed by different microdomain proteins (see Introduction

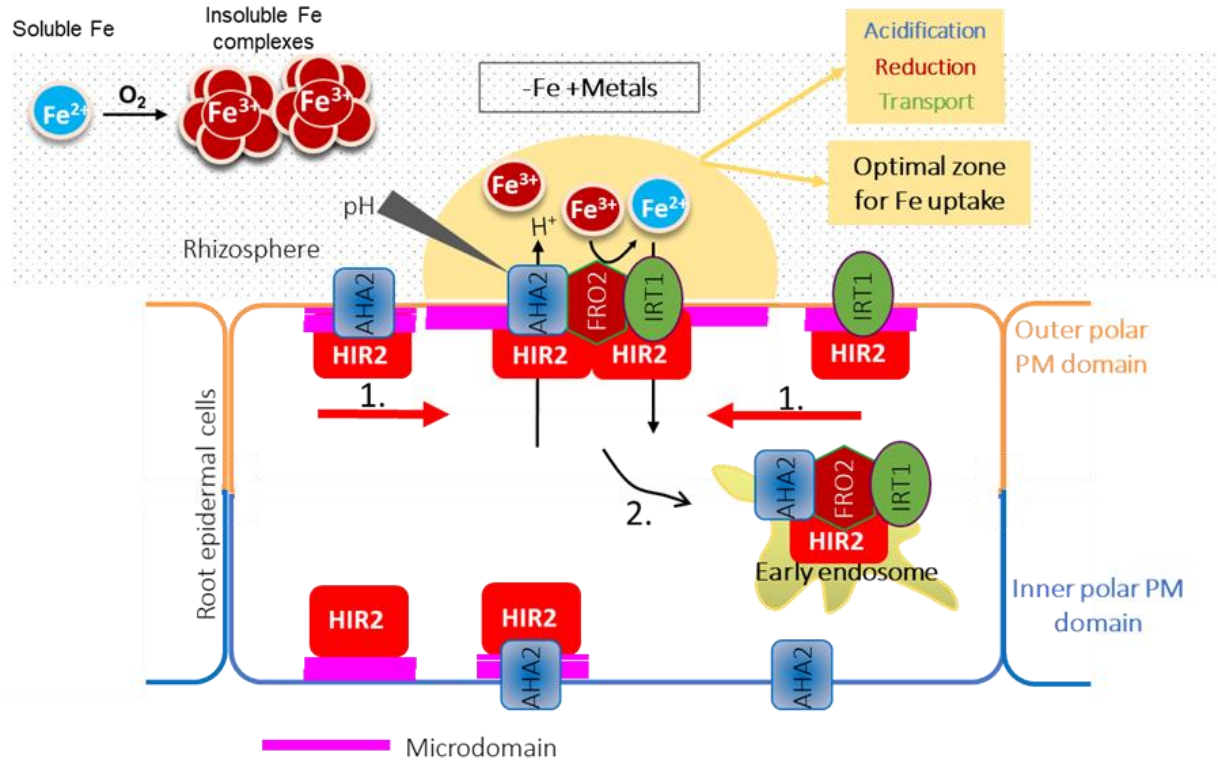

<u>Figure 29.</u> Putative regulation of the iron acquisition complex by HIR2.
Iron absorption is facilitated by the Fe acquisition complex as described in Figure 28 and implies HIR2. Two different modes of action for HIR2 are hypothesized:
1. HIR2 may act as scaffolding protein. HIR2 interacts with specific members of the Fe acquisition complex and, thus, allows their recruitment and maintenance in specific PM microdomains from root epidermal cells.
2. HIR2 may be involved in the endocytosis of members of the Fe acquisition complex. HIR2 may contribute to the creation of an endocytic platform inducing the internalization of the Fe acquisition complex.
Independently of both hypotheses, the absence of HIR2 greatly impacts Fe homeostasis in *Arabidopsis*.

Chapter III), a first hypothesis is that IRT1, and probably the whole Fe acquisition complex, may be recruited in PM microdomains by interacting with HIR2 that would act as a scaffolding protein (Figure 29). To contrast this hypothesis, it will be important to determine by microscopy approaches whether IRT1, but also FRO2 and AHA2, are still located in PM microdomains in the absence of HIR2. To this purpose, we already crossed the *hir2-2* mutant with the transgenic line expressing IRT1-mCitrine. In addition, biochemical approaches will be performed to determine whether the absence of HIR2 induces a relocalization of IRT1/FRO2/AHA2 from DIM to membrane fractions sensitive to non-ionic detergents. Finally, the capacity of IRT1 to interact with FRO2 and AHA2 in the absence of HIR2 (*hir2-2* mutant background) may be

investigated to determine whether HIR2 and membrane microdomain recruitment is required for these interactions.

So far, IRT1 endocytosis was demonstrated to be clathrin-dependent (Barberon et *al*., 2014), but, as stated in the introduction, another endocytic pathway called microdomain-associated endocytosis (MAE) exists in plants (Li et *al*., 2012). The over-accumulation of IRT1 in *hir2* mutants may be due to a stabilization of the protein resulting from a defect in IRT1 endocytosis. This result combined with the existence of an interaction between IRT1 and HIR2 led us imagine a second hypothesis in which IRT1 may undergo MAE mediated by HIR2-containing PM microdomains, although this putative mechanism would be totally novel (Figure 29). To investigate this hypothesis, we propose to compare the internalization kinetics of IRT1-mCitrine expressed in a *hir2-2* mutant background and in WT plants by TIRF microscopy. Since MAE can be regulated by environmental factors, it would be interesting to test the impact of non-iron metal nutrition on the putative MAE of IRT1. It is important to consider that the two hypotheses presented above, concerning the role of HIR2 in the regulation of IRT1, are not inevitably exclusive. For instance, HIR2 may recruit IRT1 in specific PM microdomains and may be involved in its endocytosis too. In a candidate approach, we also started to investigate the putative role of *Arabidopsis* Flot1, which participates in MAE, but also Flot2 and Flot3, in the endocytosis of IRT1. Different approaches were initiated in the frame of a collaborative project. Preliminary phenotypical analysis of *flot* mutants suggested that Flot1 and Flot3 might play a role in Fe acquisition. However, we showed that the three *Arabidopsis* flotillins do not directly interact with IRT1 (Figure 26), although we did not investigate so far whether these proteins could associate indirectly with IRT1 in a protein complex. Until now, we did not detect a co-localization between IRT1 and the three flotillins in PM microdomains in root epidermal cells (Figure 27). Despite of that, we believe that it might be interesting to investigate IRT1 internalization in the context of *flot1* mutant, thus the corresponding transgenic lines were generated. To go further in the analysis of a putative MAE of IRT1, internalization kinetic studies of IRT1-mCitrine may be performed by TIRF in the presence of drugs that disrupt the structure of microdomains, such as methyl-β-cyclodextrin, or by expressing IRT1-mCitrine in sterol biosynthesis mutants affected in the production of PM microdomains (Men *et al.*, 2008; Li *et al.*, 2011; Zauber *et al.*, 2013).

Bibliography

Adamowski, M., Narasimhan, M., Kania, U., Glanc, M., Jaeger, G. De and Friml, J. (2018) A Functional Study of AUXILIN-LIKE1 and 2, Two Putative Clathrin Uncoating Factors in *Arabidopsis*. *Plant Cell*, **30**, 700 LP-716. Available at: http://www.plantcell.org/content/30/3/700.abstract.

Alberts B, Johnson A, Lewis J, et al. Molecular Biology of the Cell. 4th edition. New York: Garland Science; 2002. The Lipid Bilayer. Available from: https://www.ncbi.nlm.nih.gov/books/NBK26871/

Ali, U., Li, H., Wang, X. and Guo, L. (2018) Emerging Roles of Sphingolipid Signaling in Plant Response to Biotic and Abiotic Stresses. *Mol. Plant*, **11**, 1328–1343. Available at: https://doi.org/10.1016/j.molp.2018.10.001.

Antonny, B., Burd, C., Camilli, P. De, et al. (2016) Membrane fission by dynamin: what we know and what we need to know. *EMBO J.*, **35**, 2270 LP-2284. Available at: http://emboj.embopress.org/content/35/21/2270.abstract.

Aridor, M. (2018) COPII gets in shape: Lessons derived from morphological aspects of early secretion. *Traffic*, **19**, 823–839. Available at: https://onlinelibrary.wiley.com/doi/abs/10.1111/tra.12603.

Asanov, A., Zepeda, A. and Vaca, L. (2010) A novel form of Total Internal Reflection Fluorescence Microscopy (LG-TIRFM) reveals different and independent lipid raft domains in living cells. *Biochim. Biophys. Acta - Mol. Cell Biol. Lipids*, **1801**, 147–155. Available at: http://dx.doi.org/10.1016/j.bbalip.2009.10.004.

Bach, J.N. and Bramkamp, M. (2013) Flotillins functionally organize the bacterial membrane. *Mol. Microbiol.*, **88**, 1205–1217.

Baisa, G.A., Mayers, J.R. and Bednarek, S.Y. (2013) Budding and braking news about clathrin-mediated endocytosis. *Curr. Opin. Plant Biol.*, **16**, 718–725. Available at: http://dx.doi.org/10.1016/j.pbi.2013.09.005.

Bar, M. and Avni, A. (2009) EHD2 inhibits ligand-induced endocytosis and signaling of the leucine-rich repeat receptor-like protein LeEix2. *Plant J.*, **59**, 600–611.

Barberon, M. (2017) The endodermis as a checkpoint for nutrients. *New Phytol.*, **213**, 1604–1610.

Barberon, M., Dubeaux, G., Kolb, C., Isono, E., Zelazny, E. and Vert, G. (2014) Polarization of IRON-REGULATED TRANSPORTER 1 (IRT1) to the plant-soil interface plays crucial role in metal homeostasis. *Proc. Natl. Acad. Sci.*, **111**, 8293–8298. Available at: http://www.pnas.org/cgi/doi/10.1073/pnas.1402262111.

Barberon, M., Vermeer, J.E.M., Bellis, D. De, et al. (2016) Adaptation of Root Function by Nutrient-Induced Plasticity of Endodermal Differentiation. *Cell*, **164**, 447-459. Available at: https://doi.org/10.1016/j.cell.2015.12.021.

Barberon, M., Zelazny, E., Robert, S., Conéjéro, G., Curie, C., Friml, J. and Vert, G. (2011) Monoubiquitin-dependent endocytosis of the transporter controls iron uptake in plants. *Proc. Natl. Acad. Sci. U. S. A.*, **108**, e450–e458.

Barbez, E., Dünser, K., Gaidora, A., Lendl, T. and Busch, W. (2017) Auxin steers root cell expansion via apoplastic pH regulation in *Arabidopsis thaliana*. *Proc. Natl. Acad. Sci.*, **114**, E4884–E4893. Available at: http://www.pnas.org/lookup/doi/10.1073/pnas.1613499114.

Bariola, P.A., Retelska, D., Stasiak, A., Kammerer, R.A., Fleming, A., Hijri, M., Frank,

S. and Farmer, E.E. (2004) Remorins form a novel family of coiled coil-forming oligomeric and filamentous proteins associated with apical , vascular and embryonic tissues in plants. *Plant Mol. Biol.* **55**, 579–594.

Bassham, D.C., Brandizzi, F., Otegui, M.S. and Sanderfoot, A.A. (2008) The Secretory System of *Arabidopsis*. *Arab. B.*, **6**, e0116. Available at: http://www.bioone.org/doi/abs/10.1199/tab.0116.

Bastow, E.L., Garcia de la Torre, V.S., Maclean, A.E., Green, R.T., Merlot, S., Thomine, S. and Balk, J. (2018) Vacuolar Iron Stores Gated by NRAMP3 and NRAMP4 Are the Primary Source of Iron in Germinating Seeds. *Plant Physiol.*, **177**, 1267–1276. Available at: http://www.plantphysiol.org/lookup/doi/10.1104/pp.18.00478.

Bellati, J., Champeyroux, C., Hem, S., Rofidal, V., Krouk, G., Maurel, C. and Santoni, V. (2016) Novel Aquaporin Regulatory Mechanisms Revealed by Interactomics. *Mol. Cell. Proteomics*, **15**, 3473–3487.

Benschop, J.J., Mohammed, S., O'Flaherty, M., Heck, A.J.R., Slijper, M. and Menke, F.L.H. (2007) Quantitative Phosphoproteomics of Early Elicitor Signaling in *Arabidopsis* . *Mol. Cell. Proteomics*, **6**, 1198–1214.

Bin, B.H., Fukada, T., Hosaka, T., et al. (2011) Biochemical characterization of human ZIP13 protein: A homo-dimerized zinc transporter involved in the spondylocheiro dysplastic Ehlers-Danlos syndrome. *J. Biol. Chem.*, **286**, 40255–40265.

Bitsikas, V., Corrêa, I.R. and Nichols, B.J. (2014) Clathrin-independent pathways do not contribute significantly to endocytic flux. *Elife*, **3**, 1–26.

Blanchet, S., Cornu, D., Argentini, M. and Namy, O. (2014) New insights into the incorporation of natural suppressor tRNAs at stop codons in Saccharomyces cerevisiae. *Nucleic Acids Res.*, **42**, 10061–10072.

Blondel, M.-O., Morvan, J., Dupré, S., Urban-Grimal, D., Haguenauer-Tsapis, R. and Volland, C. (2004) Direct sorting of the yeast uracil permease to the endosomal system is controlled by uracil binding and Rsp5p-dependent ubiquitylation. *Mol. Biol. Cell*, **15**, 883–895.

Bolle-Jones, E.W. and Mallikarjuneswara, V.R. (1957) A Beneficial Effect of Cobalt on the Growth of the Rubber Plant (Hevea brasiliensis). *Nature*, **179**, 738–739. Available at: https://doi.org/10.1038/179738a0.

Borner, G.H.H., Sherrier, D.J., Weimar, T., et al. (2005) Analysis of Detergent-Resistant Membranes in *Arabidopsis*. Evidence for Plasma Membrane Lipid Rafts1. *Plant Physiol*, **137**, 104–116.

Brandizzi, F. and Barlowe, C. (2013) Organization of the ER-Golgi interface for membrane traffic control. *Nat. Rev. Mol. Cell Biol.*, **14**, 382–392.

Briat, J. and Lobrag, S. (1997) Iron transport and storage in plants. *Trends Plant Sci.*, **2**, 187–193.

Briat, J.F., Curie, C. and Gaymard, F. (2007) Iron utilization and metabolism in plants. *Curr. Opin. Plant Biol.*, **10**, 276–282.

Briat, J.F., Dubos, C. and Gaymard, F. (2015) Iron nutrition, biomass production, and plant product quality. *Trends Plant Sci.*, **20**, 33–40.

Browman, D.T., Hoegg, M.B. and Robbins, S.M. (2007) The SPFH domain-containing proteins: more than lipid raft markers. *Trends Cell Biol.*, **17**, 394–402.

Brown, R.E. (1998) Sphingolipid organization in biomembranes: what physical studies of model membranes reveal. *J. Cell Sci.*, **111 (Pt 1**, 1–9.

Brumbarova, T. and Bauer, P. (2009) Iron Uptake and Transport in Plants. *Plant Membr. Vacuolar Transp.*, **109**, 149–172.

Brumbarova, T., Bauer, P. and Ivanov, R. (2014) Molecular mechanisms governing

Arabidopsis iron uptake. *Trends Plant Sci.*, **20**, 124–133. Available at: http://dx.doi.org/10.1016/j.tplants.2014.11.004.

Bu, S.-L., Liu, C., Liu, N., et al. (2017) Immunopurification and Mass Spectrometry Identifies Protein Phosphatase 2A (PP2A) and BIN2/GSK3 as Regulators of AKS Transcription Factors in *Arabidopsis*. *Mol. Plant*, **10**, 345–348. Available at: https://doi.org/10.1016/j.molp.2016.09.016.

Bücherl, C.A., Jarsch, I.K., Schudoma, C., Segonzac, C., Mbengue, M., Robatzek, S., MacLean, D., Ott, T. and Zipfel, C. (2017) Plant immune and growth receptors share common signalling components but localise to distinct plasma membrane nanodomains. *Elife*, **6**, e25114.

Cacas, J.L., Furt, F., Guédard, M. Le, et al. (2012) Lipids of plant membrane rafts. *Prog. Lipid Res.*, **51**, 272–299. Available at: http://dx.doi.org/10.1016/j.plipres.2012.04.001.

Cailliatte, R., Schikora, A., Briat, J.F., Mari, S. and Curie, C. (2010) High-Affinity Manganese Uptake by the Metal Transporter NRAMP1 Is Essential for *Arabidopsis* Growth in Low Manganese Conditions. *Plant Cell*, **22**, 904–917. Available at: http://www.plantcell.org/cgi/doi/10.1105/tpc.109.073023.

Cassim, A.M., Gouguet, P., Gronnier, J., et al. (2018) Plant lipids: Key players of plasma membrane organization and function. *Prog. Lipid Res.*, **73**:1-27. Available at: https://linkinghub.elsevier.com/retrieve/pii/S0163782717300711.

Castaings, L., Caquot, A., Loubet, S. and Curie, C. (2016) The high-affinity metal Transporters NRAMP1 and IRT1 Team up to Take up Iron under Sufficient Metal Provision. *Sci. Rep.*, **6**, 1–11. Available at: http://dx.doi.org/10.1038/srep37222.

Chen, X., Irani, N.G. and Friml, J. (2011) Clathrin-mediated endocytosis: The gateway into plant cells. *Curr. Opin. Plant Biol.*, **14**, 674–682.

Choi, H.W., Kim, D.S., Kim, N.H., Jung, H.W., Ham, J.H. and Hwang, B.K. (2013) Xanthomonas Filamentous Hemagglutinin-Like Protein Fha1 Interacts with Pepper Hypersensitive-Induced Reaction Protein CaHIR1 and Functions as a Virulence Factor in Host Plants . *Mol. Plant-Microbe Interact.*, **26**, 1441–1454.

Choi, H.W., Kim, Y.J. and Hwang, B.K. (2010) The Hypersensitive Induced Reaction and Leucine-Rich Repeat Proteins Regulate Plant Cell Death Associated with Disease and Plant Immunity. *Mol. Plant-Microbe Interact.*, **24**, 68–78.

Chun, H., Korolnek, T., Lee, C.-J., Jerome Coyne Iii, H., Winge, D.R., Kim, B.-E. and Petris, M.J. (2019) Extracellular zinc sensor motif in ZIP4 endocytosis 1 An extracellular histidine-containing motif in the zinc transporter ZIP4 plays a role in zinc sensing and zinc-induced endocytosis in mammalian cells. *J. Biol. Chem.*, **294**, 2815–2826. Available at: http://www.jbc.org/cgi/doi/10.1074/jbc.RA118.005203.

Chung, K.P., Zeng, Y. and Jiang, L. (2016) COPII Paralogs in Plants: Functional Redundancy or Diversity? *Trends Plant Sci.*, **21**, 758–769. Available at: https://doi.org/10.1016/j.tplants.2016.05.010.

Clough, S.J. and Bent, A.F. (1998) Floral dip: a simplified method for Agrobacterium - mediated transformation of *Arabidopsis thaliana*. *Plant J.*, **16**, 735–743. Available at: https://onlinelibrary.wiley.com/doi/abs/10.1046/j.1365-313x.1998.00343.x.

Cohen, C.K., Garvin, D.F. and Kochian, L. V. (2004) Kinetic properties of a micronutrient transporter from Pisum sativum indicate a primary function in Fe uptake from the soil. *Planta*, **218**, 784–792.

Colangelo, E.P. and Guerinot, M. Lou (2004) The Essential Basic Helix-Loop-Helix Protein FIT1 Is Required for the Iron Deficiency Response. *Plant Cell*, **16**, 3400 LP-3412. Available at: http://www.plantcell.org/content/16/12/3400.abstract.

Compeer, E.B., Kraus, F., Ecker, M., et al. (2018) A mobile endocytic network connects clathrin-independent receptor endocytosis to recycling and promotes T cell activation. *Nat. Commun.*, **9**, 1597. Available at: https://doi.org/10.1038/s41467-018-04088-w.

Connolly, E., Campbell, N., Grotz, N., Prichard, C. and Guerinot, M. (2003) Overexpression of the FRO2 Ferric Chelate Reductase Confers Tolerance to Growth on Low Iron and Uncovers Posttranscriptional Control 1. *Regulation*, **133**, 1102–1110.

Connolly, E.L., Fett, J.P. and Guerinot, M. Lou (2002) Expression of the IRT1 Metal Transporter Is Controlled by Metals at the Levels of Transcript and Protein Accumulation. *Plant Cell*, **14**, 1347 LP-1357. Available at: http://www.plantcell.org/content/14/6/1347.abstract.

Connorton, J.M., Balk, J. and Rodríguez-Celma, J. (2017) Iron homeostasis in plants - a brief overview. *Metallomics*, **9**, 813–823.

Contento, A.L. and Bassham, D.C. (2012) Structure and function of endosomes in plant cells. *J. Cell Sci.*, **125**, 3511–3518. Available at: http://jcs.biologists.org/cgi/doi/10.1242/jcs.093559.

Contreras, I., Ortiz-Zapater, E., Castilho, L.M. and Aniento, F. (2000) Characterization of Cop I Coat Proteins in Plant Cells. *Biochem. Biophys. Res. Commun.*, **273**, 176–182. Available at: http://www.sciencedirect.com/science/article/pii/S0006291X00929188.

Cooper GM. The Cell: A Molecular Approach. 2nd edition. Sunderland (MA): Sinauer Associates; 2000. Structure of the Plasma Membrane. Available from: https://www.ncbi.nlm.nih.gov/books/NBK9898/

Corradi, V., Mendez-Villuendas, E., Ingólfsson, H.I., et al. (2018) Lipid-Protein Interactions Are Unique Fingerprints for Membrane Proteins. *ACS Cent. Sci.*, **4**, 709–717.

Coskun, Ü. and Simons, K. (2011) Cell membranes: The lipid perspective. *Structure*, **19**, 1543–1548.

Cui, Y., Chen, C.L., Cui, M., Zhou, W.J., Wu, H.L. and Ling, H.Q. (2018) Four IVa bHLH Transcription Factors Are Novel Interactors of FIT and Mediate JA Inhibition of Iron Uptake in *Arabidopsis*. *Mol. Plant*, **11**, 1166–1183. Available at: https://doi.org/10.1016/j.molp.2018.06.005.

Cui, Y., He, Y., Cao, W., Gao, J. and Jiang, L. (2018) The Multivesicular Body and Autophagosome Pathways in Plants. *Front. Plant Sci.*, **9**, 1837. Available at: https://www.frontiersin.org/article/10.3389/fpls.2018.01837/full.

Cui, Y., Yu, M., Yao, X., Xing, J., Lin, J. and Li, X. (2018) Single-Particle Tracking for the Quantification of Membrane Protein Dynamics in Living Plant Cells. *Mol. Plant*, **11**, 1315–1327. Available at: http://www.sciencedirect.com/science/article/pii/S1674205218303034.

Cullen, P.J. and Korswagen, H.C. (2011) Sorting nexins provide diversity for retromer-dependent trafficking events. *Nat. Cell Biol.*, **14**, 29–37.

Curie, C., Alonso, J.M., Jean, M. Le, Ecker, J.R. and Briat, J.F. (2000) Involvement of NRAMP1 from *Arabidopsis thaliana* in iron transport. *Biochem. J.*, **347 Pt 3**, 749–755.

Curie, C., Cassin, G., Couch, D., et al. (2009) Metal movement within the plant: Contribution of nicotianamine and yellow stripe 1-like transporters. *Ann. Bot.*, **103**, 1–11.

Dalcorso, G., Manara, A., Piasentin, S. and Furini, A. (2014) Nutrient metal elements

in plants. *Metallomics*, **6**, 1770–1788. Available at: http://dx.doi.org/10.1039/C4MT00173G.

Damme, D. Van, Gadeyne, A., Vanstraelen, M., Inzé, D., Montagu, M.C.E. Van, Jaeger, G. De, Russinova, E. and Geelen, D. (2011) Adaptin-like protein TPLATE and clathrin recruitment during plant somatic cytokinesis occurs via two distinct pathways. *Proc. Natl. Acad. Sci.*, **108**, 615 LP-620. Available at: http://www.pnas.org/content/108/2/615.abstract.

Daněk, M., Valentová, O. and Martinec, J. (2016) Flotillins, Erlins, and HIRs: From Animal Base Camp to Plant New Horizons. *CRC. Crit. Rev. Plant Sci.*, **35**, 191–214. Available at: http://dx.doi.org/10.1080/07352689.2016.1249690.

Dart, C. (2010) Lipid microdomains and the regulation of ion channel function. *J. Physiol.*, **588**, 3169–3178.

Day, B., Dahlbeck, D., Huang, J., Chisholm, S.T., Li, D. and Staskawicz, B.J. (2005) Molecular Basis for the RIN4 Negative Regulation of RPS2 Disease Resistance. *Plant Cell*, **17**, 1292–1305.

Delaunay, J.-L., Breton, M., Goding, J.W., Trugnan, G. and Maurice, M. (2007) Differential detergent resistance of the apical and basolateral NPPases: relationship with polarized targeting. *J. Cell Sci.*, **120**, 1009–1016.

Demir F, Horntrich C, Blachutzik JO, et al. (2013) *Arabidopsis* nanodomain-delimited ABA signaling pathway regulates the anion channel SLAH3. *Proc Natl Acad Sci U S A*. **110**(20):8296–8301. doi:10.1073/pnas.1211667110

Dettmer, J. (2006) Vacuolar H+-ATPase Activity Is Required for Endocytic and Secretory Trafficking in *Arabidopsis*. *Plant Cell Online*, **18**, 715–730. Available at: http://www.plantcell.org/cgi/doi/10.1105/tpc.105.037978.

Dettmer, J. and Friml, J. (2011) Cell polarity in plants: When two do the same, it is not the same.... *Curr. Opin. Cell Biol.*, **23**, 686–696.

DeWitt, N.D., Hong, B., Sussman, M.R. and Harper, J.F. (1996) Targeting of two *Arabidopsis* H(+)-ATPase isoforms to the plasma membrane. *Plant Physiol.*, **112**, 833–844.

Di, C., Xu, W., Su, Z. and Yuan, J.S. (2010) Comparative genome analysis of PHB gene family reveals deep evolutionary origins and diverse gene function. *BMC Bioinformatics*, **11**.

Diaz-Rohrer, B.B., Levental, K.R., Simons, K. and Levental, I. (2014) Membrane raft association is a determinant of plasma membrane localization. *Proc. Natl. Acad. Sci.*, **111**, 8500–8505. Available at: http://www.pnas.org/cgi/doi/10.1073/pnas.1404582111.

DiDonato, R.J., Roberts, L.A., Sanderson, T., Eisley, R.B. and Walker, E.L. (2004) *Arabidopsis* Yellow Stripe-Like2 (YSL2): A metal-regulated gene encoding a plasma membrane transporter of nicotianamine-metal complexes. *Plant J.*, **39**, 403–414.

Dikic, I., Wakatsuki, S. and Walters, K.J. (2009) Ubiquitin-binding domains — from structures to functions. *Nat. Rev. Mol. Cell Biol.*, **10**, 659. Available at: https://doi.org/10.1038/nrm2767.

Dinneny, J.R., Long, T.A., Wang, J.Y., et al. (2008) Cell identity mediates the response of *Arabidopsis* roots to abiotic stress. *Science.*, **320**, 942–945.

Duan, Y., Guo, J., Shi, X., Guan, X., Liu, F., Bai, P., Huang, L. and Kang, Z. (2013) Wheat hypersensitive-induced reaction genes TaHIR1 and TaHIR3 are involved in response to stripe rust fungus infection and abiotic stresses. *Plant Cell Rep.*, **32**, 273–283.

Dubeaux, G., Neveu, J., Zelazny, E. and Vert, G. (2018) Metal Sensing by the IRT1

Transporter-Receptor Orchestrates Its Own Degradation and Plant Metal Nutrition. *Mol. Cell*, **69**, 953–964.e5. Available at: http://linkinghub.elsevier.com/retrieve/pii/S1097276518301072.

Duby, G. and Boutry, M. (2009) The plant plasma membrane proton pump ATPase: A highly regulated P-type ATPase with multiple physiological roles. *Pflugers Arch. Eur. J. Physiol.*, **457**, 645–655.

Duckett, C.M., Oparka, K.J., Prior, D. a M., Dolan, L. and Roberts, K. (1994) Dye-coupling in the root epidermis of *Arabidopsis* is progressively reduced during development. *Development*, **120**, 3247–3255.

Durrett, T.P., Gassmann, W. and Rogers, E.E. (2007) The FRD3-Mediated Efflux of Citrate into the Root Vasculature Is Necessary for Efficient Iron Translocation. *Plant Physiol.*, **144**, 197–205. Available at: http://www.plantphysiol.org/cgi/doi/10.1104/pp.107.097162.

Duy, D., Wanner, G., Meda, A.R., Wiren, N. von, Soll, J. and Philippar, K. (2007) PIC1, an Ancient Permease in *Arabidopsis* Chloroplasts, Mediates Iron Transport. *Plant Cell Online*, **19**, 986–1006. Available at: http://www.plantcell.org/cgi/doi/10.1105/tpc.106.047407.

Eide, D., Broderius, M., Fett, J. and Guerinot, M.L. (1996) A novel iron-regulated metal transporter from plants identified by functional expression in yeast. *Proc. Natl. Acad. Sci. U. S. A.*, **93**, 5624–5628.

Fajardo-Somera, R.A., Bowman, B. and Riquelme, M. (2013) The Plasma Membrane Proton Pump PMA-1 Is Incorporated into Distal Parts of the Hyphae Independently of the Spitzenkörper in Neurospora crassa. *Eukaryot. Cell*, **12**, 1097–1105.

Falhof, J., Pedersen, J.T., Fuglsang, A.T. and Palmgren, M. (2016) Plasma Membrane H+-ATPase Regulation in the Center of Plant Physiology. *Mol. Plant*, **9**, 323–337. Available at: http://dx.doi.org/10.1016/j.molp.2015.11.002.

Fan, L., Hao, H., Xue, Y., Zhang, L., Song, K., Ding, Z., Botella, M.A., Wang, H. and Lin, J. (2013) Dynamic analysis of *Arabidopsis* AP2 σ subunit reveals a key role in clathrin-mediated endocytosis and plant development. *Development*, **140**, 3826 LP-3837. Available at: http://dev.biologists.org/content/140/18/3826.abstract.

Fan, L., Li, R., Pan, J., Ding, Z. and Lin, J. (2015) Endocytosis and its regulation in plants. *Trends Plant Sci.*, **20**, 388–397. Available at: https://doi.org/10.1016/j.tplants.2015.03.014.

Filatov, V., Dowdle, J., Smirnoff, N., Ford-Lloyd, B., Newbury, H.J. and Macnair, M.R. (2007) A quantitative trait loci analysis of Zinc hyperaccumulation in *Arabidopsis* halleri. *New Phytol.*, **174**, 580–590. Available at: https://nph.onlinelibrary.wiley.com/doi/abs/10.1111/j.1469-8137.2007.02036.x.

Filatov, V., Dowdle, J., Smirnoff, N., Ford-Lloyd, B., Newbury, H.J. and Macnair, M.R. (2006) Comparison of gene expression in segregating families identifies genes and genomic regions involved in a novel adaptation, zinc hyperaccumulation. *Mol. Ecol.*, **15**, 3045–3059. Available at: https://onlinelibrary.wiley.com/doi/abs/10.1111/j.1365-294X.2006.02981.x.

Fischer, S., Spielau, T. and Clemens, S. (2017) Natural variation in *Arabidopsis thaliana* Cd responses and the detection of quantitative trait loci affecting Cd tolerance. *Sci. Rep.*, **7**, 1–14.

Flis, P., Ouerdane, L., Grillet, L., Curie, C., Mari, S. and Lobinski, R. (2016) Inventory of metal complexes circulating in plant fluids: a reliable method based on HPLC coupled with dual elemental and high-resolution molecular mass spectrometric detection. *New Phytol.*, **211**, 1129–1141.

Fourcroy, P., Sisó-Terraza, P., Sudre, D., et al. (2014) Involvement of the ABCG37 transporter in secretion of scopoletin and derivatives by *Arabidopsis* roots in response to iron deficiency. *New Phytol.*, **201**, 155–167.

Fourcroy, P., Tissot, N., Gaymard, F., Briat, J.F. and Dubos, C. (2016) Facilitated Fe Nutrition by Phenolic Compounds Excreted by the *Arabidopsis* ABCG37/PDR9 Transporter Requires the IRT1/FRO2 High-Affinity Root Fe^{2+}Transport System. *Mol. Plant*, **9**, 485–488.

Frick, M., Bright, N.A., Riento, K., Bray, A., Merrified, C. and Nichols, B.J. (2007) Coassembly of Flotillins Induces Formation of Membrane Microdomains, Membrane Curvature, and Vesicle Budding. *Curr. Biol.*, **17**, 1151–1156. Available at: https://doi.org/10.1016/j.cub.2007.05.078.

Fu, S., Xu, Y., Li, C., Li, Y., Wu, J. and Zhou, X. (2018) Rice Stripe Virus Interferes with S-acylation of Remorin and Interaction Induces Its Autophagic Degradation to Facilitate Virus Infection. *Mol. Plant*, **11**, 269–287. Available at: https://www.sciencedirect.com/science/article/pii/S1674205217303660 [Accessed April 11, 2019].

Fuglsang, A.T., Guo, Y., Cuin, T.A., et al. (2007) *Arabidopsis* Protein Kinase PKS5 Inhibits the Plasma Membrane H+-ATPase by Preventing with 14-3-3 Protein. *Plant Cell*, **19**, 1617–1634. Available at: http://www.plantcell.org/content/19/5/1617.

Fuglsang, A.T., Visconti, S., Drumm, K., Jahn, T., Stensballe, A., Mattei, B., Jensen, O.N., Aducci, P. and Palmgren, M.G. (1999) Binding of 14-3-3 protein to the plasma membrane H+-ATPase AHA2 involves the three C-terminal residues Tyr946-Thr-Val and requires phosphorylation of Thr947. *J. Biol. Chem.*, **274**, 36774–36780.

Fuji, K., Miwa, K. and Fujiwara, T. (2009) The intracellular transport of transporters : membrane trafficking of mineral transporters. *Curr. Opin. Plant Biol.*, **12**, 699–704.

Fujimoto, M., Arimura, S. -i., Ueda, T., Takanashi, H., Hayashi, Y., Nakano, A. and Tsutsumi, N. (2010) *Arabidopsis* dynamin-related proteins DRP2B and DRP1A participate together in clathrin-coated vesicle formation during endocytosis. *Proc. Natl. Acad. Sci.*, **107**, 6094–6099.

Fujimoto, M. and Tsutsumi, N. (2014) Dynamin-related proteins in plant post-Golgi traffic. *Front. Plant Sci.*, **5**, 1–8.

Furt, F., Simon-Plas, F. and Mongrand, S. (2010) Lipids of the Plant Plasma Membrane. In *Plant Cell Monographs*. pp. 3–30.

Gadeyne, A., Sánchez-Rodríguez, C., Vanneste, S., et al. (2014) The TPLATE adaptor complex drives clathrin-mediated endocytosis in plants. *Cell*, **156**, 691–704.

Gaither, L. and J. Eide, D. (2001) Eukaryotic Zinc transporters and their regulation. *Biometals*, **14**, 251–270.

Galan, J.M. and Haguenauer-Tsapis, R. (1997) Ubiquitin lys63 is involved in ubiquitination of a yeast plasma membrane protein. *EMBO J.*, **16**, 5847–5854.

Gao, C., Luo, M., Zhao, Q., Yang, R., Cui, Y., Zeng, Y., Xia, J. and Jiang, L. (2014) A Unique plant ESCRT component, FREE1, regulates multivesicular body protein sorting and plant growth. *Curr. Biol.*, **24**, 2556–2563. Available at: http://dx.doi.org/10.1016/j.cub.2014.09.014.

Gao, C., Zhuang, X., Shen, J. and Jiang, L. (2017) Plant ESCRT Complexes: Moving Beyond Endosomal Sorting. *Trends Plant Sci.*, **22**, 986–998. Available at: http://dx.doi.org/10.1016/j.tplants.2017.08.003.

García-Sáez, A.J. and Schwille, P. (2010) Stability of lipid domains. *FEBS Lett.*, **584**, 1653–1658.

Gayomba, S.R., Zhai, Z., Jung, H. and Vatamaniuk, O.K. (2015) Local and systemic signaling of iron status and its interactions with homeostasis of other essential elements. *Front. Plant Sci.*, **6**, 1–13. Available at: http://journal.frontiersin.org/article/10.3389/fpls.2015.00716/abstract.

Gehl, B. and Sweetlove, L.J. (2014) Mitochondrial Band-7 family proteins : scaffolds for respiratory chain assembly ? *Front Plant Sci*., **5**, 1–6.

Geiger, D., Maierhofer, T., Al-rasheid, K.A.S., et al. (2012) Stomatal Closure by Fast Abscisic Acid Signaling Is Mediated by the Guard Cell Anion Channel SLAH3 and the Receptor RCAR1. *Sci. Signal.*, **4**, ra32.

Geldner, N., Dénervaud-Tendon, V., Hyman, D.L., Mayer, U., Stierhof, Y.D. and Chory, J. (2009) Rapid, combinatorial analysis of membrane compartments in intact plants with a multicolor marker set. *Plant J.*, **59**, 169–178.

Geldner, N., Ueda, T., Nakano, A., et al. (2003) The *Arabidopsis* GNOM ARF-GEF Mediates Endosomal Recycling, Auxin Transport, and Auxin-Dependent Plant Growth. *Cell*, **112**, 219–230. Available at: http://www.sciencedirect.com/science/article/B6WSN-4C5HFSN-C/1/f11ba1d818b44fe5ce2cd95f8725a908\n

Gitan, R.S. and Eide, D.J. (2000) Zinc-regulated ubiquitin conjugation signals endocytosis of the yeast ZRT1 zinc transporter. *Biochem. J.*, **346 Pt 2**, 329–336.

Glebov, O.O., Bright, N.A. and Nichols, B.J. (2005) Flotillin-1 defines a clathrin-independent endocytic pathway in mammalian cells. *Nat. Cell Biol.*, **8**, 46. Available at: https://doi.org/10.1038/ncb1342.

Gratz, R., Manishankar, P., Ivanov, R., et al. (2019) CIPK11-Dependent Phosphorylation Modulates FIT Activity to Promote *Arabidopsis* Iron Acquisition in Response to Calcium Signaling. *Dev. Cell*, 1–15. Available at: https://linkinghub.elsevier.com/retrieve/pii/S1534580719300061.

Grebe, M. (2010) Cell Polarity: Lateral Perspectives. *Curr. Biol.*, **20**, R446–R448. Available at: http://dx.doi.org/10.1016/j.cub.2010.03.035.

Grefen, C. (2014) The Split-Ubiquitin System for the Analysis of Three-Component Interactions. In J. J. Sanchez-Serrano and J. Salinas, eds. *Arabidopsis Protocols*. Totowa, NJ: Humana Press, pp. 659–678. Available at: https://doi.org/10.1007/978-1-62703-580-4_34.

Grison, M.S., Brocard, L., Fouillen, L., et al. (2015) Specific Membrane Lipid Composition Is Important for Plasmodesmata Function in *Arabidopsis*. *Plant Cell*, **27**, 1228–1250. Available at: http://www.plantcell.org/lookup/doi/10.1105/tpc.114.135731.

Gronnier, J., Crowet, J.-M., Habenstein, B., et al. (2017) Structural basis for plant plasma membrane protein dynamics and organization into functional nanodomains. *Elife*, **6**.

Gronnier, J., Gerbeau-Pissot, P., Germain, V., Mongrand, S. and Simon-Plas, F. (2018) Divide and Rule: Plant Plasma Membrane Organization. *Trends Plant Sci.*, **23**, 899–917. Available at: https://doi.org/10.1016/j.tplants.2018.07.007.

Grunewald, W. and Friml, J. (2010) The march of the PINs: Developmental plasticity by dynamic polar targeting in plant cells. *EMBO J.*, **29**, 2700–2714.

Guerinot, M. and Yi, Y. (1994) Iron: Nutritious, Noxious, and Not Readily Available. *Plant Physiol*, **104**, 815–820.

Guerra, D.D. and Callis, J. (2012) Ubiquitin on the Move: The Ubiquitin Modification System Plays Diverse Roles in the Regulation of Endoplasmic Reticulum- and Plasma Membrane-Localized Proteins. *Plant Physiol.*, **160**, 56–64. Available at:

http://www.plantphysiol.org/cgi/doi/10.1104/pp.112.199869.
Hachez, C., Laloux, T., Reinhardt, H., et al. (2014) *Arabidopsis* SNAREs SYP61 and SYP121 Coordinate the Trafficking of Plasma Membrane Aquaporin PIP2;7 to Modulate the Cell Membrane Water Permeability. *Plant Cell*, **26**, 3132–3147. Available at: http://www.plantcell.org/lookup/doi/10.1105/tpc.114.127159.
Haglund, K., Sigismund, S., Polo, S., Szymkiewicz, I., Fiore, P.P. Di and Dikic, I. (2003) Multiple monoubiquitination of RTKs is sufficient for their endocytosis and degradation. *Nat. Cell Biol.*, **5**, 461. Available at: https://doi.org/10.1038/ncb983.
Hammond, G.R. V and Balla, T. (2015) Polyphosphoinositide binding domains: Key to inositol lipid biology. *Biochim. Biophys. Acta*, **1851**, 746–758.
Han, X., Yang, Y., Wu, Y., Liu, X., Lei, X. and Guo, Y. (2017) A bioassay-guided fractionation system to identify endogenous small molecules that activate plasma membrane H + -ATPase activity in *Arabidopsis*. *J. Exp. Bot.*, **68**, 2951–2962.
Haney, C.H. and Long, S.R. (2010) Plant flotillins are required for infection by nitrogen-fixing bacteria. *Proc. Natl. Acad. Sci. U. S. A.*, **107**, 478–483.
Haney, C.H., Riely, B.K., Tricoli, D.M., Cook, D.R., Ehrhardt, D.W. and Long, S.R. (2011) Symbiotic rhizobia bacteria trigger a change in localization and dynamics of the Medicago truncatula receptor kinase LYK3. *Plant Cell*, **23**, 2774–2787.
Hao, H., Fan, L., Chen, T., Li, R., Li, X., He, Q., Botella, M.A. and Lin, J. (2014) Clathrin and Membrane Microdomains Cooperatively Regulate RbohD Dynamics and Activity in *Arabidopsis*. *Plant Cell*, **26**, 1729–1745. Available at: http://www.plantcell.org/cgi/doi/10.1105/tpc.113.122358.
Haruta, M., Burch, H.L., Nelson, R.B., Barrett-Wilt, G., Kline, K.G., Mohsin, S.B., Young, J.C., Otegui, M.S. and Sussman, M.R. (2010) Molecular characterization of mutant *Arabidopsis* plants with reduced plasma membrane proton pump activity. *J. Biol. Chem.*, **285**, 17918–17929.
Haruta, M., Sabat, G., Stecker, K., Minkoff, B.B. and Sussman, M.R. (2014) A peptide hormone and its receptor protein kinase regulate plant cell expansion. *Science (80-.).*, **343**, 408–411.
Haruta, M., Tan, L.X., Bushey, D.B., Swanson, S.J. and Sussman, M.R. (2018) Environmental and Genetic Factors Regulating Localization of the Plant Plasma Membrane H+-ATPase. *Plant Physiol.*, **176**, pp.01126.2017. Available at: http://www.plantphysiol.org/lookup/doi/10.1104/pp.17.01126.
Haucke, V. and Kozlov, M.M. (2018) Membrane remodeling in clathrin-mediated endocytosis. *J. Cell Sci.*, **131**, jcs216812. Available at: http://jcs.biologists.org/content/131/17/jcs216812.abstract.
Hawes, C. (2005) Cell biology of the plant Golgi apparatus. *New Phytol.*, **165**, 29–44. Available at: https://doi.org/10.1111/j.1469-8137.2004.01218.x.
Hendry, G.A.F. and Brocklebank, K.J. (1985) Iron-Induced Oxygen Radical Metabolism in Waterlogged Plants. *New Phytol.*, **101**, 199–206. Available at: http://www.jstor.org/stable/2432545.
Heucken, N. and Ivanov, R. (2017) The retromer, sorting nexins and the plant endomembrane protein trafficking. *J. Cell Sci.*, jcs.203695. Available at: http://jcs.biologists.org/lookup/doi/10.1242/jcs.203695.
Hindt, M.N., Akmakjian, G.Z., Pivarski, K.L., Punshon, T., Baxter, I., Salt, D.E. and Guerinot, M. Lou (2017) BRUTUS and its paralogs, BTS LIKE1 and BTS LIKE2, encode important negative regulators of the iron deficiency response in *Arabidopsis thaliana*. *Metallomics*, **9**, 876–890.
Hoffmann, R.D., Olsen, L.I., Ezike, C. V, Pedersen, J.T., Manstretta, R., López-

Marqués, R.L. and Palmgren, M. Roles of plasma membrane proton ATPases AHA2 and AHA7 in normal growth of roots and root hairs in *Arabidopsis thaliana*. *Physiol. Plant.*, 1; 68(7). Available at: https://onlinelibrary.wiley.com/doi/abs/10.1111/ppl.12842.

Huang, J. and Feigenson, G.W. (1999) A microscopic interaction model of maximum solubility of cholesterol in lipid bilayers. *Biophys. J.*, **76**, 2142–2157.

Hwang, I. and Robinson, D.G. (2009) Transport vesicle formation in plant cells. *Curr. Opin. Plant Biol.*, **12**, 660–669.

Ishimaru, Y., Suzuki, M., Tsukamoto, T., et al. (2006) Rice plants take up iron as an Fe^{3+}-phytosiderophore and as Fe^{2+}. *Plant J.*, **45**, 335–346.

Ivanov, R., Brumbarova, T. and Bauer, P. (2012) Fitting into the harsh reality: Regulation of iron-deficiency responses in dicotyledonous plants. *Mol. Plant*, **5**, 27–42. Available at: http://dx.doi.org/10.1093/mp/ssr065.

Ivanov, R., Brumbarova, T., Blum, A., Jantke, A.-M., Fink-Straube, C. and Bauer, P. (2014) SORTING NEXIN1 Is Required for Modulating the Trafficking and Stability of the *Arabidopsis* IRON-REGULATED TRANSPORTER1. *Plant Cell*, **26**, 1294–1307. Available at: http://www.plantcell.org/cgi/doi/10.1105/tpc.113.116244.

Jacobson, K., Mouritsen, O.G. and Anderson, R.G.W. (2007) Lipid rafts: At a crossroad between cell biology and physics. *Nat. Cell Biol.*, **9**, 7–14.

Jahn, T., Dietrich, J., Andersen, B., Leidvik, B., Otter, C., Briving, C., Kühlbrandt, W. and Palmgren, M.G. (2001) Large scale expression, purification and 2D crystallization of recombinant plant plasma membrane H+-ATPase. *J. Mol. Biol.*, **309**, 465–476.

Jaillais, Y., Santambrogio, M., Rozier, F., Fobis-Loisy, I., Miège, C. and Gaude, T. (2007) The Retromer Protein VPS29 Links Cell Polarity and Organ Initiation in Plants. *Cell*, **130**, 1057–1070.

Jaillais, Y. and Vert, G. (2016) Brassinosteroid signaling and BRI1 dynamics went underground. *Curr. Opin. Plant Biol.*, **33**, 92–100.

Jain, A., Wilson, G.T. and Connolly, E.L. (2014) The diverse roles of FRO family metalloreductases in iron and copper homeostasis. *Front. Plant Sci.*, **5**, 100. Available at: http://journal.frontiersin.org/article/10.3389/fpls.2014.00100/abstract.

Jakoby, M., Wang, H.Y., Reidt, W., Weisshaar, B. and Bauer, P. (2004) FRU (BHLH029) is required for induction of iron mobilization genes in *Arabidopsis thaliana*. *FEBS Lett.*, **577**, 528–534.

Jarsch, I.K., Konrad, S.S.A., Stratil, T.F., Urbanus, S.L., Szymanski, W., Braun, P., Braun, K.-H. and Ott, T. (2014) Plasma Membranes Are Subcompartmentalized into a Plethora of Coexisting and Diverse Microdomains in *Arabidopsis* and Nicotiana benthamiana; *Plant Cell*, **26**, 1698 LP-1711. Available at: http://www.plantcell.org/content/26/4/1698.abstract.

Jeong, J., Cohu, C., Kerkeb, L., Pilon, M., Connolly, E.L. and Guerinot, M. Lou (2008) Chloroplast Fe(III) chelate reductase activity is essential for seedling viability under iron limiting conditions. *Proc. Natl. Acad. Sci. U. S. A.*, **105**, 10619–10624.

Jeong, J., Merkovich, A., Clyne, M. and Connolly, E.L. (2017) Directing iron transport in dicots: regulation of iron acquisition and translocation. *Curr. Opin. Plant Biol.*, **39**, 106–113. Available at: http://dx.doi.org/10.1016/j.pbi.2017.06.014.

Johnson, A. and Vert, G. (2017) Single Event Resolution of Plant Plasma Membrane Protein Endocytosis by TIRF Microscopy. *Front. Plant Sci.*, **8**, 1–11. Available at: http://journal.frontiersin.org/article/10.3389/fpls.2017.00612/full.

Johnson, A. and Vert, G. (2016) Unraveling K63 Polyubiquitination Networks by Sensor-Based Proteomics. *Plant Physiol.*, **171**, 1808–1820. Available at: http://www.plantphysiol.org/lookup/doi/10.1104/pp.16.00619.

Jung, H.W. and Hwang, B.K. (2007) The leucine-rich repeat (LRR) protein, CaLRR1, interacts with the hypersensitive induced reaction (HIR) protein, CaHIR1, and suppresses cell death induced by the CaHIR1 protein. *Mol. Plant Pathol.*, **8**, 503—514. Available at: https://doi.org/10.1111/j.1364-3703.2007.00410.x.

Jung, H.W., Lim, C.W., Lee, S.C., Choi, H.W., Hwang, C.H. and Hwang, B.K. (2008) Distinct roles of the pepper hypersensitive induced reaction protein gene CaHIR1 in disease and osmotic stress, as determined by comparative transcriptome and proteome analyses. *Planta*, **227**, 409—425. Available at: https://doi.org/10.1007/s00425-007-0628-6.

Kanczewska, J., Marco, S., Vandermeeren, C., Maudoux, O., Rigaud, J.-L. and Boutry, M. (2005) Activation of the plant plasma membrane H+-ATPase by phosphorylation and binding of 14-3-3 proteins converts a dimer into a hexamer. *Proc. Natl. Acad. Sci.*, **102**, 11675–11680. Available at: http://www.pnas.org/cgi/doi/10.1073/pnas.0504498102.

Karandur, D., Nawrotek, A., Kuriyan, J. and Cherfils, J. (2017) Multiple interactions between an Arf/GEF complex and charged lipids determine activation kinetics on the membrane. *Proc. Natl. Acad. Sci.*, **114**, 201707970. Available at: http://www.pnas.org/lookup/doi/10.1073/pnas.1707970114.

Karlova, R., Boeren, S., Russinova, E., Aker, J., Vervoort, J. and Vries, S. de (2006) You have access The *Arabidopsis* Somatic Embryogenesis Receptor-like kinase1 protein complex includes brassinosteroid-insensitive1. *Plant Cell*, **18**, 626 LP-638. Available at: http://www.plantcell.org/content/18/3/626.abstract.

Kasai, K., Takano, J., Miwa, K., Toyoda, A. and Fujiwara, T. (2011) High boron-induced ubiquitination regulates vacuolar sorting of the BOR1 borate transporter in *Arabidopsis thaliana*. *J. Biol. Chem.*, **286**, 6175–6183.

Keinath, N.F., Kierszniowska, S., Lorek, J., et al. (2010) PAMP (Pathogen-associated Molecular Pattern)-induced changes in plasma membrane compartmentalization reveal novel components of plant immunity. *J. Biol. Chem.*, **285**, 39140–39149.

Kim, D.-Y., Bovet, L., Maeshima, M., Martinoia, E. and Lee, Y. (2007) The ABC transporter AtPDR8 is a cadmium extrusion pump conferring heavy metal resistance. *Plant J.*, **50**, 207–218. Available at: https://onlinelibrary.wiley.com/doi/abs/10.1111/j.1365-313X.2007.03044.x.

Kim, D.-Y., Scalf, M., Smith, L.M. and Vierstra, R.D. (2013) Advanced Proteomic Analyses Yield a Deep Catalog of Ubiquitylation Targets in *Arabidopsis* . *Plant Cell*, **25**, 1523–1540.

Kim, H.T., Kim, K.P., Lledias, F., Kisselev, A.F., Scaglione, K.M., Skowyra, D., Gygi, S.P. and Goldberg, A.L. (2007) Certain Pairs of Ubiquitin-conjugating Enzymes (E2s) and Ubiquitin-Protein Ligases (E3s) Synthesize Nondegradable Forked Ubiquitin Chains Containing All Possible Isopeptide Linkages. *J. Biol. Chem.*, **282**, 17375–17386. Available at: http://www.jbc.org/content/282/24/17375.abstract.

Kim, S.A., Punshon, T., Lanzirotti, A., Li, A., Alonso, J.M., Ecker, J.R., Kaplan, J. and Guerinot, M. Lou (2006) Localization of iron in *Arabidopsis* seed requires the vacuolar membrane transporter VIT1. *Science (80-.).*, **314**, 1295–1298.

Kim, S.J. and Brandizzi, F. (2016) The plant secretory pathway for the trafficking of cell wall polysaccharides and glycoproteins. *Glycobiology*, **26**, 940–949.

Kim, S.-J. and Brandizzi, F. (2012) News and Views into the SNARE Complexity in

Arabidopsis. *Front. Plant Sci.*, **3**, 1–6.
Klatte, M., Schuler, M., Wirtz, M., Fink-Straube, C., Hell, R. and Bauer, P. (2009) The Analysis of *Arabidopsis* Nicotianamine Synthase Mutants Reveals Functions for Nicotianamine in Seed Iron Loading and Iron Deficiency Responses. *Plant Physiol.*, **150**, 257–271. Available at: http://www.plantphysiol.org/cgi/doi/10.1104/pp.109.136374.
Kleine-Vehn, J., Leitner, J., Zwiewka, M., Sauer, M., Abas, L., Luschnig, C. and Friml, J. (2008) Differential degradation of PIN2 auxin efflux carrier by retromer-dependent vacuolar targeting. *Proc. Natl. Acad. Sci. U. S. A.*, **105**, 17812–17817.
Klemm, R.W., Ejsing, C.S., Surma, M.A., et al. (2009) Segregation of sphingolipids and sterols during formation of secretory vesicles at the trans-Golgi network. *J. Cell Biol.*, **185**, 601–612.
Kobayashi, T., Nagasaka, S., Senoura, T., Itai, R.N., Nakanishi, H. and Nishizawa, N.K. (2013) Iron-binding haemerythrin RING ubiquitin ligases regulate plant iron responses and accumulation. *Nat. Commun.*, **4**, 1–12. Available at: http://dx.doi.org/10.1038/ncomms3792.
Kobayashi, T., Nakanishi Itai, R. and Nishizawa, N.K. (2014) Iron deficiency responses in rice roots. *Rice*, **7**, 1–11.
Kobayashi, T. and Nishizawa, N.K. (2012) Iron Uptake, Translocation, and Regulation in Higher Plants. *Annu. Rev. Plant Biol.*, **63**, 131–152. Available at: http://www.annualreviews.org/doi/10.1146/annurev-arplant-042811-105522.
Komander, D. (2009) *The emerging complexity of protein ubiquitination*,.
Konrad, S.S.A. and Ott, T. (2015) Molecular principles of membrane microdomain targeting in plants. *Trends Plant Sci.*, **20**, 351–361.
Konrad, S.S.A., Popp, C., Stratil, T.F., Jarsch, I.K., Thallmair, V., Folgmann, J., Marín, M. and Ott, T. (2014) S-acylation anchors remorin proteins to the plasma membrane but does not primarily determine their localization in membrane microdomains. *New Phytol.*, **203**, 758–769.
Kozik, P., Francis, R.W., Seaman, M.N.J. and Robinson, M.S. (2010) A screen for endocytic motifs. *Traffic*, **11**, 843–855.
Lahner, B., Gong, J., Mahmoudian, M., et al. (2003) Genomic scale profiling of nutrient and trace elements in *Arabidopsis thaliana*. *Nat. Biotechnol.*, **21**, 1215–1221.
Langhorst, M.F., Reuter, A., Jaeger, F.A., Wippich, F.M., Luxenhofer, G., Plattner, H. and Stuermer, C.A.O. (2008) Trafficking of the microdomain scaffolding protein reggie-1/flotillin-2. *Eur. J. Cell Biol.*, **87**, 211–226.
Langhorst, M.F., Solis, G.P., Hannbeck, S., Plattner, H. and Stuermer, C.A.O. (2007) Linking membrane microdomains to the cytoskeleton: Regulation of the lateral mobility of reggie-1/flotillin-2 by interaction with actin. *FEBS Lett.*, **581**, 4697–4703.
Łangowski, Ł., Růžička, K., Naramoto, S., Kleine-Vehn, J. and Friml, J. (2010) Trafficking to the Outer Polar Domain Defines the Root-Soil Interface. *Curr. Biol.*, **20**, 904–908. Available at: https://doi.org/10.1016/j.cub.2010.03.059.
Lanquar, V., Lelièvre, F., Bolte, S., et al. (2005) Mobilization of vacuolar iron by AtNRAMP3 and AtNRAMP4 is essential for seed germination on low iron. *EMBO J.*, **24**, 4041–4051.
Lanquar, V., Ramos, M.S., Lelièvre, F., Barbier-Brygoo, H., Krieger-Liszkay, A., Krämer, U. and Thomine, S. (2010) Export of vacuolar manganese by AtNRAMP3 and AtNRAMP4 is required for optimal photosynthesis and growth under manganese deficiency. *Plant Physiol.*, **152**, 1986–99. Available at:

http://www.pubmedcentral.nih.gov/articlerender.fcgi?artid=2850043&tool=pmcentrez&rendertype=abstract.

Laude, A. and Prior, I. (2004) Plasma membrane microdomains: organization, function and trafficking. *Mol. Membr. Biol.*, **21**, 193–205. Available at: http://informahealthcare.com/doi/abs/10.1080/09687680410001700517.

Lauwers, E., Erpapazoglou, Z., Haguenauer-Tsapis, R. and André, B. (2010) The ubiquitin code of yeast permease trafficking. *Trends Cell Biol.*, **20**, 196–204.

Lauwers, E., Jacob, C. and André, B. (2009) K63-linked ubiquitin chains as a specific signal for protein sorting into the multivesicular body pathway. *J. Cell Biol.*, **185**, 493–502.

Leborgne-Castel, N. and Luu, D. (2009) Regulation of endocytosis by external stimuli in plant cells. *Plant Biosyst.*, **143**, 630–635.

Lederkremer, G.Z., Cheng, Y., Petre, B.M., Vogan, E., Springer, S., Schekman, R., Walz, T. and Kirchhausen, T. (2001) Structure of the Sec23p/24p and Sec13p/31p complexes of COPII. *Proc. Natl. Acad. Sci.*, **98**, 10704 LP-10709. Available at: http://www.pnas.org/content/98/19/10704.abstract.

Lee, M.C.S., Orci, L., Hamamoto, S., Futai, E., Ravazzola, M. and Schekman, R. (2005) Sar1p N-Terminal Helix Initiates Membrane Curvature and Completes the Fission of a COPII Vesicle. *Cell*, **122**, 605–617. Available at: https://doi.org/10.1016/j.cell.2005.07.025.

Lefebvre, B. (2004) Targeting of a Nicotiana plumbaginifolia H+-ATPase to the Plasma Membrane Is Not by Default and Requires Cytosolic Structural Determinants. *Plant Cell Online*, **16**, 1772–1789. Available at: http://www.plantcell.org/cgi/doi/10.1105/tpc.022277.

Lefebvre, B., Furt, F., Hartmann, M.-A., et al. (2007) Characterization of Lipid Rafts from Medicago truncatula Root Plasma Membranes: A Proteomic Study Reveals the Presence of a Raft-Associated Redox System1. *Plant Physiol.*, **144**, 402 LP-418. Available at: http://www.plantphysiol.org/content/144/1/402.abstract.

Lefebvre, B., Timmers, T., Mbengue, M., et al. (2010) A remorin protein interacts with symbiotic receptors and regulates bacterial infection. *Proc. Natl. Acad. Sci. U. S. A.*, **107**, 2343–2348.

Lefèvre, F., Fourmeau, J., Pottier, M., Baijot, A., Cornet, T., Abadía, J., Álvarez-Fernández, A. and Boutry, M. (2018) The Nicotiana tabacum ABC transporter NtPDR3 secretes O-methylated coumarins in response to iron deficiency. *J. Exp. Bot.*, **69**, 4419–4431.

Leitner, J., Petrasek, J., Tomanov, K., Retzer, K., Parezova, M., Korbei, B., Bachmair, A., Zazimalova, E. and Luschnig, C. (2012) Lysine63-linked ubiquitylation of PIN2 auxin carrier protein governs hormonally controlled adaptation of *Arabidopsis* root growth. *Proc. Natl. Acad. Sci.*, **109**, 8322–8327. Available at: http://www.pnas.org/cgi/doi/10.1073/pnas.1200824109.

Li, L.-Y., Cai, Q.-Y., Yu, D.-S. and Guo, C.-H. (2010) Overexpression of AtFRO6 in transgenic tobacco enhances ferric chelate reductase activity in leaves and increases tolerance to iron-deficiency chlorosis. *Mol. Biol. Rep.*, **38**, 3605–3613.

Li, R., Liu, P., Wan, Y., et al. (2012) A Membrane Microdomain-Associated Protein, *Arabidopsis* Flot1, Is Involved in a Clathrin-Independent Endocytic Pathway and Is Required for Seedling Development. *Plant Cell*, **24**, 2105–2122. Available at: http://www.plantcell.org/cgi/doi/10.1105/tpc.112.095695.

Li, X., Wang, X., Yang, Y., Li, R., He, Q., Fang, X., Luu, D.-T., Maurel, C. and Lin, J. (2011) Single-Molecule Analysis of PIP2;1 Dynamics and Partitioning Reveals

Multiple Modes of *Arabidopsis* Plasma Membrane Aquaporin Regulation. *Plant Cell*, **23**, 3780 LP-3797. Available at: http://www.plantcell.org/content/23/10/3780.abstract.

Liang, P., Stratil, T.F., Popp, C., Marín, M., Folgmann, J., Mysore, K.S., Wen, J. and Ott, T. (2018) Symbiotic root infections in Medicago truncatula require remorin-mediated receptor stabilization in membrane nanodomains. *Proc. Natl. Acad. Sci.*, **115**, 5289 LP-5294. Available at: http://www.pnas.org/content/115/20/5289.abstract.

Lichtenthaler, H.K. and Buschmann, C. (2001) Chlorophylls and Carotenoids: Measurement and Characterization by UV-VIS Spectroscopy. *Curr. Protoc. Food Anal. Chem.*, **1**, F4.3.1-F4.3.8. Available at: https://doi.org/10.1002/0471142913.faf0403s01.

Liu, J., DeYoung, S.M., Zhang, M., Dold, L.H. and Saltiel, A.R. (2005) The stomatin/prohibitin/flotillin/HflK/C domain of flotillin-1 contains distinct sequences that direct plasma membrane localization and protein interactions in 3T3-L1 adipocytes. *J. Biol. Chem.*, **280**, 16125–16134.

Long, T.A., Tsukagoshi, H., Busch, W., Lahner, B., Salt, D.E. and Benfey, P.N. (2010) The bHLH Transcription Factor POPEYE Regulates Response to Iron Deficiency in *Arabidopsis* Roots. *Plant Cell Online*, **22**, 2219–2236. Available at: http://www.plantcell.org/cgi/doi/10.1105/tpc.110.074096.

Lopez, M.M., Zelent, B. and Kosk-Kosicka, D. (2000) Effects of volatile anesthetic on the Ca2+-ATPase activation by dimerization. Distance-dependent quenching analysis and fluorescence energy transfer studies. *Eur. J. Biochem.*, **267**, 3345–3350.

Lu, D., Lin, W., Gao, X., et al. (2011) Direct ubiquitination of pattern recognition receptor FLS2 attenuates plant innate immunity. *Science*, **332**, 1439–1442.

Lucas, M., Gershlick, D.C., Vidaurrazaga, A., Rojas, A.L., Bonifacino, J.S. and Hierro, A. (2016) Structural Mechanism for Cargo Recognition by the Retromer Complex. *Cell*, **167**, 1623–1635.e14.

Luschnig, C. and Vert, G. (2014) The dynamics of plant plasma membrane proteins: PINs and beyond. *Development*, **141**, 2924–2938. Available at: http://dev.biologists.org/cgi/doi/10.1242/dev.103424.

Luu, D.T., Martinière, A., Sorieul, M., Runions, J. and Maurel, C. (2012) Fluorescence recovery after photobleaching reveals high cycling dynamics of plasma membrane aquaporins in *Arabidopsis* roots under salt stress. *Plant J.*, **69**, 894–905.

Lv, X., Jing, Y., Xiao, J., Zhang, Y., Zhu, Y., Julian, R. and Lin, J. (2017) Membrane microdomains and the cytoskeleton constrain AtHIR1 dynamics and facilitate the formation of an AtHIR1-associated immune complex. *Plant J.*, **90**, 3–16.

Ma, J.F., Tamai, K., Yamaji, N., Mitani, N., Konishi, S., Katsuhara, M., Ishiguro, M., Murata, Y. and Yano, M. (2006) A silicon transporter in rice. *Nature*, **440**, 688–691. Available at: https://doi.org/10.1038/nature04590.

Ma, J.F., Yamaji, N., Mitani, N., Tamai, K., Konishi, S., Fujiwara, T., Katsuhara, M. and Yano, M. (2007) An efflux transporter of silicon in rice. *Nature*, **448**, 209. Available at: https://doi.org/10.1038/nature05964.

Macháň, R. and Hof, M. (2010) Lipid diffusion in planar membranes investigated by fluorescence correlation spectroscopy. *Biochim. Biophys. Acta - Biomembr.*, **1798**, 1377–1391.

Mai, H.J., Pateyron, S. and Bauer, P. (2016) Iron homeostasis in *Arabidopsis thaliana*: Transcriptomic analyses reveal novel FIT-regulated genes, iron deficiency marker genes and functional gene networks. *BMC Plant Biol.*, **16**, 1–22. Available at:

http://dx.doi.org/10.1186/s12870-016-0899-9.
Malinsky, J., Opekarová, M., Grossmann, G. and Tanner, W. (2013) Membrane Microdomains, Rafts, and Detergent-Resistant Membranes in Plants and Fungi. *Annu. Rev. Plant Biol*, **64**, 501–29.
Mamode Cassim, A., Gouguet, P., Gronnier, J., et al. (2019) Plant lipids: Key players of plasma membrane organization and function. *Prog. Lipid Res.*, **73**, 1–27. Available at: https://doi.org/10.1016/j.plipres.2018.11.002.
Mao, H., Nakamura, M., Viotti, C. and Grebe, M. (2016) A Framework for Lateral Membrane Trafficking and Polar Tethering of the PEN3 ATP-Binding Cassette Transporter. *Plant Physiol.*, **172**, 2245–2260.
Marín, M. and Ott, T. (2012) Phosphorylation of intrinsically disordered regions in remorin proteins. *Front. Plant Sci.*, **3**, 1–6.
Marquès-Bueno, M.M., Morao, A.K., Cayrel, A., et al. (2016) A versatile Multisite Gateway-compatible promoter and transgenic line collection for cell type-specific functional genomics in *Arabidopsis*. *Plant J.*, **85**, 320–333.
Marschner, H. and Römheld, V. (1994) Strategies of plants for acquisition of iron Strategies in iron acquisition of higher plants. *Plant Soil*, **165**, 261–274. A
Marschner, H., Romheld, V. and Kissel, M. (1986) Different strategies in higher plants in mobilization and uptake of iron. *J. Plant Nutr.*, **9**, 695–713.
Martinez, D., Legrand, A., Gronnier, J., et al. (2019) Coiled-coil oligomerization controls localization of the plasma membrane REMORINs. *J. Struct. Biol.*, **206**, 12–19. Available at: http://www.sciencedirect.com/science/article/pii/S1047847718300467.
Martiniere, A., Fiche, J.B., Smokvarska, M., et al. (2019) Osmotic stress activates two reactive oxygen species pathways with distinct effects on protein nanodomains and diffusion. *Plant Physiol.*, pp.01065.2018.
Martiniere, A., Lavagi, I., Nageswaran, G., et al. (2012) Cell wall constrains lateral diffusion of plant plasma-membrane proteins. *Proc. Natl. Acad. Sci.*, **109**, 12805–12810.
Martins, S., Dohmann, E.M.N., Cayrel, A., et al. (2015) Internalization and vacuolar targeting of the brassinosteroid hormone receptor BRI1 are regulated by ubiquitination. *Nat. Commun.*, **6**.
Matsuoka, K., Furukawa, J., Bidadi, H., Asahina, M., Yamaguchi, S. and Satoh, S. (2014) Gibberellin-induced expression of fe uptake-related genes in *Arabidopsis*. *Plant Cell Physiol.*, **55**, 87–98.
Maurer, F., Müller, S. and Bauer, P. (2011) Suppression of Fe deficiency gene expression by jasmonate. *Plant Physiol. Biochem.*, **49**, 530–536.
McMahon, H.T. and Boucrot, E. (2011) Molecular mechanism and physiological functions of clathrin-mediated endocytosis. *Nat. Rev. Mol. Cell Biol.*, **12**, 517–533. Available at: http://dx.doi.org/10.1038/nrm3151.
Meer, G. Van and Sprong, H. (2004) Membrane lipids and vesicular traffic. *Curr. Opin. Cell Biol.*, **16**, 373–378.
Meer, G. Van, Voelker, D.R. and Feigenson, G.W. (2009) Membrane lipids: where they are and how they behave. *Nat. Rev. Mol. Cell Biol.*, **101**, 1–4.
Meister, M. and Tikkanen, R. (2014) Endocytic trafficking of membrane-bound cargo: A flotillin point of view. *Membranes (Basel).*, **4**, 356–371.
Men, S., Boutté, Y., Ikeda, Y., Li, X., Palme, K., Stierhof, Y.-D., Hartmann, M.-A., Moritz, T. and Grebe, M. (2008) Sterol-dependent endocytosis mediates post-cytokinetic acquisition of PIN2 auxin efflux carrier polarity. *Nat. Cell Biol.*, **10**, 237.

Available at: https://doi.org/10.1038/ncb1686.
Mettlen, M., Chen, P.-H., Srinivasan, S., Danuser, G. and Schmid, S.L. (2018) Regulation of Clathrin-Mediated Endocytosis. *Annu. Rev. Biochem.*, **87**, 871–896.
Mevissen, T.E.T. and Komander, D. (2017) Mechanisms of Deubiquitinase Specificity and Regulation. *Annu. Rev. Biochem.*, **86**, 159–192. Available at: https://doi.org/10.1146/annurev-biochem-061516-044916.
Mikosch, M., Hurst, A.C., Hertel, B. and Homann, U. (2006) Diacidic Motif Is Required for Efficient Transport of the K+ Channel KAT1 to the Plasma Membrane. *Plant Physiol.*, **142**, 923–930.
Miller, E.A., Beilharz, T.H., Malkus, P.N., Lee, M.C.S., Hamamoto, S., Orci, L. and Schekman, R. (2003) Multiple Cargo Binding Sites on the COPII Subunit Sec24p Ensure Capture of Diverse Membrane Proteins into Transport Vesicles. *Cell*, **114**, 497–509. Available at: https://doi.org/10.1016/S0092-8674(03)00609-3.
Miwa, K., Takano, J., Omori, H. and Seki, M. (2007) Plants Tolerant of High Boron Levels. *Science (80-.).*, **318**, 1417.
Mongrand, S., Morel, J., Laroche, J., et al. (2004) Lipid Rafts in Higher Plant Cells. *J. Biol. Chem.*, **279**, 36277–36286.
Morrissey, J., Baxter, I.R., Lee, J., Li, L., Lahner, B., Grotz, N., Kaplan, J., Salt, D.E. and Guerinot, M.L. (2009) The Ferroportin Metal Efflux Proteins Function in Iron and Cobalt Homeostasis in *Arabidopsis*. *Plant Cell*, **21**, 3326–3338. Available at: http://www.plantcell.org/cgi/doi/10.1105/tpc.109.069401.
Morrow, I.C., Rea, S., Martin, S., Prior, I.A., Prohaska, R., Hancock, J.F., James, D.E. and Parton, R.G. (2002) Flotillin-1/reggie-2 traffics to surface raft domains via a novel Golgi-independent pathway. Identification of a novel membrane targeting domain and a role for palmitoylation. *J. Biol. Chem.*, **277**, 48834–48841.
Morsomme, P., Dambly, S., Maudoux, O. and Boutry, M. (1998) Single point mutations distributed in 10 soluble and membrane regions of the Nicotiana plumbaginifolia plasma membrane PMA2 H+-ATPase activate the enzyme and modify the structure of the C-terminal region. *J. Biol. Chem.*, **273**, 34837–34842.
Mossessova, E., Bickford, L.C. and Goldberg, J. (2003) SNARE Selectivity of the COPII Coat. *Cell*, **114**, 483–495. Available at: https://doi.org/10.1016/S0092-8674(03)00608-1.
Mukhopadhyay, D. and Riezman, H. (2007) Proteasome-independent functions of ubiquitin in endocytosis and signaling. *Science (80-.).*, **315**, 201–205.
Munch, D., Teh, O.-K., Malinovsky, F.G., et al. (2015) Retromer contributes to immunity-associated cell death in *Arabidopsis*. *Plant Cell*, **27**, 463–479.
Murashige, T. and Skoog, F. (1962) A revised medium for rapid growth and bioassays with tobacco tissue cultures. *Physiol. Plant.*, 473–97.
Nakamura, M. and Grebe, M. (2018) Outer , inner and planar polarity in the *Arabidopsis* root. *Curr. Opin. Plant Biol.*, **41**, 46–53. Available at: http://dx.doi.org/10.1016/j.pbi.2017.08.002.
Nakamura, Y. (2017) Plant Phospholipid Diversity: Emerging Functions in Metabolism and Protein–Lipid Interactions. *Trends Plant Sci.*, **22**, 1027–1040. Available at: http://dx.doi.org/10.1016/j.tplants.2017.09.002.
Naseer, S., Lee, Y., Lapierre, C., Franke, R., Nawrath, C. and Geldner, N. (2012) Casparian strip diffusion barrier in *Arabidopsis* is made of a lignin polymer without suberin. *Proc. Natl. Acad. Sci.*, **109**, 10101–10106. Available at: http://www.pnas.org/cgi/doi/10.1073/pnas.1205726109.
Niittylä, T., Fuglsang, A.T., Palmgren, M.G., Frommer, W.B. and Schulze, W.X. (2007)

Temporal Analysis of Sucrose-induced Phosphorylation Changes in Plasma Membrane Proteins of *Arabidopsis*. *Mol. Cell. Proteomics*, **6**, 1711–1726. Available at: http://www.mcponline.org/lookup/doi/10.1074/mcp.M700164-MCP200.

Nikolovski, N., Rubtsov, D., Segura, M.P., Miles, G.P., Stevens, T.J., Dunkley, T.P.J., Munro, S., Lilley, K.S. and Dupree, P. (2012) Putative glycosyltransferases and other plant Golgi apparatus proteins are revealed by LOPIT proteomics. *Plant Physiol.*, **160**, 1037–1051.

Norman, J.M. Van (2016) Asymmetry and cell polarity in root development. *Dev. Biol.*, **419**, 165–174. Available at: http://dx.doi.org/10.1016/j.ydbio.2016.07.009.

Nozoye, T., Nagasaka, S., Kobayashi, T., Takahashi, M., Sato, Y., Sato, Y., Uozumi, N., Nakanishi, H. and Nishizawa, N.K. (2011) Phytosiderophore efflux transporters are crucial for iron acquisition in graminaceous plants. *J. Biol. Chem.*, **286**, 5446–5454.

Nühse, T.S., Bottrill, A.R., Jones, A.M.E. and Peck, S.C. (2007) Quantitative phosphoproteomic analysis of plasma membrane proteins reveals regulatory mechanisms of plant innate immune responses. *Plant J.*, **51**, 931–940.

Oh, Y.J., Kim, H., Seo, S.H., et al. (2016) Cytochrome b5 Reductase 1 Triggers Serial Reactions that Lead to Iron Uptake in Plants. *Mol. Plant*, **9**, 501–513. Available at: http://dx.doi.org/10.1016/j.molp.2015.12.010.

Olsen, R.A., Clark, R.B. and Bennett, J.H. (1981) The Enhancement of Soil Fertility by Plant Roots: Some plants, often with the help of microorganisms, can chemically modify the soil close to their roots in ways that increase or decrease the absorption of crucial ions. *Am. Sci.*, **69**, 378–384. Available at: http://www.jstor.org/stable/27850529.

Ortega-Rodes, P., Grimm, B. and Ortega, E. (2014) Evolutionary, physiological and biotechnological aspects of ferrochelatase and heme in higher plants. *Biotecnol. Apl.*, **31**, 176–186.

Pacifici, E., Mambro, R. Di, Ioio, R. Dello, Costantino, P. and Sabatini, S. (2018) Acidic cell elongation drives cell differentiation in the *Arabidopsis* root. *EMBO J.*, **37**, e99134. Available at: http://emboj.embopress.org/content/37/16/e99134.abstract.

Paez Valencia, J., Goodman, K. and Otegui, M.S. (2016) Endocytosis and Endosomal Trafficking in Plants. *Annu. Rev. Plant Biol.*, **67**, 309–335. Available at: http://www.annualreviews.org/doi/10.1146/annurev-arplant-043015-112242.

Palmer, C. and Guerinot, M. Lou (2009) A question of balance: facing the challenges of Cu, Fe and Zn homeostasis. *Nat Chem Biol*, **5**, 333–340.

Palmgren, M., Sommarin, M., Serrano, R. and Larsson, C. (1991) Identification of an autoinhibitory domain in the C-terminal region of the plant plasma membrane H(+)-ATPase. *J. Biol. Chem.*, **266 30**, 20470–20475.

Parsons, H.T., Christiansen, K., Knierim, B., et al. (2012) Isolation and proteomic characterization of the *Arabidopsis* Golgi defines functional and novel components involved in plant cell wall biosynthesis. *Plant Physiol.*, **159**, 12–26.

Pedrazzini, E., Komarova, N.Y., Rentsch, D. and Vitale, A. (2013) Traffic Routes and Signals for the Tonoplast. *Traffic*, **14**, 622–628.

Perraki, A., Cacas, J., Crowet, J.-M., Lins, L., Castroviejo, M., German-Retana, S., Mongrand, S. and Raffaele, S. (2012) Plasma Membrane Localization of Solanum tuberosum Remorin from Group 1 , Homolog 3 Is Mediated by Conformational Changes in a Novel C-Terminal Anchor and Required for the Restriction of Potato Virus. *Plant Physiol.*, **160**, 624–637.

Perraki, A., Gronnier, J., Gouguet, P., et al. (2018) REM1.3's phospho-status defines its plasma membrane nanodomain organization and activity in restricting PVX cell-to-cell movement. *PLOS Pathog.*, **14**, e1007378. Available at: https://doi.org/10.1371/journal.ppat.1007378.

Pfaffl, M.W. (2001) A new mathematical model for relative quantification in in real-time RT–PCR. *Nucleic Acids Res.*, **29**, 16–21.

Pickart, C.M. and Fushman, D. (2004) Polyubiquitin chains: polymeric protein signals. *Curr. Opin. Chem. Biol.*, **8**, 610–616. Available at: http://www.sciencedirect.com/science/article/pii/S1367593104001413.

Piechota, J., Bereza, M., Sokołowska, A., Suszyn, K., Lech, K. and Jan, H. (2015) Unraveling the functions of type II - prohibitins in *Arabidopsis* mitochondria. , **1**.

Pimpl, P., Movafeghi, A., Coughlan, S., Denecke, J., Hillmer, S. and Robinson, D.G. (2000) In Situ Localization and in Vitro Induction of Plant COPI-Coated Vesicles. *Plant Cell*, **12**, 2219 LP-2235. Available at: http://www.plantcell.org/content/12/11/2219.abstract.

Piper, R.C., Dikic, I. and Lukacs, G.L. (2016) Ubiquitin-dependent sorting in endocytosis . PubMed Commons. *Cold Spring Harb. Perspect. Biol.*, **6**, 24384571.

Piper, R.C. and Lehner, P.J. (2011) Endosomal transport via ubiquitination. *Trends Cell Biol.*, **21**, 647–655.

Polo, S., Sigismund, S., Faretta, M., Guidi, M., Capua, M.R., Bossi, G., Chen, H., Camilli, P. De and Fiore, P.P. Di (2002) A single motif responsible for ubiquitin recognition and monoubiquitination in endocytic proteins. *Nature*, **416**, 451–455. Available at: https://doi.org/10.1038/416451a.

Qi, X. and Zheng, H. (2013) Rab-A1c GTPase defines a population of the trans-Golgi network that is sensitive to endosidin1 during cytokinesis in *Arabidopsis*.*Mol. Plant*, **6**, 847–859. Available at: https://doi.org/10.1093/mp/sss116.

Qi, Y. and Katagiri, F. (2012) Membrane microdomain may be a platform for immune signaling. *Plant Signal. Behav.*, **7**, 454–456.

Qi, Y., Tsuda, K., Nguyen, L. V., Wang, X., Lin, J., Murphy, A.S., Glazebrook, J., Thordal-Christensen, H. and Katagiri, F. (2011) Physical association of *Arabidopsis* Hypersensitive Induced Reaction proteins (HIRs) with the immune receptor RPS2. *J. Biol. Chem.*, **286**, 31297–31307.

Qiao, Z., Brechenmacher, L., Smith, B., Strout, G.W., Mangin, W., Taylor, C., Russell, S.D., Stacey, G. and Libault, M. (2017) The GmFWL1 (FW2-2-like) nodulation gene encodes a plasma membrane microdomain-associated protein. *Plant. Cell Environ.*, **40**, 1442–1455. Available at: https://onlinelibrary.wiley.com/doi/abs/10.1111/pce.12941.

Qiao, Z. and Libault, M. (2017) Function of plasma membrane microdomain-associated proteins during legume nodulation. *Plant Signal. Behav.*, **12**, e1365215. Available at: https://doi.org/10.1080/15592324.2017.1365215.

Quinn, P.J. (2010) A lipid matrix model of membrane raft structure. *Prog. Lipid Res.*, **49**, 390–406. Available at: http://dx.doi.org/10.1016/j.plipres.2010.05.002.

Raad, H., Paclet, M.H., Boussetta, T., Kroviarski, Y., Morel, F., Quinn, M.T., Gougerot-Pocidalo, M.A., Dang, P.M.C. and El-Benna, J. (2009) Regulation of the phagocyte NADPH oxidase activity: Phosphorylation of gp91phox/NOX2 by protein kinase C enhances its diaphorase activity and binding to Rac2, p67phox, and p47phox. *FASEB J.*, **23**, 1011–1022.

Raffaele, S., Bayer, E., Lafarge, D., et al. (2009) Remorin, a solanaceae protein resident in membrane rafts and plasmodesmata, impairs potato virus X movement. *Plant*

Cell, **21**, 1541–1555.

Raffaele, S., Mongrand, S., Gamas, P., Niebel, A. and Ott, T. (2007) Genome-Wide Annotation of Remorins, a Plant-Specific Protein Family: Evolutionary and Functional Perspectives. *Plant Physiol.*, **145**, 593 LP-600. Available at: http://www.plantphysiol.org/content/145/3/593.abstract.

Rajniak, J., Giehl, R.F.H., Chang, E., Murgia, I., Wirén, N. von and Sattely, E.S. (2018) Biosynthesis of redox-active metabolites in response to iron deficiency in plants. *Nat. Chem. Biol.*, **14**, 442–450. Available at: https://doi.org/10.1038/s41589-018-0019-2.

Ravet, K., Touraine, B., Boucherez, J., Briat, J.F., Gaymard, F. and Cellier, F. (2009) Ferritins control interaction between iron homeostasis and oxidative stress in *Arabidopsis*. *Plant J.*, **57**, 400–412.

Regenberg, B., Villalba, J.M., Lanfermeijer, F.C. and Palmgren, M.G. (1995) C-terminal deletion analysis of plant plasma membrane H(+)-ATPase: yeast as a model system for solute transport across the plant plasma membrane. *Plant Cell*, **7**, 1655–66. Available at: http://www.ncbi.nlm.nih.gov/pubmed/7580256.

Rellán-Álvarez, R., Giner-Martínez-Sierra, J., Orduna, J., Orera, I., Rodríguez-Castrilln, J.Á., García-Alonso, J.I., Abadía, J. and Álvarez-Fernández, A. (2010) Identification of a Tri-Iron(III), Tri-Citrate Complex in the Xylem Sap of Iron-Deficient Tomato Resupplied with Iron: New Insights into Plant Iron Long-Distance Transport. *Plant Cell Physiol.*, **51**, 91–102.

Reynolds, G.D., Wang, C., Pan, J. and Bednarek, S.Y. (2018) Inroads into Internalization: Five Years of Endocytic Exploration. *Plant Physiol.*, **176**, 208–218.

Reyt, G., Boudouf, S., Boucherez, J., Gaymard, F. and Briat, J.F. (2015) Iron- and ferritin-dependent reactive oxygen species distribution: Impact on *Arabidopsis* root system architecture. *Mol. Plant*, **8**, 439–453.

Rivera-Milla, E., Stuermer, C.A.O. and Málaga-Trillo, E. (2006) Ancient origin of reggie (flotillin), reggie-like, and other lipid-raft proteins: Convergent evolution of the SPFH domain. *Cell. Mol. Life Sci.*, **63**, 343–357.

Robinson, N.J., Procter, C.M., Connolly, E.L. and Guerinot, M.L. (1999) A ferric-chelate reductase for iron uptake from soils. *Nature*, **397**, 694–697.

Rodríguez-Celma, J. and Schmidt, W. (2013) Reduction-based iron uptake revisited. *Plant Signal. Behav.*, **8**, e26116. Available at: http://www.tandfonline.com/doi/abs/10.4161/psb.26116.

Rogers, E.E., Eide, D.J. and Guerinot, M.L. (2000) Altered selectivity in an *Arabidopsis* metal transporter. *Proc. Natl. Acad. Sci.*, **97**, 12356–12360. Available at: http://www.pnas.org/cgi/doi/10.1073/pnas.210214197.

Romero-Barrios, N. and Vert, G. (2018) Proteasome-independent functions of lysine-63 polyubiquitination in plants. *New Phytol.*, **217**, 995–1011.

Roschzttardtz, H., Conejero, G., Curie, C. and Mari, S. (2009) Identification of the Endodermal Vacuole as the Iron Storage Compartment in the *Arabidopsis* Embryo. *Plant Physiol.*, **151**, 1329–1338.

Roschzttardtz, H., Conéjéro, G., Divol, F., Alcon, C., Verdeil, J.-L., Curie, C. and Mari, S. (2013) New insights into Fe localization in plant tissues. *Front. Plant Sci.*, **4**, 350.

Roschzttardtz, H., Grillet, L., Isaure, M.P., Conéjéro, G., Ortega, R., Curie, C. and Mari, S. (2011) Plant cell nucleolus as a hot spot for iron. *J. Biol. Chem.*, **286**, 27863–27866.

Roschzttardtz, H., Seguela-Arnaud, M., Briat, J.-F., Vert, G. and Curie, C. (2011) The FRD3 Citrate Effluxer Promotes Iron Nutrition between Symplastically

Disconnected Tissues throughout *Arabidopsis* Development. *Plant Cell*, **23**, 2725–2737. Available at: http://www.plantcell.org/cgi/doi/10.1105/tpc.111.088088.

Rotin, D. and Kumar, S. (2009) Physiological functions of the HECT family of ubiquitin ligases. *Nat. Rev. Mol. Cell Biol.*, **10**, 398–409. Available at: https://doi.org/10.1038/nrm2690.

Sager, R. and Lee, J.Y. (2014) Plasmodesmata in integrated cell signalling: Insights from development and environmental signals and stresses. *J. Exp. Bot.*, **65**, 6337–6358.

Saini, S., Sharma, I. and Pati, P.K. (2015) Versatile roles of brassinosteroid in plants in the context of its homoeostasis, signaling and crosstalks. *Front. Plant Sci.*, **6**, 1–17. Available at: http://journal.frontiersin.org/Article/10.3389/fpls.2015.00950/abstract.

Sánchez-Rodríguez, C., Shi, Y., Kesten, C., et al. (2018) The Cellulose Synthases Are Cargo of the TPLATE Adaptor Complex. *Mol. Plant*, **11**, 346–349.

Sancho-Andrés, G., Soriano-Ortega, E., Gao, C., et al. (2016) Sorting motifs involved in the trafficking and localization of the PIN1 auxin efflux carrier. *Plant Physiol.*, **3**, 1965–1982. Available at: http://www.plantphysiol.org/content/early/2016/05/12/pp.16.00373.abstract.

Sandor, R., Der, C., Grosjean, K., Anca, I., Noirot, E., Leborgne-Castel, N., Lochman, J., Simon-Plas, F. and Gerbeau-Pissot, P. (2016) Plasma membrane order and fluidity are diversely triggered by elicitors of plant defence. *J. Exp. Bot.*, **67**, 5173–5185.

Santi, S. and Schmidt, W. (2009) Dissecting iron deficiency-induced proton extrusion in *Arabidopsis* roots. *New Phytol.*, **183**, 1072–1084.

Sarabipour, S. and Hristova, K. (2016) Mechanism of FGF receptor dimerization and activation. *Nat. Commun.*, **7**, 1–12. Available at: http://dx.doi.org/10.1038/ncomms10262.

Schaaf, G., Honsbein, A., Meda, A.R., Kirchner, S., Wipf, D. and Wirén, N. Von (2006) AtIREG2 encodes a tonoplast transport protein involved in iron-dependent nickel detoxification in *Arabidopsis thaliana* roots. *J. Biol. Chem.*, **281**, 25532–25540.

Schaaf, G., Schikora, A., Häberle, J., Vert, G., Ludewig, U., Briat, J.F., Curie, C. and Wirén, N. Von (2005) A putative function for the *Arabidopsis* Fe-phytosiderophore transporter homolog AtYSL2 in Fe and Zn homeostasis. *Plant Cell Physiol.*, **46**, 762–774.

Schagerlöf, U., Wilson, G., Hebert, H., Al-Karadaghi, S. and Hägerhäll, C. (2006) Transmembrane topology of FRO2, a ferric chelate reductase from *Arabidopsis thaliana*. *Plant Mol. Biol.*, **62**, 215–221.

Schmid, M., Davison, T.S., Henz, S.R., Pape, U.J., Demar, M., Vingron, M., Schölkopf, B., Weigel, D. and Lohmann, J.U. (2005) A gene expression map of *Arabidopsis thaliana* development. *Nat. Genet.*, **37**, 501. Available at: https://doi.org/10.1038/ng1543.

Schmid, N.B., Giehl, R.F.H., Doll, S., Mock, H.-P., Strehmel, N., Scheel, D., Kong, X., Hider, R.C. and Wiren, N. von (2014) Feruloyl-CoA 6'-Hydroxylase1-Dependent Coumarins Mediate Iron Acquisition from Alkaline Substrates in *Arabidopsis*. *Plant Physiol.*, **164**, 160–172. Available at: http://www.pubmedcentral.nih.gov/articlerender.fcgi?artid=3875798&tool=pmcentrez&rendertype=abstract%5Cnhttp://www.plantphysiol.org/cgi/doi/10.1104/pp.113.228544.

Séguéla, M., Briat, J.F., Vert, G. and Curie, C. (2008) Cytokinins negatively regulate the root iron uptake machinery in *Arabidopsis* through a growth-dependent pathway.

Plant J., **55**, 289–300.
Shin, L.-J., Lo, J.-C., Chen, G.-H., Callis, J., Fu, H. and Yeh, K.-C. (2013) IRT1 Degradation Factor1, a RING E3 Ubiquitin Ligase, Regulates the Degradation of Iron-Regulated Transporter1 in *Arabidopsis*. *Plant Cell*, **25**, 3039–3051. Available at: http://www.plantcell.org/cgi/doi/10.1105/tpc.113.115212.
Sieben, C., Mikosch, M., Brandizzi, F. and Homann, U. (2008) Interaction of the K+-channel KAT1 with the coat protein complex II coat component Sec24 depends on a di-acidic endoplasmic reticulum export motif. *Plant J.*, **56**, 997–1006.
Singer, A.S.J. and Nicolson, G.L. (1972) The Fluid Mosaic Model of the Structure of Cell Membranes. *Science*, **175**, 720–731.
Sisó-Terraza, P., Luis-Villarroya, A., Fourcroy, P., Briat, J.-F., Abadía, A., Gaymard, F., Abadía, J. and Álvarez-Fernández, A. (2016) Accumulation and Secretion of Coumarinolignans and other Coumarins in *Arabidopsis thaliana* Roots in Response to Iron Deficiency at High pH. *Front. Plant Sci.*, **7**, 1–22. Available at: http://journal.frontiersin.org/article/10.3389/fpls.2016.01711/full.
Sivitz, A., Grinvalds, C., Barberon, M., Curie, C. and Vert, G. (2011) Proteasome-mediated turnover of the transcriptional activator FIT is required for plant iron-deficiency responses. *Plant J.*, **66**, 1044–1052.
Sivitz, A.B., Hermand, V., Curie, C. and Vert, G. (2012) *Arabidopsis* bHLH100 and bHLH101 Control Iron Homeostasis via a FIT-Independent Pathway. *PLoS One*, **7**.
Socha, A.L. and Guerinot, M. Lou (2014) Mn-euvering manganese: the role of transporter gene family members in manganese uptake and mobilization in plants. *Front. Plant Sci.*, **5**, 1–16. Available at: http://journal.frontiersin.org/article/10.3389/fpls.2014.00106/abstract.
Solis, G.P., Hoegg, M., Munderloh, C., Schrock, Y., Malaga-Trillo, E., Rivera-Milla, E. and Stuermer, C.A.O. (2007) Reggie/flotillin proteins are organized into stable tetramers in membrane microdomains. *Biochem. J.*, **403**, 313–322.
Solis, G.P., Hülsbusch, N., Radon, Y., Katanaev, V.L., Plattner, H. and Stuermer, C.A.O. (2013) Reggies/flotillins interact with Rab11a and SNX4 at the tubulovesicular recycling compartment and function in transferrin receptor and E-cadherin trafficking. *Mol. Biol. Cell*, **24**, 2689–2702.
Song, J., Lee, M.H., Lee, G.-J., Yoo, C.M. and Hwang, I. (2006) *Arabidopsis* EPSIN1 plays an important role in vacuolar trafficking of soluble cargo proteins in plant cells via interactions with clathrin, AP-1, VTI11, and VSR1. *Plant Cell*, **18**, 2258–2274.
Song, K., Jang, M., Kim, S.Y., Lee, G., Lee, G.-J., Kim, D.H., Lee, Y., Cho, W. and Hwang, I. (2012) An A/ENTH Domain-Containing Protein Functions as an Adaptor for Clathrin-Coated Vesicles on the Growing Cell Plate in *Arabidopsis* Root Cells. *Plant Physiol.*, **159**, 1013–1025.
Sorieul, M., Santoni, V., Maurel, C. and Luu, D.T. (2011) Mechanisms and Effects of Retention of Over-Expressed Aquaporin AtPIP2;1 in the Endoplasmic Reticulum. *Traffic*, **12**, 473–482.
Stacey, M.G., Koh, S., Becker, J. and Stacey, G. (2002) AtOPT3, a Member of the Oligopeptide Transporter Family, Is Essential for Embryo Development in *Arabidopsis*. *Plant Cell*, **14**, 2799–2811. Available at: http://www.plantcell.org/lookup/doi/10.1105/tpc.005629.
Staehelin, L.A. and Kang, B.-H. (2008) Nanoscale Architecture of Endoplasmic Reticulum Export Sites and of Golgi Membranes as Determined by Electron Tomography. *Plant Physiol.*, **147**, 1454–1468.
Steccanella, V., Hansson, M. and Jensen, P.E. (2015) Linking chlorophyll biosynthesis

to a dynamic plastoquinone pool. *Plant Physiol. Biochem.*, **97**, 207–216. Available at: http://dx.doi.org/10.1016/j.plaphy.2015.10.009.

Sutter, J.-U., Campanoni, P., Tyrrell, M. and Blatt, M.R. (2006) S Selective mobility and sensitivity to SNAREs is exhibited by the *Arabidopsis* KAT1 K+ channel at the plasma membrane.. *Plant Cell*, **18**, 935 LP-954. Available at: http://www.plantcell.org/content/18/4/935.abstract.

Sutter, J.U., Sieben, C., Hartel, A., Eisenach, C., Thiel, G. and Blatt, M.R. (2007) Abscisic Acid Triggers the Endocytosis of the *Arabidopsis* KAT1 K+ Channel and Its Recycling to the Plasma Membrane. *Curr. Biol.*, **17**, 1396–1402.

Swatek, K.N. and Komander, D. (2016) Ubiquitin modifications. *Cell Res.*, **26**, 399–422. Available at: http://dx.doi.org/10.1038/cr.2016.39.

Takagi, J., Renna, L., Takahashi, H., et al. (2013) MAIGO5 Functions in Protein Export from Golgi-Associated Endoplasmic Reticulum Exit Sites in *Arabidopsis*. *Plant Cell*, **25**, 4658 LP-4675.

Takano, J., Tanaka, M., Toyoda, A., Miwa, K., Kasai, K., Fuji, K., Onouchi, H., Naito, S. and Fujiwara, T. (2010) Polar localization and degradation of *Arabidopsis* boron transporters through distinct trafficking pathways. *Proc. Natl. Acad. Sci.*, **107**, 5220–5225. Available at: http://www.pnas.org/cgi/doi/10.1073/pnas.0910744107.

Tan, S., Zhang, P., Xiao, W., et al. (2017) TMD1 domain and CRAC motif determine the association and disassociation of MxIRT1 with detergent-resistant membranes. *Traffic*, **19**.

Tanner, W., Malinsky, J. and Opekarová, M. (2011) In Plant and Animal Cells, Detergent-Resistant Membranes Do Not Define Functional Membrane Rafts. *Plant Cell*, **23**, 1191–1193.

Tapken, W. and Murphy, A.S. (2015) Membrane nanodomains in plants: Capturing form, function, and movement. *J. Exp. Bot.*, **66**, 1573–1586.

Terrell, J., Shih, S., Dunn, R. and Hicke, L. (1998) A Function for Monoubiquitination in the Internalization of a G Protein–Coupled Receptor. *Mol. Cell*, **1**, 193–202. Available at: https://doi.org/10.1016/S1097-2765(00)80020-9.

Terry, N. and Abadía, J. (1986) Function of iron in chloroplast. *J. Plant Nutr. - J PLANT NUTR*, **9**, 609–646.

Thomine, S. and Vert, G. (2013) Iron transport in plants: Better be safe than sorry. *Curr. Opin. Plant Biol.*, **16**, 322–327.

Tomasi, N., Nobili, M. De, Gottardi, S., Zanin, L., Mimmo, T., Varanini, Z., Römheld, V., Pinton, R. and Cesco, S. (2013) Physiological and molecular characterization of Fe acquisition by tomato plants from natural Fe complexes. *Biol. Fertil. Soils*, **49**, 187–200.

Traub, L.M. (2009) Tickets to ride: Selecting cargo for clathrin-regulated internalization. *Nat. Rev. Mol. Cell Biol.*, **10**, 583–596.

Trimble, W.S. and Grinstein, S. (2015) Barriers to the free diffusion of proteins and lipids in the plasma membrane. *J. Cell Biol.*, **208**, 259–271.

Truong-Quang, B.-A. and Lenne, P.-F. (2014) Membrane microdomains: from seeing to understanding. *Front. Plant Sci.*, **5**, 1–14.

Vert, G., Briat, J.F. and Curie, C. (2001) *Arabidopsis* IRT2 gene encodes a root-periphery iron transporter. *Plant J.*, **26**, 181–189.

Vert, G., Briat, J.-F. and Curie, C. (2003) Dual Regulation of the *Arabidopsis* High-Affinity Root Iron Uptake System by Local and Long-Distance Signals. *Plant Physiol.*, **132**, 796–804. Available at: http://www.plantphysiol.org/cgi/doi/10.1104/pp.102.016089.

Vert, G., Grotz, N., Dédaldéchamp, F., Gaymard, F., Guerinot, M. Lou, Briat, J.-F. and Curie, C. (2002) IRT1, an *Arabidopsis* Transporter Essential for Iron Uptake from the Soil and for Plant Growth. *Plant Cell*, **14**, 1223 LP-1233. Available at: http://www.plantcell.org/content/14/6/1223.abstract.

Viehweger, K. (2014) How plants cope with heavy metals. *Bot. Stud.*, **55**.

Vitale, A. and Boston, R.S. (2008) Endoplasmic reticulum quality control and the unfolded protein response: Insights from plants. *Traffic*, **9**, 1581–1588.

Voinnet, O., Rivas, S., Mestre, P. and Baulcombe, D. (2003) An enhanced transient expression system in plants based on suppression of gene silencing by the p19 protein of tomato bushy stunt virus. *Plant J.*, **33**, 949–956.

Walker, E.L. and Connolly, E.L. (2008) Time to pump iron: iron-deficiency-signaling mechanisms of higher plants. *Curr. Opin. Plant Biol.*, **11**, 530–535.

Walton, A., Stes, E., Cybulski, N., et al. (2016) It's Time for Some "Site"-Seeing: Novel Tools to Monitor the Ubiquitin Landscape in *Arabidopsis thaliana* *Plant Cell*, **28**, 6 LP-16. Available at: http://www.plantcell.org/content/28/1/6.abstract.

Wang, C., Hu, T., Yan, X., et al. (2016) Differential Regulation of Clathrin and Its Adaptor Proteins during Membrane Recruitment for Endocytosis. *Plant Physiol.*, **171**, 215–229.

Wang, C., Yan, X., Chen, Q., et al. (2013) Clathrin Light Chains Regulate Clathrin-Mediated Trafficking, Auxin Signaling, and Development in *Arabidopsis*. *Plant Cell*, **25**, 499 LP-516. Available at: http://www.plantcell.org/content/25/2/499.abstract.

Wang, H.Y., Klatte, M., Jakoby, M., Bäumlein, H., Weisshaar, B. and Bauer, P. (2007) Iron deficiency-mediated stress regulation of four subgroup Ib BHLH genes in *Arabidopsis thaliana*. *Planta*, **226**, 897–908.

Wang, L., Li, H., Lv, X., et al. (2015) Spatiotemporal dynamics of the BRI1 receptor and its regulation by membrane microdomains in living *Arabidopsis* cells. *Mol. Plant*, **8**, 1334–1349.

Wang, L., Xue, Y., Xing, J., Song, K. and Lin, J. (2018) Exploring the Spatiotemporal Organization of Membrane Proteins in Living Plant Cells. *Annu. Rev. Plant Biol.*, **69**, 525–551.

Wang, N., Cui, Y., Liu, Y., Fan, H., Du, J., Huang, Z., Yuan, Y., Wu, H. and Ling, H.Q. (2013) Requirement and functional redundancy of Ib subgroup bHLH proteins for iron deficiency responses and uptake in *Arabidopsis thaliana*. *Mol. Plant*, **6**, 503–513.

Wang, Q., Zhao, Y., Luo, W., et al. (2013) Single-particle analysis reveals shutoff control of the *Arabidopsis* ammonium transporter AMT1;3 by clustering and internalization. *Proc. Natl. Acad. Sci.*, **110**, 13204 LP-13209. Available at: http://www.pnas.org/content/110/32/13204.abstract.

Wang, S., Yoshinari, A., Shimada, T., Hara-Nishimura, I., Mitani-Ueno, N., Feng Ma, J., Naito, S. and Takano, J. (2017) Polar Localization of the NIP5;1 Boric Acid Channel Is Maintained by Endocytosis and Facilitates Boron Transport in *Arabidopsis* Roots. *Plant Cell*, **29**, 824–842. Available at: http://www.plantcell.org/lookup/doi/10.1105/tpc.16.00825.

Wattelet-Boyer, V., Brocard, L., Jonsson, K., et al. (2016) Enrichment of hydroxylated C24- and C26-acyl-chain sphingolipids mediates PIN2 apical sorting at trans-Golgi network subdomains. *Nat. Commun.*, **7**, 12788.

White, P.J. and Brown, P.H. (2010) Plant nutrition for sustainable development and

global health. *Ann. Bot.*, **105**, 1073–1080.
Widjaja, I., Naumann, K., Roth, U., Wolf, N., Mackey, D., Dangl, J.L., Scheel, D. and Lee, J. (2009) Combining subproteome enrichment and Rubisco depletion enables identification of low abundance proteins differentially regulated during plant defense. *Proteomics*, **9**, 138–147.
Xing, S., Wallmeroth, N., Berendzen, K.W. and Grefen, C. (2016) Techniques for the analysis of protein-protein interactions in vivo. *Plant Physiol.*, **171**, pp.00470.2016.
Xiong, H., Kakei, Y., Kobayashi, T., et al. (2013) Molecular evidence for phytosiderophore-induced improvement of iron nutrition of peanut intercropped with maize in calcareous soil. *Plant, Cell Environ.*, **36**, 1888–1902.
Yadav, P.K., Gupta, A.K., Sharma, B., Bhatt, T.K. and Joshi, D. (2016) Role of Ubiquitin-Mediated Degradation System in Plant Biology. *Front. Plant Sci.*, **7**, 1–8.
Yamada, K., Nagano, A.J., Nishina, M., Hara-Nishimura, I. and Nishimura, M. (2013) Identification of two novel endoplasmic reticulum body-specific integral membrane proteins. *Plant Physiol.*, **161**, 108–120.
Yi, Y. and Guerinot, M. Lou (1996) Genetic evidence that induction of root Fe(III) chelate reductase activity is necessary for iron uptake under iron deficiency. *Plant J.*, **10**, 835–844.
Yoshinari, A., Fujimoto, M., Ueda, T., Inada, N., Naito, S. and Takano, J. (2016) DRP1-dependent endocytosis is essential for polar localization and boron-induced degradation of the borate transporter BOR1 in *Arabidopsis thaliana*. *Plant Cell Physiol.*, **57**, 1985–2000.
Yoshinari, A., Hosokawa, T., Amano, T., Beier, M.P., Kunieda, T., Shimada, T., Hara-Nishimura, I., Naito, S. and Takano, J. (2019) Polar Localization of the Borate Exporter BOR1 Requires AP2-Dependent Endocytosis. *Plant Physiol.*, pp.01017.2018. Available at: http://www.plantphysiol.org/content/early/2019/02/01/pp.18.01017.abstract.
Yuan, W., Zhang, D., Song, T., et al. (2017) *Arabidopsis* plasma membrane H+-ATPase genes AHA2 and AHA7 have distinct and overlapping roles in the modulation of root tip H+efflux in response to low-phosphorus stress. *J. Exp. Bot.*, **68**, 1731–1741.
Yuan, Y., Wu, H., Wang, N., Li, J., Zhao, W., Du, J., Wang, D. and Ling, H.Q. (2008) FIT interacts with AtbHLH38 and AtbHLH39 in regulating iron uptake gene expression for iron homeostasis in *Arabidopsis*. *Cell Res.*, **18**, 385–397.
Žárský, V., Kulich, I., Fendrych, M. and Pečenková, T. (2013) Exocyst complexes multiple functions in plant cells secretory pathways. *Curr. Opin. Plant Biol.*, **16**, 726–733. Available at: http://www.sciencedirect.com/science/article/pii/S1369526613001623.
Zauber, H., Szymanski, W. and Schulze, W.X. (2013) Unraveling sterol-dependent membrane phenotypes by analysis of protein abundance-ratio distributions in different membrane fractions under biochemical and endogenous sterol depletion. *Mol. Cell. Proteomics*, **12**, 3732–3743.
Zelazny, E., Barberon, M., Curie, C. and Vert, G. (2011) Ubiquitination of transporters at the forefront of plant nutrition. *Plant Signal. Behav.*, **6**, 1597–1599.
Zelazny, E., Borst, J.W., Muylaert, M., Batoko, H., Hemminga, M.A. and Chaumont, F. (2007) FRET imaging in living maize cells reveals that plasma membrane aquaporins interact to regulate their subcellular localization. *Proc. Natl. Acad. Sci. U. S. A.*, **104**, 12359–12364. Available at: http://www.pubmedcentral.nih.gov/articlerender.fcgi?artid=1941474&tool=pmcentrez&rendertype=abstract.

Zelazny, E., Miecielica, U., Borst, J.W., Hemminga, M.A. and Chaumont, F. (2009) An N-terminal diacidic motif is required for the trafficking of maize aquaporins ZmPIP2;4 and ZmPIP2;5 to the plasma membrane. *Plant J.*, **57**, 346–355.

Zelazny, E., Santambrogio, M., Pourcher, M., Chambrier, P., Berne-Dedieu, A., Fobis-Loisy, I., Miège, C., Jaillais, Y. and Gaude, T. (2013) Mechanisms governing the endosomal membrane recruitment of the core retromer in *Arabidopsis*. *J. Biol. Chem.*, **288**, 8815–8825.

Zelazny, E. and Vert, G. (2014) Plant Nutrition: Root Transporters on the Move. *Plant Physiol.*, **166**, 500–508. Available at: http://www.plantphysiol.org/cgi/doi/10.1104/pp.114.244475.

Zelazny, E. and Vert, G. (2015) Regulation of Iron Uptake by IRT1: Endocytosis Pulls the Trigger. *Mol. Plant*, **8**, 977–979.

Zhai, Z., Gayomba, S.R., Jung, H.-I., et al. (2014) OPT3 Is a Phloem-Specific Iron Transporter That Is Essential for Systemic Iron Signaling and Redistribution of Iron and Cadmium in *Arabidopsis*. *Plant Cell*, **26**, 2249–2264. Available at: http://www.plantcell.org.memex.lehman.cuny.edu:2048/content/26/5/2249.short.

Zhang, T., Sui, D. and Hu, J. (2016) Structural insights of ZIP4 extracellular domain critical for optimal zinc transport. *Nat. Commun.*, **7**, 11979. Available at: http://www.nature.com/doifinder/10.1038/ncomms11979.

Zhang, Y., Persson, S., Hirst, J., Robinson, M.S., Damme, D. van and Sánchez-Rodríguez, C. (2015) Change your Tplate, change your fate: Plant CME and beyond. *Trends Plant Sci.*, **20**, 41–48.

Zhao, F.J., Jiang, R.F., Dunham, S.J. and McGrath, S.P. (2006) Cadmium uptake, translocation and tolerance in the hyperaccumulator *Arabidopsis* halleri. *New Phytol.*, **172**, 646–654.

Zhao, H. and Eide, D. (2002) The yeast ZRT1 gene encodes the zinc transporter protein of a high-affinity uptake system induced by zinc limitation. *Proc. Natl. Acad. Sci.*, **93**, 2454–2458.

Zhou, J., Liu, D., Wang, P., et al. (2018) Regulation of *Arabidopsis* brassinosteroid receptor BRI1 endocytosis and degradation by plant U-box PUB12/PUB13-mediated ubiquitination. *Proc. Natl. Acad. Sci.*, **115**, E1906 LP-E1915. Available at: http://www.pnas.org/content/115/8/E1906.abstract.

Zhou, L., Cheung, M.-Y., Li, M.-W., Fu, Y., Sun, Z., Sun, S.-M. and Lam, H.-M. (2010) Rice hypersensitive induced reaction protein 1 (OsHIR1) associates with plasma membrane and triggers hypersensitive cell death. *BMC Plant Biol.*, **10**, 290.

Zhou, L., Cheung, M.-Y., Zhang, Q.I., Lei, C.-L., Zhang, S.-H., Sun, S.S.-M. and Lam, H.-M. (2009) A novel simple extracellular leucine-rich repeat (eLRR) domain protein from rice (OsLRR1) enters the endosomal pathway and interacts with the hypersensitive-induced reaction protein 1 (OsHIR1). *Plant. Cell Environ.*, **32**, 1804–1820. Available at: https://onlinelibrary.wiley.com/doi/abs/10.1111/j.1365-3040.2009.02039.x.

Rôle de la protéine HIR2 et des microdomaines de la membrane plasmique dans le contrôle de la machinerie d'acquisition du fer chez les plantes

Mots clés : IRT1, endocytose, microdomaines membranaires, acquisition du fer.

Résumé Le fer est essentiel à la croissance et au développement des plantes. Chez Arabidopsis thaliana, le transporteur IRT1 permet l'absorption du fer par les cellules épidermiques de la racine et est, par conséquent, un des acteurs majeurs de la nutrition en fer. IRT1 est cependant un transporteur peu spécifique qui transporte également des métaux non ferreux que sont le zinc (Zn), le manganèse (Mn) et le cobalt, qui constituent les substrats secondaires d'IRT1 et qui ont été récemment démontrés dans notre laboratoire comme régulant l'endocytose d'IRT1. Afin d'identifier des protéines potentiellement impliquées dans le trafic ou dans la régulation de l'activité d'IRT1, nous avons isolé des interactants de ce transporteur via des immunopurifications d'IRT1 combinées à des analyses de spectrométrie de masse. Cette approche nous a permis d'établir le premier intéractome d'IRT1. Parmi les protéines interagissant avec IRT1, nous avons isolé AHA2 et FRO2 qui participent toutes les deux au processus d'absorption du fer chez Arabidopsis, ainsi que la protéine à domaine SPFH appelée HIR2. HIR2 est localisée dans des microdomaines membranaires chez Arabidopsis, mais sa fonction reste jusqu'à présent assez énigmatique. Cependant, chez les animaux, les protéines à domaine SPFH ont été proposées comme étant impliquées dans la formation des microdomaines membranaires; de plus certaines protéines à domaines SPFH appelées Flotillines interviennent dans des mécanismes d'endocytose chez les animaux et les plantes. Après avoir validé les interactions entre les protéines IRT1 et FRO2/AHA2/HIR2 par des approches complémentaires, nous avons analysé la dynamique intracellulaire de ces protéines par microscopie. Nos résultats suggèrent l'existence d'un complexe protéique regroupant les trois acteurs majeurs de l'homéostasie du fer chez Arabidopsis : IRT1, FRO2 et AHA2, dont la fonction pourrait être d'optimiser l'absorption du fer dans la racine. Contrairement à ce qui est observé pour IRT1, les protéines FRO2 et AHA2 ne sont pas massivement endocytées en réponse à un excès de métaux (Zn,Mn, Co) et ceci bien qu'elles puissent être présentes au sein d'un complexe contenant IRT1. Nous avons en outre montré que FRO2 et AHA2 étaient ubiquitinées, mais contrairement à IRT1, de façon indépendante de la concentration en métaux non ferreux. En utilisant des approches de génétique inverse, nous avons mis en évidence que HIR2 était impliquée dans le maintien de l'homéostasie du fer, les mutants hir2 étant extrêmement sensibles à la carence en fer. D'autre part nous avons montré que l'accumulation de la protéine IRT1 était dérégulée chez le mutant hir2 et ceci de façon post-transcriptionnelle. Nous cherchons actuellement à déterminer comment HIR2 régule la dynamique et/ou la stabilité d'IRT1 dans la cellule. HIR2 pourrait assurer le recrutement d'IRT1 et plus généralement du complexe d'acquisition du fer décrit ci-dessus dans des microdomaines membranaires spécifiques. D'autre part, nous avons également émis l'hypothèse que HIR2 pourrait être impliquée dans une voie d'endocytose d'IRT1 indépendante de la clathrine

Role of HIR2 protein and plasma membrane microdomains in the control of iron acquisition machinery in plants

Keywords : IRT1, endocytosis, membrane microdomains, iron acquisition.

Abstract : Iron is an essential nutrient for plant growth and development. In Arabidopsis thaliana, the transporter IRT1, which allows iron absorption through the epidermic cells of the root, is a major actor in iron nutrition. Bessides, IRT1 also transports the non-iron metals zinc (Zn), manganese (Mn) and cobalt (Co). These metals are considered as the secondary substrates of IRT1, and therefore this transporter is considered as poorly specific. Our laboratory has recently uncovered that these secondary substrates regulate IRT1 endocytosis. In order to uncover the different proteins that can be implicated in the traffic or in the regulation of IRT1 activity, we performed IRT1 immnopurification, followed by mass spectrometry analysis. This approach allowed us to produce a first interactome list of IRT1. Among the proteins that interact with IRT1, we isolated AHA2 and FRO2, both well known in the process of iron acquisition in Arabidopsis, and also a SPFH domain containing protein known as HIR2. Although it is known that HIR2 is contained in membrane microdomains in Arabidopsis, its function is still to be determined. Nevertheless, in the animal kingdom, SPFH domain containing proteins have been proposed as implicated in the formation of membrane microdomains. This is especially the case of the specific SPFH domain containing proteins known as Flotillins, which have the ability to mediate endocytosis in animals as in plants. After validation of the interaction between IRT1 and FRO2/AHA2/HIR2 by different complementary approaches, we microscopically analyzed the intracellular dynamics of these proteins. Our results suggest the existence of a protein complex that reunites the three major actors of iron homeostasis in Arabidopsis: IRT1, FRO2 and AHA2. We suspect that the main function of this complex is to optimize the process of iron absorption in the root. In spite of what is known for IRT1 and despite being part of a same complex, FRO2 and AHA2 are not massively endocytosed in response to a non-iron metal excess (Zn, Mn, Co). Furthermore, we have shown that FRO2 and AHA2 are ubiquitinated, although their ubiquitination is also independent of the concentration of the non-iron metals, unlike the ubiquitination of IRT1. Finally, using reverse genetic approaches, we have been able to show that HIR2 is implicated in the maintenance of the iron homeostasis. Indeed, hir2 mutants are extremely sensitive to lack of Fe, even though they present posttranslational deregulations that result in the overaccumulation of the protein IRT1. We are currently trying to determine how HIR2 regulates the dynamics and/or the stability of IRT1 inside the cell. HIR2 could be assuring the recruiting of IRT1,or the recruitment of the whole iron acquisition complex, into specific membrane microdomains. On the other hand, HIR2 could be implicated in a new pathway of internalization of IRT1, independent of clathrin